Dielectric and optical properties of dense plasmas

Article *in* Annales de Physique · July 2005

DOI: 10.1051/anphys:2006004

CITATIONS
53

READS
589

1 author:

H. Reinholz
University of Rostock
112 PUBLICATIONS **2,591** CITATIONS

SEE PROFILE

Dielectric and Optical Properties of Dense Plasmas

Heidi Reinholz
Institut für Physik, Universität Rostock, 18051 Rostock, Germany

August 18, 2006

Dedicated to Tim, Falk, Ben and Rob

Contents

1 Plasma and Radiation

1.1 Introduction

The interaction of matter with radiation is a very broad subject and concerns almost every area in physics[1]. Radiation as a diagnostic tool is used to investigate the properties of matter. Another aspect is the exposure of matter to radiation in order to change or influence the behavior of matter via excitation of matter by radiation. In any case, the particular effects and properties which can be obtained are determined by the coupling of the electromagnetic radiation (light) to the charged particles. This is also the case for neutral matter, gases, liquids or the condensed state, since it consists of bound states made up from charged particles, electrons and atomic nuclei. The forces are indirectly given by the electromagnetic interaction. However, we will be concerned with the so–called fourth state of matter, the plasma. Its properties are mainly determined by the bare Coulomb interaction since its constituents are free charged particles. The long range character of the interaction leads to special features. There is a broad range of systems which can be considered and treated as Coulomb systems. Ionic plasmas are the most long–standing investigated systems. They are not only relevant in the physics of stellar and planetary systems but also in various technical systems and applications, as e.g. in light sources and fusion. Of particular interest for fundamental research are high-dense plasmas produced with shock waves , Z-pinches or heavy ion beams, see e.g. [3, 2] where further references can be found. In recent years, high-intense laser pulses have become available. The radiation is used to produce plasmas as well as subsequently to probe its properties. A non-exhaustive list of references which are relevant in the context of this paper is [4, 5, 6, 7, 8]. It is expected that in the near future also relativistic plasmas will be produced leading to new theoretical and experimental challenges.

Beside these standard systems we will also refer to electron-hole plasmas in semiconductors, where systems of reduced dimensionality (quantum well, quantum wire, quantum dot) became of increasing interest due to recent advances in semiconductor technologies. Dusty plasmas are typically two dimensional structures. Such systems can be found in astrophysical applications. They have become available experimentally recently, e.g. they have been produced under the condition of zero gravity in space stations. Quark–gluon plasmas can also be treated with similar methods as Coulomb plasmas and exhibit analogous effects, see Röpke [9].

Considering the physics of charged particle systems, a variety of different phenomena are of interest. The properties of ionized, high temperature plasmas such as the solar plasma or magnetically confined fusion plasmas are determined by screening, collisions and radiation. The formation or presence of bound states, i.e. atoms, molecules, clusters, condensed matter is a further aspect which is due to the interactions within the plasma itself. The physics of nonideal plasmas or, more general, of strongly coupled Coulomb systems was described in

[1] Presently, particular attention is paid to Einstein's paper on the photoelectric effect [1] which appeared 100 years ago, in the *annus mirabilis*.

numerous monographs. We would like to name a few which are particularly relevant and are in parts predecessors to the quantum-statistical approach presented within this work: *Theory of bound states and ionization equilibrium in plasmas and solids* by Ebeling, Kraeft and Kremp [10], *Quantum Statistics of Charged Particle Systems* by Kraeft, Kremp, Ebeling and Röpke [11], *Physics of Nonideal Plasma* by Iakubov and Fortov [12], *Thermophysical properties of Hot Dense Plasmas* by Ebeling *et al.* [13], the report article by Redmer [14] and the most recent one, *Quantum Statistics of Nonideal Plasmas* by Kremp, Schlanges and Kraeft [15]. Within a regular series of international workshops and conferences, the topics of *Physics of Nonideal Plasmas* (PNP) [16] and *Strongly Coupled Coulomb Systems* (SCCS) [17] has been extensively discussed and published.

The main focus of the present work is the description of various dielectric properties. We will consider homogeneous systems near thermal equilibrium, described by the temperature T and, in the case of a neutral plasma consisting of electrons and singly charged ions, by the particle density $n = n_e = n_i$. Instead of temperature and particle density, the dimensionless plasma parameter

$$\Gamma = \frac{e^2}{4\pi\epsilon_0 k_B T} \left(\frac{4\pi n}{3}\right)^{1/3} \tag{1}$$

and the degeneracy parameter

$$\Theta = \frac{2m_e k_B T}{\hbar^2} (3\pi^2 n)^{-2/3} \tag{2}$$

are introduced for further classification. They describe the ratio between the mean potential energy and the kinetic energy (Γ) and denote the degree of degeneracy of the electron gas (Θ). Usually, plasmas are classified as ideal ($\Gamma \ll 1$) and nonideal ($\Gamma \geq 1$) as well as degenerate ($\Theta \ll 1$) and nondegenerate ($\Theta \gg 1$) systems, respectively.

In chapter 2, we will give a microscopic, quantum statistical approach for the evaluation of the dielectric properties of Coulomb systems expressed via the dielectric function $\epsilon(\vec{k}, \omega)$. The observable quantities which can be derived and expressed, e.g., via the response function $\chi(\vec{k}, \omega)$ of an electron-ion plasma can be considered in the entire frequency–wavelength–space $(\vec{k}, \omega)$. Applying generalized linear response theory, they are expressed in terms of equilibrium correlation functions which allow for a systematic perturbative treatment. A Green's function perturbation theory is used to evaluate the correlation functions which will be outlined in chapter 3. General expressions for the dynamical local-field factor $G(\vec{k}, \omega)$ are given. In the long-wavelength limit, it can be related to a dynamical collision frequency $\nu(\omega) = -i\omega_{\rm pl}\, G(0, \omega)/\omega$ with the plasma frequency

$$\omega_{\rm pl} = \sqrt{\frac{ne^2}{\epsilon_0 m_e}}. \tag{3}$$

Thus, a systematic approach to the optical conductivity is given within a dielectric function formalism. The following chapter 4 focuses on the long-wavelength limit and the calculation of the frequency dependent conductivity or collision frequency. At arbitrary degeneracy,

different approximations for the ω-dependent collision frequency are considered. The implementation of the quantum statistical theory of the dc-conductivity of a two-component plasma into the evaluation of the dynamical local-field factor is shown. It allows the consistent treatment of screening and strong collisions. Sum rules are considered. In particular, the convergence of the third-moment sum rule can be shown analytically. Numerical calculations are presented for the dielectric function and the optical conductivity of the electron-ion plasma in adiabatic approximation. The validity of this perturbative approach depends on an expansion parameter to be small. In our case it is the particle density or the plasma parameter Γ which limits the applicability of this perturbative approach. The comparison with numerical solutions obtained from molecular dynamics simulations or path integral Monte Carlo simulations will extend the region where such physical properties are evaluated, see chapter 5.

We investigate transport properties, in particular the dynamical conductivity and optical absorption. Bremsstrahlung, Compton and Thomson scattering, and reflectivity are interesting applications, which are discussed in chapter 6. In principle, bound state formation can also be treated and included using the many-particle formalism as given above, but will not shown in detail. The formation of bound states, the composition of partially ionized plasmas, optical line spectra, the physics of the transition from a dielectric to a metal-like behavior (Mott transition) at increasing density, degeneration and Pauli blocking are only briefly commented on in the Outlook, chapter 7. Our calculations so far are performed for the nonrelativistic case. A relativistic generalization is necessary in view of expected experiments. The latter also demand the treatment of short-time behavior, strong non-equilibrium and strong electric fields. Our results given below which are applicable to present experiments are open for corresponding improvements. Such envisaged experiments need for a non-equilibrium quantum electrodynamic (QED).

The aim of the present work is an improvement of the theory of the dielectric response, which is relevant for the interaction of matter with external fields, in particular electromagnetic fields. Instead of a simple Drude formula which introduces a relaxation time in a semi-empiric way, a systematic quantum statistical approach is given which is able to describe the dynamical behavior of the collision frequency. In this way, a systematic many-particle approach to the ac and dc conductivity has been worked out on the basis of the second fluctuation-dissipation theorem, which relates the inverse response function to a generalized force-force correlation function. Our approach is particularly suitable for the unified description of experiments which are related to the interaction of radiation and matter.

1.2 Quantum Electrodynamics: Lagrangian

The current most fundamental and complete theory for describing the properties of electromagnetic radiation and its interaction with electrically charged matter is quantum electrodynamics (QED). While quantum mechanics of charged particles is generalized to a relativistic treatment, the electromagnetic fields of photons are quantized leading to a consistent approach to all phenomena exhibited by charged point particles, such as electrons and positrons,

and the particles of light (photons), interacting by electromagnetism. There are excellent and comprehensive reviews and advanced treatises of QED, see e.g. textbooks by Itzykson and Zuber [18], Peshkin and Schroeder [19], Bogolyubov and Shirkov [20], or Schweber [21].

In the following, we will present a few fundamental relationships related to the subject of this work, in particular to the state of the many-particle system describing matter and radiation and its time evolution. We will briefly outline how the equations of motion (Maxwell equations and Dirac equation) as well as a Hamiltonian can be found. We follow the notation given by Itzykson and Zuber [18] and adopt the MKSA system of electromagnetic units (SI units) which has the virtue of overall convenience, especially in applications[2].

We consider a system of fermionic charged particles (electrons, protons) described by the Dirac spinor fields $\psi(x)$ (Dirac indices and labeling of species are omitted). The interaction is mediated by electromagnetic fields $\vec{E}(x), \vec{B}(x)$ at $x = x^\mu = (ct, \vec{r})$ which are related to the 4-vector potential $A^\mu(x) = (U(x)/c, \vec{A}(x))$ according to

$$\vec{E}(x) = -\nabla U(x) - \frac{\partial}{\partial t}\vec{A}(x), \qquad \vec{B}(x) = \nabla \times \vec{A}(x)\,. \tag{4}$$

For a compact and covariant presentation, the field strength tensor $F^{\mu\nu} = \partial^\mu A^\nu - \partial^\nu A^\mu$ is introduced, $\partial_\mu = \partial/\partial x^\mu = (\partial/\partial ct, \partial/\partial \vec{r}) = (\partial/\partial ct, \nabla)$ is the derivative operator. The components of the field strength tensor are the electromagnetic fields,

$$F^{\mu\nu} = \begin{pmatrix} 0 & -E_x/c & -E_y/c & -E_z/c \\ E_x/c & 0 & -B_z & B_y \\ E_y/c & B_z & 0 & -B_x \\ E_z/c & -B_y & B_x & 0 \end{pmatrix}.$$

On the microscopic level, the time evolution of the system is described by the Lagrangian density

$$\mathcal{L}(x) = \bar{\psi}(x)\left(i\hbar c\gamma^\mu\partial_\mu - mc^2\right)\psi(x) - \frac{\epsilon_0}{4}c^2 F_{\mu\nu}(x)F^{\mu\nu}(x) - j_\mu(x)A^\mu(x) \tag{5}$$

with the Hermitian adjoint $\bar{\psi}(x) = \psi(x)^\dagger\gamma^0$, the Dirac matrices $\gamma^\mu = (\gamma^0, \vec{\gamma})$, the electron charge $e = -1.6021917 \times 10^{-19}$ As. The 4-vector fermion current density is given by

$$j^\mu(x) = ec\bar{\psi}(x)\gamma^\mu\psi(x) = (c\rho(x), \vec{J}(x))\,, \tag{6}$$

where $\rho(x)$ is the charge density and $\vec{J}(x)$ the electrical current density, and it is easily shown that $F_{\mu\nu}(x)F^{\mu\nu}(x) = -2[\vec{E}^2(x)/c^2 - \vec{B}^2(x)]$.

[2]Note that in textbooks of QED often the Gaussian system (or the Heaviside - Lorentz system) of units is used which is more suitable for microscopic, relativistic problems. A detailed discussion of this topic can be found in J. D. Jackson, Classical Electrodynamics, Second Edition, Wiley, New York 1974, p. 811 ff: Appendix on Units and Dimensions.

With the QED Lagrangian density (5) the action $S = \int d^4x \mathcal{L}(x)$ can be introduced. The equations of motion for the fields $\psi(x), \bar{\psi}(x), A^\mu(x)$ are obtained from the condition of extremal action. By variation with respect to $\bar{\psi}(x)$, the Dirac equation

$$i\hbar c\gamma^\mu \partial_\mu \psi(x) - ec\gamma^\mu A_\mu(x)\psi(x) - mc^2\psi(x) = 0 \tag{7}$$

follows, and its adjoint by variation with respect to $\psi(x)$. The Maxwell equations

$$\nabla \cdot \vec{E}(x) = \frac{\rho(x)}{\epsilon_0}, \qquad \nabla \times \vec{B}(x) - \frac{1}{c^2}\frac{\partial}{\partial t}\vec{E}(x) = \frac{\vec{J}(x)}{\epsilon_0 c^2}\ , \tag{8}$$

are found by variation with respect to $A^\mu(x)$, whereas the remaining Maxwell equations

$$\nabla \cdot \vec{B}(x) = 0, \qquad \nabla \times \vec{E}(x) + \frac{\partial}{\partial t}\vec{B}(x) = 0 \tag{9}$$

follow directly from the definition of the electromagnetic fields in terms of the 4-vector potential (4). We also find from Eqs. (8) the continuity equation for the charge density,

$$\partial_\mu j^\mu = \frac{\partial \rho(x)}{\partial t} + \nabla \cdot \vec{J}(x) = 0\,. \tag{10}$$

With respect to the application to the many-particle system considered in the following we discuss briefly three issues concerning the Lagrangian density (5).

i) The Lagrangian density $\mathcal{L}(x)$ is Lorentz invariant. However, for some technical purposes it is more convenient to break Lorentz invariance and to select a special frame of reference, in particular in order to introduce a Hamiltonian, perform canonical quantization, introduce a density operator, or describe initial correlations within the considerd system. It is possible to take an arbitrary frame of reference, the velocity of which is the so-called boost vector. Final results can then be given in a covariant form of all physical relations, not explicitly depending on the boost vector. For further details see the hyper-plane formalism developed by Fleming [22] and later by Morozov *et al.* [23, 24, 25].

ii) The Lagrangian density $\mathcal{L}(x)$ is gauge invariant. The equations of motion (7), (8) remain unchanged if $A^\mu(x)$ is replaced by $A^\mu(x) + \partial^\mu f(x)$ and the local phase of the Dirac field is changed multiplying $\psi(x)$ by $\exp(ief(x)/\hbar c)$, with $f(x)$ denoting an arbitrary scalar function. We will fix the gauge using the Coulomb gauge $\nabla \cdot \vec{A}(x) = 0$. This condition can only be given in a specific frame of reference and therefore breaks the Lorentz invariance[3]. With Eqs. (4), (8) follows the Poisson equation $\Delta U(x) = -\rho(x)/\epsilon_0$. No time derivatives appear in this relation which plays the role of a constraint.

iii) Another important issue is the decomposition of the field into internal and external fields, $A^\mu(x) = A^\mu{}_{\rm int}(x) + A^\mu{}_{\rm ext}(x)$. The sources of the internal field are considered to be the

[3]There are alternative gauges such as the manifestly covariant Lorentz (Feynman) gauge $\partial_\mu A^\mu(x) = 0$ leading to separate wave equations for the vector potential and the scalar potential, or the axial gauge $A^3(x) = 0$. However, they give rise to problems in the interpretation if applied within the context considered here and will not be discussed any further, see, e.g., Itzykson and Zuber [18].

charged particles belonging to the system under consideration, described by the dynamical degrees of freedom. On the other hand, the sources of the external fields are prescribed distributions of charge and current densities in space and time, which are assumed not to be influenced by the dynamical evolution of the system so that no feedback is considered[4]. In this work we will investigate the response of the system to such external fields.

Instead of using the condition of extremal actions, the equations of motion for the charged particles and fields can also be found via the canonical formalism. Within this approach, a Hamiltonian is derived which allows to find a non-relativistic limit. Since the Hamiltonian is fundamental in the standard approach to many-particle systems, we will briefly outline this.

We fix a system of reference and consider the fields $\psi(\vec{r},t), \bar{\psi}(\vec{r},t), U(\vec{r},t), \vec{A}(\vec{r},t)$ as generalized coordinates $Q_i(\vec{r},t)$. The corresponding generalized momenta are derived from the Lagrangian $L = \int d^3r \mathcal{L}(x)$ via $P_i(\vec{r},t) = \delta L/\delta \dot{Q}_i(\vec{r},t)$. Only the time derivatives of $\psi(\vec{r},t)$ and $\vec{A}(\vec{r},t)$ occur in the Lagrangian, equation (5), and we find

$$P_\psi(\vec{r},t) = i\hbar\bar{\psi}(\vec{r},t)\gamma^0 = i\hbar\psi^\dagger(\vec{r},t), \qquad \vec{P}_{\vec{A}}(\vec{r},t) = \epsilon_0\left(\nabla U(\vec{r},t) + \frac{\partial}{\partial t}\vec{A}(\vec{r},t)\right) = -\epsilon_0\vec{E}(\vec{r},t)\ . \tag{11}$$

For the remaining fields $\bar{\psi}(\vec{r},t), U(\vec{r},t)$ no canonical momenta can be defined as a dynamical variable. The Hamiltonian reads

$$H = \int d^3r[i\hbar\bar{\psi}\gamma^0\frac{\partial\psi}{\partial t} + \epsilon_0(\nabla U + \frac{\partial}{\partial t}\vec{A})\cdot\frac{\partial}{\partial t}\vec{A}] - L \tag{12}$$

$$= \int d^3r\left[\bar{\psi}(-i\hbar c\vec{\gamma}\cdot\nabla - ec\vec{\gamma}\cdot\vec{A} + mc^2)\psi + \frac{\epsilon_0 c^2}{2}(\nabla\times\vec{A})^2 - \frac{1}{2\epsilon_0}\vec{P}^2_{\vec{A}} + eU\bar{\psi}\gamma^0\psi + \vec{P}_{\vec{A}}\cdot\frac{\partial}{\partial t}\vec{A}\right]$$

$$= \int d^3r\left[P_\psi\gamma^0\left(-c\vec{\gamma}\cdot\nabla - \frac{ec}{i\hbar}\vec{\gamma}\cdot\vec{A} + \frac{mc^2}{i\hbar}\right)\psi + \frac{\epsilon_0 c^2}{2}(\nabla\times\vec{A})^2 + \frac{1}{2\epsilon_0}\vec{P}^2_{\vec{A}}\right]\ . \tag{13}$$

Using equation (11), the field $\bar{\psi}(\vec{r},t)$ has been eliminated, and there is no explicit dependence on the scalar field $U(\vec{r},t)$ in (13). It results in $\vec{P}_{\vec{A}}\cdot\frac{\partial}{\partial t}\vec{A} = \vec{P}^2_{\vec{A}}/\epsilon_0 - \vec{P}_{\vec{A}}\cdot\nabla U$ and partial integration of the last term into $U\nabla\cdot\vec{P}_{\vec{A}}$, if one applies the constraint $e\bar{\psi}\gamma^0\psi + \nabla\cdot\vec{P}_{\vec{A}} = \rho - \epsilon_0\nabla\cdot\vec{E} = 0$. This is one of Maxwell's equations, the Gauss law, which is not related to time evolution, but gives a constraint on the field $\vec{E}$. If this constraint holds at a certain initial time, it is easily shown that it holds for any time because of charge conservation (10). The other Maxwell equation $\nabla\cdot\vec{B} = 0$ that is not related to time evolution, follows from the definition $\vec{B} = \nabla\times\vec{A}$.

[4]In general we are considering open systems defined by the volume Ω. 'External' fields are not only fields, caused by charges and currents inside (e.g. the field of atomic nuclei in adiabatic approximation) and outside Ω which are not considered as dynamical variables, but also currents of particles and photons entering the volume under consideration.

The remaining Maxwell equations follow as equations of motion within the canonical formalism according to $\partial Q_i/\partial t = \delta H/\delta P_i$ and $\partial P_i/\partial t = -\delta H/\delta Q_i$. Considering the vector potential $\vec{A}(\vec{r},t)$, we find a relationship for $\partial\vec{A}(\vec{r},t)/\partial t$ which is identical with the definition of the canonical momentum $\vec{P}_{\vec{A}}(\vec{r},t)$ as given above in (11). Applying the operator $\nabla\times$ and substituting the definition of the vector potential $\vec{A}(\vec{r},t)$, Eq.(4), the Maxwell equation (9) $\partial\vec{B}/\partial t = -\nabla\times\vec{E}$ is obtained. The second canonical equation

$$\frac{\partial\vec{P}_{\vec{A}}}{\partial t} = -\epsilon_0 c^2\nabla\times[\nabla\times\vec{A}] + ec\bar{\psi}\vec{\gamma}\psi \tag{14}$$

yields the Maxwell equation (8) $\partial\vec{E}/\partial t = c^2\nabla\times\vec{B} - \vec{J}/\epsilon_0$ where $\vec{J}$ is substituted from (6). Considering the Dirac field $\psi(\vec{r},t)$, the Dirac equation (7) and its hermitian adjoint is obtained. Therefore, we identified the dynamical variables Q_i to be only $\psi(\vec{r},t), \vec{A}(\vec{r},t)$ and the corresponding momenta as given in Eqs. (11).

Note, that due to the Coulomb gauge the field $\vec{A}(\vec{r},t)$ is transverse so that only the transverse part of $\vec{P}_{\vec{A}}$ can be considered as a canonical conjugate momentum. The longitudinal part has to be eliminated. For this, the generalized momentum $\vec{P}_{\vec{A}} = \vec{P}_{\rm transv} + \vec{P}_{\rm long}$ or the corresponding electric field $\vec{E}$ should be decomposed into a solenoidal ($\nabla\cdot\vec{P}_{\rm transv} = 0$) and an irrotational ($\nabla\times\vec{P}_{\rm long} = 0$) part. Using the Coulomb gauge $\nabla\cdot\vec{A} = 0$ the transverse part is easily identified as $\vec{P}_{\rm transv} = \partial\vec{A}/\partial t$. The longitudinal part $\epsilon_0\vec{P}_{\rm long} = \nabla U$ can be directly related to the Coulomb interactions and decouples from the vector potential. We now write the Hamiltonian

$$H = \int d^3r\left[\bar{\psi}\left(-i\hbar c\vec{\gamma}\cdot\nabla - ec\vec{\gamma}\cdot\vec{A} + mc^2\right)\psi + \frac{\epsilon_0 c^2}{2}(\nabla\times\vec{A})^2 + \frac{\epsilon_0}{2}\vec{E}^2_{\rm transv} + \frac{1}{2}\rho U\right]. \tag{15}$$

In the last term, the scalar potential can also be expressed through the charge density $\rho(\vec{r},t) = e\psi^\dagger(\vec{r},t)\psi(\vec{r},t)$ via the Poisson equation given above[5]

$$\nabla^2 U(\vec{r},t) = -\frac{\rho(\vec{r},t)}{\epsilon_0}, \qquad U(\vec{r},t) = \int d^3\vec{r}\,'\frac{\rho(\vec{r}\,',t)}{4\pi\epsilon_0|\vec{r}-\vec{r}\,'|}\,. \tag{16}$$

The charge density is eliminated from the Hamiltonian replacing it by the ψ field according to Eq. (6). The canonical quantization can be performed by defining the respective anti-commutation or commutation relations with respect to $\vec{A}$ and ψ fields, which will not be detailed here any further.

[5]The Coulomb interaction looks formally like an instantaneous interaction at a distance. However, the charge densities change with time as described by the dynamics of the system. An explicit presentation of the interaction with other charges situated on the past light cone can be formulated in other gauges. In particular, in the Lorentz gauge the propagators of the electromagnetic field are introduced, and the quantization is given in terms of the corresponding Green's functions, see Itzykson and Zuber [18].

1.3 Nonrelativistic Limit: Hamiltonian

Undoubtedly a fundamental treatment of plasmas and radiation should be formulated within a many-particle QED. The nonequilibrium quantum statistical mechanics for such systems has been put forward by different authors, see, e.g. Morozov *et al.* [23, 24], DuBois *et al.* [26, 27] and Bechler [28]. The elaboration of a consequent relativistic theory of plasmas and radiation is an important issue for future work, in particular with respect to recent developments in laser and accelerator facilities. However, the relativistic treatment of correlations in charged fermion system is quite complex. Also, the non-relativistic limit is possible in many applications. Therefore, it is worthwile to elaborate this approximation as it is the aim of the present work.

In order to obtain the nonrelativistic limit for a plasma interacting with radiation, the 4-component Dirac spinor

$$\psi(x) = \begin{pmatrix} \phi_\uparrow(x) \\ \phi_\downarrow(x) \\ \chi_\uparrow(x) \\ \chi_\downarrow(x) \end{pmatrix} e^{-\frac{i}{\hbar}mc^2 t} \tag{17}$$

is decomposed into the fields of particle $\phi_c(x)$ and antiparticle $\chi_c(x)$[6]. Assuming that the absolute values of $i\hbar(\partial\chi/\partial t)/mc^2\chi$ and eU/mc^2 are small compared with 1, the Dirac equation (7) can be expanded with respect to these quantities, and after some algebra with Pauli matrices $\vec{\sigma}$ the Pauli equation is obtained, see e.g. Itzykson [18], Röpke and Hitzschke [29], Mahan [30], or Schiff [31]. Neglecting the contribution of the antiparticle fields χ, the corresponding Hamiltonian (15) reads in the non–relativistic case[7]

$$\begin{aligned} H = &\sum_c \int \mathrm{d}^3\vec{r}\, \phi_c^\dagger(\vec{r},t) \left[\frac{1}{2m_c} \left(\frac{\hbar}{i}\vec{\nabla} - e_c\vec{A}(\vec{r},t) \right)^2 - \frac{\hbar e_c}{2m_c}\vec{\sigma}\cdot(\nabla\times\vec{A}(\vec{r},t)) \right] \phi_c(\vec{r},t) \\ &+ \int \mathrm{d}^3\vec{r} \left[\frac{1}{2\epsilon_0}\vec{P}^2_{\mathrm{transv}}(\vec{r},t) + \frac{\epsilon_0 c^2}{2}(\nabla\times\vec{A}(\vec{r},t))^2 \right] \\ &+ \frac{1}{2}\sum_{c,d} \int \mathrm{d}^3\vec{r} \int \mathrm{d}^3\vec{r}\,' \phi_c^\dagger(\vec{r},t)\phi_d^\dagger(\vec{r}\,',t) \frac{e_c e_d}{4\pi\epsilon_0\,|\vec{r}-\vec{r}\,'|} \phi_d(\vec{r}\,',t)\phi_c(\vec{r},t)\,. \end{aligned} \tag{18}$$

Here, the indices c, d denote not only spin, but also the species (electron, proton) if a multicomponent plasma is considered. We will ignore the interaction between spin ($\vec{\sigma}$) and magnetic field $\vec{B} = \nabla\times\vec{A}$ so that the corresponding term is omitted, the spin occurs only

[6]The notation reminds of the fact that for an electron at rest the spinors describe eigenstates of σ^3 with eigenvalue +1 (spin "up") and -1 (spin "down"). For nonvanishing momentum $\vec{p}$ they are eigenstates of the helicity operator $\vec{\sigma}\cdot\vec{p}/|\vec{p}|$

[7]Relativistic corrections to the Pauli hamiltonian (18) can be derived considering higher orders in m_c^{-1} (see Itzykson [18], p. 71), in particular the spin–orbit coupling and the so–called Darwin term, which may be traced to the fluctuations of the electron's position (zitterbewegung) on a scale of the order of its Compton wavelength.

in the index c. The second line is the well known contribution of the field energy which can also be given in the familiar form $\epsilon_0[E^2_{\rm transv}(\vec{r},t)+c^2B^2(\vec{r},t)]/2$. The third line describes the Coulomb interaction between the particles and can be expressed in terms of a scalar potential $U(\vec{r},t)$, see Eqs. (15), (16) or the charge density (6)

$$\rho(\vec{r},t)=\sum_c e_c\phi_c^\dagger(\vec{r},t)\phi_c(\vec{r},t). \tag{19}$$

The time dependence of the fields follows from the Hamiltonian equations for the generalized coordinates $\phi_c(\vec{r},t)$, $\vec{A}(\vec{r},t)$ and the generalized momenta $P_{\phi,c}(\vec{r},t)=i\hbar\phi_c^\dagger(\vec{r},t)$ and $\vec{P}_{\rm transv}(\vec{r},t)$. In particular, for the charge density we find (10)

$$\frac{\partial\rho(\vec{r},t)}{\partial t}=\sum_c e_c\left\{\left[\frac{\partial}{\partial t}\phi_c^\dagger(\vec{r},t)\right]\phi_c(\vec{r},t)+\phi_c^\dagger(\vec{r},t)\left[\frac{\partial}{\partial t}\phi_c(\vec{r},t)\right]\right\}=-\nabla\cdot\vec{J}(\vec{r},t)\,, \tag{20}$$

with the electrical current density

$$\vec{J}(\vec{r},t)=\sum_c\frac{e_c}{2m_c}\left\{\phi_c^\dagger(\vec{r},t)\left[\frac{\hbar}{i}\nabla\phi_c(\vec{r},t)\right]-\left[\frac{\hbar}{i}\nabla\phi_c^\dagger(\vec{r},t)\right]\phi_c(\vec{r},t)-2e_c\phi_c^\dagger(\vec{r},t)\vec{A}(\vec{r},t)\phi_c(\vec{r},t)\right\}. \tag{21}$$

In a quantum field theory, the fields are replaced by operators, and the generalized coordinates and the generalized momenta obey equal time anti-commutation relation in the case of fermions, and commutation relations in the case of bosons[8]. The time dependence of operators is due to the Heisenberg picture, e.g. for an operator $O(t)$ holds

$$i\hbar\frac{\partial}{\partial t}O(t)=[O(t),H]+i\hbar\frac{\partial O(t)}{\partial t}\bigg|_{\rm expl}\,, \tag{22}$$

where the last contribution concerns only the explicit time dependence, such as an external, time dependent potential[9]. For an explicitly time independent operator, the time evolution can be given as

$$O(t)=\mathrm{e}^{-iH/\hbar}\,O\,\mathrm{e}^{iH/\hbar}\,. \tag{24}$$

[8]The corresponding expressions [18] $\{\phi_c(\vec{r},t),P_{\phi,c'}(\vec{r}\,',t)\}_+=i\hbar\delta_{cc'}\delta^3(\vec{r}-\vec{r}\,')$, $[A_i(\vec{r},t),\vec{P}_{\rm transv,j}(\vec{r}\,',t)]_-=i\hbar[\delta_{ij}\delta^3(\vec{r}-\vec{r}\,')-\nabla_i\nabla_j(4\pi|\vec{r}-\vec{r}\,'|)^{-1}]$ become more simple in the Fourier representation given below.

[9]Sometimes a twofold dependence on time is introduced, $O^t(t)$, to discriminate between the different time dependences, the parametric, explicit one given as upper index, and the dynamical one according to the Heisenberg picture. – Using the commutator relations, the time dependence according to the Heisenberg picture leads to the same expressions (20), (21) for the electrical current density given above. In particular, we find for the particle velocity

$$\vec{v}_c=\dot{\vec{r}}_c=\frac{1}{m_c}(\hbar\vec{p}-e_c\vec{A}(\vec{r})). \tag{23}$$

The electrical current density (21) which is the experimentally measured current density is determined by the velocity of the charged particles.

A macroscopic description is obtained if we consider averaged quantities, calculated as trace with the statistical operator $\varrho(t)$. In the Schrödinger picture, the time dependence of any linear operator O is given as $\langle O\rangle^t = \mathrm{Tr}[\varrho(t)O]$.

The evaluation of physical properties of systems described by the Hamiltonian (18) is the subject of many-particle theory. The methods of quantum statistics have been applied to investigate systems in equilibrium and non-equilibrium, see comprehensive textbooks such as Kremp *et al.* [11], Mahan [30], Kadanoff and Baym [32], Fetter and Walecka [33], or Zubarev *et al.* [34, 35]. In particular, we are interested in the response properties with respect to external perturbations and follow the notations of Zubarev *et al.* [34, 35].

To find a more compact description of the many-particle system, creation and annihilation operators are introduced. For homogeneous systems it is advantageous to consider the Fourier transform $\tilde{f}(\vec{k})$ of the function $f(\vec{r})$ according to

$$\tilde{f}(\vec{k}) = \int_\Omega d^3\vec{r} e^{-i\vec{k}\cdot\vec{r}} f(\vec{r}) \,, \qquad f(\vec{r}) = \frac{1}{\Omega}\sum_{\vec{k}} e^{i\vec{k}\cdot\vec{r}} \tilde{f}(\vec{k}) \,. \tag{25}$$

Similarly, the time Fourier transform is defined as

$$\tilde{f}(\omega) = \int_{-\infty}^{\infty} dt e^{i\omega t} f(t) \,, \qquad f(t) = \frac{1}{2\pi}\int_{-\infty}^{\infty} d\omega e^{-i\omega t} \tilde{f}(\omega) \,. \tag{26}$$

To preserve normalization, the particle fields are transformed as (time dependence is due to the Heisenberg picture and will not be given explicitly)

$$\phi_c(\vec{r}) = \frac{1}{\sqrt{\Omega}}\sum_p e^{i\vec{p}\cdot\vec{r}} a_{c,p} \,, \qquad \phi_c^\dagger(\vec{r}) = \frac{1}{\sqrt{\Omega}}\sum_p e^{-i\vec{p}\cdot\vec{r}} a_{c,p}^\dagger \,. \tag{27}$$

The anti-commutation relations now read

$$\{a_{c,p}, a_{c',p'}^\dagger\}_+ = \delta_{cc'}\delta_{pp'} \,, \qquad \{a_{c,p}, a_{c',p'}\}_+ = \{a_{c,p}^\dagger, a_{c',p'}^\dagger\}_+ = 0. \tag{28}$$

With the short notation $\vec{A}_k = \tilde{\vec{A}}(\vec{k})$ and correspondingly $\tilde{\vec{P}}_{\mathrm{transv}}(\vec{k}) = \vec{P}_{\mathrm{trans,k}}$ (note that $\vec{A}_k^\dagger = \vec{A}_{-k}$ so that $\vec{A}(\vec{r})$ is a real field) we find in canonical variables, cf. Eq. (11),

$$\begin{aligned} H = \quad & \sum_{c,p} E_c(\vec{p}) a_{c,p}^\dagger a_{c,p} + \frac{1}{\Omega}\sum_k \left[\frac{1}{2\epsilon_0}\vec{P}_{\mathrm{transv},k}\cdot\vec{P}_{\mathrm{transv},-k} + \frac{\epsilon_0 c^2}{2}k^2 \vec{A}_k\cdot\vec{A}_{-k}\right] \\ & -\frac{1}{\Omega}\sum_{c,pk}\frac{e_c}{m_c} a_{c,p-k/2}^\dagger a_{c,p+k/2}\hbar\vec{p}\cdot\vec{A}_{-k} + \frac{1}{\Omega^2}\sum_{c,pkk'}\frac{e_c^2}{2m_c} a_{c,p-k'/2}^\dagger a_{c,p+k'/2}\vec{A}_k\cdot\vec{A}_{-k-k'} \\ & +\frac{1}{2}\sum_{cd,pp'k} V_{cd}(k) a_{c,p-k}^\dagger a_{d,p'+k}^\dagger a_{d,p'} a_{c,p} \end{aligned} \tag{29}$$

with $E_c(p) = \hbar^2 p^2/2m_c$ and $V_{cd}(k) = e_c e_d/(\epsilon_0\Omega k^2)$. Besides the free particles and the free radiation fields, this Hamiltonian contains the coupling of the current density to the vector potential as well as the Coulomb interaction between the charge densities.

Introducing the Wigner transform of the single-particle occupation operator[10] [11]

$$n^c_{p,k} = a^\dagger_{c,p-k/2} a_{c,p+k/2} \tag{35}$$

the Fourier transforms of the charge density $\rho(\vec{r})$, Eq. (19), and the electrical current density $\vec{J}(\vec{r})$, Eq. (21), can be represented as

$$\tilde{\rho}(\vec{k}) = \sum_{c,p} e_c n^c_{p,k} \;, \qquad \tilde{\vec{J}}(\vec{k}) = \sum_{c,p} \frac{e_c}{m_c} \hbar \vec{p}\, n^c_{p,k} - \frac{1}{\Omega} \sum_{c,pk'} \frac{e_c^2}{m_c} n^c_{p,k'} \vec{A}_{k-k'} \;, \tag{36}$$

respectively. Here, $\tilde{\rho}(0)/\Omega$ has the meaning of the spacially averaged charge density, and $\tilde{\vec{J}}(0)/\Omega$ the spacially averaged current density.

In the Fourier representation of the Hamiltonian, Eq. (29), the fifth contribution is simplified if no density gradients are considered so that the components with $k' \neq 0$ can be neglected. Introducing the plasma frequency

$$\omega_{\rm pl}^2 = \frac{1}{\Omega} \sum_{c,p} \frac{e_c^2}{\epsilon_0 m_c} n^c_{p,0} \,, \tag{37}$$

---

[10] Related to the density operator in coordinate space by $\Omega^{-1} \int d^3\vec{r} e^{-i\vec{k}\cdot\vec{r}} \int d^3\vec{x} e^{-i\vec{p}\cdot\vec{x}} \phi_c^\dagger(\vec{r}-\vec{x}/2)\phi_c(\vec{r}+\vec{x}/2)$.

[11] As for the particle fields, we could introduce photon creation and annihilation operators according to ($\vec{\epsilon}_{k\lambda}$ denotes the direction of two polarizations orthogonal to $\vec{k}$)

$$\vec{A}_k = \sum_\lambda \vec{\epsilon}_{k\lambda} \left(\frac{\hbar\Omega}{2\epsilon_0\omega_k} \right)^{1/2} (a^\dagger_{k\lambda} + a_{-k\lambda}) \,, \tag{30}$$

$$\vec{P}_{{\rm transv},k} = i \sum_\lambda \vec{\epsilon}_{k\lambda} \left(\frac{\hbar\Omega\epsilon_0\omega_k}{2} \right)^{1/2} (a^\dagger_{k\lambda} - a_{-k\lambda}) \,, \tag{31}$$

with commutator relations

$$[a_{-k\lambda}, a^\dagger_{k'\lambda'}]_- = \delta_{\lambda\lambda'}\delta_{kk'} \;, \qquad [a_{-k\lambda}, a_{k'\lambda'}]_- = [a^\dagger_{-k\lambda}), a^\dagger_{k'\lambda'}]_- = 0 \,. \tag{32}$$

The contribution to the photon field (no vacuum contribution) reads

$$H_{\rm field} = \sum_{k\lambda} \hbar\omega_k a^\dagger_{k\lambda} a_{-k\lambda} \,. \tag{33}$$

Standard perturbation theory can be applied, starting with the Hamiltonian

$$\begin{aligned} H = & \sum_{c,p} E_c(\vec{p}) a^\dagger_{c,p} a_{c,p} + \sum_{k\lambda} \hbar\omega_k a^\dagger_{k\lambda} a_{-k\lambda} \\ & - \sum_{k\lambda} \vec{j}_k \cdot \vec{\epsilon}_{k\lambda} \left(\frac{\hbar\Omega}{2\epsilon_0\omega_k} \right)^{1/2} (a^\dagger_{-k\lambda} + a_{k\lambda}) + \frac{1}{2} \sum_{cd,pp'k} V_{cd}(k) a^\dagger_{c,p-k} a^\dagger_{d,p'+k} a_{d,p'} a_{c,p} \,. \end{aligned} \tag{34}$$

This expression which is quite similar to the electron–phonon Hamiltonian serves as a basis for perturbation expansions or Green's function approaches. In the present work we mainly treat the Coulomb interaction so that the propagation of photon modes in the plasma will not be elaborated in detail.

this so–called condensate term can be merged into the term $\epsilon_0 c^2 k^2 \vec{A}_k \cdot \vec{A}_{-k}/2$ so that the dispersion relation $\omega_k^2 = \omega_{\rm pl}^2 + c^2 k^2$ results. Furthermore, using this approximation, $\tilde{\vec{J}}(\vec{k}) \approx \Omega \vec{j}_k - \epsilon_0 \omega_{\rm pl}^2 \vec{A}_k$ follows for the electrical current with

$$\vec{j}_k = \frac{1}{\Omega} \sum_{c,p} \frac{e_c}{m_c} \hbar \, \vec{p} \, n_{p,k}^c \, . \tag{38}$$

The electrical current $\tilde{\vec{J}}(\vec{k}) = \tilde{\vec{J}}_{\rm long}(\vec{k}) + \tilde{\vec{J}}_{\rm transv}(\vec{k})$ can be decomposed into a longitudinal component with $\vec{k} \times \tilde{\vec{J}}_{\rm long}(\vec{k}) = 0$ and a transverse one with $\vec{k} \cdot \tilde{\vec{J}}_{\rm transv}(\vec{k}) = 0$. Note that $\vec{A}_k$ is transverse and couples only to the transverse component of $\tilde{\vec{J}}(\vec{k})$. We consider the time evolution according to the Heisenberg picture and perform the Fourier transform of the averages, Eq. (26), so that $\tilde{O}(\vec{k}, \omega) = \int dt e^{i\omega t} \langle O \rangle^t$. The longitudinal part of the electrical current $\tilde{\vec{J}}_{\rm long}(\vec{k}, \omega) = \tilde{J}_{\rm long}(\vec{k}, \omega) \vec{k}/k$ is related to the charge density according to the conservation of charge (10),

$$-i\omega \tilde{\rho}(\vec{k}, \omega) + ik \, \tilde{J}_{\rm long}(\vec{k}, \omega) = 0 \, , \tag{39}$$

and contains no independent information.

Similarly, the equation of motions for the radiation fields from (22) will lead to the Maxwell equation, as does the application of the canonical formalism,

$$\begin{aligned} \dot{\vec{A}}_k &= \frac{1}{\epsilon_0} \vec{P}_{{\rm transv},k} = -\tilde{\vec{E}}_{\rm transv}(\vec{k}) \, , \\ \dot{\vec{P}}_{{\rm transv},k} &= \tilde{\vec{J}}_{\rm transv}(\vec{k}) - \epsilon_0 c^2 k^2 \vec{A}_k \, , \end{aligned} \tag{40}$$

or, for the Fourier transform of the averages,

$$\begin{aligned} -i\omega \vec{A}_k(\omega) &= \frac{1}{\epsilon_0} \vec{P}_{{\rm transv},k}(\omega) = -\tilde{\vec{E}}_{\rm transv}(\vec{k}, \omega) \, , \\ -i\omega \vec{P}_{{\rm transv},k}(\omega) &= -\epsilon_0 \omega^2 \vec{A}_k(\omega) = \tilde{\vec{J}}_{\rm transv}(\vec{k}, \omega) - \epsilon_0 c^2 k^2 \vec{A}_k(\omega) \, . \end{aligned} \tag{41}$$

We obtain an equation which gives the average vector potential in terms of the transverse current[12],

$$\vec{A}_k(\omega) = \frac{1}{\epsilon_0 (c^2 k^2 - \omega^2)} \tilde{\vec{J}}_{\rm transv}(\vec{k}, \omega) \, . \tag{42}$$

Together with

$$\tilde{U}(\vec{k}, \omega) = U_k(\omega) = \frac{\tilde{\rho}(\vec{k}, \omega)}{\epsilon_0 k^2} = \frac{\tilde{J}_{\rm long}(\vec{k}, \omega)}{\epsilon_0 \omega k} \tag{43}$$

according to Eq. (16), the potentials are algebraically related to the sources.

[12]The decomposition into a longitudinal and a transverse current, given by $\tilde{J}_{{\rm transv},i}(\vec{k}, \omega) = \sum_j (\delta_{ij} - k_i k_j / k^2) \tilde{J}_j(\vec{k}, \omega)$, is simplified if the direction of the wave vector $\vec{k}$ coincides with, e.g., the z axis. Then, the commutator relations have the simple form $[A_{k,x}, P_{k',x}] = i\hbar \delta_{kk'}$.

1.4 Response to External Perturbations

Now we go on to open systems, *i.e.* systems under external influences. In particular, the charge density as well as the electrical current density will be decomposed into an external part and a part induced within the system. The external sources are externally controlled, and we assume that the feedback of the system back to these sources can be neglected so that we represent the effects of these sources by the c-number charge density $\rho^{\rm ext}(\vec{r},t)$ and electrical current density $\vec{J}^{\rm ext}(\vec{r},t)$, see DuBois [27].

Within a macroscopic description where in the Schrödinger picture the time dependence of any linear operator O is given as $\langle O\rangle^t = {\rm Tr}[\varrho(t)O]$, we define

$$\begin{aligned}\langle\tilde{\rho}^{\rm tot}(\vec{k})\rangle^t &= \tilde{\rho}^{\rm ext}(\vec{k},t) + \langle\tilde{\rho}(\vec{k})\rangle^t,\\ \langle\tilde{\vec{J}}^{\rm tot}(\vec{k})\rangle^t &= \tilde{\vec{J}}^{\rm ext}(\vec{k},t) + \langle\tilde{\vec{J}}(\vec{k})\rangle^t,\end{aligned} \tag{44}$$

reflecting the different origins of the sources. Formally, out of the sum over the components one component $c = {\rm ext}$ can be considered as causing the external perturbation.

In the same way, the decomposition of the vector and scalar potentials into an external and an induced contribution has been discussed before. The external part is a classical quantity, described in space and time and not influenced by the dynamical evolution of the system. In contrast, the induced part has to be considered as an operator, related to the dynamical degrees of freedom of the system.

We can introduce new fields $\vec{D}(\vec{r},t), \vec{H}(\vec{r},t)$ which are determined by the external contributions of charge and current densities in a similar fashion as the total fields (8). In Fourier representation these relations read

$$\begin{aligned}i\vec{k}\cdot\tilde{\vec{D}}(\vec{k},\omega) &= \tilde{\rho}^{\rm ext}(\vec{k},\omega),\\ i\vec{k}\times\tilde{\vec{H}}(\vec{k},\omega) &= i\omega\tilde{\vec{D}}(\vec{k},\omega) + \tilde{\vec{J}}^{\rm ext}(\vec{k},\omega)\,.\end{aligned} \tag{45}$$

We define the following relationships between the new fields and the averaged fields[13]

$$\begin{aligned}\tilde{\vec{D}}(\vec{k},\omega) &= \epsilon_0\hat{\epsilon}(\vec{k},\omega)\tilde{\vec{E}}(\vec{k},\omega)\\ \tilde{\vec{B}}(\vec{k},\omega) &= \frac{1}{\epsilon_0 c^2}\tilde{\vec{H}}(\vec{k},\omega)\,.\end{aligned} \tag{46}$$

A linear relation defining the tensors of the dielectric function $\hat{\epsilon}(\vec{k},\omega)$ is supported by empirical experience if confined to not too large fields. Otherwise nonlinear contributions exist which are not considered here. For isotropic systems, the dielectric tensor can be decomposed

[13]We consider systems which are homogeneous in space and time. Then, in co-ordinate space the linear relation between external and induced charge and current densities depends only on the difference in position and time, having the form of a convolution. In Fourier representation an algebraic relation results which is diagonal in $\vec{k}$ and ω.

into a longitudinal and a transverse part[14]

$$\epsilon_{ij}(\vec{k},\omega) \;=\; \epsilon_{\rm long}(\vec{k},\omega)\frac{k_i k_j}{k^2} + \epsilon_{\rm transv}(\vec{k},\omega)\left(\delta_{ij} - \frac{k_i k_j}{k^2}\right) \;=\; \begin{pmatrix} \epsilon^{\rm T} & 0 & 0 \\ 0 & \epsilon^{\rm T} & 0 \\ 0 & 0 & \epsilon^{\rm L} \end{pmatrix}. \qquad (49)$$

where the matrix representation is valid assuming $\vec{k} = k\vec{e}_z$. In particular, we have from (45) and (46)

$$i\vec{k}\cdot\tilde{\vec{D}}(\vec{k},\omega) \;=\; i\epsilon_0\epsilon_{\rm long}(\vec{k},\omega)\vec{k}\cdot\tilde{\vec{E}}(\vec{k},\omega) = \tilde{\rho}^{\rm ext}(\vec{k},\omega), \qquad (50)$$

$$i\epsilon_0 c^2\vec{k}\times\tilde{\vec{B}}(\vec{k},\omega) \;=\; i\omega\epsilon_0\epsilon_{\rm transv}\tilde{\vec{E}}_{\rm transv}(\vec{k},\omega) + \tilde{\vec{J}}^{\rm ext}_{\rm transv}(\vec{k},\omega). \qquad (51)$$

From the Maxwell equation (8) and Eq. (50) follows a relationship between the averaged charge density and the external charge density

$$\tilde{\rho}^{\rm ext}(\vec{k},\omega) = \epsilon_{\rm long}(\vec{k},\omega)\tilde{\rho}^{\rm tot}(\vec{k},\omega) \qquad (52)$$

so that with (44) and under consideration of the continuity equation (20) follows

$$\epsilon_{\rm long}(\vec{k},\omega) = 1 - \frac{\tilde{\rho}(\vec{k},\omega)}{\tilde{\rho}^{\rm tot}(\vec{k},\omega)} = 1 - \frac{\tilde{J}_{\rm long}(\vec{k},\omega)}{\tilde{J}^{\rm tot}_{\rm long}(\vec{k},\omega)}\,. \qquad (53)$$

With respect to the transverse part, similar relations are obtained. Eq. (51) can be rewritten as

$$\epsilon_0 c^2 k^2 \vec{A}_k(\omega) = \omega^2\epsilon_0\epsilon_{\rm transv}(\vec{k},\omega)\vec{A}_k(\omega) + \tilde{\vec{J}}^{\rm ext}_{\rm transv}(\vec{k},\omega) \qquad (54)$$

if using the Fourier transformed definition of the vector potential (4) and the relation for the transverse electric field (41). With (42) we find for the components in any transverse direction[15]

$$\epsilon_{\rm transv}(\vec{k},\omega) \;=\; 1 - \left(1 - \frac{c^2k^2}{\omega^2}\right)\frac{\tilde{J}_{\rm transv}(\vec{k},\omega)}{\tilde{J}^{\rm tot}_{\rm transv}(\vec{k},\omega)}\,. \qquad (55)$$

[14] Alternatively, a magnetic susceptibility can be introduced according to

$$\tilde{\vec{B}}(\vec{k},\omega) \;=\; \frac{1}{\epsilon_0 c^2}\mu(\vec{k},\omega)\tilde{\vec{H}}(\vec{k},\omega) \qquad (47)$$

and the dielectric tensor is then restricted to a longitudinal component. In this case, the term with $\tilde{\vec{D}}(\vec{k},\omega)$ in the second equation of (45) doesn't exist. There is a relationship between those two definitions

$$1 - \frac{1}{\mu} = \frac{\omega^2}{c^2k^2}(\epsilon_{\rm long} - \epsilon_{\rm transv})\,. \qquad (48)$$

[15] Because of isotropy, no direction in the plane transverse to the longitudinal direction which is set by the vector $\vec{k} = k\vec{e}_z$ can be distinguished. Therefore we represent the transverse vectors by the modulus of the x component

As well known, in the long wavelength limit ($k \to 0$) the longitudinal and transverse dielectric functions are identical, since in this case no direction in space is singled out by the wave vector $\vec{k}$. From Eqs. (53) and (55) it can be seen that also the response to external sources becomes identical.

1.5 Dielectric Function, Optical and Transport Properties

The dielectric function introduced in the previous section is a fundamental quantity, related to various properties of charged particle systems. There are several exact relations for the dielectric function of a homogeneous charged particle system of particle density n which can be shown analytically. We will give a short summary since we refer to them later on. For an extended account see Mahan [30] and Forster [36]. General relations are important in so far as the consistency of any approximation can be tested. Other approaches do use the sum rules explicitely to construct improved approximations, see Gold [37], Adamyan *et al.* [38] and Hong and Lee [39].

As a consequence of the causality of the system's response, the Kramers-Kronig relation gives a relation between the real and the imaginary part of the dielectric function

$$\mathrm{Re}\,\epsilon(\vec{k},\omega) \;=\; 1 \;-\; \mathcal{P}\int_{-\infty}^{\infty} \frac{d\omega'}{\pi}\,\frac{\mathrm{Im}\,\epsilon(\vec{k},\omega'+i0)}{\omega-\omega'}\,, \tag{56}$$

which can in fact be given in a more general way for any other response function. The so-called sum rules, although integrals over frequency, give general relations for certain frequency moments of the dielectric or inverse dielectric function,

$$\int_{-\infty}^{\infty} \frac{d\omega}{\pi}\,\omega^n\,\mathrm{Im}\,\epsilon^{\pm 1}(\vec{k},\omega) \;=\; C_n^{\pm}(\vec{k})\;. \tag{57}$$

The first moment of the inverse dielectric function known as the f-sum rule $C_1^- = -\omega_{\mathrm{pl}}^2$ follows from particle conservation. It gives the sum of oscillator strengths for transitions from the ground state to excited states. The conductivity sum rule $C_1^+ = \omega_{\mathrm{pl}}^2$ integrates over the dissipative part of the longitudinal conductivity $\sigma_{\mathrm{long}}(\vec{k},\omega)$. Amongst the higher moments the third moment sum rule C_3^- is of particular interest. It should converge. However, in RPA as well as for the Drude formula this sum rule diverges as will be discussed in chapter 3. There are also some rigorous limiting cases which should be considered in connection with any approximation. These are the perfect screening

$$\lim_{k\to 0}\int_{-\infty}^{\infty} \frac{d\omega}{\pi}\,\frac{1}{\omega}\,\mathrm{Im}\,\epsilon^{-1}(k,\omega) \;=\; -1 \tag{58}$$

and the compressibility (K) sum rule

$$\lim_{k\to 0}\,\mathrm{Re}\,\epsilon(\vec{k},0) \;=\; 1 \;+\; \frac{n^2e^2}{\epsilon_0 k^2}\,\Omega\,K \tag{59}$$

for the long-wavelength limit as well as the high-frequency behaviour

$$\lim_{\omega\to\infty} \mathrm{Re}\,\epsilon(\vec{k},\omega) \;=\; 1 - \frac{\omega_{\mathrm{pl}}^2}{\omega^2} + O(\omega^{-4})\;. \tag{60}$$

Further properties of a dense plasma can be directly derived from the dielectric function. Some of them will be calculated and analyzed in the course of this review. The non-local dynamical conductivity gives the response of the system to the total electric field and determines the induced electrical current wich can be measured, according to

$$\tilde{\vec{J}}(\vec{k},\omega) = \hat{\sigma}(\vec{k},\omega)\tilde{\vec{E}}(\vec{k},\omega). \tag{61}$$

Using the Gauss law (8) and the continuity equation (10) for the longitudinal and Eqs. (41), (42) for the transverse electric fields and the corresponding electric current densities, we deduct

$$\sigma_{\mathrm{long}} \;=\; i\epsilon_0\omega\frac{\tilde{J}_{\mathrm{long}}(\vec{k},\omega)}{\tilde{J}^{\mathrm{tot}}_{\mathrm{long}}(\vec{k},\omega)}\,, \tag{62}$$

$$\sigma_{\mathrm{transv}} \;=\; i\epsilon_0\omega\left(1-\frac{c^2k^2}{\omega^2}\right)\frac{\tilde{J}^{\mathrm{transv}}(\vec{k},\omega)}{\tilde{J}^{\mathrm{tot}}_{\mathrm{transv}}(\vec{k},\omega)}\;, \tag{63}$$

and the relationship

$$\hat{\epsilon}(\vec{k},\omega) = \hat{I} + \frac{i}{\epsilon_0\omega}\hat{\sigma}(\vec{k},\omega) \tag{64}$$

holds.

Another important quantity is the polarization tensor which describes the relation between the induced electrical current or charge densities and the total vector or scalar potential, respectively. It can be introduced in different ways. If we use the definition

$$\begin{aligned}\epsilon_{ij}(\vec{k},\omega) &= \delta_{ij} - \frac{1}{\epsilon_0\omega^2}\tilde{\Pi}_{ij}(\vec{k},\omega)\\ &= \delta_{ij} - \frac{1}{\epsilon_0\omega^2}\left[\tilde{\Pi}_{\mathrm{long}}(\vec{k},\omega)\frac{k_ik_j}{k^2} + \tilde{\Pi}_{\mathrm{transv}}(\vec{k},\omega)\left(\delta_{ij}-\frac{k_ik_j}{k^2}\right)\right]\end{aligned} \tag{65}$$

we have with (55) and (42)

$$\tilde{\Pi}_{\mathrm{transv}}(\vec{k},\omega) = \epsilon_0(\omega^2-c^2k^2)\frac{\tilde{J}_{\mathrm{transv}}(\vec{k},\omega)}{\tilde{J}^{\mathrm{tot}}_{\mathrm{transv}}(\vec{k},\omega)} = -\frac{\tilde{J}_{\mathrm{transv}}(\vec{k},\omega)}{A_k(\omega)} \tag{66}$$

and from (53) and (43)

$$\tilde{\Pi}_{\mathrm{long}}(\vec{k},\omega) = \epsilon_0\omega^2\frac{\tilde{J}_{\mathrm{long}}(\vec{k},\omega)}{\tilde{J}^{\mathrm{tot}}_{\mathrm{long}}(\vec{k},\omega)} = \frac{\omega^2}{k^2}\frac{\tilde{\rho}(\vec{k},\omega)}{U^{\mathrm{tot}}_k(\omega)}\;. \tag{67}$$

The latter relation gives the motivation for an alternative definition

$$\Pi_{\rm long}(\vec{k},\omega) = \frac{k^2}{\omega^2}\tilde{\Pi}_{\rm long}(\vec{k},\omega) = \frac{\tilde{\rho}(\vec{k},\omega)}{U_k^{\rm tot}(\omega)} \ . \tag{68}$$

Thus we will use

$$\epsilon_{\rm long}(\vec{k},\omega) = 1 - \frac{1}{\epsilon_0 k^2}\Pi_{\rm long}(\vec{k},\omega)\,, \qquad \epsilon_{\rm transv}(\vec{k},\omega) = 1 - \frac{1}{\epsilon_0\omega^2}\tilde{\Pi}_{\rm transv}(\vec{k},\omega)\,. \tag{69}$$

To describe the relation between the induced electrical current or charge densities and the external vector or scalar potential, respectively, we introduce the response function. With

$$\tilde{\chi}_{\rm transv}(\vec{k},\omega) = \epsilon_0(\omega^2 - c^2k^2)\frac{\tilde{J}_{\rm transv}(\vec{k},\omega)}{\tilde{J}^{\rm ext}_{\rm transv}(\vec{k},\omega)} = -\frac{\tilde{J}_{\rm transv}(\vec{k},\omega)}{A_k(\omega)} \tag{70}$$

we have

$$\tilde{\chi}_{\rm transv}(\vec{k},\omega) = \frac{\tilde{\Pi}_{\rm transv}(\vec{k},\omega)}{1 - \frac{1}{\epsilon_0(\omega^2-c^2k^2)}\tilde{\Pi}_{\rm transv}(\vec{k},\omega)} = \epsilon_0\omega^2(\epsilon_{\rm transv}(\vec{k},\omega) - 1)\frac{\omega^2 - c^2k^2}{c^2k^2 - \epsilon_{\rm transv}(\vec{k},\omega)\omega^2} \ . \tag{71}$$

With

$$\chi_{\rm long}(\vec{k},\omega) = \frac{\tilde{\rho}(\vec{k},\omega)}{U_k^{\rm ext}(\omega)} \tag{72}$$

we find

$$\chi_{\rm long}(\vec{k},\omega) = \frac{\Pi_{\rm long}(\vec{k},\omega)}{1 - \frac{1}{\epsilon_0 k^2}\Pi_{\rm long}(\vec{k},\omega)} = \epsilon_0 k^2(\frac{1}{\epsilon_{\rm long}(\vec{k},\omega)} - 1)\,. \tag{73}$$

The optical properties, refraction index $n(\omega)$ and absorption coefficient $\alpha(\omega)$ are determined by the long-wavelength limit of the transverse dielectric function

$$\lim_{k\to 0}\epsilon_{\rm transv}(\vec{k},\omega) = \left(en(\omega) + \frac{ic}{2\omega}\alpha(\omega)\right)^2 \tag{74}$$

as well as the surface impedance of a plasma surface

$$Z(\omega) \ = \ -\frac{i\omega}{c\pi}\int \frac{d^3k}{k^2 - \frac{\omega^2}{c^2}[\epsilon_{\rm transv}(\vec{k},\omega) - 1]} \tag{75}$$

The longitudinal dielectric function is related to the stopping power, the energy loss per path length of ions penetrating a charged particle system. This will not be addressed within this review. For a detailed presentation of this topic see Zwicknagel *et al.* [40].

A further important quantity, related and relevant to various theoretical and experimental situations, is the dynamical structure factor, defined via the Laplace transformation of the density–density correlation function, see e.g. Mahan [30] or Hansen and McDonald [41],

$$S(\vec{k},\omega) \ = \ \frac{1}{2\pi\Omega n}\int_{-\infty}^{\infty} dt\langle\tilde{\rho}(\vec{k},t)\tilde{\rho}(-\vec{k})\rangle e^{i\omega t}\,. \tag{76}$$

With respect to the dielectric function it is given as

$$S(\vec{k},\omega) \;=\; \frac{\hbar}{n}\,\frac{\epsilon_0 k^2}{e^2}\,\frac{1}{\mathrm{e}^{-\beta\hbar\omega}-1}\,\mathrm{Im}\,\epsilon^{-1}_{\mathrm{long}}(\vec{k},\omega)\,. \tag{77}$$

Furthermore, the static structure factor $S(\vec{k})$,

$$S(\vec{k}) = \frac{1}{\Omega n}\langle\tilde{\rho}(\vec{k})\tilde{\rho}(-\vec{k})\rangle \tag{78}$$

follows from the dynamical one according to

$$S(\vec{k}) = \int_{-\infty}^{\infty}\mathrm{d}\omega\, S(\vec{k},\omega). \tag{79}$$

We restricted ourselves to a limited number of quantities which are relevant for our further considerations. A more exhaustive presentation of the dielectric function and the dynamic structure factor is found in the monographs by, e.g., Mahan [30], Forster [36], or Hansen and McDonald [41]. Further details such as the structure factor for a multicomponent system will be given in chapter 5 in connection with molecular dynamics simulations.

2 Linear Response Theory of Dielectric Function

2.1 Polarization and Response Function

After considering the properties of a charged particle system interacting with external sources, we will give a microscopic, quantum statistical approach for the evaluation of the induced charge and electrical current densities, which allows to calculate the dielectric function, the response and the polarization function as well as other related quantities as defined in section 1.5. We will focus on a nonrelativistic linear response theory. The covariant formulation can be found in papers by Morozov *et al.* [23, 24, 25].

As in the previous Chapter, we consider a charge-neutral plasma consisting of two components with masses m_c and charges e_c, where the index c denotes species (electron e, ion i) and spin, under the influence of classical external fields

$$F^{\rm ext}(\vec{r},t) = {\rm e}^{i(\vec{k}\vec{r}-\omega t)}\tilde{F}^{\rm ext}(\vec{k},\omega) + {\rm c.c.} \tag{80}$$

produced by external charge and current densities. The addition of the complex conjugate in Eq. (80) guaranties that the external field is real. Within this chapter, we will employ a short notation for the densities of the Fourier transforms (25), e.g. for the external forces

$$F^{\rm ext}_k(\omega) = \frac{1}{\Omega}\tilde{F}^{\rm ext}(\vec{k},\omega) \tag{81}$$

with Ω the normalization volume. The spacial averaged charge and current densities in Fourier space shall be defined in analogy to this as $\rho_k = \tilde{\rho}(\vec{k})/\Omega$ and $\vec{J}_k = \tilde{\vec{J}}(\vec{k})/\Omega$, respectively.

The total Hamiltonian $H^{\rm tot}(t) = H + H^{\rm ext}(t)$ contains the system Hamiltonian H and the external part $H^{\rm ext}(t)$ which is explicitly time dependent. The general form of H is given by Eq. (29). It contains the contribution of the transverse components of the Maxwell fields which are necessary to describe radiation processes in a plasma. For standard plasmas, the dominant interaction is the Coulomb interaction within the system. Any contribution due to the transverse part of Maxwell fields (transverse vector potential) caused by moving charges (currents) within the system will be neglected. This would only be relevant for very high temperatures, if the velocity of the system charges leads to noticeable radiation corrections (transverse contributions). This is not the case in our considerations. We describe Coulomb systems with the hamiltonian

$$H = \sum_{c,p} E_c(p)\; a^\dagger_{c,p} a_{c,p} + \frac{1}{2}\sum_{cd,pp'q} V_{cd}(q)\; a^\dagger_{c,p-q}\, a^\dagger_{d,p'+q}\, a_{d,p'}\, a_{c,p}\;, \tag{82}$$

where $E_c(p) = \hbar^2 p^2/2m_c$ denotes the kinetic energy, $V_{cd}(q) = e_c e_d/(\epsilon_0 \Omega q^2)$ the Coulomb interaction.

The coupling to the external perturbations according to Eq. (44) is found from the general Hamiltonian (18) by singling out one component as an external one,

$$H^{\rm ext}(t) = \int d^3r \left\{ \rho^{\rm ext}(\vec{r},t) U(\vec{r}) - \vec{J}^{\rm ext}(\vec{r},t)\cdot\vec{A}(\vec{r}) - \frac{e_{\rm ext}}{2m_{\rm ext}} \rho^{\rm ext}(\vec{r},t)\vec{A}^2(\vec{r}) \right\} . \tag{83}$$

The longitudinal coupling to the external charge density is mediated by the scalar potential (16). The transverse part contains the external current as well as the charge density. Written in phase space,

$$\begin{aligned} H^{\rm ext}(t) = \quad & \sum_k \int \frac{d\omega}{4\pi} \left\{ \rho^{\rm ext}_k(\omega) U_{-k} - \vec{J}^{\rm ext}_k(\omega)\cdot\vec{A}_{-k} - \frac{e_{\rm ext}}{2m_{\rm ext}} \sum_{k'} \rho^{\rm ext}_{k'}(\omega)\vec{A}_{k-k'}\vec{A}_{-k} \right\} {\rm e}^{-i\omega t} \\ & + {\rm c.c.} \end{aligned} \tag{84}$$

A factor 1/2 arises because each value $\vec{k},\omega$ occurs also in the complex conjugate. Within linear response it is sufficient to consider only one mode with respect to $\vec{k},\omega$ as already done in the ansatz for the external perturbations, Eq. (80). Different Fourier components will superpose independently.

Due to these perturbations, charge densities $\langle\rho_k\rangle^t$ and electrical current densities $\langle\vec{J}_k\rangle^t$ are induced, having the same wave number $\vec{k}$ and frequency ω as a consequence of the homogeneity in space and time. They are related to the average of the Wigner transform $n^c_{p,k}$ of the single-particle occupation operator (35) according to (36) in the following way

$$\rho_k(\omega) = {\rm e}^{i\omega t}\langle\rho_k\rangle^t = \frac{{\rm e}^{i\omega t}}{\Omega} \sum_{p,c} e_c \langle \delta n^c_{p,k}\rangle^t , \tag{85}$$

$$\begin{aligned} \vec{J}_k(\omega) = {\rm e}^{i\omega t}\langle\vec{J}_k\rangle^t &= \vec{j}_k(\omega) - \frac{{\rm e}^{i\omega t}}{\Omega}\epsilon_0\omega^2_{\rm pl}\langle\vec{A}_k\rangle^t , \\ &= \vec{j}_k(\omega) - \frac{1}{\Omega}\epsilon_0\omega^2_{\rm pl}\vec{A}_k(\omega) , \end{aligned} \tag{86}$$

$$\vec{j}_k(\omega) = {\rm e}^{i\omega t}\langle\vec{j}_k\rangle^t = \frac{{\rm e}^{i\omega t}}{\Omega}\sum_{p,c}\frac{e_c}{m_c}\hbar\vec{p}\,\langle n^c_{p,k}\rangle^t . \tag{87}$$

Here, $\delta n^c_{p,k} = n^c_{p,k} - {\rm Tr}\left\{n^c_{p,k}\ \varrho_0\right\}$ denotes the deviation from equilibrium given by the equilibrium statistical operator

$$\varrho_0 = \frac{\exp(-\beta H + \beta\sum_c \mu_c N_c)}{{\rm Tr}\exp(-\beta H + \beta\sum_c \mu_c N_c)} , \tag{88}$$

where β denotes the inverse temperature, μ_c the chemical potential of species c, and N_c its total particle number. The average $\langle\ldots\rangle^t = {\rm Tr}\left\{\ldots\varrho(t)\right\}$ has to be performed with the nonequilibrium statistical operator $\varrho(t)$, which will be derived below in linear response with respect to the external perturbations.

As discussed in the previous Chapter, from standard electrodynamics the dielectric function is introduced via the ratio between the induced electrical current density and the total

electrical current density. In the case of the longitudinal dielectric function, the more natural way to pursue is the calculation of the inverse dielectric function, see Eqs. (72) and (73), as

$$\chi_{\rm long}(\vec{k},\omega) = \epsilon_0 k^2 \frac{\rho_k(\omega)}{\rho_k^{\rm ext}(\omega)} = \epsilon_0 k^2 \frac{k}{\omega} \frac{J_k^{\rm long}(\omega)}{\rho_k^{\rm ext}(\omega)} = \epsilon_0 k^2 \frac{J_k^{\rm long}(\omega)}{J_k^{\rm long,ext}(\omega)} = \epsilon_0 k^2 \frac{k}{\omega} {\rm e}^{i\omega t} \frac{\langle J_k^{\rm long}\rangle^t}{\rho_k^{\rm ext}(\omega)}\,, \quad (89)$$

where the continuity Eq. (39) as well as the relations (43) and (86) have been taken into account. The longitudinal polarization function can be found from Eqs. (73), (69) and (64) as

$$\Pi_{\rm long}(\vec{k},\omega) \;=\; -\frac{ik^2}{\omega}\sigma_{\rm long}(\vec{k},\omega) = \epsilon_0 k^2 \frac{J_k^{\rm long}(\omega)}{J_k^{\rm ext,long}(\omega)} \; \frac{1}{1+\frac{J_k^{\rm long}(\omega)}{J_k^{\rm ext,long}(\omega)}}. \quad (90)$$

For the transverse case, for the polarization function (66) follows

$$\tilde{\Pi}_{\rm transv}(\vec{k},\omega) \;=\; \epsilon_0 \left(\omega^2 - c^2k^2\right) \frac{J_k^{\rm transv}(\omega)}{J_k^{\rm ext,transv}(\omega)} \; \frac{1}{1+\frac{J_k^{\rm transv}(\omega)}{J_k^{\rm ext,transv}(\omega)}}. \quad (91)$$

Alternatively, we can consider the transverse response function $\tilde{\chi}_{\rm transv}(\vec{k},\omega)$ according to (70). The structure for the polarization function and the response function in the transverse case is very similar.

The main problem in evaluating the mean value of the charge density $\langle\rho_k\rangle^t$ or the current density $\langle\vec{J}_k\rangle^t$ is the determination of the non–equilibrium statistical operator $\varrho(t)$. In linear response theory, the external potential is considered to be weak so that an expansion up to first order is possible. Explicit solutions can be given in this special case.

2.2 Generalized Linear Response Theory

Linear response theory has been derived by Kubo [42] and was later further developed in different directions by Mori [43], Zubarev *et al.* [44, 45, 46], Tserkovnikov [47] and Lee [48] to name just a few. For a recent presentation see Zubarev *et al.* [34, 35].

The main idea of a generalized linear response theory is the construction of the statistical operator

$$\varrho(t) = \varrho_{\rm rel}(t) + \varrho_{\rm irrel}(t) \quad (92)$$

by introducing a relevant statistical operator $\varrho_{\rm rel}(t)$. The latter characterizes the non-equilibrium state of the system by the mean values $\langle A_n\rangle^t$ of a set of relevant observables $\{A_n\}$[16]. A generalized Gibbs state

$$\varrho_{\rm rel}(t) = {\rm e}^{-S(t)/k_B}\;, \quad (93)$$

[16]The index n may include also a continuous variable such as the position $\vec{r}$. Then, summation over n in (94) and following expressions also means integration over $\vec{r}$.

where

$$\frac{1}{k_B} S(t) = \Phi(t) + \sum_n \alpha_n(t)\, A_n \tag{94}$$

is the entropy operator and

$$\Phi(t) = \ln \mathrm{Tr} \exp \left\{ - \sum_n \alpha_n(t) A_n \right\} \tag{95}$$

is the Massieu-Planck function, follows from the maximum of the entropy

$$\langle S(t) \rangle^t = -k_B \, \mathrm{Tr}\{ \varrho_{\mathrm{rel}}(t) \, \ln \varrho_{\mathrm{rel}}(t) \} \tag{96}$$

at given mean values

$$\mathrm{Tr}\{ \varrho_{\mathrm{rel}}(t) \; A_n \} = \langle A_n \rangle^t \; . \tag{97}$$

The thermodynamic parameters (Lagrange multipliers) $\alpha_n(t)$ are determined by the self-consistency conditions (97) and will be evaluated within linear response theory below.

The relevant statistical operator (93) does not solve the Liouville von Neumann equation, but it can serve to formulate the correct boundary conditions to obtain the retarded solution of the von Neumann equation. Using the principle of the weakening of initial correlations, the irrelevant part of the statistical operator can be found with the help of the time evolution operator $U(t, t')$ via Abel's theorem [34, 35, 44].

$$i\hbar \frac{\partial}{\partial t} U(t, t') = H^{\mathrm{tot}}(t) \; U(t, t'); \qquad U(t', t') = 1, \tag{98}$$

as

$$\varrho(t) = \eta \int_{-\infty}^{t} dt' \; \mathrm{e}^{-\eta(t-t')} \; U^{\dagger}(t, t') \; \varrho_{\mathrm{rel}}(t') \; U(t', t) \; , \tag{99}$$

where the limit $\eta \to 0$ has to be taken after the thermodynamic limit. Partial integration of (99) gives $\varrho(t) = \varrho_{\mathrm{rel}}(t) + \varrho_{\mathrm{irrel}}(t)$ with

$$\varrho_{\mathrm{irrel}}(t) = - \int_{-\infty}^{t} dt' \; \mathrm{e}^{-\eta(t-t')} U^{\dagger}(t, t') \; \left\{ \frac{i}{\hbar} \left[H^{\mathrm{tot}}(t') \, , \; \varrho_{\mathrm{rel}}(t') \right] + \frac{\partial}{\partial t'} \, \varrho_{\mathrm{rel}}(t') \right\} U(t', t). \tag{100}$$

Alternatively, from the expression for the statistical operator, a Liouville-von-Neumann equation

$$\frac{\partial \varrho(t)}{\partial t} + \frac{i}{\hbar} \left[H_{\mathrm{tot}}(t), \varrho(t) \right] = - \lim_{\eta \to 0} \; \eta \left\{ \varrho(t) - \varrho_{\mathrm{rel}}(t) \right\} \tag{101}$$

is found, where the initial conditions are incorporated via a source term containing the relevant statistical operator. The self-consistency conditions (97) which determine the Lagrange multipliers take the form

$$\mathrm{Tr}\{ A_n \; \varrho_{\mathrm{irrel}}(t) \} = 0 \tag{102}$$

and the external perturbation shall be written in the general way

$$H^{\rm ext}(t) = F_k^{\rm ext}(\omega) C_{-k} {\rm e}^{-i\omega t} + {\rm c.c.} \tag{103}$$

where the operator C contains system specific quantum mechanical operators, see, e.g., Eq. (84). Note that $C_{-k} = C_k^\dagger$, the normalization factor $1/4\pi$ is included into the external field. We now specify the set of relevant observables $\{A_n\}$ as $\{H, N_c, B_n(\vec{r})\}$ and the corresponding Lagrange parameters $\{\alpha_n\}$ as $\{\beta, -\beta\mu_c, -\beta\phi_n(\vec{r},t)\}$,

$$\varrho_{\rm rel} = \exp\left\{ -\Phi(t) - \beta H + \beta \sum_c \mu_c \, N_c + \beta \sum_n \int d^3r \; \phi_n(\vec{r},t) \; B_n(\vec{r}) \right\} \; . \tag{104}$$

The meaning of the Langrange multipliers $\beta = 1/(k_B T)$ and the chemical potential μ_c is known from thermodynamic equilibrium already[17]. Thermal perturbations can be included by allowing a position dependence in these terms, see Reinholz [49].

For a weak external field $F^{\rm ext}$, the system remains near thermal equilibrium described by ϱ_0 (88), so that $\varrho(t)$ (92) can be expanded up to the first order with respect to $F^{\rm ext}$ and the Langrange multipliers ϕ_n. For this, it is convenient to use the Fourier representation so that for a single mode $(\vec{k}, \omega)$ in Fourier space

$$\int d^3r \; \phi_n(\vec{r},t) \; B_n(\vec{r}) = \phi_n(\vec{k},\omega) \; {\rm e}^{-i\omega t} \; B_{n,k}^\dagger + {\rm c.c.} \tag{105}$$

with[18]

$$\phi_n(\vec{r},t) = {\rm e}^{i(\vec{k}\cdot\vec{r} - \omega t)} \; \phi_n(\vec{k},\omega) \; , \qquad B_{n,k} = \int d^3r \; B_n(\vec{r}) \; {\rm e}^{-i\vec{k}\cdot\vec{r}} \; . \tag{106}$$

The relevant contribution to (92) is

$$\varrho_{\rm rel}(t) = \varrho_0 + {\rm e}^{-i\omega t} \int_0^\beta d\tau \sum_n B_{n,k}^\dagger(i\hbar\tau) \; \phi_n(\vec{k},\omega) \; \varrho_0 + {\rm c.c.} \tag{107}$$

where the dependence on the imaginary time is given according to the Heisenberg time dependence (24). From (100) follows

$$\begin{aligned} \rho_{\rm irrel}(t) = & - \int_{-\infty}^t dt' {\rm e}^{-\eta(t-t')} U(t,t') \left\{ \frac{i}{\hbar} \left[H_{\rm ext}(t'), \rho_0 \right] \right. \\ & \left. + \rho_0 \int_0^\beta d\tau \int d^3\vec{r} \left(\phi_n(\vec{r},t') \frac{i}{\hbar} \left[H, B_n(\vec{r}; -i\hbar\tau) \right] + \frac{\partial}{\partial t'} \phi_n(\vec{r},t') B_n(\vec{r}; -i\hbar\tau) \right) \right\} U(t',t). \end{aligned} \tag{108}$$

[17] In principle, all Lagrange multipliers are functions of t. However, in the case of β and μ_c this is of second order with respect to the external perturbation and can be neglected within linear response theory.

[18] In general, we have $\phi_n(\vec{r},t) = \sum_{k'} \int \frac{d\omega'}{2\pi} {\rm e}^{i(\vec{k}'\cdot\vec{r} - \omega' t)} \phi_n(\vec{k}',\omega')$ and $B_{n,k'} = \int d^3r \, B_n(\vec{r}) \, {\rm e}^{-i\vec{k}'\cdot\vec{r}}$. The selfconsistency Eqs. (102) must be fulfilled for any time t so that $\omega' = \omega$ follows. Furthermore, the equilibrium correlation functions ${\rm Tr}(A_k B_{k'}^+ \rho_0)$ do vanish except if $k' = k$ so that $\langle A_k(\eta - i\omega); B_{k'} \rangle \sim \delta_{kk'}$. The well-known property of linear response that only such fluctuations are induced where the wave vector and frequency coincide with the external potential is a consequence of homogeneity in space and time.

and, applying the Kubo identity [34]

$$[A, \varrho_0] = \int_0^\beta d\tau \ \mathrm{e}^{-\tau H} \ [H, A] \ e^{\tau H} \ \varrho_0 \ , \tag{109}$$

where A shall be an arbitrary operator and the total particle number N_c occurring in ϱ_0 (88) is assumed to commute with H, A, we find

$$\varrho_{\mathrm{irrel}}(t) = -\int_{-\infty}^{t} dt' \ \mathrm{e}^{-\eta(t-t')} \ \mathrm{e}^{-i\omega t'} \int_0^\beta d\tau \left\{ \dot{C}_k^\dagger(t' - t + i\hbar\tau) \ F^{\mathrm{ext}}(\vec{k}, \omega) \right.$$
$$\left. + \sum_n \left(\dot{B}_{n,k}^\dagger(t' - t + i\hbar\tau) - i\omega B_{n,k}^\dagger(t' - t + i\hbar\tau) \right) \ \phi_n(\vec{k}, \omega) \right\} \varrho_0 + \mathrm{c.c.} \tag{110}$$

where $\dot{O} = i[H, O]/\hbar$. Inserting this result in the self-consistency conditions (102) we get the response equations (the index k is merged with the index n, m)

$$-\ \langle B_m; \dot{C}_k \rangle_{\omega + i\eta} \ F_k^{\mathrm{ext}}(\omega) = \sum_n \langle B_m; \left\{ \dot{B}_n - i\omega B_n \right\} \rangle_{\omega + i\eta} \ \phi_n(\vec{k}, \omega) \, , \tag{111}$$

where the equilibrium correlation functions are defined as the Kubo scalar product

$$(A; B) \ = \ (B^\dagger; A^\dagger) = \frac{1}{\beta} \int_0^\beta d\tau \mathrm{Tr} \left\{ A(-i\hbar\tau) B^\dagger \varrho_0 \right\} \tag{112}$$

and it's Laplace transform

$$\langle A; B \rangle_z \ = \ \int_0^\infty dt \ \mathrm{e}^{izt} \, (A(t); B) \, . \tag{113}$$

To make the relation between the response Eqs. (111) and the Boltzmann equation more obvious, see Röpke [50], we introduce the 'stochastic' part of forces applying partial integrations

$$\langle A; B \rangle_z = \frac{i}{z} \left\{ (A; B) + \langle \dot{A}; B \rangle_z \right\} = \frac{i}{z} \left\{ (A; B) - \langle A; \dot{B} \rangle_z \right\} \tag{114}$$

and evaluate $(B_m; \dot{C}_k) \langle B_m; C_k \rangle_{\omega + i\eta} / \langle B_m; \dot{C}_k \rangle_{\omega + i\eta}$ as shown by Christoph and Röpke [46, 51]. The response equations (111) can be rewritten as

$$-M_{m0} \ F_k^{\mathrm{ext}}(\omega) = \sum_n M_{mn} \ \phi_n(k, \omega) \tag{115}$$

with

$$M_{m0} = \left(B_m; \dot{C}_k \right) \tag{116}$$

and

$$M_{mn} = \left(B_m; \{ \dot{B}_n - i\omega B_n \} \right) + \left\langle \left\{ \dot{B}_m - \frac{\langle \dot{B}_m; \dot{C}_k \rangle_{\omega + i\eta}}{\langle B_m; \dot{C}_k \rangle_{\omega + i\eta}} \ B_m \right\}; \{ \dot{B}_n - i\omega B_n \} \right\rangle_{\omega + i\eta} . \tag{117}$$

These were interpreted as generalized linear response equations by Röpke [51]. The M_{nm} are generalized transition probabilities (collision term) and the l.h.s describes the influence of the external forces (drift term) such representing also a generalized Boltzmann equation.

The system of Eqs. (111) or (115) can be solved applying Cramer's rule, see the following section. Then, the response parameters ϕ_n are represented as a ratio of two determinants containing equilibrium correlation functions. With these expressions for ϕ_n the explicit form of the non-equilibrium statistical operator $\varrho(t)$ is known, and we can evaluate mean values of arbitrary observables.

In particular, we are interested in the evaluation of $\langle \vec{J}_k \rangle^t \exp(i\omega t)$ in order to calculate the dielectric function via either the response function (89) or the polarization function (90) and (91), using (107) and (110),

$$\langle \vec{J}_k \rangle^t \ \mathrm{e}^{i\omega t} = \beta \sum_n \Big\{ (\vec{J}_k; B_n) - \langle \vec{J}_k; [\dot{B}_n - i\omega B_n] \rangle_{\omega + i\eta} \Big\} \phi_n(\vec{k}, \omega) - \beta \langle \vec{J}_k; \dot{C}_k \rangle_{\omega + i\eta} F_k^{\mathrm{ext}}(\omega). \tag{118}$$

If $\vec{J}_k$ can be represented by a linear combination of the relevant observables $\{B_n\}$, we can directly use the selfconsistency conditions (97) and have

$$\langle \vec{J}_k \rangle^t \ \mathrm{e}^{i\omega t} = \mathrm{Tr} \Big\{ \vec{J}_k \ \varrho_{\mathrm{rel}}(t) \Big\} \ \mathrm{e}^{i\omega t} \, . \tag{119}$$

After expanding $\varrho_{\mathrm{rel}}(t)$, Eq. (107), up to first order in $\phi_n(\vec{k}, \omega)$ we have

$$\langle \vec{J}_k \rangle^t \ \mathrm{e}^{i\omega t} = \beta \sum_n (\vec{J}_k; B_n) \ \phi_n(\vec{k}, \omega) \ . \tag{120}$$

This is consistent with Eq. (118) because the remaining terms on the r.h.s of (118) compensate due to the response Eqs. (111).

The linear response theory expresses the response of a system (dissipation) via equilibrium correlation functions (fluctuations) which allows the systematic perturbative treatment in analogy to equilibrium properties. The generalized linear response theory as sketched here has been successfully applied to mechanical and non-mechanical (heat and particle exchange) perturbations and the principal equivalence to the application of kinetic equations has been shown. Expressions for thermoelectric transport coefficients have been derived and, e.g., used to describe partially ionized plasmas [52, 53, 14], semiconductors [54], magnetic metals [55] and expanded liquid metals [56]. However, this approach has the potential to calculate non-linear properties as well if the statistical operator is considered beyond the linear expansion, for conceptional examples and references see Zubarev *et al.* [34, 35].

2.3 Specification of the Set of Relevant Operators

Before we evaluate the dielectric function within the generalized linear response theory as outlined in the previous section we would like to discuss two general aspects concerning the evaluation of expressions such as Eq. (120) for the quantum statistical average of the induced current density:

(i) The set of quantum operators $\{B_1, B_2, \ldots, B_l, \ldots\}$ needs to be specified. It defines the rank of the matrices which emerge when the response parameters ϕ_n are calculated via Cramers rule from Eq. (115).

(ii) The equilibrium correlation functions (112), (113) for an interacting many-body system have to be evaluated which can be done by perturbation theory[19].

Both aspects are closely related. It can be shown by formal manipulations [34, 46] that the results for the physical quantities given above are independent on the choice made for the set of quantum operators $\{B_l\}$ as long as the correlation functions are evaluated rigorously (and the limit $\eta \to 0$ is performed in the final expressions). In contrast, finite order perturbation theory will lead to different results depending on the choice of quantum operators $\{B_l\}$.

For a many-body system described by the Hamiltonian, Eq. (82), quantum statistical approaches allow to evaluate the equilibrium correlation functions by systematic perturbation expansions. In order to produce reasonable approximations one can use two different strategies which are directly related to the above mentioned main problems. Perturbation expansion can be extended by considering higher orders and performing partial summations. The other option is the extension of the set of relevant observables which leads to a finer description of the nonequilibrium state of the system so that already in low-order perturbation theory relevant results are obtained [46]. As has been shown for the electrical conductivity [57, 45], results from finite order perturbation theory are the better the more relevant observables are considered.

Let us now discuss the particular choice of the set of quantum operators $\{B_l\}$. In the simplest case where this set is empty [51, 46], the Kubo density matrix [42] for the statistical operator is obtained. It is identical with choosing the equilibrium statistical operator as the relevant statistical operator. The solution for the induced current density can be immediately obtained from Eq. (118) as

$$\langle \vec{J}_k(\omega) \rangle = \langle \vec{J}_k \rangle^t \; \mathrm{e}^{i\omega t} = -\beta \langle \vec{J}_k ; \dot{C}_k \rangle_{\omega + i\eta} \, F_k^{\mathrm{ext}}(\omega). \tag{121}$$

In the case of the longitudinal dielectric function, the Kubo formula is obtained which will be discussed in the next section.

On the other hand, one can follow the framework known from standard transport theory by Spitzer [58, 59] such as the Chapman-Enskog [60] or the Grad method [61] for the dc-conductivity. For this, the set of quantum operators $\{B_l\}$ is chosen as moments (Sonine or Hermite polynoms, respectively) of the single-particle distribution function of each component of the system [51, 53]. This has also been done in the context of the dielectric function by Wierling, Reinholz *et al.* [50, 62, 63], taking

$$\{ \, B_l \, \} \quad \to \quad \vec{P}^c_{k,n} = \sum_p \hbar \vec{p} \left(\beta \, E^c_p \right)^n n^c_{p,k} \; . \tag{122}$$

The first moments ($n = 0$; $c = e, i$) are the linear momentum operators of the corresponding species. The electrical current can be expressed as a linear combination of these observables

[19] Alternatively, numerical simulations such as molecular dynamics or path integral Monte Carlo can be applied, independently from small parameters necessary for perturbative expansions.

according to (87),

$$\vec{j}_k = \frac{1}{\Omega} \sum_c \frac{e_c}{m_c} \vec{P}^c_{k,0} \ . \tag{123}$$

The second moments ($n = 1$) are relevant in connection with the thermopower and thermal conductivity since they describe the current of kinetic energy, see Reinholz *et al.* [53]. For finite wavenumber $\vec{k}$, the general form of the moments will contain not only powers of p^2, but also of $\vec{k} \cdot \vec{p}$, see Röpke and Wierling [62]. The general expression for the induced current density is obtained from (120) with ϕ_n from (115) as

$$\langle \vec{J}_k \rangle^t \ \mathrm{e}^{i\omega t} = -\frac{1}{M(\vec{k},\omega)} \, F^{\mathrm{ext}}_k(\omega). \tag{124}$$

with

$$M(\vec{k},\omega) \ = \frac{|M_{mn}(\vec{k},\omega)|}{\begin{vmatrix} 0 & M_{0n}(\vec{k},\omega) \\ M_{m0}(\vec{k},\omega) & M_{mn}(\vec{k},\omega) \end{vmatrix}}, \tag{125}$$

where the elements in the determinants are given by Eqs. (116), (117) and

$$M_{0n}(\vec{k},\omega) \ \ = \ \ (\vec{J}_k; B_n). \tag{126}$$

We emphasize that the equivalence of the approach based on a finite set of moments of the single-particle distribution function with the Kubo formula (121) can be shown. However, different results are obtained evaluating the correlation functions in a given approximation.

An interesting point is the close relation to kinetic theory. The linearized Boltzmann equation results if the single particle occupation number is taken as relevant observable, expressing the collision term as the correlation function of orthogonal, "stochastic" forces [44, 51].

As a rule, Markovian approximations are the better the more details of the correlations are taken into account to describe the nonequilibrium state. For instance, also higher order distribution functions such as the two-particle distribution function can be included [51].

2.4 Longitudinal Response

For the longitudinal dielectric function we consider the following external perturbation of the system

$$H^{\mathrm{ext}}(t) = \rho^{\mathrm{ext}}_k(\omega) U_{-k} \mathrm{e}^{-i\omega t} + c.c. \tag{127}$$

which is a special case of Eq. (84). Comparing this with the general expression (103), we find

$$C_k = U_k = \frac{\Omega \rho_k}{\epsilon_0 k^2} = \frac{\Omega}{\epsilon_0 k^2} \frac{k}{\omega} J^{\mathrm{long}}_k. \tag{128}$$

In order to obtain the last expression, the continuity Eq. (39) in Fourier space was applied. We derive an expression for the longitudinal response function (89) using the Kubo expression (121) with $F_k^{\rm ext}(\omega) = \rho_k^{\rm ext}(\omega)$ and C_k given in (128),

$$\chi_{\rm long}(\vec{k},\omega) \;\; = \;\; -i\beta\Omega\,\frac{k^2}{\omega}\langle J_k^{\rm long};J_k^{\rm long}\rangle_{\omega+i\eta}\;. \tag{129}$$

This Kubo formula [42, 30] expresses the response function in terms of the correlation function of the longitudinal electrical current operator $J_k^{\rm long}$. Note that

$$\dot{\rho}_k = \frac{i}{\hbar}[H,\rho_k] = ik\,J_k^{\rm long} \tag{130}$$

was used. Whereas at high frequencies the perturbative treatment of expression (129) is immediately possible, divergences appearing in the zero-frequency limit have to be dealt with by partial summations.

The polarization function is obtained from (73) and (129) as

$$\Pi_{\rm long}(\vec{k},\omega) = \frac{\chi_{\rm long}(\vec{k},\omega)}{1+\frac{1}{\epsilon_0 k^2}\chi_{\rm long}(\vec{k},\omega)} = -i\beta\Omega\frac{k^2}{\omega}\frac{\langle J_k^{\rm long};J_k^{\rm long}\rangle_{\omega+i\eta}}{1-\frac{i\beta\Omega}{\epsilon_0\omega}\langle J_k^{\rm long};J_k^{\rm long}\rangle_{\omega+i\eta}}. \tag{131}$$

If the current density operator $J_k^{\rm long}$ can be represented as superposition of the relevant observables B_n, we find the following expression for the response function [34, 45, 62]

$$\chi_{\rm long}(k,\omega) = -\,i\beta\Omega\,\frac{k^2}{\omega}\;\frac{1}{M(\vec{k},\omega)}\;, \tag{132}$$

where the expression (117) is now called the inverse response function and has the specific elements[20]

$$\begin{aligned} M_{0n}(\vec{k},\omega) &= (J_k^{\rm long};B_n)\;, \qquad M_{m0}(\vec{k},\omega) = (B_m;J_k^{\rm long})\;,\\ M_{mn}(\vec{k},\omega) &= (B_m;[\dot{B}_n - i\omega B_n]) + \langle \dot{B}_m;[\dot{B}_n - i\omega B_n]\rangle_{\omega+i\eta}\\ &\quad -\frac{\langle \dot{B}_m;J_k^{\rm long}\rangle_{\omega+i\eta}}{\langle B_m;J_k^{\rm long}\rangle_{\omega+i\eta}}\;\langle B_m;[\dot{B}_n - i\omega B_n]\rangle_{\omega+i\eta}\;. \end{aligned} \tag{134}$$

The evaluation of the correlation functions can be done by standard many particle methods such as perturbation theory for thermodynamic Green's functions or molecular dynamic simulations which will be outlined in the following chapters 3-5.

[20] A different representation of the matrix elements is given in [62, 64].

$$\begin{aligned} M_{mn}(\vec{k},\omega) &= (B_m;[\dot{B}_n - i\omega B_n]) \;+\; \langle \dot{B}_m;\dot{B}_n\rangle_{\omega+i\eta}\\ &\quad + \begin{vmatrix} 0 & \langle \dot{B}_m;B_j\rangle_{\omega+i\eta}\\ \langle B_i;\dot{B}_n\rangle_{\omega+i\eta} & \langle B_i;B_j\rangle_{\omega+i\eta}\end{vmatrix} \Big/ |\langle B_i;B_j\rangle_{\omega+i\eta}|\;. \end{aligned} \tag{133}$$

The simplest choice for a relevant observable B_n characterizing the nonequilibrium state of the system is the longitudinal current density (36)

$$B_n = J_k^{\rm long} = j_k^{\rm long} \tag{135}$$

itself which is also the lowest moment of the distribution function. We will treat this approach in more detail before discussing possible extensions to more general sets of relevant observables. From the approach given by Eq. (135), we have

$$\chi_{\rm long}(k,\omega) = -\,i\beta\Omega\frac{k^2}{\omega}\;\frac{(J_k^{\rm long};J_k^{\rm long})^2}{M_{jj}(\vec{k},\omega)}\;, \tag{136}$$

with

$$M_{jj}(\vec{k},\omega) = -i\omega\;(J_k^{\rm long};J_k^{\rm long}) + \langle \dot{J}_k^{\rm long};\dot{J}_k^{\rm long}\rangle_{\omega+i\eta} - \frac{\langle \dot{J}_k^{\rm long};J_k^{\rm long}\rangle_{\omega+i\eta}}{\langle J_k^{\rm long};J_k^{\rm long}\rangle_{\omega+i\eta}}\;\langle J_k^{\rm long};\dot{J}_k^{\rm long}\rangle_{\omega+i\eta}\;. \tag{137}$$

Using the property

$$(\dot{A};B) = \frac{i}{\hbar\beta}\;{\rm Tr}\{[A,B^\dagger]\varrho_0\} \tag{138}$$

it is easy to see that $(J_k^{\rm long};\dot{J}_k^{\rm long}) = 0$. Applying partial integration (114), the expression (136) can be rewritten as

$$\chi_{\rm long}(k,\omega) = -\,i\beta\Omega\frac{k^2}{\omega}\;\frac{(J_k^{\rm long}J_k^{\rm long})\;\langle J_k^{\rm long};J_k^{\rm long}\rangle_{\omega+i\eta}}{(J_k^{\rm long};J_k^{\rm long}) - \eta\;\langle J_k^{\rm long};J_k^{\rm long}\rangle_{\omega+i\eta}}\,. \tag{139}$$

Performing the limit $\eta \to 0$, for finite values of the current–current correlation function the Kubo formula (129) is obtained again. As mentioned before, expressions (136) and (129) are differently suited to perform perturbation expansions, see the following chapter.

The applicability of correlation functions for the inverse transport coefficients has been widely discussend [34, 35, 44]. Sometimes also the relations (129) or (136) are denoted as fluctuation–dissipation theorems of the first or second kind, respectively.

The approach to the dielectric function is based on the choice (135) for the set of relevant observables and may be considered as the generalization of the force–force correlation function method for the electrical resistivity, see [51], to the dielectric function. In particular, the choice of single-particle occupation numbers $n^c_{p,0}$ as set of relevant observables leads to a generalized Boltzmann equation (115), thus bridging between the Kubo formula (129) and the generalized linear response expression (136). Also the Chapman-Enskog or Grad method to solve the Boltzmann equation becomes a special version of generalized linear response theory where the moments of the distribution function are taken as relevant observables. Possible extensions of the set of relevant observables have been investigated in evaluating the dc conductivity in Ref. [45], considering not only the full single-particle distribution function, but also two-particle correlations. It is the main advantage of the generalized response formula (136) in comparison with the Kubo formula (129) that finite order perturbation expansion can be performed also near $\vec{k} = 0,\ \omega = 0$. This will be further detailed in chapter 3.

2.5 Transverse Response

We now consider the response of a system to a transverse field. An external current will induce a transverse current in the system. The coupling of the system to the external sources according to Eq. (84) shall now be written in a slightly different way in order to emphasize the separation between the external charge and current densities and the operators within the system. We follow the Hamiltonian (29) with the definitions (38) and the spacial charge density,

$$H^{\rm ext}(t) = -\sum_k \vec{j}_k^{\rm ext}(t)\cdot\vec{A}_{-k} + \frac{1}{\Omega}\frac{e_{\rm ext}}{2m_{\rm ext}}\sum_{k,k'}\rho_{k'}^{\rm ext}(t)\vec{A}_{k-k'}\vec{A}_{-k}\,. \tag{140}$$

The time dependence of the operators is given by the Heisenberg picture, whereas the external sources are explicitly time dependent. If we consider the case that the relevant statistical operator is the equilibrium statistical operator, the statistically averaged transverse current density can be given directly from relation (121)

$$\langle J_k^{\rm transv}\rangle^t = -\beta\langle J_k^{\rm transv};\dot{H}^{\rm ext}\rangle_{\omega+i\eta}{\rm e}^{-i\omega t}, \tag{141}$$

where the time derivative is only to be taken with respect to the Heisenberg picture of the system operators and can be executed via the commutator with the system Hamiltonian. It follows

$$\begin{aligned}\dot{H}^{\rm ext} &= \frac{i}{\hbar}[H;H^{\rm ext}]\\ &= -\sum_k \vec{j}_k^{\rm ext}(t)\cdot\dot{\vec{A}}_{-k} + \frac{1}{\Omega}\frac{e_{\rm ext}}{2m_{\rm ext}}\sum_{k,k'}\rho_{k'}^{\rm ext}(t)\left\{\dot{\vec{A}}_{-k}\vec{A}_{k-k'} + \vec{A}_{k-k'}\dot{\vec{A}}_{-k}\right\}.\end{aligned} \tag{142}$$

Using the defintion of $\vec{J}_k$ (86) in terms of the canonical current density $\vec{j}_k$ and the plasma frequency for the external quantities, the total external current density is defined in analogy to (36),

$$\vec{J}_k^{\rm ext}(t) = \vec{j}_k^{\rm ext}(t) - \frac{e_{\rm ext}}{m_{\rm ext}}\sum_{k'}\rho_{k'}^{\rm ext}(t)\vec{A}_{k-k'} \tag{143}$$

and is to be considered as the classical quantity which is measured. A contribution according to the commutator at $2k$ is neglected. Note that the external current density does couple onto the considered system in a system specific way via the average of the vector potential. For Eq. (141) we write

$$J_k^{\rm transv}(\omega) = {\rm e}^{i\omega t}\langle J_k^{\rm transv}\rangle^t = \beta\langle J_k^{\rm transv};\dot{\vec{A}}_k\rangle_{\omega+i\eta}\cdot J_k^{\rm ext,transv}\,. \tag{144}$$

To simplify the notation, we put $\vec{J}_k^{\rm ext}(t) = J_k^{\rm ext}(t)\vec{e}_x$ so that only the x-components of $\vec{A}_k$ and of $J_k^{\rm transv}$ have to be considered. For the transverse polarization function (91) follows

$$\tilde{\Pi}_{\rm transv}(\vec{k},\omega) = \epsilon_0\left(\omega^2 - c^2k^2\right)\frac{\beta\langle J_k^{\rm transv};\dot{A}_k\rangle_{\omega+i\eta}}{1+\beta\langle J_k^{\rm transv};\dot{A}_k\rangle_{\omega+i\eta}} \tag{145}$$

Using partial integration we find

$$\langle J_k^{\rm transv};\dot{A}_k\rangle_{\omega+i\eta}=\frac{1}{c^2k^2-\omega^2}\left\{\frac{i\Omega\omega}{\epsilon_0}\langle J_k^{\rm transv};J_k^{\rm transv}\rangle_{\omega+i\eta}+c^2k^2(J_k^{\rm transv};A_k)-i\omega(J_k^{\rm transv};\dot{A}_k)\right\} \tag{146}$$

which can be further treated using the classical or averaged quantities (41),(42)

$$\langle J_k^{\rm transv};\dot{A}_k\rangle_{\omega+i\eta}=\frac{1}{c^2k^2-\omega^2}\,\frac{\Omega}{\epsilon_0}\left\{i\omega\langle J_k^{\rm transv};J_k^{\rm transv}\rangle_{\omega+i\eta}-(J_k^{\rm transv};J_k^{\rm transv})\right\}\,. \tag{147}$$

Subsequently, the dielectric function (69) in the classical limit is

$$\epsilon_{\rm transv}(\vec{k},\omega)=1+\frac{\beta\Omega}{\epsilon_0\omega^2}\,\frac{i\omega\langle J_k^{\rm transv};J_k^{\rm transv}\rangle_{\omega+i\eta}-(J_k^{\rm transv};J_k^{\rm transv})}{1+\frac{\beta\Omega}{\epsilon_0(c^2k^2-\omega^2)}\left\{i\omega\langle J_k^{\rm transv};J_k^{\rm transv}\rangle_{\omega+i\eta}-(J_k^{\rm transv};J_k^{\rm transv})\right\}} \tag{148}$$

Thus the expressions for the transverse and longitudinal dielectric function have the same structure in the limit $k\to 0$, as well as the auto-correlation functions for the electrical current. The denominator reflects the well known prescription from the diagram representation that the polarisation function (self-energy of the photon propagator) contains only irreducible diagrams with respect to the photon propagator.

If the coupling to the photon field, i.e. to the transverse fields $\vec{A}$ or $\vec{E}_{\rm transv}$, is neglected, this is identical with considering Coulomb systems where solely the Coulomb interaction remains. Then also the current auto-correlation function is determined by the equation of motions accounting only for Coulomb interaction, and no photonic interaction is considered. Consequently there are no reducible diagrams in the transverse polarization function, and the denominator in Eq. (148) has to be replaced by 1. This is also possible from the argument that the remaining contribution is of higher order in the transverse coupling. Therefore, for Coulomb systems we have for the dielectric function (69) in the classical limit

$$\epsilon_{\rm transv}^{\rm Coulomb}(\vec{k},\omega)=1+\frac{\beta\Omega}{\epsilon_0\omega^2}\left\{i\omega\,\langle J_k^{\rm transv};J_k^{\rm transv}\rangle_{\omega+i\eta}-\left(J_k^{\rm transv};J_k^{\rm transv}\right)\right\}. \tag{149}$$

This expression has been considered as a starting expression for numerical simulations [65].

Alternatively, the transverse response can also be calculated using the canonical current density $j_k^{\rm transv}$. The total current density is decomposed into an internal current density (86) and an external current density according to (44) which is given after Fourier transformation as

$$\vec{J}_k^{\rm tot}(\omega)=\vec{J}_k(\omega)+\vec{J}_k^{\rm ext}(\omega)\,. \tag{150}$$

Using again the classical relation between the total current density and the vector field (42) as well as the relationship for the internal current density (86), the total current density (150) can be written in terms of the external current density and the canonical current density,

$$J_k^{\rm tot,transv}(\omega)=\left(1+\frac{\omega_{\rm pl}^2}{c^2k^2-\omega^2}\right)^{-1}\left(j_k^{\rm transv}(\omega)+J_k^{\rm ext,transv}(\omega)\right), \tag{151}$$

Subsequently, the transverse dielectric function (55) can be expressed in terms of the canonical current density and the external current density,

$$\epsilon_{\rm transv}(\vec{k},\omega) \;=\; 1-\frac{\omega_{\rm pl}^2}{\omega^2}-\left(1-\frac{c^2k^2+\omega_{\rm pl}^2}{\omega^2}\right)\,\frac{j_k^{\rm transv}}{J_k^{\rm ext,trans}\left(1+\frac{j_k^{\rm transv}}{J_k^{\rm ext,trans}}\right)}\,. \tag{152}$$

In analogy to (144), we find for the canonical current density

$$j_k^{\rm transv}(\omega)=\mathrm{e}^{i\omega t}\langle j_k^{\rm transv}\rangle^t=\beta\langle j_k^{\rm transv};\dot{\vec{A}}_k\rangle_{\omega+i\eta}\cdot J_k^{\rm ext,transv}\,. \tag{153}$$

Substitution into the expression for the dielectric function (152) leads to

$$\epsilon_{\rm transv}(\vec{k},\omega) \;=\; 1-\frac{\omega_{\rm pl}^2}{\omega^2}-\left(1-\frac{c^2k^2+\omega_{\rm pl}^2}{\omega^2}\right)\,\frac{\beta\langle j_k^{\rm transv};\dot{A}_k\rangle_{\omega+i\eta}}{1+\beta\langle j_k^{\rm transv};\dot{A}_k\rangle_{\omega+i\eta}}\,. \tag{154}$$

Using partial integration in analogy to (146), we find

$$\langle j_k^{\rm transv};\dot{A}_k\rangle_{\omega+i\eta}=\frac{1}{c^2k^2-\omega^2}\left\{\frac{i\Omega\omega}{\epsilon_0}\langle j_k^{\rm transv};J_k^{\rm transv}\rangle_{\omega+i\eta}+c^2k^2(j_k^{\rm transv};A_k)-i\omega(j_k^{\rm transv};\dot{A}_k)\right\} \tag{155}$$

which can be further treated using the classical or averaged quantities (41),(42) as well as (143), $\vec{J}(k)=\Omega\,\vec{j}_k-\epsilon_0\omega_{\rm pl}^2\,\vec{A}_k$, which is partially intergrated again. Then,

$$\langle j_k^{\rm transv};\dot{A}_k\rangle_{\omega+i\eta}=\frac{i\Omega\omega}{\epsilon_0}\frac{\langle j_k^{\rm transv};j_k^{\rm transv}\rangle_{\omega+i\eta}}{c^2k^2-\omega^2+\omega_{\rm pl}^2}+(j_k^{\rm transv};A_k^{\rm transv})\,. \tag{156}$$

Since the expressions of correlation functions have been derived within linear response theory, the further analysis can be done neglecting external fields. Thus, the vector potential in the Kubo scalar product can be replaced by the canonical curents via (151) and (42),

$$\langle j_k^{\rm transv};\dot{A}_k\rangle_{\omega+i\eta}=\frac{1}{c^2k^2-\omega^2+\omega_{\rm pl}^2}\,\frac{\Omega}{\epsilon_0}\left\{i\omega\langle j_k^{\rm transv};j_k^{\rm transv}\rangle_{\omega+i\eta}+(j_k^{\rm transv};j_k^{\rm transv})\right\} \tag{157}$$

which is the analogy to (147) with the quantum mechanical phonon propagator in the denominator. Subsequently, the dielectric function (154) in the quantum mechanical limit is

$$\begin{aligned}\epsilon_{\rm transv}(\vec{k},\omega) \quad &= 1-\frac{\omega_{\rm pl}^2}{\omega^2} \\ &+ \quad \frac{\beta\Omega}{\epsilon_0\omega^2}\,\frac{i\omega\langle j_k^{\rm transv};j_k^{\rm transv}\rangle_{\omega+i\eta}+(j_k^{\rm transv};j_k^{\rm transv})}{1-\frac{\beta\Omega}{\epsilon_0(c^2k^2-\omega^2+\omega_{\rm pl}^2)}\left\{i\omega\langle j_k^{\rm transv};j_k^{\rm transv}\rangle_{\omega+i\eta}+(j_k^{\rm transv};j_k^{\rm transv})\right\}}.\end{aligned} \tag{158}$$

A discussion of this expression similar to the one in front of (149) leads to

$$\epsilon_{\rm transv}^{\rm Coulomb}(\vec{k},\omega) \;=\; 1-\frac{\omega_{\rm pl}^2}{\omega^2}+\frac{\beta\Omega}{\epsilon_0\omega^2}\,\left\{i\omega\langle j_k^{\rm transv};j_k^{\rm transv}\rangle_{\omega+i\eta}+(j_k^{\rm transv};j_k^{\rm transv})\right\}\,. \tag{159}$$

3 Quantum Statistical Approach for Dielectric Function

3.1 Equilibrium Correlation Functions

Within this chapter, the microscopic expressions for the dielectric function and related quantities which have been derived applying a generalized linear response theory will be calculated. This involves primarily the calculation of equilibrium correlation functions which are determined using the following Hamiltonian (82)

$$H = \sum_{c,p} E_c(p)\ a^\dagger_{c,p} a_{c,p} + \frac{1}{2} \sum_{cd,pp'q} V_{cd}(q)\ a^\dagger_{c,p-q}\, a^\dagger_{d,p'+q}\, a_{d,p'}\, a_{c,p}\ , \tag{160}$$

where $E_c(p) = \hbar^2 p^2/2m_c$ denotes the kinetic energy, $V_{cd}(q) = e_c e_d/(\epsilon_0 \Omega q^2)$ the Coulomb interaction. Correlation functions can be evaluated basically in two different approaches. Computer simulations, see e.g. [41], are not related to any expansion with respect to a small parameter. However, numerical accuracy may become poor in some limiting cases so that analytical approaches may be in favor. Also, the rigorous quantum treatment is not easily incorporated into molecular dynamics and related simulations. A more detailed discussion will be presented in the context of the dynamical collision frequency in chapter 4.

The other option is the kinetic theory or a thermodynamic Green's function approach. The latter will be pursued in the following. It allows for a systematic perturbation expansion that can be represented by Feynman diagrams. It also highlights the close connection between the thermodynamic properties and non-equilibrium properties when considered within linear response. The relations between the equilibrium correlation functions (112), (113) and

the Green's functions are given according to [34][21]

$$\begin{aligned}(A;B) &= \frac{1}{\beta}\int_{-\infty}^{\infty}\frac{d\omega}{\pi}\,\frac{1}{\omega}\mathrm{Im}\,\mathcal{G}_{AB^\dagger}(\omega+i\eta)\;,\\ \langle A;B\rangle_z &= \frac{i}{\beta}\int_{-\infty}^{\infty}\frac{d\omega}{\pi}\,\frac{1}{z-\omega}\,\frac{1}{\omega}\mathrm{Im}\,\mathcal{G}_{AB^\dagger}(\omega+i\eta)\;.\end{aligned} \tag{165}$$

The thermodynamic Green's functions are obtained from the analytical continuation of $\mathcal{G}_{AB^\dagger}(\omega_\mu)$, calculated at the Matsubara frequencies ω_μ using perturbation theory represented by diagram techniques [11, 30]. Of course, rigorous results are obtained only for some limiting cases where the perturbation expansion is controlled by a small parameter. Partial summations can be performed which allow to take into account effects in higher order of the interaction strength (strong collisions) or due to higher density. It is the main objective of this work to show how the effects of local field corrections and collisions can be included consistently in the theory of dielectric function of non-ideal plasmas.

As was shown in the previous chapter 2, the most relevant quantity in the context of the dielectric function is the electrical current operator $\tilde{\vec{J}}(\vec{k})$ (36) or its spatial density $\vec{J}_k = \tilde{\vec{J}}(\vec{k})/\Omega$. The latter was used throughout chapter 2. From now on we will restrict ourselves to the canonical current density (38)

$$\vec{j}_k = \sum_c \vec{j}_k^{\,c} = \frac{1}{\Omega}\sum_{c,p}\frac{e_c}{m_c}\hbar\,\vec{p}\,n_{p,k}^c\,. \tag{166}$$

unless otherwise stated. While the current densities J are the macroscopic property measurable in experiments and directly related to the classical velocity which is used in computer

[21] This relation can be derived in the following way: Using the eigensolution of the Hamiltonian $H - \sum_c \mu_c N_c|n\rangle = \epsilon_n|n\rangle$, the integrand in the correlation function (112)

$$\mathrm{Tr}\left\{A(t)B^\dagger\varrho_0\right\} = \int_{-\infty}^{\infty}\frac{\mathrm{d}\omega}{2\pi}I_{AB^\dagger}(\omega)\,\mathrm{e}^{i\omega t} \tag{161}$$

can be written as the Fourier transform of the spectral function

$$I_{AB^\dagger}(\omega) = 2\pi\hbar\sum_{nm}\frac{\mathrm{e}^{-\beta\epsilon_n}}{Z}\langle n|A|m\rangle\langle m|B^\dagger|n\rangle\delta(\epsilon_n-\epsilon_m-\hbar\omega)\,. \tag{162}$$

On the other hand, the Matsubara Green's functions can also be expressed via the spectral function [33] according to

$$\mathcal{G}_{AB^+}(z_\nu) = \int_{-\infty}^{\infty}\frac{\mathrm{d}\omega}{2\pi}\frac{e^{\beta\hbar\omega}-1}{z_\nu-\omega}I_{AB^\dagger}(\omega) \tag{163}$$

with $z_\nu = i\nu/(\beta\hbar)$; $\nu = 0, \pm 2, \ldots$ for Bose like operators A, B. Thus we derive the relation

$$\mathrm{Tr}\left\{A(t)B^\dagger\varrho_0\right\} = \frac{1}{\pi}\int_{-\infty}^{\infty}\mathrm{d}\omega\frac{1}{e^{\beta\hbar\omega}-1}\mathrm{Im}\mathcal{G}_{AB^\dagger}(\omega-i\eta)e^{i\omega t}\,. \tag{164}$$

Now, the integrals in (112), (113) can be performed with the result (165) given above.

simulations, the canonical current density is expressed in terms of creation and annihilation operators and therefore directly accessible for perturbation theories based on Feynman diagrams. In the longitudinal response both current densities are identical, see (135). The term which makes the difference between the two definitions is a transverse contribution. However, we are mainly interested in the following in the Coulomb interaction, restricting ourselves to Coulomb systems. The internal transverse fields of photons will not be considered unless otherwise explicitly stated.

The main quantity in the expressions for the longitudinal and transverse response functions and polarization functions are the current–current correlation functions

$$\langle \vec{j}^{\,c}_k; \vec{j}^{\,c'}_k \rangle_{\omega+i\eta} \;=\; \left(\frac{\hbar}{\Omega}\right)^2 \sum_{pp'} \frac{e_c e_{c'}}{m_c m_{c'}} \vec{p}\cdot\vec{p}\,' \langle n^c_{p,k}; n^{c'}_{p',k} \rangle_{\omega+i\eta} \;. \tag{167}$$

According to the Eqs. (165), the equilibrium correlation functions can be expressed in terms of thermodynamic Green's functions. For instance, the density-density correlation function

$$\langle n^c_{p,k}; n^{c'}_{p',k} \rangle_{\omega+i\eta} \;=\; \langle a^\dagger_{p-\frac{k}{2},c} a_{p+\frac{k}{2},c}; a^\dagger_{p'-\frac{k}{2},c'} a_{p'+\frac{k}{2},c'} \rangle_{\omega+i\eta} \tag{168}$$

can be evaluated considering the two–particle Green's function $\mathcal{G}_{nn}(p-\frac{k}{2}, p+\frac{k}{2}; p'-\frac{k}{2}, p'+\frac{k}{2}; \omega_\mu)$, spin and species (c, c') are not given explicitly and should be combined with the momentum variables. In the presentation by Feynman diagrams, $\mathcal{G}_{nn}$ is a four–point Green's function with frequency ω_μ, on the left hand side with incoming $p-\frac{k}{2}$ and outgoing $p+\frac{k}{2}$, on the right hand side with incoming $p'+\frac{k}{2}$ and outgoing $p'-\frac{k}{2}$.

It shall be mentioned for later reference that the correlation function (167) is related to the Kubo scalar product (112) via a partial integration (114). It can be expressed as the commutator of position and linear momentum (cf. [51]). With the particle density n_c we find

$$(\vec{j}^{\,c}_k; \vec{j}^{\,c'}_k) \;=\; \delta_{cc'} \frac{3 e_c^2 n_c}{m_c \beta \Omega} \qquad \text{and} \qquad (\vec{j}_k; \vec{j}_k) \;=\; \frac{3\epsilon_0 \omega_{\rm pl}^2}{\beta\Omega} \tag{169}$$

if the system is considered to be 3 dimensional and isotropic. The plasma frequency is defined as

$$\omega_{\rm pl}^2 = \sum_c \frac{e_c^2 n_c}{\epsilon_0 m_c} \tag{170}$$

see Eq. (37), and appears in Eq. (136) for the longitudinal response. For the transverse response, we derived expression (159). If the last term is rewritten using Eq. (169), the second term is cancelled and leads to

$$\epsilon^{\rm Coulomb}_{\rm transv}(\vec{k}, \omega) = 1 + \frac{i\beta\Omega}{\epsilon_0 \omega} \langle j_k^{\rm transv}; j_k^{\rm transv} \rangle_{\omega+i\eta}. \tag{171}$$

As pointed out in the discussion leading to Eq. (149), there are no reducible diagrams contributing to the transverse current-current correlation function as long as only Coulomb interaction is considered. This expression can be directly analysed in perturbation theory.

In the longitudinal case, we have two different possibilities to carry out the perturbation expansion. Firstly, we can expand the current-current correlation function occurring in the Kubo formula (129). Note that the canonical current density and the quantummechanical current density are identical in the longitudinal case, see Eq. (135). The inverse longitudinal dielectric function (73) is then given as

$$\epsilon_{\rm long}^{-1}(\vec{k},\omega) = 1 + \frac{1}{\epsilon_0 k^2}\chi_{\rm long}(\vec{k},\omega) = 1 - \frac{i\beta\Omega}{\epsilon_0\omega}\langle j_k^{\rm long}; j_k^{\rm long}\rangle_{\omega+i\eta}. \tag{172}$$

Inspection of the perturbation expansion of the current-current correlation function, Eq. (167), using the representation by Feynman diagrams shows that $\langle j_k^{\rm long}; j_k^{\rm long}\rangle_{\omega+i\eta} = \langle j_k^{\rm long}; j_k^{\rm long}\rangle_{\omega+i\eta}^{\rm (irred)}$ / $\epsilon_{\rm long}(\vec{k},\omega)$. The index (irred) denotes such irreducible diagrams contributing to the current-current correlation function which cannot be separated into two pieces by cutting a single interaction line. In fact, we are performing a perturbation expansion for the longitudinal polarization function $\Pi_{\rm long}(\vec{k},\omega)$, Eq. (69), or the longitudinal dielectric function

$$\epsilon_{\rm long}(\vec{k},\omega) = 1 + \frac{i\beta\Omega}{\epsilon_0\omega}\langle j_k^{\rm long}; j_k^{\rm long}\rangle_{\omega+i\eta}^{\rm (irred)} \tag{173}$$

which is in analogy to the transverse case (171).

Secondly, the response function (132) is applied giving

$$\epsilon_{\rm long}^{-1}(\vec{k},\omega) = 1 - \frac{i\beta\Omega}{\epsilon_0\omega}\,\frac{1}{M(\vec{k},\omega)}\,. \tag{174}$$

Specifying the set of quantum operators $\{B_n\}$ as the electrical current $\vec{j}_k$ only, the inverse response function is given according to Eqs. (137) as

$$\begin{aligned} M(\vec{k},\omega) &= \frac{M_{jj}(\vec{k},\omega)}{(j_k^{\rm long}; j_k^{\rm long})^2} = \frac{1}{\langle j_k^{\rm long}; j_k^{\rm long}\rangle_{\omega+i\eta}}, \qquad (175)\\ M_{jj}(\vec{k},\omega) &= -i\omega\ (j_k^{\rm long}; j_k^{\rm long}) + \langle \dot{j}_k^{\rm long}; \dot{j}_k^{\rm long}\rangle_{\omega+i\eta} - \frac{\langle \dot{j}_k^{\rm long}; j_k^{\rm long}\rangle_{\omega+i\eta}}{\langle j_k^{\rm long}; j_k^{\rm long}\rangle_{\omega+i\eta}}\ \langle j_k^{\rm long}; \dot{j}_k^{\rm long}\rangle_{\omega+i\eta}\ . \end{aligned}$$

The perturbation expansion of $M_{jj}(\vec{k},\omega)$ is considered with respect to the coupling parameter e^2 on which we will focus now. The generalization to a more extended set of quantum operators $\{B_n\}$ is straightforward, see Sec. 4.4 (Chap. 4).

Apart from the particle current operators $\vec{j}_k^{\,c}$ further correlation functions arise due to the appearance of time derivatives ("forces") $\dot{\vec{j}}_k^{\,c}$. Taking the time derivative by applying the commutator relation with the Hamiltonian for Coulomb systems (82) according to (22), we arrive at expressions containing

$$\begin{aligned} \dot{n}_{p,k}^c &= \frac{i}{\hbar}[H, n_{p,k}^c] = -\frac{i\vec{k}}{m_c}\,\hbar\vec{p}\,n_{p,k}^c + v_{p,k}^c\ , \\ v_{p,k}^c &= \frac{i}{\hbar}\sum_{p'q\bar{p}d} V_{cd}(q)\,\left\{\delta_{\bar{p},p-\frac{q}{2}} - \delta_{\bar{p},p+\frac{q}{2}}\right\}\,a^\dagger_{\bar{p}-\frac{k}{2}-\frac{q}{2},c}a^\dagger_{p'+\frac{q}{2},d}a_{p'-\frac{q}{2},d}a_{\bar{p}+\frac{k}{2}+\frac{q}{2},c}\ . \end{aligned} \tag{176}$$

Due to the potential dependent part $v^c_{p,k}$ higher order correlation functions will occur. However, this second approach is more suitable to a perturbative treatment and is directly related to the dynamical collision frequency, as shown in Section 3.4. The systematic evaluation of the correlation functions will be given in chapter 4.

3.2 Collisionless Plasma - Random Phase Approximation

Before presenting the perturbation expansions using a diagram technique, we discuss in this Section the lowest approximation to the dielectric function. The Hamiltonian H (29) contains the free fermion and photon fields as well as interaction terms, the latter contain the charge e which may be considered as coupling constant. Perturbation expansion can be performed with respect to e, starting in zeroth order with an ideal fermion gas for the different components and photons. In this approximation, all correlation functions can be evaluated using Wick's theorem [30, 33]. In particular, expressions for the electrical charge density or current density auto-correlation functions are obtained.

However, such a definition of a zeroth order approximation describes no response of the system to external perturbations because any coupling is neglected, and the trivial result $\epsilon(\vec{k},\omega) = 1$ follows. To describe the response to external fields we need the coupling to the external charge or current densities. Then, the starting point for a perturbation expansion is the mean field approximation. In the well-known way, the Hamiltonian H is replaced by an optimal single-particle Hamiltonian $H^{\rm mf}$ which is obtained rewriting the interaction term in (160) according to

$$\frac{1}{2}\sum_{cd,pp'k} V_{cd}(k) a^\dagger_{c,p-k} a^\dagger_{d,p'+k} a_{d,p'} a_{c,p} \approx \sum_{cd,pp'k} V_{cd}(k) a^\dagger_{c,p-k} a_{c,p} \langle a^\dagger_{d,p'+k} a_{d,p'}\rangle \tag{177}$$

and neglecting the quadratic term describing fluctuations around the mean values. Here we assume that the anomal averages such as $\langle a_{d,p'} a_{c,p}\rangle$ describing a superfluid state vanish. The remaining Hamiltonian $H^{\rm mf}$ can be diagonalized, and similar to the free particle case all correlation functions are calculated using Wick's theorem. The new quasiparticles contain the mean field $\propto \langle a^\dagger_{d,p'+k} a_{d,p'}\rangle$ which has to be determined in a self-consistent way, using the equilibrium statistical operator with $H^{\rm mf}$.

Because any correlations in the plasma are neglected in this approximation, collisions cannot be described, and this approximation is denoted as collisionless plasma or the Random-Phase-Approximation (RPA). Within a kinetic approach, see also Sect. 2.3, this corresponds to the Vlasov equation which is obtained from the Boltzmann equation if any contribution from the collision term beyond the mean field is neglected. Derivations within the kinetic theory can be found in [66, 67]. We will follow the scheme of the generalized linear response theory as derived in the previous chapter and section.

The density-density correlation function (168) can easily be calculated for the zeroth order by using the Wick theorem [33, 30]. Since we want to consider higher perturbation theory later on we use the connection to Green's functions and Feynman diagrams. The

Born approximation is obtained if incoming and outgoing lines are connected, corresponding to a simple bubble (single loop) $\mathcal{G}^{(0)}_{nn}$. It means that the two-particle Green's function is approximated by the product of two single-particle Green's functions of the ideal system

$$\mathcal{G}^{(0)}_{nn}\left(p-\frac{k}{2},p+\frac{k}{2};p'-\frac{k}{2},p'+\frac{k}{2};\omega_\mu\right) \;=\; \delta_{cc'}\delta_{pp'}\sum_{z_\nu}\frac{1}{z_\nu-E^c_{p+\frac{k}{2}}}\,\frac{1}{z_\nu+\omega_\mu-E^{c'}_{p-\frac{k}{2}}}.$$

With the relation (162), this leads to

$$\langle n^c_{p,k};n^{c'}_{p',k}\rangle^{(0)}_{\omega+i\eta} \;=\; \delta_{cc'}\,\delta_{pp'}\,\frac{\hbar}{i\beta}\,\frac{1}{\Delta E^c_{p,k}}\,\frac{f^c_{p+\frac{k}{2}}-f^c_{p-\frac{k}{2}}}{\Delta E^c_{p,k}-\hbar(\omega+i\eta)} \tag{178}$$

with $\Delta E^c_{p,k}=E^c_{p+\frac{k}{2}}-E^c_{p-\frac{k}{2}}=\hbar^2\vec{k}\cdot\vec{p}/m_c$, and $f^c_p=[\exp(\beta E^c_p-\beta\mu_c)+1]^{-1}$ denotes the Fermi distribution function, $\beta=1/(k_BT)$ the inverse temperature, and μ_c the chemical potential of species c. The limit $\eta\to 0$ has to be taken after the thermodynamic limit. Here and in all what follows we will omit the index $\omega+i\eta$ when writing correlation functions of the type $\langle A;B\rangle_{\omega+i\eta}$.

Expression (178) gives the irreducible part in the zeroth order with respect to e. Taking it as the lowest order of the perturbation expansion of the polarization function $\Pi(\vec{k},\omega)$, Eq. (131), given by the irreducible part of the current-current correlation function, the RPA expression for the dielectric function of a non-interacting fermion gas [68, 69][22],

$$\Pi^{(0)}_{\rm long}(\vec{k},\omega)=\Pi^{\rm RPA}(\vec{k},\omega) \;=\; \sum_c\Pi^{\rm c,RPA}(\vec{k},\omega)=\frac{1}{\Omega}\sum_{p,c}e_c^2\,\frac{f^c_{p+\frac{k}{2}}-f^c_{p-\frac{k}{2}}}{\Delta E^c_{p,k}-\hbar(\omega+i\eta)}, \tag{179}$$

is found. The limit $\eta\to 0$ can be performed using Dirac's identity. Analytical expressions for various limiting cases can be found in [70, 71]. Note, that due to the structure of the polarization function the validity of the Kramers-Kronig relation (56) can be seen readily. Expression (179) is of second order with respect to e. Correspondingly, the response function χ contains arbitrary orders with respect to e. The dielectric function and related quantities are found in the RPA according to the expressions given above.

For the transverse polarization function we find from (171),(69) and the current–current correlation function (167) with (178) the following expression [68, 72]

$$\tilde{\Pi}^{(0)}_{\rm transv}(\vec{k},\omega) \;=\; \epsilon_0\omega^2_{\rm pl}-\frac{\hbar^2}{\Omega}\sum_{p,c}\frac{e_c^2}{m_c^2}\,p_x^2\,\frac{f^c_{p+\frac{k}{2}}-f^c_{p-\frac{k}{2}}}{\Delta E^c_{p,k}-\hbar(\omega+i\eta)}. \tag{180}$$

If the distribution functions f^c_p are taken as Boltzmann distributions and the long-wavelength limit is considered, the classical expression [67]

$$\tilde{\Pi}^{(0)}_{\rm transv}(\vec{k},\omega) \;=\; \epsilon_0\omega^2_{\rm pl}\left\{1-\beta\sum_c m_c\int{\rm d}^3\vec{v}\,\frac{kv_z}{kv_z-\omega}\,\frac{{\rm e}^{-\beta m_cv^2/2}}{\int{\rm d}^3\vec{v}\,{\rm e}^{-\beta m_cv^2/2}}\right\} \tag{181}$$

[22]This expression is valid for 2 as well as 3 dimensional systems. In the following only the 3 dimensional system is considered. Explicit results for 2 dimensional systems will be given as footnotes.

is obtained.

In the static limit, the imaginary part of (179) vanishes whereas the real part can be written as

$$\lim_{\omega\to 0}\ \Pi^{\rm RPA}(\vec{k},\omega) \ = \ \frac{1}{\Omega}\sum_{p,c} e_c^2\, f_p^c \left(\frac{1}{E_p^c - E_{p-k}^c} - \frac{1}{E_{p+k}^c - E_p^c}\right) .$$

For the longitudinal dielectric function (69), we consider the limits for small and large wave vectors[23]

$$\begin{aligned}
\lim_{k\to\infty}\ \epsilon_{\rm long}(\vec{k},\omega) &= 1 + 4\sum_c \frac{n_c\, e_c^2 m_c}{\epsilon_0 \hbar^2 k^4} , \\
\lim_{k\to 0}\ \epsilon_{\rm long}(\vec{k},\omega) &= 1 + \left(\frac{\kappa}{k}\right)^2 .
\end{aligned} \tag{182}$$

The screening parameter κ is expressed via a Fermi integral

$$\kappa^2 \ = \ \sum_c \frac{e_c^2 m_c^{3/2}}{\sqrt{2}\pi^2\epsilon_0\hbar^3} \int_0^\infty dE_p^c\, (E_p^c)^{-1/2}\, f_p^c \tag{183}$$

for arbitrary degeneracy and reduces to Debye screening $\kappa_D^2 = \beta\, e^2 n/\epsilon_0$ in the nondegenerate limit and the Thomas-Fermi parameter $\kappa_{TF}^2 = e^2 m k_F/(\pi^2\hbar^2\epsilon_0)$ in the degenerate limit[24]. The Debye radius can vary in dependence of temperature and density over a wide range. Typical values for a dense non-degenerate plasma would be between $10\, a_B$ and $10^4\, a_B$.

In the long wavelength limit, the relation

$$\lim_{k\to 0} \langle j_k^{\rm long}; j_k^{\rm long}\rangle_{\omega+i\eta}^{(0)} \ = \ \frac{i}{3\omega}\, (\vec{j}_k; \vec{j}_k) \tag{184}$$

holds and with (169) we find

$$\lim_{k\to 0}\ \Pi^{\rm RPA}(\vec{k},\omega) \ = \ \epsilon_0 k^2\, \frac{\omega_{\rm pl}^2}{\omega^2} , \tag{185}$$

with the plasma frequency $\omega_{\rm pl}$, see (170)[25].

[23] For 2dim systems, the second expression of the long-wavelength limit is $\lim_{k\to 0}\ \epsilon_{\rm long}(\vec{k},0) = 1 + \kappa_{2D}/k$. The screening parameter $\kappa_{2D} = e^2 m/(2\pi\epsilon_0\hbar^2)$ is density independent and comparable with the atomic size $a_B = 2/\kappa_{2D}$, see e.g. [63]

[24] The limiting cases are given for a one component system.

[25] In the 2-dimensional case, the plasma frequency $\omega_{\rm pl}^2 = e^2 n k/(2\epsilon_0 m)$ is dependent on the wave vector. The Fourier transforms of the Coulomb potential $V(r) = 1/(4\pi\epsilon_0 r)$ is $V_{2D}(q) = 1/(2\epsilon_0\Omega q)$. Ω denotes the normalization area. The RPA dielectric function in the long-wavelength limit is $\lim_{k\to 0}\ \Pi^{\rm RPA}(\vec{k},\omega) = 2\epsilon_0 k\omega_{\rm pl}^2/\omega^2$.

Performing the integrations in (179) explicitely, we find the RPA dielectric function for arbitrary degeneracy as given by Arista *et al.* [70][26].

$$\begin{aligned} \mathrm{Re}\,\epsilon_{\mathrm{long}}(k,\omega) &= 1 + \frac{2\,k_F^2}{\pi\,a_B\,k^3}\,\left[g(u+z) - g(u-z)\right] \quad , \\ \mathrm{Im}\,\epsilon_{\mathrm{long}}(k,\omega) &= \frac{8\pi\epsilon_0}{\beta e^2 a_B^2\,k^3}\ln\frac{1+\exp(\beta\mu - (u-z)^2\beta\,E_F)}{1+\exp(\beta\mu-(u+z)^2\beta\,E_F)} \end{aligned}$$

with

$$\begin{aligned} g(x) &= \int_0^\infty dy\,y\ln\left(\frac{|x+y|}{|x-y|}\right)\,f(y^2E_F)\,, \\ u = \frac{m\,\omega}{\hbar\,k\,k_F}, \qquad z &= \frac{k}{2\,k_F} \qquad \text{and} \qquad k_F^3 = 3\pi^2 n\,. \end{aligned} \tag{186}$$

In the non–degenerate case (classical limit $\beta E_F \ll 1$), this can be written as

$$g(x) = \frac{2}{3}\sqrt{\beta E_F}\mathcal{D}(\sqrt{\beta E_F}\,x) \tag{187}$$

with the Dawson integral

$$\mathcal{D}(x) = \frac{1}{\sqrt{\pi}}\int_{-\infty}^{\infty}\frac{\mathrm{e}^{-t^2}\mathrm{d}t}{x-t}. \tag{188}$$

The dielectric function follows as

$$\epsilon_{\mathrm{long}}(\vec{k},\omega) = 1 + \frac{\beta e^2 n}{\epsilon_0 k^2}\left\{1 + x\mathcal{D}(x)\right\} = 1 + \frac{\kappa_D^2}{k^2}\left\{1 + x\mathcal{D}(x)\right\} \tag{189}$$

with $x = \sqrt{m/2k_BT}\,\omega/k$. In analogy, the relation (181) for the transverse dielectric function can be expressed in terms of Dawson intergrals as well,

$$\epsilon_{\mathrm{transv}}(\vec{k},\omega) = 1 + \frac{\omega_{\mathrm{pl}}^2}{\omega^2}\mathcal{D}(x) \tag{190}$$

[26]The general expression (179) is valid for two-dimensional systems as well. The explicit treatment of the integrals for $T = 0$ was first given by Stern [73]. For arbitrary temperature, the expression for the dielectric function is [74]

$$\begin{aligned} \mathrm{Re}\,\epsilon_{\mathrm{long}}(k,\omega) &= 1 + \frac{k_F}{a_B\,k^2}\,\left[h_1(u+z) - h_1(u-z)\right]\,, \\ \mathrm{Im}\,\epsilon_{\mathrm{long}}(k,\omega) &= \frac{k_F}{a_B\,k^2}\,\left[h_2(u-z) - h_2(u+z)\right]\,. \end{aligned}$$

The variables u, z are defined as in (186), but the Fermi wave vector is $k_F^2 = 2\pi n$. The functions introduced above are integrals over the Fermi functions,

$$\begin{aligned} h_1(x) &= \int_0^1 dy\,\frac{y}{\sqrt{1-y}}\,f[yx^2E_F], \\ h_2(x) &= \int_0^\infty \frac{dy}{\sqrt{u}}\,f[(y+x^2)E_F]\,. \end{aligned}$$

The RPA approximation, which describes the collisionless plasma, satifies the first moment sum rules (57) and limiting relations (58) - (60) given in Section 1.5. However, it can't describe electrical transport (conductivity) since interactions are not taken into account. Going beyond the RPA, two important effects should be included to describe the optical properties as well as the electrical conductivity. We have to take into account (i) scattering processes between the particles and (ii) the formation of bound states. Referring to other works [11, 29, 75] for the inclusion of bound states into the dielectric function, we will focus on the treatment of collisions to bridge between the theory of dielectric function and the conductivity for the fully ionized plasma.

3.3 Dynamical Local-Field Corrections

Traditionally, the static limit ($\omega = 0$) has been improved by using the concept of local-field factors as proposed by Hubbard empirically. Hubbard [76] introduced a correction factor $G(\vec{k})$ to the RPA in order to account for the exchange and correlation hole around an electron. It increases the dielectric screening. The concept of local-field factors for 2 and 3-dimensional systems, see [37, 77, 78, 79, 80] and references therein, in the static limit ($\omega = 0$) has been extended to finite frequencies by introducing dynamical local-field factors $G(\vec{k}, \omega)$ in precisely the same form as the Hubbard corrections according to[27]

$$\Pi_{\rm long}(\vec{k},\omega) \;=\; \frac{1}{(\Pi^{\rm RPA})^{-1}(\vec{k},\omega) + G(\vec{k},\omega)/(\epsilon_0 k^2)} \; . \tag{192}$$

Different approximative methods to determine $G(\vec{k}, \omega)$ have been developed such as perturbation expansions [81][28] and the parameterization of the dielectric function via sum rules [39, 71]. In particular, it has been shown that the third moment sum rule (57) is important in the construction of dynamic approximations [71, 80]. A study of the dynamical local-field factors within a time-dependent mean-field theory neglecting damping effects was reported by Kalman *et al.* [82].

Rearranging Eq. (192) as

$$G(\vec{k},\omega) = \epsilon_0 k^2 \left[\frac{1}{\Pi_{\rm long}(\vec{k},\omega)} - \frac{1}{\Pi^{\rm RPA}(\vec{k},\omega)} \right] \tag{193}$$

[27] Alternatively, the local-field factor can be defined via

$$\Pi_{\rm long}(\vec{k},\omega) = \frac{\Pi^{\rm RPA}(\vec{k},\omega)}{1 + G(\vec{k},\omega)\,\Omega V(k) \Pi^{\rm RPA}(\vec{k},\omega)} \tag{191}$$

which is then valid for the 2-dim and 3-dim case.

[28] A similar procedure is common when performing the perturbation expansion of Green's functions. Near the poles of the unperturbed Green's functions such an expansion is not possible. However, with the help of the Dyson equation the self-energy is introduced in the denominator, and for the latter quantity a perturbation expansion is possible.

shows, that the local field corrections are rather expansions with respect to the inverse polarization function. Replacing the polarization function by the response function $\chi(\vec{k},\omega)$ via (73) with (132), the dynamical local-field factors $G(\vec{k},\omega)$ are directly related to the inverse response function $M(\vec{k},\omega)$, which was introduced in Eq. (174), according to

$$G(\vec{k},\omega) \;=\; -i\,\frac{\epsilon_0\omega}{\beta\Omega}M(\vec{k},\omega) - \epsilon_0 k^2 \frac{1}{\Pi^{\rm RPA}(\vec{k},\omega)} + 1. \tag{194}$$

where the general expression (169) was used.

Let us analyse the perturbation expansion of the expression of the inverse response function $M(\vec{k},\omega)$ (137). We are considering all diagrams, corresponding to the perturbation expansion of $\chi(\vec{k},\omega)$, in contrast to $\Pi(\vec{k},\omega)$ where only irreducible diagrams are considered. In lowest order with respect to e^2 we have[29]

$$M^{(0)}(\vec{k},\omega) = i\frac{\beta\Omega k^2}{\omega}\frac{1}{\Pi^{\rm RPA}(\vec{k},\omega)} \tag{195}$$

and $G^{(0)}(0,\omega)$ is zero[30] since the last term in Eq. (194) contributes in next order only. Notice that contributions in the lowest order arise from $\dot{\vec{J}}_k^{\rm el}$ which are produced from the kinetic part of $\dot{n}^c_{p,k}$ in Eq. (176), not from the interaction part $\upsilon^c_{p,k}$.

In the next order of perturbation expansion, diagrams with one interaction line have to be considered. The irreducible first-order contributions of Eq. (168)

$$\begin{aligned}
\langle n^c_{p,k}; n^{c'}_{p',k}\rangle^{(\rm irred,1)}_{\omega+i\eta} \;&=\; \delta_{cc'}\,\frac{\hbar}{i\beta}\,\frac{1}{\Delta E^c_{p,k}}\,\frac{f^c_{p-\frac{k}{2}} - f^c_{p+\frac{k}{2}}}{\Delta E^c_{p,k} - \hbar(\omega+i\eta)} \\
&\times\Bigg[\;-\; \delta_{pp'}\sum_{p''} V_{cc}(p-p'')\,\frac{1}{\Delta E^c_{p,k}}\,\frac{f^c_{p''-\frac{k}{2}} - f^c_{p''+\frac{k}{2}}}{\Delta E^c_{p,k} - \hbar(\omega+i\eta)}\,\left(2\Delta E^c_{p,k} - \hbar\omega\right) \\
&\quad +\; V_{cc}(p-p')\,\frac{1}{\Delta E^c_{p',k}}\,\frac{f^c_{p'-\frac{k}{2}} - f^c_{p'+\frac{k}{2}}}{\Delta E^c_{p',k} - \hbar(\omega+i\eta)}\,\left(\Delta E^c_{p,k} + \Delta E^c_{p',k} - \hbar\omega\right)\Bigg]
\end{aligned} \tag{196}$$

are due to self-energy and vertex corrections which arise from the corresponding Feynman diagrams when expanding the Green's function $\mathcal{G}_{nn}$ up to first order in e^2. For the current-current correlation function the first-order contribution follows as

$$\begin{aligned}
\langle \vec{j}_k; \vec{j}_k\rangle^{(\rm irred,1)}_{\omega+i\eta} = \;& -\frac{i}{2}\,\frac{\omega}{\hbar^4\Omega^2\beta k^4}\sum_{pp'c}(m_c e_c)^2\left(f^c_{p+\frac{k}{2}} - f^c_{p-\frac{k}{2}}\right)V_{cc}(\vec{p}-\vec{p}')\left(f^c_{p'+\frac{k}{2}} - f^c_{p'-\frac{k}{2}}\right) \\
&\times\left(\frac{1}{p_z - m_c(\omega+i\eta)/(\hbar k)} - \frac{1}{p'_z - m_c(\omega+i\eta)/(\hbar k)}\right)^2.
\end{aligned} \tag{197}$$

[29]The upper index coincides with the power of e^2 in the perturbation expansion of the density–density correlation function

[30]Of course, this can also be directly seen from (193).

In addition, there are further reducible diagrams of first order where the interaction line connects two loops. The latter are immediately evaluated with the result

$$M^{(\mathrm{red},1)}(\vec{k},\omega) = -i\,\frac{\beta\Omega}{\epsilon_0\omega}\ . \tag{198}$$

Together with the contribution, cf. Eq. (197),

$$M^{(\mathrm{irred},1)}(\vec{k},\omega) = \frac{\langle\vec{j}_k;\vec{j}_k\rangle^{(\mathrm{irred},1)}_{\omega+i\eta}}{\left[\langle\vec{j}_k;\vec{j}_k\rangle^{(0)}_{\omega+i\eta}\right]^2} \tag{199}$$

to the first order contribution of the inverse response function, we find within the single-moment approach for the dynamical local-field factor, Eq. (194), the result

$$G^{(1)}(\vec{k},\omega) = \, i\,\frac{\epsilon_0\beta\Omega k^4}{\omega}\,\left[\Pi^{\mathrm{RPA}}(\vec{k},\omega)\right]^{-2}\,\langle\vec{j}_k;\vec{j}_k\rangle^{(\mathrm{irred},1)}_{\omega+i\eta}\,, \tag{200}$$

see also [83] for the expression of an one-component system. Note that the reducible first order term is compensated by the 1 in Eq. (194). Thus, the account of only one reducible term $M^{(\mathrm{red},1)}(\vec{k},\omega)$ is equivalent to an infinite partial summation in $\chi(\vec{k},\omega)$ leading to the RPA result. There are no cross terms between different components in the first order.

An analytical expression for $G^{(1)}(\vec{k},\omega)$ at zero temperature as given in [81] and the result for the static limit $G^{(1)}(\vec{k},0)$ as given in [84], can be recovered from our expression. The limiting cases are in accordance with the compressibility sum rule, $\lim_{k\to 0} G^{(1)}(\vec{k},0) = k^2/(4\,k_F^2)$, and the relation to the pair distribution at zero distance, $\lim_{k\to\infty} G^{(1)}(\vec{k},0) = 1/3$, which are correct within the order of perturbation theory considered here, i.e. comparing with properties of the uncorrelated fermion gas [85]. The analytical evaluation in the full $(\vec{k},\omega)$-plane is possible following the same procedure as in [81], but will not be given here. The static local field corrections are important for large wave vectors (small distances) and low densities. A better approach should go beyond the first order contributions and relate the local field corrections self-consistently to the structure factor or pair distribution function as proposed in the classical work of Singwi *et al.* [77] and elaborated further by others. Similar relations should be derived for the dynamical local field factor.

The long-wavelength limit $k \to 0$ is of particular interest when calculating optical conductivities. Using the relations

$$\begin{aligned}
\lim_{k\to 0}\,(f_{p+\frac{k}{2}} - f_{p-\frac{k}{2}}) &= -\beta\, f_p(1-f_p)\,\frac{\hbar^2 k}{m}\,p_z\ , \\
\lim_{k\to 0}\,\left(\frac{1}{p_z - \frac{m\omega}{\hbar k} - i\eta} - \frac{1}{p'_z - \frac{m\omega}{\hbar k} - i\eta}\right) &= \left(\frac{\hbar k}{\omega}\right)^2\,(p'_z - p_z)
\end{aligned}$$

as well as (185) it follows from (200)

$$\lim_{k\to 0} G^{(1)}(k,\omega) = \frac{k^2}{2\Omega_0}\,\frac{\epsilon_0\hbar^4\beta^2}{(e\,m\,n)^2}\,\sum_{pp'}\,f_p(1-f_p)\,V(|\mathbf{p}-\mathbf{p}'|)f_{p'}(1-f_{p'})\,p_z p'_z(p_z-p'_z)^2\ . \tag{201}$$

Thus, this expression is $\propto k^2$ and no contribution from terms of first order in V will modify the behavior in the long-wavelength limit $k \to 0$ [63, 86].

3.4 Dynamical Collision Frequency

The dynamical conductivity tensor has been defined in the first chapter (64). Within this section we are mainly interested in the longitudinal dynamical conductivity according to

$$\epsilon(\vec{k},\omega) = 1 + \frac{i}{\epsilon_0 \omega}\sigma_{\rm long}(\vec{k},\omega) \tag{202}$$

In order to describe it on an appropriate approximation level, we have to go beyond the zeroth and first order contributions with respect to the interaction strength and include collisions. For this we define a dynamical collision frequency [87] according to

$$\sigma_{\rm long}(\vec{k},\omega) = \frac{\epsilon_0\, \omega_{\rm pl}^2}{-i\,\omega\, + \nu(\vec{k},\omega)} \tag{203}$$

It is also called the *internal conductivity* [88, 89]. Similar expressions have been suggested and used by Kurilenko *et al.* [90, 91]. Expression (203) is a generalization of the phenomenological Drude formula, see e.g. Ref. [30][31].

The discussion of the dielectric function can be based on the perturbation expansion of the current-current correlation function $\langle \vec{j}_k; \vec{j}_k\rangle^{\rm (irred)}_{\omega+i\eta}$, see (173). However, such an expansion will not converge near frequency $\omega = 0$ in the long-wavelength limit where the dc-conductivity is obtained. This is already clearly seen from the lowest order result, equation (185), which is diverging in the limit $\omega \to 0$. Making use of partial integration and the fact that due to the Kubo identity $(A; \dot{A}) = i/(\hbar\beta)\,\langle [A, A]\rangle = 0$, we can express the current-current correlation function as

$$\langle \vec{j}_k; \vec{j}_k\rangle_{\omega+i\eta} \;=\; \frac{i}{\omega}\,\left(\vec{j}_k; \vec{j}_k\right) + \frac{1}{\omega^2}\,\langle \dot{\vec{j}}_k; \dot{\vec{j}}_k\rangle_{\omega+i\eta} \tag{205}$$

by the Kubo scalar product, Eq. (169), and a force-force correlation function $\langle \dot{\vec{j}}_k; \dot{\vec{j}}_k\rangle_{\omega+i\eta}$.

Expressing the time derivative $\dot{\vec{j}}^{\,c}_k$ of the particle current operators according to Eq. (176)

[31] The transverse conductivity is defined in analogy to the longitudinal (203) as

$$\sigma_{\rm transv}(\vec{k},\omega) = \frac{\epsilon_0\, \omega_{\rm pl}^2}{-i\,\omega\, + \widetilde{\nu}(\vec{k},\omega)} \tag{204}$$

where $\widetilde{\nu}(\vec{k},\omega)$ is commonly called memory function [92, 93]. It's relation to correlation functions will be further discussed in paragraph 5.6 in the context of implementation of MD simulations.

we have

$$\langle \dot{\vec{j}}^{c}_{k}; \dot{\vec{j}}^{c'}_{k} \rangle_{\omega+i\eta} = \frac{\hbar^2}{\Omega^2} \frac{e_c e_{c'}}{m_c m_{c'}} \sum_{pp'} \vec{p}\vec{p}\prime \Bigg[\langle v^{c}_{p,k}; v^{c'}_{p,k'} \rangle_{\omega+i\eta} + \frac{\hbar^2 k^2}{m_c m_{c'}} p_z p'_z \langle n^{c}_{p,k}; n^{c'}_{p',k} \rangle_{\omega+i\eta} + i\frac{\hbar k}{m_{c'}} p'_z \langle v^{c}_{p,k}; n^{c'}_{p',k} \rangle_{\omega+i\eta} - i\frac{\hbar k}{m_c} p_z \langle n^{c}_{p,k}; v^{c'}_{p',k} \rangle_{\omega+i\eta} \Bigg] . \tag{206}$$

In order to collect all contributions to the time dependent correlation function in second order Born approximation we apply the following relations ($z = \omega + i\eta$)

$$\begin{aligned} \langle n^{c}_{p,k}; n^{c'}_{p',k} \rangle_z &= -i\hbar \frac{(n^{c}_{p,k}; n^{c'}_{p',k}) + \langle v^{c}_{p,k}; n^{c'}_{p',k} \rangle_z}{\Delta E^{c}_{p,k} - \hbar z} = -i\hbar \frac{(n^{c}_{p,k}; n^{c'}_{p',k}) - \langle n^{c}_{p,k}; v^{c'}_{p',k} \rangle_z}{\Delta E^{c'}_{p',k} - \hbar z}, \\ \langle n^{c}_{p,k}; v^{c'}_{p',k} \rangle_z &= -i\hbar \frac{(n^{c}_{p,k}; v^{c'}_{p',k}) + \langle v^{c}_{p,k}; v^{c'}_{p',k} \rangle_z}{\Delta E^{c}_{p,k} - \hbar z} \end{aligned} \tag{207}$$

which can be proven by partial integration. Substituting these into Eq. (206), we write the force-force correlation function as

$$\begin{aligned} \langle \dot{\vec{j}}^{c}_{k}; \dot{\vec{j}}^{c'}_{k} \rangle_z = \frac{\hbar^2}{\Omega^2} \frac{e_c e_{c'}}{m_c m_{c'}} \sum_{pp'} \vec{p}\cdot\vec{p}\prime \Bigg[& (\hbar\omega)^2 \frac{\langle v^{c}_{p,k}; v^{c'}_{p,k'} \rangle_z}{\left(\Delta E^{c}_{p,k} - \hbar z\right)\left(\Delta E^{c'}_{p',k} - \hbar z\right)} \\ & - \frac{i}{\hbar} \frac{\Delta E^{c}_{p,k} \Delta E^{c'}_{p',k}}{\Delta E^{c}_{p,k} - \hbar z} \left(n^{c}_{p,k}; n^{c'}_{p',k}\right) - \frac{\Delta E^{c}_{p,k}}{\Delta E^{c}_{p,k} - \hbar z} \left(n^{c}_{p,k}; v^{c'}_{p',k}\right) \\ & - \hbar\omega \frac{\Delta E^{c}_{p,k}}{\left(\Delta E^{c}_{p,k} - \hbar z\right)\left(\Delta E^{c'}_{p',k} - \hbar z\right)} \left(v^{c}_{p,k}; n^{c'}_{p',k}\right) \Bigg] . \end{aligned} \tag{208}$$

In this expression, the first term is explicitly proportional to e^6, thus the correlation function $\langle v^{c}_{p,k}; v^{c'}_{p',k} \rangle_z$ itself can be treated at zeroth order when evaluating $\langle \vec{j}_k; \vec{j}_k \rangle^{(\mathrm{irred},2)}_{\omega+i\eta}$. All other terms have to be evaluated within first or second-order perturbation theory.

Because of $\Delta E^{c}_{p,k} = \hbar p_z k/m_c \propto k$ they do not contribute to the second order in the long-wavelength limit, cf. [51] and we arrive at the force-force correlation function

$$\lim_{k\to 0} \langle \vec{j}_k; \vec{j}_k \rangle^{(\mathrm{irred},2)}_{\omega+i\eta} = \frac{1}{\omega^2} \langle \dot{\vec{j}}_0; \dot{\vec{j}}_0 \rangle^{(2)}_{\omega+i\eta} = \frac{\hbar^2}{\Omega^2\omega^2} \sum_{pp',cc'} \frac{e_c e_{c'}}{m_c m_{c'}} \vec{p}\cdot\vec{p}\prime \lim_{k\to 0} \langle v^{c}_{p,k}; v^{c'}_{p',k} \rangle_{\omega+i\eta} . \tag{209}$$

As can be seen, higher orders in ω^{-1} occur when considering the long-wavelength limit of higher order contributions to $\langle \vec{j}_k; \vec{j}_k \rangle^{(\mathrm{irred})}_{\omega+i\eta}$, see Eqs. (205), (209). The dc–conductivity calculated in this way is divergent.

A possible way out is to anticipate the validity of a Drude formula for the optical conductivity

$$\sigma_{\mathrm{long}}(\omega) = \frac{\epsilon_0\, \omega_{\mathrm{pl}}^2}{-i\left[\omega + i/\tau\right]} \tag{210}$$

with a relaxation time τ not depending on frequency. Applying the Drude formula in the high-frequency limit and adjusting the terms of the expansion by comparing with the expansion of $\langle \vec{j}_k; \vec{j}_k \rangle^{(\mathrm{irred})}_{\omega+i\eta}$ in a region where convergence may be achieved, i.e. at large ω, a finite value for the dc-conductivity may be obtained according to the $\omega = 0$ limit of the Drude formula (210) [30]. For this ansatz, it can easily be seen that the f-sume rule (57) C_n^- is fulfilled. However, the third-moment sum rule is not convergent for the Drude approximation given by Eq. (210) with a relaxation time independent of frequency. Therefore, the assumption of the validity of the Drude formula with a constant relaxation time cannot be justified. Furthermore, such a procedure will result in a wrong static limit if compared with results from kinetic or linear response theory.

The standard Drude model (e.g. [30]) is an empirical approach. It is obtained from Eq. (203) by taking the static limit of the real part of the collision frequency leading to a frequency independent real parameter $\tau = \nu(0,0)^{-1}$. Being able to actually derive a relation (203) microscopically allows to investigate the validity of the empirical expression as well as suggested improvements. As was shown before, the approach via the irreducible parts of the current–current correlation function are not suitable. Instead, we will continue the perturbation approximation as was done in the previous section for the local field corrections. In fact, a comparison of the dynamical local–field corrections according to (192) and the definition of the dynamical collision frequency in (203) leads to the relation

$$\lim_{k\to 0} \nu(\vec{k},\omega) = -i\,\frac{\omega_{\mathrm{pl}}^2}{\omega}\, G(0,\omega) \tag{211}$$

in the long-wavelength limit. The first order term $G^{(1)}(0,\omega)$ vanishes as discussed in the previous Section. We identify the next order of e^2 in which the correlation functions in Eqs. (194) with (175) contribute. Because $\langle \vec{j}_k; \dot{\vec{j}}_k \rangle_{\omega+i\eta} = -\langle \dot{\vec{j}}_k; \vec{j}_k \rangle_{\omega+i\eta} = (1/\omega)\,\langle \dot{\vec{j}}_k; \dot{\vec{j}}_k \rangle_{\omega+i\eta}$, and $\langle \dot{\vec{j}}_k; \dot{\vec{j}}_k \rangle^{(2)}_{\omega+i\eta}$ is of the order e^6, see Eq. (209), the only second order contribution to the dynamical collision frequency in the long-wavelength limit is

$$G^{(2)}(0,\omega) \;=\; i\omega\,\frac{\beta\Omega}{\epsilon_0\omega_{\mathrm{pl}}^4}\langle \dot{\vec{j}}_0; \dot{\vec{j}}_0 \rangle^{(2)}_{\omega+i\eta}\,. \tag{212}$$

The dynamical force-force correlation function, see Eqs. (176),(209), contains the correlation function

$$\begin{aligned}\langle v^c_{p,k}; v^{c'}_{p',k} \rangle_{\omega+i\eta} = \frac{1}{\hbar^2} \sum_{dd'qq'll'\bar{p}\bar{p}'} V_{cd}(q)\, V_{c'd'}(q') \left\{ \delta_{\bar{p},p-\frac{q}{2}} - \delta_{\bar{p},p+\frac{q}{2}} \right\} \left\{ \delta_{\bar{p}',p'-\frac{q'}{2}} - \delta_{\bar{p}',p'+\frac{q'}{2}} \right\} \\ \times \langle a^\dagger_{\bar{p}-\frac{k}{2}-\frac{q}{2},c} a^\dagger_{l+\frac{q}{2},d} a_{l-\frac{q}{2},d} a_{\bar{p}+\frac{k}{2}+\frac{q}{2},c}; a^\dagger_{\bar{p}'-\frac{k}{2}-\frac{q'}{2},c'} a^\dagger_{l'+\frac{q'}{2},d'} a_{l'-\frac{q'}{2},d'} a_{\bar{p}'+\frac{k}{2}+\frac{q'}{2},c'} \rangle_{\omega+i\eta}\end{aligned} \tag{213}$$

The evaluation of this correlation function leads to a finite contribution in the long-wavelength limit for the dc– conductivity and is therefore a more appropriate approach for a calculation of static thermoelectric properties. The detailed evaluation will be shown in the following

chapter using the relation (165) to the corresponding four-particle Green's's function $\mathcal{G}_{vv}(\omega_\mu)$ (the single-particle variables are omitted), see Fig. 1 in section 4.1.

Concluding this section, we point out that more general discussions with respect to the use of perturbation expansions can be found in [34, 35]. Divergences which may occur in higher orders of the perturbation theory are avoided by extending the set of relevant quantum operators $\{B_n\}$ specifying the nonequilibrium state, so that a virial expansion of the response function is possible, see section 2.2 and [51]. Before focussing on the optical conductivity to bridge between the theory of dielectric function and dc-conductivity, the dielectric function for arbitrary wave numbers $\vec{k}$ will be discussed in the next section.

3.5 Mermin Approach

The approach and the expressions given in the previous chapters are valid in the complete $(\vec{k}, \omega)$ space. The case of arbitrary wavenumbers $\vec{k}$ is necessary in order to calculate the structure factor of the system and related properties. However, the evaluation proves to be quite involved. Therefore, it is of practical interest to have tractable expressions which describe the effects of collisions in the entire $(\vec{k}, \omega)$ plane. For this, simpler and more phenomenological attempts have been explored which will be presented here and set in the context of our more consistent linear response theory.

An approach by Ichimaru *et al.* [78] uses an interpolation of its low- and high-frequency limit for the frequency dependent local field corrections

$$G(k, \omega) = \frac{\omega I(k) + i\nu_e G(k)}{\omega + i\nu_e}. \tag{214}$$

where $I(k)$ is defined in Ref. [78] and $G(k)$ is the static local field factor, see section 3.3. Here, the focus is on a detailed description of the k-dependence of the static local field correction $G(k)$. The approach taken in this review is to emphasize the correct description of the dynamical collision frequency.

A simple phenomenological way to include collisions is the concept of relaxation time. The RPA result for the collisionless case as discussed in Sect. 3.2 could be generalized by introducing a complex frequency, replacing the small parameter η in Eq. (179) by a relaxation time $1/\tau$ which is then a finite quantity and has to be chosen in an appropriate way. However, a simple implemention of the relaxation time into the RPA polarization function, $\Pi^{\mathrm{RPA}}(k, \omega + i/\tau)$, shows serious shortcomings. In the long-wavelength limit (185), it does not lead to the Drude formula (210) as would be expected. Additionally, the sum rules are not fulfilled any more as they are for the RPA expression. It can be shown analytically, that the deviations from the exact results are proportional to $1/\tau$.

These inconsistencies were removed by Mermin starting from a kinetic theory [72, 94]. He postulated the existence of a local equilibrium distribution function which the system relaxes to. The distribution function contains a shift in the chemical potential $\delta\mu$ which ensures the particle number conservation in a microscopic plasma volume. Solving the linearized Boltzmann equation in relaxation time approximation and respecting the particle number

conservation by a particular choice of the relaxation term, he gave a special form of the polarization function in terms of the Lindhard expression $\Pi^{\rm RPA}(\vec{k},z)$, Eq. (179),

$$\Pi^{\rm M}(k,\omega) \quad = (1-i\omega\tau)\,\frac{\Pi^{\rm RPA}(k,\omega+i/\tau)\Pi^{\rm RPA}(k,0)}{\Pi^{\rm RPA}(k,\omega+i/\tau)-i\omega\tau\Pi^{\rm RPA}(k,0)}\,. \tag{215}$$

The relaxation time τ is a parameter which has to be fixed in an appropriate way[32].

Recently, the Mermin-like polarization function (215) was derived within the generalized linear response theory [96, 95]. In the context of the Mermin approach, it was shown that the conservation of particle density has to be ensured for a consistent approximation. In contrast to the approach of Mermin who treated the single-particle density matrix of an ideal fermion gas, in the Zubarev approach the full statistical operator is considered, containing also correlations. The result is given in terms of correlation functions which allow for a systematic perturbation expansion. In order to derive the equation of motion for the quantum statistical average of any observable A, the Liouville von Neumann equation (101) can be utilized,

$$\begin{aligned}\frac{\rm d}{{\rm d}t}\langle A\rangle^t &= \frac{\partial}{\partial t}{\rm Tr}\{\rho(t)A\} \\ &= {\rm Tr}\{-\frac{i}{\hbar}[H_{\rm tot},\rho(t)]A\}-\eta\left({\rm Tr}\{\rho(t)A\}-{\rm Tr}\{\rho_{\rm rel}(t)A\}\right).\end{aligned} \tag{216}$$

If the equation of motion for relevant observables B_n is considered, the self-consistency condition (97) can be used to eliminate the terms containing η. This means, that already at finite η the time evolution of the relevant observables is given after cyclic permutation of the operators in the first term by the pure Hamiltonian dynamics according to

$$\frac{\rm d}{{\rm d}t}\langle B_n\rangle^t \;=\; \frac{i}{\hbar}\langle[H_{\rm tot},B_n]\rangle. \tag{217}$$

In the limit $\eta\to 0$ results within linear response theory should not depend on the special choice made for the relevant distribution. However, as soon as approximations are made, like finite orders of perturbation theory, this changes and the appropriate choice of one set or the other can make calculations more convenient. In contrast, in the case of finite η the source term can be interpreted as relaxation term, so that the non-equilibrium statistical operator $\rho(t)$ relaxes to the relevant one with a relaxation time $\tau=1/\eta$. The advantage of the Zubarev approach is, that the dynamics of the set of the relevant observables $\{B_n\}$ is not influenced by this relaxation term, but is still determined by the Hamiltonian as shown above (217). Therefore, this Zubarev approach allows to divide the observables into relevant observables for which the equation of motion is exactly described by the Hamiltonian, and irrelevant variables which underlie an additional relaxation process as long as η is finite.

In the following, we will utilize this aspect of the Zubarev approach. For a certain set of relevant variables such as conserved quantities the exact equation of motions in form of

[32] An expression for each component $\Pi^{c,{\rm M}}(\vec{k},z)$ was given by Selchow *et al.* [95] via partial Lindhard expressions $\Pi^{c,{\rm RPA}}(\vec{k},z)$, see Eq. (223) below, similar to expression (215) using the same relaxation time for each component.

balance equations are fulfilled, whereas for the remaining irrelevant variables the effect of interaction is globaly taken into account by introducing a relaxation term. In particular, in order to realize particle number conservation, the corresponding density will be taken as relevant observable, see [96] and below. An extension of this choice to include energy conservation was considered in [95]. Furthermore, we approximate the time evolution of the irrelevant variables. In particular, we consider

$$\frac{\partial \tilde{\rho}_\eta(t)}{\partial t} + \frac{i}{\hbar}\left[H_{\rm kin}(t) + H_{\rm ext}(t), \tilde{\rho}_\eta(t)\right] = -\,\eta\left\{\tilde{\rho}_\eta(t) - \tilde{\rho}_{\rm rel}(t)\right\}\,. \tag{218}$$

Instead of the dynamical treatment of collisions as described by the interaction part of the Hamiltonian, the term $i\left[H_{\rm int}(t), \tilde{\rho}_\eta(t)\right]/\hbar$ in the Liouville-von Neumann equation is replaced by a relaxation term. The relevant operator as well as the statistical operator are constructed with the interaction free Hamiltonian. At the same time, the consistency condition for the mean values of the relevant observables is preserved and their time evolution is still governed by (217) with $H_{\rm tot}$ replaced by $H_{\rm kin} + H_{\rm ext}$. Thus they are still conserved quantities, e.g. the particle density.

We specify this general approach by considering the density $n_k^c = \sum_p n_{p,k}^c/\Omega$ of the components c as relevant observables B_n, and shifts in the chemical potentials $\delta\mu_c(k,\omega)$ as the corresponding response parameters ϕ_n. The response equations (111) which determine the response parameters read with the external perturbation $H^{\rm ext} = \rho_k^{\rm ext}(\omega)\Omega\sum_c e_c n_k^c/(\epsilon_0 k^2)$ according to (127),(128)

$$-\frac{\Omega e_c}{\epsilon_0 k^2}\,\langle n_k^c; \dot{n}_k^c\rangle_{\omega+i\eta}\;\rho_k^{\rm ext}(\omega) \;\;=\;\; \langle n_k^c; (\dot{n}_k^c + i\omega n_k)\rangle_{\omega+i\eta}\delta\mu_c(k,\omega)\,.$$

Furthermore, utilizing the selfconsistency condition (97) we find in analogy to Eq. (120)

$$\rho_k(\omega) = \sum_c e_c\langle n_k^c\rangle^t\;{\rm e}^{i\omega t} = \beta\sum_c e_c(n_k^c; n_k^c)\;\delta\mu_c(k,\omega)\,. \tag{219}$$

The response function follows from (89) as

$$\chi_{\rm long}(k,\omega) \;\;=\;\; -\beta\Omega\sum_c e_c^2\frac{(n_k^c; n_k^c)\,\langle n_k^c; \dot{n}_k^c\rangle_{\omega+i\eta}}{\langle n_k^c; (\dot{n}_k^c + i\omega n_k^c)\rangle_{\omega+i\eta}}. \tag{220}$$

Applying partial integration (111) of the correlation function, it can readily be seen that the relation (220) is identical with the Kubo formula (129). This emphasizes that the choice of the relevant observables is not important in the limit $\eta \to 0$ as long as no approximations are made.

However, in the light of the discussion above, we will assume that η is finite and evaluate the correlation functions neglecting the interaction term in the Hamiltonian. This is identical with considering the dynamics via the Liouville-von Neumann equation (218). In this case

the zeroth order of the density-density correlation function (168) is already the complete solution and can be expressed by the RPA solution (179). We find [96]

$$
\begin{aligned}
(n_k^c; n_k^c) &= \frac{1}{\beta\Omega^2} \sum_p \frac{f^c_{p+k/2} - f^c_{p-k/2}}{\Delta E^c_{p,k}} = \frac{1}{\beta\Omega}\, \Pi^{c,\mathrm{RPA}}(\vec{k}, 0), && (221)\\
\langle n_k^c; n_k^c \rangle_{\omega+i\eta} &= \frac{\hbar}{i\beta\Omega^2} \sum_p \frac{1}{\Delta E^c_{p,k}} \frac{f^c_{p+\frac{k}{2}} - f^c_{p-\frac{k}{2}}}{\Delta E^c_{p,k} - \hbar(\omega + i\eta)} \\
&= \frac{1}{\beta\Omega} \frac{i}{\omega + i\eta} \left[\Pi^{c,\mathrm{RPA}}(k, \omega + i\eta) - \Pi^{c,\mathrm{RPA}}(k, 0) \right], && (222)\\
\langle n_k^c; \dot{n}_k^c \rangle_{\omega+i\eta} &= \frac{1}{\beta\Omega}\, \Pi^{c,\mathrm{RPA}}(k, \omega + i\eta). && (223)
\end{aligned}
$$

Inserting the expressions (221) to (223) into Eq. (220) we obtain

$$
\chi^M_{\mathrm{long}}(k,\omega) = \sum_c \frac{\Pi^{c,\mathrm{RPA}}(k, \omega + i\eta)}{1 - \frac{1}{1 - i\omega/\eta} \left[1 - \frac{\Pi^{c,\mathrm{RPA}}(k,\omega+i\eta)}{\Pi^{c,\mathrm{RPA}}(k,0)} \right]}. \qquad (224)
$$

In the approximations considered here, the polarization function and the response function are identical since interactions are neglected. The Mermin result (215) is obtained after replacing the parameter η by a relaxation time $1/\tau$. The dielectric function is

$$
\epsilon^{\mathrm{Mermin}}(k,\omega) = 1 + \frac{1}{\epsilon_0 k^2} \sum_c \frac{\Pi^{c,\mathrm{RPA}}(k, \omega + i\eta)}{1 - \frac{1}{1 - i\omega/\eta} \left[1 - \frac{\Pi^{c,\mathrm{RPA}}(k,\omega+i\eta)}{\Pi^{c,\mathrm{RPA}}(k,0)} \right]} \qquad (225)
$$

Neglecting interactions by taking the limit $\eta \to 0$ the RPA result is recovered. In the long wavelength limit, relation (185) can be applied. This leads to

$$
\epsilon^{\mathrm{Mermin}}(0,\omega) = 1 - \frac{\omega_{\mathrm{pl}}^2}{\omega(\omega + i\eta)} \qquad (226)
$$

which is the Drude formula (203) if the parameter η is identified as the collision frequency $\nu(\vec{k}, \omega)$ or the inverse of a relaxation time. In that way, the physical meaning of the parameter η is identified in the same way as was discussed for the Mermin Liouville-von Neumann equation (218).

The idea is that an expression for η obtained in the long-wavelength limit (near $k = 0$) can be applied also for a large region in the k space. In the kinetic approach as well as in the linear response theory, the inclusion of collisions without simplifying restrictions leads to tedious calculations in the derivation of the dielectric function $\epsilon(k, \omega)$ for arbitrary values of k and ω, what is circumvented with the Mermin ansatz.

This approach can be generalized by extending the set of relevant observables. In particular, besides particle number conservation, also total momentum and energy are conserved

quantities, see [95, 97]. The corresponding densities will be taken as relevant observables. The relevant statistical operator is characterizing a local equilibrium as well-known from hydrodynamics. For instance, higher moments of the distribution function such as the current of kinetic energy have been taken into account in the theory of conductivity [49, 98] and dielectric function [62]. Improvements of the Mermin expression by including the energy conservation [95] leads to redefinitions of $\eta(k,\omega)$. Also nonideality corrections related to the two-particle distribution function have been incorporated. Performing the limit $\eta \to 0$, the appropriate choice of the relevant statistical operator ρ_{rel} is essential for the convergence of the perturbation expansion.

4 Frequency Dependent Conductivity

It is the main objective of this chapter to show how the effects of dynamical screening and strong binary collisions can be included in the theory of dielectric function of charged particle systems. This allows us to reproduce well-known results for the dc-conductivity as a limiting case, but also to find new expressions describing these effects at arbitrary frequencies. In the previous chapters, a systematic quantum statistical approach to the interaction between a charged particle system and radiation has been given within linear response theory, where dissipative properties are related to equilibrium correlation functions. The evaluation of the latter is the focus of this chapter. As a result, we deduce convenient renormalization procedures necessary for the consistent description of the response[33].

As starting point, the longitudinal dielectric function (202) $\epsilon_{\rm long}(\vec{k},\omega)$ or correspondingly the longitudinal dynamical conductivity (203) $\sigma_{\rm long}(\vec{k},\omega)$ are considered. Both are related to the dynamical collision frequency $\nu(\vec{k},\omega)$ according to a generalized Drude formula

$$\epsilon_{\rm long}(\vec{k},\omega) = 1 - \frac{\omega_{\rm pl}^2}{\omega[\omega + i\nu(\vec{k},\omega)]}, \qquad \sigma_{\rm long}(\vec{k},\omega) = \frac{\epsilon_0\omega_{\rm pl}^2}{-i\omega + \nu(\vec{k},\omega)}. \tag{227}$$

In particular, we will consider the long wavelength limit $k \to 0$, which relates the frequency dependent conductivity[34]

$$\sigma(\omega) = \lim_{k\to 0} \sigma_{\rm long}(\vec{k},\omega) = \frac{\epsilon_0\omega_{\rm pl}^2}{-i\omega + \nu(\omega)} \tag{228}$$

to the frequency dependent collision frequency $\nu(\omega) = \lim_{k\to 0}\nu(\vec{k},\omega)$.

We will also discuss limiting cases, in particular the high frequency behavior and the dc–conductivity

$$\sigma_{\rm dc} = \frac{\epsilon_0\,\omega_{\rm pl}^2}{\nu(0)}\,. \tag{229}$$

The central quantity, $\nu(\omega)$, is given by the correlation function of the interaction potentials (3.53) taken in the long-wavelength limit (212), (209)

$$\nu(\omega) = \frac{\beta\hbar^2}{\Omega\epsilon_0\omega_{\rm pl}^2} \sum_{pp',cc'} \frac{e_c e_{c'}}{m_c m_{c'}}\,\vec{p}\cdot\vec{p}'\, \lim_{k\to 0}\langle v^c_{p,k}; v^{c'}_{p',k}\rangle_{\omega+i\eta}\,. \tag{230}$$

The correlation function is expressed in terms of creation and annihilation operators, see Eq. (213)

$$\langle v^c_{p,k}; v^{c'}_{p',k}\rangle_{\omega+i\eta} = \frac{1}{\hbar^2} \sum_{dd'qq'll'\bar{p}\bar{p}'} V_{cd}(q)\,V_{c'd'}(q') \left\{\delta_{\bar{p},p-\frac{q}{2}} - \delta_{\bar{p},p+\frac{q}{2}}\right\} \left\{\delta_{\bar{p}',p'-\frac{q'}{2}} - \delta_{\bar{p}',p'+\frac{q'}{2}}\right\}$$
$$\times\langle a^\dagger_{\bar{p}-\frac{k}{2}-\frac{q}{2},c} a^\dagger_{l+\frac{q}{2},d} a_{l-\frac{q}{2},d} a_{\bar{p}+\frac{k}{2}+\frac{q}{2},c}; a^\dagger_{\bar{p}'-\frac{k}{2}-\frac{q'}{2},c'} a^\dagger_{l'+\frac{q'}{2},d'} a_{l'-\frac{q'}{2},d'} a_{\bar{p}'+\frac{k}{2}+\frac{q'}{2},c'}\rangle_{\omega+i\eta} \tag{231}$$

[33] An alternative approach is the kinetic theory via collision integrals, which shall not be detailed here. [34, 35]. Calculations within numerical simulations will be explained in the following chapter.

[34] The index *long* will be omitted. Note, that longitudinal and transverse case coincide in the long–wavelength limit anyway.

if we consider a two–component system of electrons (mass m_e, charge e_e) and ions (mass m_i, charge e_i) and $c, d, = e, i$. The interaction is Coulombic. Transverse coupling to external perturbations is not considered.

The evaluation of the correlation functions using quantum statistical methods will be given in this chapter, leading to the corresponding expressions for σ and ϵ. According to Eq. (165), we represent the equlibrium correlation functions by thermal Green's functions, see FIG. 1, and use diagram expansions to perform appropriate partial summations[35]. Born approximation, the summation of ring diagrams describing screening and the sum of ladder diagrams describing binary collisions will be detailed. For a systematic perturbation expansion, two options could be considered. Either contributions from higher moments of the correlations functions have to be taken into account, as will also be discussed in section 4.4 leading to a renormalization factor. Alternatively, further contributions within a one moment approximation have to be taken into account. This means to go beyond expression (230) up to terms in higher order of e^2 as given in (175).

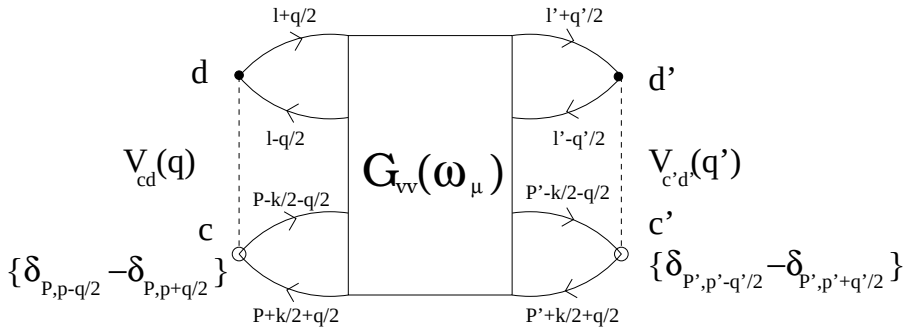

Figure 1: Representation of the Green's function $\mathcal{G}_{vv}(\omega_\mu)$ by Feynman diagrams.

4.1 Born Approximation

In order to evaluate the dynamical collision frequency (230) in lowest approximation with respect to the interaction we treat the four-particle Green's function $\mathcal{G}_{vv}(\omega_\mu)$ which corresponds to the correlation function (231) as a product of four single-particle Green's functions, see FIG. 2.

Alternatively, one can directly evaluate the correlation function (231) in lowest order

[35]For diagram techniques see e.g. Fetter andWalecka [33]. The interactions are shown as dashed line and the particle propagators as full line with arrow.

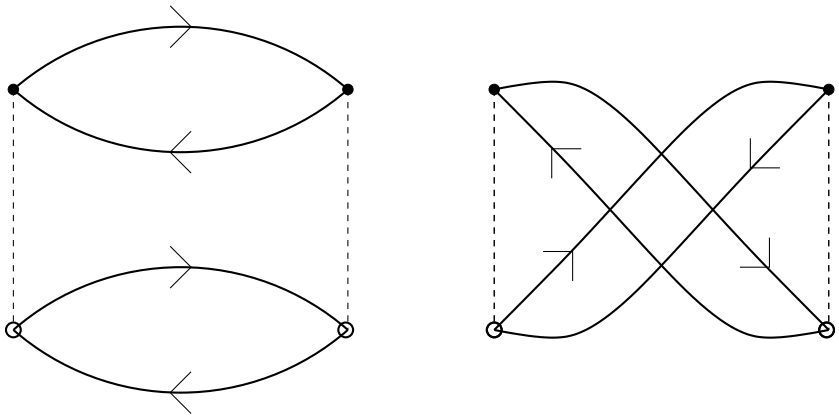

Figure 2: Green's function $\mathcal{G}_{vv}(\omega_\mu)$ in Born approximation.

with respect to the interaction using Wick's theorem. They are of order of e^4. We find

$$\begin{aligned}\langle v^c_{p,k}; v^{c'}_{p',k}\rangle^{(2)}_z = \frac{i}{\beta\hbar}\sum_{\bar{p}lqd}\frac{\mathrm{e}^{\beta(\Delta E^d_{l,q}-\Delta E^c_{\bar{p},k+q})}-1}{\hbar z+\Delta E^d_{l,q}-\Delta E^c_{\bar{p},k+q}}\frac{V_{cd}(q)}{\Delta E^d_{l,q}-\Delta E^c_{\bar{p},k+q}} \qquad (232)\\ \times f^d_{l+\frac{q}{2}}\left(1-f^d_{l-\frac{q}{2}}\right)\, f^c_{\bar{p}-\frac{k}{2}-\frac{q}{2}}\left(1-f^c_{\bar{p}+\frac{k}{2}+\frac{q}{2}}\right)\,\{\delta_{p,\bar{p}+\frac{q}{2}}-\delta_{p,\bar{p}-\frac{q}{2}}\}\\ \times\Big[V_{cd}(q)\delta_{cc'}\{\delta_{p',\bar{p}+\frac{q}{2}}-\delta_{p',\bar{p}-\frac{q}{2}}\}\,+\,V_{cd}(q+k)\delta_{dc'}\{\delta_{p',l-\frac{k}{2}-\frac{q}{2}}-\delta_{p',l+\frac{k}{2}+\frac{q}{2}}\}+exch.\,contr.\Big]\end{aligned}$$

with $\Delta E^c_{p,q} = E^c_{p+q/2} - E^c_{p-q/2} = \hbar^2\vec{p}\cdot\vec{q}/m_c$, $E^c_p = \hbar^2p^2/(2m_c)$ and $V_{cd}(q) = e_ce_d/(\epsilon_0q^2\Omega)$ for the Coulomb interaction, and $f^c_p = [\exp\{\beta(E^c_p-\mu_c)+1]^{-1}$ the Fermi function. This expression is substituted into Eq. (230) taking the long-wavelength limit. We execute the sum over the species of singly charged particles with $e_e = -e_i = e$, spin $s_e = s_i = 1/2$, and the reduced mass $\mu_r^{-1} = m_e^{-1}+m_i^{-1}$. The notation *exch. contr.* denotes further contributions which arise when the collision partners are indentical and exchange their quantum state after interaction. We get the result for the complex frequency dependent dynamical collision frequency in Born approximation

$$\nu^{\mathrm{Born}}(\omega) = \frac{4i\hbar e^2}{\Omega\epsilon_0\omega^2_{\mathrm{pl}}\mu_r^2}\sum_{pp'q}\frac{\mathrm{e}^{\beta(\Delta E^i_{p',q}-\Delta E^e_{p,q})}-1}{\Delta E^i_{p',q}-\Delta E^e_{p,q}}q_z^2\,V^2_{ei}(q)\frac{f^i_{p'+\frac{q}{2}}\left(1-f^i_{p'-\frac{q}{2}}\right)f^e_{p-\frac{q}{2}}\left(1-f^e_{p+\frac{q}{2}}\right)}{\hbar(\omega+i\eta)+\Delta E^i_{p',q}-\Delta E^e_{p,q}}. \qquad (233)$$

Due to momentum conservation, there is no contribution from the interactions between particles of the same component in this one-moment approach. The factor 4 is due to summation over spin variables.

Alternatively, the inclusion of ion dynamics can also be done via a dynamical structure factor $S(q,\omega)$ according to (77) [41, 99].

Adiabatic Limit

In adiabatic approximation $\lim(m_i/m_e) \to \infty$, the electrons are considered to scatter from ions at positions $\mathbf{R}_j$. From (233), we find the following expression for the dynamical collision frequency,

$$\nu^{\mathrm{Born}}(\omega) = \frac{2i\hbar n_i}{n_e m_e} \sum_{pq} V_{ei}^2(q)\, S_i(q)\, q_z^2\, \frac{f^e_{p+\frac{q}{2}} - f^e_{p-\frac{q}{2}}}{\Delta E^e_{p,q} - \hbar(\omega + i\eta)}\, \frac{1}{\Delta E^e_{p,q}}\,, \tag{234}$$

$$= -i\, \frac{\epsilon_0 n_i\, \Omega^2}{6\pi^2 e^2\, n_e m_e} \int_0^\infty dq\, q^6\, V_{ei}^2(q)\, S_i(q)\, \frac{1}{\omega} \left[\epsilon_{\mathrm{RPA},e}(q,\omega) - \epsilon_{\mathrm{RPA},e}(q,0)\right]. \tag{235}$$

The latter expression was already given and used by [90, 91, 99, 100, 101, 102, 103]. In the RPA dielectric function, only the electronic part contributes while the ionic distribution is taken into account by the ionic structure factor [104, 30] (78)

$$S_i(q) = \frac{1}{n_i \Omega} \sum_{jl} \exp\left[i\mathbf{q}\cdot(\mathbf{R}_j - \mathbf{R}_l)\right] \tag{236}$$

on the static level. If the ion distribution function is uncorrelated, we have only contributions from $l = j$ and $S(q) = 1$.

4.2 Dynamical Screening

After having considered the collision term in Born approximation for arbitrary ω in the long-wavelength limit, we will now discuss higher orders of perturbation theory. Ring diagrams are produced replacing a single loop by a chain of loops, see FIG. 3.

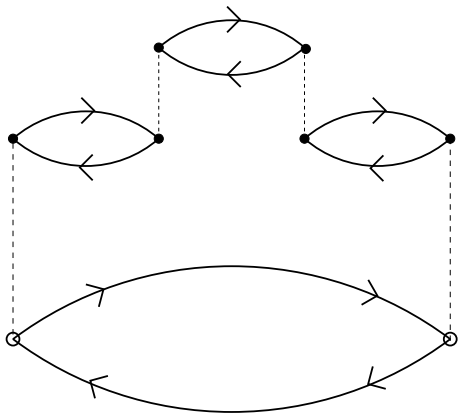

Figure 3: Example of a contribution to the Green's function $\mathcal{G}_{vv}(\omega_\mu)$ in a dynamically screened approximation.

The summation of all loop diagrams is included by introducing a dynamically screened potential $V^s_{cc'}(q,z) = V_{cc'}(q)/\epsilon_{\mathrm{long}}(q,z)$. In this expression, the longitudinal dielectric function $\epsilon_{\mathrm{long}}(q,z)$ can be expressed in terms of the polarization function $\Pi(q,z)$ (69) and taken

in different approximations. For instance, the random-phase approximation $\epsilon^{\rm RPA}(q,z)$ (179) corresponds to the summation of simple loop diagrams. Representing the screened interaction $V^s(q,\omega_\nu)$ diagrammatically by a wavy line, the summation over loop diagrams leads to the diagrams for $\mathcal{G}_{vv}(\omega_\mu)$ shown in FIG. 4, see also [11, 51]. In the following we shall detail only the evaluation of the first diagram of FIG. 4.

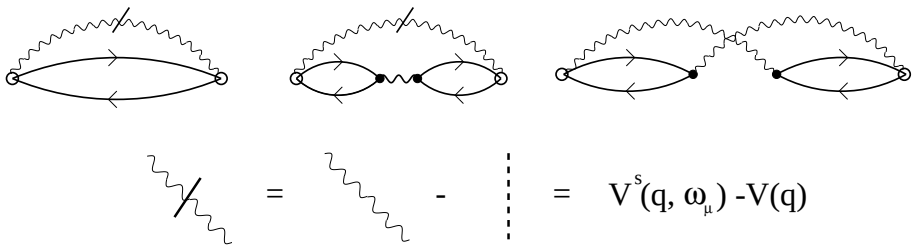

Figure 4: Contributions to the Green's function $\mathcal{G}_{vv}(\omega_\mu)$ in a dynamically screened Born approximation.

We use the spectral representation of the screened potential, see e.g. [11],

$$V^s_{cc'}(q,\omega_\nu) \;=\; V_{cc'}(q) \;+\; V_{cc'}(q) \int \frac{d\omega}{\pi} \frac{\mathrm{Im}\,\epsilon^{-1}_{\rm long}(q,\omega+i0)}{\omega-\omega_\nu}, \tag{237}$$

in order to evaluate its contribution to the Green's function (163) $\mathcal{G}_{vv}(\omega_\mu)$ corresponding to the expression (213),

$$\begin{aligned}
\mathcal{G}_{vv}(\omega_\mu) &= -\delta_{cc'}\delta_{pp'} \sum_\lambda \frac{f^c_{p+\frac{k}{2}+\frac{q}{2}} - f^c_{p-\frac{k}{2}-\frac{q}{2}}}{\Delta E^c_{p,k+q} - \hbar\omega_\lambda} V_{cc}(q) \int \frac{d\bar\omega}{\pi} \frac{\mathrm{Im}\,\epsilon^{-1}_{\rm long}(q,\bar\omega+i0)}{\omega_\lambda+\omega_\mu-\bar\omega} \\
&= -\delta_{cc'}\delta_{pp'} \left[f^c_{p+\frac{k}{2}+\frac{q}{2}} - f^c_{p-\frac{k}{2}-\frac{q}{2}} \right] V_{cc}(q) \int \frac{d(\hbar\bar\omega)}{\pi} \frac{\mathrm{Im}\,\epsilon^{-1}_{\rm long}(q,\bar\omega+i0)}{\Delta E^c_{p,k+q} + \hbar\omega_\mu - \hbar\bar\omega} \\
&\quad \times \left[g\left(\Delta E^c_{p,k+q}\right) - g(\hbar\bar\omega) \right]
\end{aligned} \tag{238}$$

where $g(E) = [\exp(\beta E)-1]^{-1}$ is the Bose-Einstein distribution function. After analytical continuation $\omega_\mu \to z$, the imaginary part of this expression reads

$$\begin{aligned}
\mathrm{Im}\,\mathcal{G}_{vv}(\omega+i\eta) &= \delta_{cc'}\delta_{pp'} \left[f^c_{p+\frac{k}{2}+\frac{q}{2}} - f^c_{p-\frac{k}{2}-\frac{q}{2}} \right] \left[g\left(\Delta E^c_{p,k+q}\right) - g\left(\Delta E^c_{p,k+q} + \hbar\omega\right) \right] \\
&\quad \times V_{cc}(q)\, \mathrm{Im}\,\epsilon^{-1}_{\rm long}(q, \Delta E^c_{p,k+q}/\hbar + \omega + i0)
\end{aligned} \tag{239}$$

which leads to a contribution to the correlation function

$$\begin{aligned}
\langle v^c_{pk}; v^{c'}_{p'k} \rangle^{(2,s)}_{\omega+i\eta} &= -\frac{i}{\beta\hbar^2}\,\delta_{cc'} \sum_{\bar p q} \left[f^c_{\bar p+\frac{k}{2}+\frac{q}{2}} - f^c_{\bar p-\frac{k}{2}-\frac{q}{2}} \right] V_{cc}(q) \int_{-\infty}^{\infty} \frac{d\bar\omega}{\pi} \\
&\quad \times \frac{\mathrm{Im}\,\epsilon^{-1}_{\rm long}(q, \Delta E^c_{\bar p,k+q}/\hbar + \bar\omega + i0)}{(\omega+i\eta-\bar\omega)\,\bar\omega} \left\{ \delta_{p,\bar p+\frac{q}{2}} - \delta_{p,\bar p-\frac{q}{2}} \right\} \\
&\quad \times \left[g\left(\Delta E^c_{\bar p,k+q}\right) - g\left(\Delta E^c_{\bar p,k+q} + \hbar\bar\omega\right) \right] \left\{ \delta_{p',\bar p+\frac{q}{2}} - \delta_{p',\bar p-\frac{q}{2}} \right\} .
\end{aligned} \tag{240}$$

Using relation (69), we express the inverse dielectric function by the longitudinal polarization function

$$\mathrm{Im}\,\epsilon^{-1}_{\mathrm{long}}(q,\omega+i0) \;=\; \frac{\mathrm{Im}\,\Pi_{\mathrm{long}}(q,\omega+i0)}{\epsilon_0 q^2\,|\epsilon_{\mathrm{long}}(q,\omega)|^2}\;. \tag{241}$$

Since we are interested in the second order contribution we can take the polarization function in the RPA limit, Eq. (179). Using

$$\frac{1}{\epsilon_0 q^2}\mathrm{Im}\,\Pi^{\mathrm{RPA}}(q,\omega+i0) \;=\; -\pi\sum_{p,c} V_{cc}(q)\,\left[f^c_{p+\frac{q}{2}}-f^c_{p-\frac{q}{2}}\right]\,\delta(\Delta E^c_{p,q}-\hbar\omega) \tag{242}$$

we carry out the $\bar\omega$ integration in the correlation function, Eq. (240), and take the long-wavelength limit

$$\lim_{k\to 0}\,\langle v^c_{pk};v^{c'}_{p'k}\rangle^{(2,s)}_{\omega+i\eta} \;=\; \frac{i}{\beta\hbar}\,\delta_{cc'}\sum_{\bar p\bar p' q\bar c}\frac{V^2_{c\bar c}(q)}{|\epsilon_{\mathrm{RPA}}(q,\Delta E^{\bar c}_{\bar p',q}/\hbar)|^2}\,\left[g\left(\Delta E^c_{\bar p,q}\right)-g\left(\Delta E^{\bar c}_{\bar p',q}\right)\right] \tag{243}$$

$$\times\,\frac{f^{\bar c}_{\bar p'+\frac{q}{2}}-f^{\bar c}_{\bar p'-\frac{q}{2}}}{\hbar(\omega+i\eta)-\Delta E^{\bar c}_{\bar p',q}+\Delta E^c_{\bar p,q}}\,\frac{f^c_{\bar p+\frac{q}{2}}-f^c_{\bar p-\frac{q}{2}}}{\Delta E^{\bar c}_{\bar p',q}-\Delta E^c_{\bar p,q}}\left\{\delta_{p,\bar p+\frac{q}{2}}-\delta_{p,\bar p-\frac{q}{2}}\right\}\left\{\delta_{p',\bar p+\frac{q}{2}}-\delta_{p',\bar p-\frac{q}{2}}\right\}\;.$$

The second diagram in FIG. 4 cannot be interpreted by a single scattering event. Its contribution is of order n^2 and does not contribute in the low-density limit, see [51]. The third diagram has the same structure as Eq. (243) after performing the frequency summations [51] in the lowest order of density. Note that in the lowest order of interaction, this diagram leads to the double-exchange term of the Born approximation, which corresponds to the second term in Eq. (232) and the second diagramm of FIG. 2. Finally, the collision frequency in the long-wavelength limit (230) is obtained,

$$\nu^{\mathrm{LB}}(\omega) \;=\; \frac{i\hbar}{\Omega\epsilon_0\omega^2_{\mathrm{pl}}}\sum_{pp'qcc'}\frac{q_z^2\,V^2_{cc'}(q)}{|\epsilon_{\mathrm{RPA}}(q,\Delta E^{c'}_{p',q}/\hbar)|}\,\frac{f^c_{p+\frac{q}{2}}-f^c_{p-\frac{q}{2}}}{\hbar(\omega+i\eta)-\Delta E^{c'}_{p',q}+\Delta E^c_{p,q}}\,\frac{f^{c'}_{p'+\frac{q}{2}}-f^{c'}_{p'-\frac{q}{2}}}{\Delta E^{c'}_{p',q}-\Delta E^c_{p,q}}$$

$$\times\,\left[g\left(\Delta E^c_{p,q}\right)-g\left(\Delta E^{c'}_{p',q}\right)\right]\,\left[\frac{e_c^2}{m_c^2}\frac{1}{|\epsilon_{\mathrm{RPA}}(q,\Delta E^{c'}_{p',q}/\hbar)|}-\frac{e_ce_{c'}}{m_cm_{c'}}\frac{1}{|\epsilon_{\mathrm{RPA}}(q,\Delta E^c_{p,q}/\hbar)|}\right], \tag{244}$$

where the term proportional to $e_ce_{c'}/(m_cm_{c'})$ originates from the third diagram in FIG. 4. Executing the summation over the species leads to the collision frequency in screened Born approximation

$$\nu^{\mathrm{LB}}(\omega) \;=\; -\frac{4i\hbar e^2\mu}{\Omega\,\epsilon_0\omega^2_{\mathrm{pl}}}\sum_{pp'q}\frac{\mathrm{e}^{\beta(\Delta E^i_{p',q}-\Delta E^e_{p,q})}-1}{\Delta E^i_{p',q}-\Delta E^e_{p,q}}\,q_z^2\,V^2_{ei}(q)\,\frac{f^e_{p-\frac{q}{2}}\left(1-f^e_{p+\frac{q}{2}}\right)\,f^i_{p'+\frac{q}{2}}\left(1-f^i_{p'-\frac{q}{2}}\right)}{\hbar(\omega+i\eta)+\Delta E^i_{p',q}-\Delta E^e_{p,q}}$$

$$\times\,\left[\frac{1}{m_e\,|\epsilon_{\mathrm{RPA}}(q,\Delta E^i_{p',q}/\hbar)|}\;+\;\frac{1}{m_i\,|\epsilon_{\mathrm{RPA}}(q,\Delta E^e_{p,q}/\hbar)|}\right]^2\;. \tag{245}$$

This expression has the same structure as the Born approximation, Eq. (233), except the bare Coulomb interaction is screened by the full RPA expression of the dielectric function. With Eq. (245), we have found a collision frequency in screened Born approximation for arbitrary frequencies.

In the zero-frequency limit, the imaginary part of the collision frequency vanishes. The inverse relaxation time, derived from (245),

$$\begin{aligned}\frac{1}{\tau^{\mathrm{LB}}(0)} &= \mathrm{Re}\,\nu^{\mathrm{LB}}(0) = -\frac{4i\pi\beta e^2}{\Omega\,\epsilon_0\omega_{\mathrm{pl}}^2\mu}\sum_{pp'q}\int d(\hbar\omega)\,q_z^2\,\frac{V_{ei}^2(q)}{|\epsilon_{\mathrm{RPA}}(q,\omega)|^2} \\ &\times f^e_{p-\frac{q}{2}}\left(1-f^e_{p+\frac{q}{2}}\right)\,f^i_{p'+\frac{q}{2}}\left(1-f^i_{p'-\frac{q}{2}}\right)\,\delta(\Delta E^i_{p',q}-\hbar\omega)\,\delta(\Delta E^e_{p,q}-\hbar\omega)\end{aligned} \tag{246}$$

follows. It coincides with the well-known Lenard-Balescu collision integral [105, 106, 107] and has been derived before within the linear response theory, see Refs. [51, 108].

Adiabatic Limit

Neglecting the ion dynamics and introducing the static ionic structure factor $S_i(\vec{q})$ to replace the ionic part of the dielectric function, thus making an adiabatic approximation, we find in analogy to Eq. (234),

$$\nu^{\mathrm{LB}}(\omega) = -\frac{2i\hbar n_i}{n_e m_e}\sum_{pq}\frac{V_{ei}^2(q)\,S_i(q)}{|\epsilon_{\mathrm{RPA},e}(q,\Delta E^e_{p,q}/\hbar)|^2}\,q_z^2\,\frac{f^e_{p+\frac{q}{2}}-f^e_{p-\frac{q}{2}}}{\Delta E^e_{p,q}-\hbar(\omega+i\eta)}\,\frac{1}{\Delta E^e_{p,q}} \tag{247}$$

$$= -i\,\frac{\epsilon_0 n_i\,\Omega^2}{6\pi^2e^2\,n_e m_e}\int_0^\infty dq\,q^6\,V_{ei}^2(q)\,S_i(q)\,\frac{1}{\omega}\left[\epsilon^{-1}_{\mathrm{RPA},e}(q,\omega)\;-\;\epsilon^{-1}_{\mathrm{RPA},e}(q,0)\right]. \tag{248}$$

The dielectric function is to be taken only from the electron subsystem as discussed above. The structure of these expressions is similar to the Born approximation, Eqs. (234), (235). However, the bare Coulomb potential is replaced by the dynamically screened one. As can be seen from the static limit of the RPA dielectric function, Eq. (183), the divergences in the Born approximation for small q-values are now removed. A generalization of the Drude formula with a frequency dependent relaxation time of electron-phonon systems was derived in [109] using correlation functions. Their result resembles the analogy to the relaxation time derived from the real part of the collision frequency, Eq. (248). However, the complex character of the correlation functions had not been investigated. Evaluating the adiabatic expression (248) for a classical plasma (non-degenerate case), we find an expression as given before by Bekefi [110] whereas the zero-temperature limit for a simple metal was considered by Hopfield [111].

4.3 Strong collisions

For Coulomb systems, the collision integral in Born approximation is divergent not only for small transfer momenta q which is cured considering the dynamically screened interaction

as discussed in the previous section. As well known, see e.g. [14, 51, 98, 112], for large values[36] of q the collision integral in Born approximation is divergent if the classical limit is considered. In the quantum case, the divergence disappears, because the corresponding short range part of the Coulomb potential is averaged out due to quantum effects. However, the correct result in the low-density limit for the dc-conductivity cannot be obtained from Born approximation [51].

Divergences are avoided and correct limiting cases are obtained if higher orders of the perturbation expansion are taken into account. The behavior for large values of q or correspondingly at small distances r is determined by strong binary collisions which are accounted for by summing up the so-called ladder diagrams in the perturbation expansion, see FIG. 5. In the following, we will show the evaluation of the collision frequency when including strong collisions.

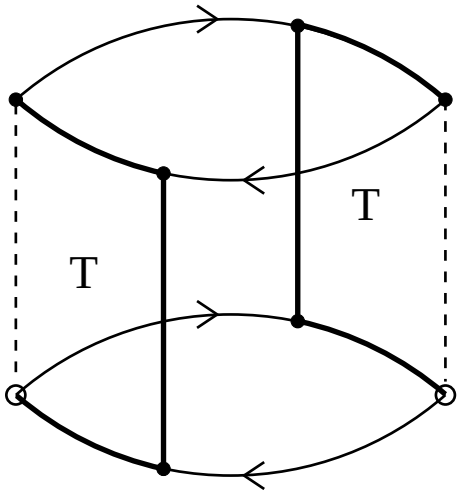

Figure 5: Green's function $\mathcal{G}_{vv}(\omega_\mu)$ in ladder approximation.

We start with the correlation function $\langle v^c_{p,k}; v^{c'}_{p',k}\rangle_z$, Eq. (231), in the long-wavelength limit $k \to 0$. The observables $v^c_{p,k=0}$, Eq. (176), shall be written as

$$v^c_{p,0} \;=\; \frac{i}{\hbar}\sum_{12} V(1,2)\,\{\delta_{p,p_2} \,-\, \delta_{p,p_1}\}\,\delta_{cc_1}\; a^\dagger_{p_1,c_1} a^\dagger_{p'_1,c'_1} a_{p'_2,c'_2} a_{p_2,c_2}\,. \tag{249}$$

Within this section, the abbreviation $1 = (p_1, c_1; p'_1, c'_1)$ refers to the state of a pair of charges and

$$V(1,2) = V_{c_1 c'_1}(|\vec{p}_2 - \vec{p}_1|)\delta_{c_1 c_2}\delta_{c_{1'} c_{2'}}\delta_{p_2 - p_1; p'_1 - p'_2}. \tag{250}$$

Now, the Feynman diagram for the Green's function $\mathcal{G}_{vv}(\omega_\mu)$ corresponding to the correlation function according to Eq. (165) was shown in FIG. 1. The Born approximation was already discussed in Subsection 4.1. while the summation of ring diagrams leads to the screened

[36]The typical length scale is the thermal wave length.

interaction, see FIG. 4 and Subsection 4.2. In order to take into account strong collisions, we perform the summation of ladder diagrams, corresponding to FIG. 5. The analytical expression reads

$$\mathcal{G}_{vv}(\omega_\mu) = \sum_{1234,\omega_\lambda} V(1,2)\,[K_p(2) - K_p(1)]\,\mathcal{G}_2(1,3;\omega_\lambda+\omega_\mu)\,V(3,4)\,[K_{p'}(4) - K_{p'}(3)]\,\mathcal{G}_2(4,2;\omega_\lambda) \tag{251}$$

with $K_p(1) = \delta_{p,p_1}$[37].

In the low-density limit where $f_p^c \ll 1$, the two-particle propagator is given as the bilinear expansion in terms of the solution of the two-particle Schrödinger equation [11],

$$\mathcal{G}_2(1,2;\omega_\lambda) = \sum_{nP} \frac{\psi_{nP}(1)\psi^*_{nP}(2)}{\hbar\omega_\lambda - E_{nP}}\ . \tag{252}$$

Inserting this into Eq. (251), performing the summation over ω_λ and some further straightforward calculations the result for the collision frequency (230)

$$\begin{aligned}\nu^{\rm ladder}(\omega) &= \frac{i\hbar}{\Omega_0 n_e m_e}\sum_{nn'P}\frac{\mathrm{e}^{\beta(E_{nP}-E_{n'P})}-1}{E_{nP}-E_{n'P}}\,\frac{g^{ei}(E_{nP})[1+g^{ei}(E_{n'P})]}{\hbar(\omega+i\eta)+E_{nP}-E_{n'P}} \\ &\quad\times\left|\sum_{p_e,p_i,q}\psi^*_{n'P}(p_e,p_i)\,V(q)\,q_z\,\psi_{nP}(p_e+q,p_i-q)\right|^2\end{aligned} \tag{253}$$

is obtained, with $\psi_{nP}(p_e,p_i)$ being the wavefunction, E_{nP} the energy eigenvalue for the two-particle state with c.o.m. momentum P and internal quantum number n, and $g^{ei}(E) = \{\exp[\beta(E-\mu_e-\mu_i)]-1\}^{-1}$ the Bose distribution function.

Alternatively, we express the dynamical collision frequency in terms of the T–matrix in order to make the connection to scattering phase shifts and transport cross section. We use the operator form[38] and give the representation with respect to the two-particle basis at the end. With the relation

$$\mathcal{G}_2(z) = \int_{-\infty}^{\infty}\frac{d\omega}{\pi}\frac{\mathrm{Im}\mathcal{G}_2^+(\omega)}{z-\omega}\,, \tag{254}$$

where $\mathcal{G}_2^+(\omega) = \lim_{\eta\to 0}\mathcal{G}_2(\omega+i\eta)$, we express (251)

$$\mathcal{G}_{vv}(\omega_\mu) = \int_{-\infty}^{\infty}\frac{d\omega}{\pi}\int_{-\infty}^{\infty}\frac{d\omega'}{\pi}[V,K_p]\mathrm{Im}\mathcal{G}_2^+(\omega)[V,K_{p'}]\mathrm{Im}\mathcal{G}_2^+(\omega)F(\omega_\mu,\omega,\omega')\ \ , \tag{255}$$

with

$$F(\omega_\mu,\omega,\omega') = \sum_{\omega_\lambda}\frac{1}{\omega_\lambda+\omega_\mu-\omega}\frac{1}{\omega_\lambda-\omega'} = \frac{\mathrm{e}^{\beta(\omega-\omega')}-1}{\omega'+\omega_\mu-\omega}g^{ei}(\omega)[1+g^{ei}(\omega')]\ \ . \tag{256}$$

[37] In the case of higher moments (122), the $K_p(1)$ become more involved linear momentum dependent expressions. For generality, we replace $K_p(1)$ by δ functions for the lowest moment at the end only.

[38] An alternative derivation using the Bethe-Salpeter equation, the free two-particle propagator and the definition of the ladder–T matrices is given in the Appendix 4.8.

Now we utilize the optical theorem[39]

$$\mathrm{Im}\mathcal{G}_2^+(\omega+i\eta) = \frac{1}{V}T^+(\omega)\mathrm{Im}\mathcal{G}_2^{0+}(\omega)T^-(\omega)\frac{1}{V} \tag{260}$$

with the free two–particle propagator $\mathcal{G}_2^0(z) = [\hbar z - H^0]^{-1}$. Insertion gives

$$\begin{aligned}\mathcal{G}_{vv}(\omega_\mu) &= \int_{-\infty}^{\infty}\frac{d\omega}{\pi}\int_{-\infty}^{\infty}\frac{d\omega'}{\pi} \\ &\times\mathrm{Im}\mathcal{G}_2^{0+}(\omega)T^-(\omega)[K_{p'},\frac{1}{V}]T^-(\omega')\mathrm{Im}\mathcal{G}_2^{0+}(\omega')T^+(\omega')[K_p,\frac{1}{V}]T^+(\omega)F(\omega_\mu,\omega,\omega')\,.\end{aligned} \tag{261}$$

Using relation (259), we have

$$T^-(\omega)[K_{p'},\frac{1}{V}]T^-(\omega') = T^-(\omega)K_{p'} - K_{p'}T^-(\omega') + T^-(\omega)[K_{p'}\mathcal{G}_2^{0-}(\omega') - \mathcal{G}_2^{0-}(\omega)K_{p'}]T^-(\omega') \tag{262}$$

and using the matrix representation with respect to the linear momentum states, the correlation functions (231) can be expressed as

$$\begin{aligned}\langle v^c_{p,0};v^{c'}_{p',0}\rangle_z^{\mathrm{ladder}} &= \frac{i}{\hbar\beta}\sum_{1234}\frac{\mathrm{e}^{\beta(E_1-E_3)}-1}{\hbar z+(E_1-E_3)}\,\frac{\delta_{cc_1}\delta_{c'c_3}}{E_1-E_3}\,f^{c_1}_{p_1}[1-f^{c_3}_{p_3}]\,f^{c'_1}_{p'_1}[1-f^{c'_3}_{p'_3}] \\ &\times\Big[T^-(1,3;E_3)K_p(1) - T^-(1,3;E_1)K_p(3) \\ &\quad + T^-(1,2;E_1)\left\{\frac{1-f_2}{E_1-E_2}-\frac{1-f_2}{E_3-E_2}\right\}T^-(2,3;E_3)K_p(2)\Big] \\ &\times\Big[T^+(3,1;E_1)K_{p'}(3) - T^+(3,1;E_3)K_{p'}(1) \\ &\quad + T^+(3,4;E_3)\left\{\frac{1-f_4}{E_3-E_4}-\frac{1-f_4}{E_1-E_4}\right\}T^+(4,1;E_1)K_{p'}(4)\Big]\,.\end{aligned} \tag{263}$$

The arguments are given in the compact notation according to (249) and the shorthand notations $E_1 = E^{c_1}_{p_1} + E^{c'_1}_{p'_1}$, $f_1 = f^{c_1}_{p_1} + f^{c'_1}_{p'_1}$, see also the defintions below Eq. (232). In the following we consider the one-moment approach replacing $K_p(1) = \delta_{p,p_1}$. Using Eq. (230), the dynamical collision frequency can be given[40].

[39]The optical theorem is

$$\mathrm{Im}\mathcal{G}_2^+(\omega) = \frac{-i\eta}{(\hbar\omega - H + i\eta)(\hbar\omega - H - i\eta)} = \mathcal{G}_2^+(\omega)[\mathcal{G}_2^{0+}(\omega)]^{-1}\mathrm{Im}\mathcal{G}_2^{0+}(\omega)[\mathcal{G}_2^{0-}(\omega)]^{-1}\mathcal{G}_2^-(\omega)\,.$$

Furthermore, the following relations hold

$$V\mathcal{G}_2^\pm(\omega) = T^\pm(\omega)\mathcal{G}_2^{0\pm}(\omega) \tag{257}$$

$$T^\pm(\omega) = V + V\mathcal{G}_2^{0\pm}(\omega)T^\pm(\omega) = V + T^\pm(\omega)\mathcal{G}_2^{0\pm}(\omega)V \tag{258}$$

$$\frac{1}{V}T^-(\omega) = 1 + \mathcal{G}_2^{0-}(\omega)T^-(\omega)\,. \tag{259}$$

[40]In lowest order, the T-matrices (258) are approximated by the potential, Eq. (250), and only terms

Adiabatic limit

The summation of ladder diagrams in the corresponding Matsubara Green's function $\mathcal{G}_{vv}^{\rm ladder}(\omega_\mu)$ was shown for arbitrary mass ratios m_i/m_e. Here, we will restrict ourselves to the adiabatic limit $m_e/m_i \to 0$, thus

$$\nu^{\rm ladder}(\omega) = \frac{4\beta\hbar}{n_e m_e \Omega} \sum_{pp'} p_z p'_z \, \langle v^e_{p,0}; v^e_{p',0} \rangle^{\rm ladder}_{\omega+i\eta} \ . \tag{265}$$

As already pointed out in the discussion of the Born approximation, because of conservation of the total linear momentum only the interaction between electrons and ions will contribute in the first moment approach. Representing the operators with respect to a two-particle basis in Eq. (263), we find

$$\begin{aligned}
\nu^{\rm ladder}(\omega) = \frac{4i\,\hbar}{n_e m_e \Omega} \sum_{p_e p_i q} & \frac{{\rm e}^{\beta(E^{ei}_{p,0}-E^{ei}_{p,q})}-1}{\hbar(\omega+i\eta)+E^{ei}_{p,0}-E^{ei}_{p,q}} \, \frac{1}{E^{ei}_{p,0}-E^{ei}_{p,q}} \, f^e_{p_e}\left(1-f^e_{p_e+q}\right) \qquad (266) \\
\times f^i_{p_i}\left(1-f^i_{p_i-q}\right) & \Bigg\{ (p_{e,z}+q_z)\; T^-_{ei}(p_e,p_i;q;E^{ei}_{p,0}) \;-\; p_{e,z}\; T^-_{ei}(p_e,p_i;q;E^{ei}_{p,q}) \\
& - \sum_{q'} (p_{e,z}+q'_z)\, T^-_{ei}(p_e,p_i;q';E^{ei}_{p,0}) \left[\frac{1}{E^{ei}_{p,0}-E^{ei}_{p,q'}-i\hbar\eta} - \frac{1}{E^{ei}_{p,q}-E^{ei}_{p,q'}-i\hbar\eta} \right] \\
\times T^-_{ei}(p_e+q',p_i-q';-q'+q;E^{ei}_{p,q}) & \Bigg\} \Bigg\{ (p_{e,z}+q_z)\; T^+_{ei}(p_e+q,p_i-q;-q;E^{ei}_{p,0}) \\
\times - \; p_{e,z}\; T^+_{ei}(p_e+q,p_i-q;-q;E^{ei}_{p,q}) & + \sum_{q''} (p_{e,z}+q''_z) T^+_{ei}(p_e+q,p_i-q;-q+q'';E^{ei}_{p,q}) \\
& \times \left[\frac{1}{E^{ei}_{p,q}-E^{ei}_{p,q''}+i\hbar\eta} - \frac{1}{E^{ei}_{p,0}-E^{ei}_{p,q''}+i\hbar\eta} \right] T^+_{ei}(p_e+q'',p_i-q'';-q'';E^{ei}_{p,0}) \Bigg\},
\end{aligned}$$

where the abbreviations $T^\pm_{ei}(p_e,p_i;q;E) = T^\pm_{ei}(p_e,p_i;p_e+q,p_i-q;E)$ and $E^{ei}_{p,q} = E^e_{p_e+q}+E^i_{p_i-q}$ were used. The Fermi functions occurring in the T-matrices such as $(1-f^e_{p_e}-f^i_{p_i})$ were ne-

---

proportional to the second order in the potential are considered. A suitable choice of variables in accordance with the δ-functions as $p_1 = \bar{p}-\frac{q}{2}; p_3 = \bar{p}+\frac{q}{2}; p'_1 = l+\frac{q}{2}; p'_3 = l-\frac{q}{2}$ and $c'_1 = d$ allows to perform most of the integrations in Eq. (263) for the first moments and leads to

$$\begin{aligned}
\langle v^c_{p,0}; v^{c'}_{p',0} \rangle^{\rm ladder}_z \;=\; & \frac{i}{\hbar\beta} \sum_{\bar{p}lqd} \frac{{\rm e}^{\beta(\Delta E^d_{l,q}-\Delta E^c_{\bar{p},q})}-1}{\hbar z+\Delta E^d_{l,q}-\Delta E^c_{\bar{p},q}} \, \frac{1}{\Delta E^d_{l,q}-\Delta E^c_{\bar{p},q}} \, f^d_{l+\frac{q}{2}}\left(1-f^d_{l-\frac{q}{2}}\right) \qquad (264) \\
& \times f^c_{\bar{p}-\frac{q}{2}}\left(1-f^c_{\bar{p}+\frac{q}{2}}\right) [V_{cd}(q)]^2\, \delta_{cc'}\, \{\delta_{p,\bar{p}+\frac{q}{2}}-\delta_{p,\bar{p}-\frac{q}{2}}\}\, \{\delta_{p',\bar{p}+\frac{q}{2}}-\delta_{p',\bar{p}-\frac{q}{2}}\} \ .
\end{aligned}$$

This is the same expression as the first term in the Born approximation, Eq. (232), taken in the long-wavelength limit $k = 0$. The second term in Eq. (232) originates from double-exchange contribution which has not been considered within the derivation of the T–matrix approximation given here.

glected since we will consider only the non-degenerate case in the following. Eq. (266) contains the half off-shell T-matrices for the electron-ion scattering, where the energy coincides with either the incoming or the outgoing energy, respectively. In general, Eq. (258)

$$\begin{aligned} T^{\pm}_{ei}(p_e,p_i;q;E) &= V_{ei}(q)+\sum_{q'} V_{ei}(q')\,\frac{1}{E-E^{ei}_{p,q'}\pm i\eta}\,T^{\pm}_{ei}(p_e+q',p_i-q';-q'+q;E) \\ &= \sum_{l=0}^{\infty}(2l+1)T^{\pm}_{l}(p_r,|\vec{p}_r+\vec{q}|;E)P_l(\cos\theta) \end{aligned} \tag{267}$$

holds for arbitrary values of energy E. For the partial wave decomposition of the T–matrix in the second expression, the relative linear momentum $\vec{p}_r = (m_i\vec{p}_e - m_e\vec{p}_i)/(m_e+m_i) \approx \vec{p}_e$ were used. In the Legendre polynomials $P_l(\cos\theta)$, θ is the angle between $\vec{p}_r$ and $(\vec{p}_r+\vec{q})$.

In the following, the higher order products of the T-matrices occurring in Eq. (266) will be neglected. Insertion of the Lippmann-Schwinger equation in partial wave expansion, Eq. (267), yields, after performing the integrals over the angular parts,

$$\begin{aligned} \mathrm{Re}\,\nu^{\mathrm{ladder}}(\omega) &= \frac{\beta\,\Omega^2}{3\pi^3\hbar}\int_0^\infty dp\,p^2\int_0^\infty dp'\,p'^2\delta(p^2-p'^2+\frac{2m_e\omega}{\hbar})\;f^e_p\;\frac{1-\mathrm{e}^{-\beta\hbar\omega}}{\beta\hbar\omega} \\ &\times\sum_{l=0}^{\infty}(l+1)\;\Big[\Big\{p'T^-_l(p,p';E^e_p)-pT^-_{l+1}(p,p';E^e_{p'})\Big\}\Big\{p'T^+_l(p',p;E^e_p)-pT^+_{l+1}(p',p;E^e_{p'})\Big\} \\ &+\Big\{pT^-_l(p,p';E^e_{p'})-p'T^-_{l+1}(p,p';E^e_p)\Big\}\Big\{pT^+_l(p',p;E^e_{p'})-p'T^+_{l+1}(p',p;E^e_p)\Big\}\Big]\;. \end{aligned} \tag{268}$$

With the help of the δ-function one integral can be performed, e.g. putting $p'^2 = p^2+2m_e\omega/\hbar$.

In lowest order, the T-matrices $T^{\pm}_{ei}(p_e,p_i;q;E)$ in Eq. (267) or Eq. (268) are replaced by the interaction potential $V_{ei}(q)$, and we reproduce the Born approximation, see Eq. (233). However, the Coulomb interaction $V_{ei}(q)$ is now replaced by a statically screened electron-ion interaction

$$V^{\mathrm{st.sc.}}_{ei}(q) = \frac{V_{ei}(q)}{|\epsilon(k,0)|^2} = \frac{e^2}{\epsilon_0\Omega}\,\frac{1}{(q^2+\kappa^2)^2} \tag{269}$$

with the definition of the screening parameter κ given in Eq. (183). The second Born approximation can be derived from the general expression (266). The result in adiabatic approximation is

$$\begin{aligned} \nu^{2.\mathrm{Born}}(\omega) &= \frac{2i\,\hbar\beta\Omega^3}{3(2\pi)^9 m_e}\int d^3p\int d^3p'\int d^3p''\frac{\mathrm{e}^{\beta(E^e_p-E^e_{p'})}-1}{\beta(E^e_p-E^e_{p'})}\,\frac{1}{\hbar(\omega+i\eta)+E^e_p-E^e_{p'}} \\ &\times f^e_p(1-f^e_{p'})V_{ei}(\vec{p}'-\vec{p})V_{ei}(\vec{p}''-\vec{p}')V_{ei}(\vec{p}-\vec{p}'')(\vec{p}'-\vec{p}) \\ &\times\left(\frac{\vec{p}''-\vec{p}'}{E^e_p-E^e_{p''}+i\hbar\eta}-\frac{\vec{p}''-\vec{p}}{E^e_{p'}-E^e_{p''}+i\hbar\eta}\right) \end{aligned} \tag{270}$$

which can be further simplified in the limit of large β (small temperatures) at appropriately fixed values of κ_D, in order to justify to take the non-degenerate limit.

From the general symmetry property r.h.s.$(\omega) = [\text{r.h.s.}(-\omega)]^*$ of the right hand side of Eq. (266), we conclude that the dynamical collision frequency in the zero-frequency limit $\nu^{\text{ladder}}(0)$ must be real. Therefore, in the decomposition due to the Dirac identity $i/(\omega - \omega' + i\eta) = \pi\delta(\omega-\omega') + i\mathcal{P}/(\omega-\omega')$ only the δ function describing the conservation of kinetic energy gives a contribution. Then, products of two on-shell T-matrices remain which can be expressed in terms of scattering phase shifts. The higher order products of T-matrices in Eq. (266) vanish because the difference in the square brackets is equal to zero. We obtain

$$\begin{aligned}\nu^{\text{ladder}}(0) &= \frac{4\pi\,\beta\,\hbar}{\Omega n_e m_e}\sum_{p_e p_i q} q_z^2\, f^e_{p_e}\left(1-f^e_{p_e+q}\right)\, f^i_{p_i}\left(1-f^i_{p_i-q}\right)\,\delta(E^{ei}_{p,q}-E^{ei}_{p,0}) \\ &\quad\times T^-_{ei}(p_e,p_i;q;E^{ei}_{p,0})T^+_{ei}(p_e+q,p_i-q;-q;E^{ei}_{p,0})\,. \end{aligned} \tag{271}$$

In adiabatic approximation, we perform the integration over p_i to give a factor $n_i\Omega$ and relate the product of the T-matrices to the transport cross section

$$\mathcal{Q}^T_{ei}(k) = \frac{4\pi}{k^2}\sum_{l=0}^{\infty}(l+1)\,\sin^2\left[\delta^{ei}_{l+1}(k)-\delta^{ei}_l(k)\right]\,, \tag{272}$$

as detailed in Refs. [51, 98, 112, 108, 113], $\delta^{ei}_l(k)$ are the scattering phase shifts. Taking the non-degenerate limit, we obtain

$$\nu^{\text{ladder}}(0) = \frac{8}{3\sqrt{\pi}}\frac{\hbar n_i}{m_e}\left(\frac{\beta\hbar^2}{2m_e}\right)^{5/2}\int_0^\infty dk\; k^5\;\mathrm{e}^{-\frac{\beta\hbar^2k^2}{2m_e}}\,\mathcal{Q}^T_{ei}(k)\,. \tag{273}$$

This way, the correct zero frequency limit for the collision frequency is reproduced. Numerical results will be given in section 4.6.

4.4 DC Conductivity and Virial Expansion

In the static limit, the imaginary part of the collision frequency is zero. The dc-conductivity (229) is directly related to the real part of the collision frequency. In the following, we will apply the various approximations for the treatment of the correlation functions (231) which were presented in the previous sections in order to derive an expression for the dc–conductivity considering the adiabatic limit in a systematic manner. Furthermore, we will discuss the extension of the set of relevant observables in order to include higher order perturbation contributions. Subsequently, we derive generalized expressions via introducing a renormalization factor. On this basis, Esser *et al.* [114] constructed an interpolation formula which is valid over a wide parameter range of temperature and density.

In Born approximation, the static collision frequency (234) can be transformed to give

$$\sigma^{\text{Born}}_{\text{dc}} = \frac{\epsilon_0\omega^2_{\text{pl}}}{\nu^{\text{Born}}(0)} = \frac{12\pi^3\hbar^3e^2n_e^2}{\Omega^2m_e^2n_i}\left[\int_0^\infty dq\,q^3\;V^2_{ei}(q)\,S_i(q)\;f^e_{q/2}\right]^{-1}\,. \tag{274}$$

The interaction is a pure Coulombic one. Since the Coulomb interaction is long-ranged the Born approximation diverges for small absolute values of $\vec{q}$ in the static case. On a practical level, the Coulomb potential could be replaced by a statically screened potential (Debye potential) or a pseudopotential. The latter one would also take into account the structure and finite size of the ions (if not hydrogen).

A more consistent treatment requires dynamical screening as outlined in section 4.2. From (247), the Ziman formula [115, 116]

$$\sigma_{\rm dc}^{\rm Ziman} \;=\; \frac{\epsilon_0\omega_{\rm pl}^2}{\nu^{\rm LB}(0)} \;=\; \frac{12\pi^3\hbar^3e^2n_e^2}{\Omega^2m_e^2n_i}\left[\int_0^\infty dq\,q^3\;\frac{V_{ei}^2(q)\,S_i(q)}{|\epsilon_{\rm RPA}(q,0)|^2}\,f_{q/2}^e\right]^{-1} \tag{275}$$

is obtained. The inclusion of ion dynamics considering the dynamical ionic structure factor is straightforward and should coincide with the expression (245) for the two-component system. Only in this case, the dc-conductivity is influenced by dynamical screening and the frequency argument of the dielectric function is an energy dependent variable. The connection between the Ziman formula and the Lenard-Balescu result was also investigated in Ref. [117] taking into account the relation between the dielectric function and the structure factor, Eq. (77).

Further evaluation of the Ziman formula (275) using the long-wavelength limit of the RPA dielectric function (182) in the non-degenerate case and for uncorrelated ions ($S_i(\vec{q}) = 1$) yields

$$\sigma_{\rm dc}^{\rm Ziman} \;=\; \frac{3}{4\sqrt{2\pi}}\;\frac{(4\pi\epsilon_0)^2}{\beta^{3/2}m_e^{1/2}e^2}\,\frac{n_e}{n_i}\,\frac{1}{L_{\rm BH}} \tag{276}$$

with the Brooks-Herring Coulomb logarithm [118, 119]

$$L_{\rm BH} = \frac{1}{2}\int_0^\infty \frac{x\,dx}{(x+\kappa_D^2)^2}{\rm e}^{-\beta\hbar^2x/8m_e} \tag{277}$$

and the Debye screening κ_D according to the nondegenerate limit of Eq. (184). This approximation is valid for high temperatures ($\Gamma^2\Theta \ll 1$, see Eqs. (1), (2) for definitions). In its low–density limit, the following expansion can be given [51, 108, 114]

$$L_{\rm BH} = -\frac{1}{2}\,\ln\zeta - \frac{1}{2}(C+1) - \zeta\ln\zeta + \ldots \tag{278}$$

with $\zeta = (2/3\pi^2)^{1/3}\Gamma/\Theta$ and C=0.5772...the Euler's constant. From calculations of the Lenard-Balescu collision term, Eq. (245), for the dynamic screening in a symmetric plasma ($n_e = n_i$), the static limit

$$L_{\rm LB} = \frac{1}{2}\,\left(\ln\frac{\Theta}{\Gamma} + 0.4807\right) \tag{279}$$

is obtained. Comparing with expansion (278) for the Born approximation of a statically screened potential, an effective screening parameter

$$\kappa_{\rm eff}^2 = 1.47\,n_ee^2\beta/\epsilon_0 \tag{280}$$

is derived [51, 108] which will be used in further calculations. Thus, the Born approximation of a statically screened collision term accounts for the effects of dynamic screening via an effective screening parameter.

Taking into account strong binary collisions as outlined in section 4.3 leads to expression (273). If we take the transport cross section $\mathcal{Q}_{ei}^T(k)$ in quasiclassical approximation [51, 98, 108]

$$\mathcal{Q}_{ei}^T(k) = \frac{4\pi}{a_B^2 k^4} \ln\left(0.681 \frac{k^2 a_{\rm B}}{\kappa_D}\right) , \tag{281}$$

where $a_{\rm B} = 4\pi\epsilon_0\hbar^2/(m_e e^2)$ is the Bohr radius and perform the integral over k in Eq. (273) we find for the dc-conductivity (229)

$$\sigma_{\rm dc}^{\rm ladder} = \frac{3}{4\sqrt{2\pi}} \frac{(4\pi\epsilon_0)^2}{\beta^{3/2} m_e^{1/2} e^2} \frac{n_e}{n_i} \frac{1}{L_{\rm ladder}} , \qquad L_{\rm ladder} = \ln\left(0.765 \frac{4\pi\epsilon_0}{\beta e^2 \kappa_D}\right) . \tag{282}$$

The exact low-density limit for the dc conductivity of a Lorentz plasma[41] was derived by Spitzer [58, 59],

$$\sigma_{\rm dc}^{\rm Lorentz} = \frac{4\sqrt{2}}{\pi^{3/2}} \frac{(4\pi\epsilon_0)^2}{\beta^{3/2} m_e^{1/2} e^2} \frac{n_e}{n_i} \frac{1}{L_{\rm Sp}} , \qquad L_{\rm Sp} = \ln \frac{3}{\sqrt{2}} \frac{4\pi\epsilon_0}{\beta e^2 \kappa_{\rm D}} = \frac{1}{2} \ln\left(\frac{3}{2}\Gamma^{-3}\right) . \tag{283}$$

The Spitzer Coulomb logarithm is a good approximation only in the low density limit. It coincides with the Coulomb logarithm $L_{\rm ladder}$ in ladder approximation for the statically screened interaction potential up to an additive constant reflecting the different treatment of the screening of the Coulomb interaction. A possible improvement is the use of an effective screening parameter $\kappa_{\rm eff}$ as introduced above. However, the prefactors of ladder and Lorentz limit differ from each other. This discrepancy can be resolved by considering higher moments of the distribution functions as will be discussed below. Furthermore, for a correct treatment of a fully ionized plasma in the low–density limit a different prefactor is obtained [58, 59]

$$\sigma_{\rm dc}^{\rm Sp} = 0.591 \frac{(4\pi\epsilon_0)^2}{\beta^{3/2} m_e^{1/2} e^2} \frac{n_e}{n_i} \frac{1}{L_{\rm Sp}} . \tag{284}$$

The origin of the prefactor will be shown to come from electron–electron interactions, see below.

4.4.1 Renormalization Factor

Using the linear response approach as presented here, the incorporation of contributions due to higher order perturbation theory for the dc–conductivity of a fully ionized plasma has been considered in several papers, e.g. [51]. For this, correlation functions additional to the force–force correlation functions in Eq. (230) have to be considered, see Eq. (175). It was

[41] A Lorentz plasma is a fully ionized plasma in which electrons interact with ions at fixed positions and the electron-electron interaction is neglected.

shown that the incorporation of higher moments of the single-particle distribution function (122) is an alternative. Restricting ourselves to higher moments of the electron distribution function (adiabatic approximation), Eq. (122), with $c = e$,

$$\vec{P}^{e}_{k,n} = \sum_{p} \hbar\vec{p}\left(\beta\, E^{e}_{p}\right)^{n} n^{e}_{p,k}\,, \tag{285}$$

the number of observables in the relevant statistical operator is systematically increased. This leads to the inclusion of the electron–electron interaction and contributions due to the kinetic energy current. In analogy to the discussion in section 3.4, the only contributions to the submatrix elements, Eq. (133), in second order, come from the generalized force-force correlation function

$$\langle \dot{\vec{P}}^{c}_{0,l}; \dot{\vec{P}}^{c'}_{0,m} \rangle_{\omega+i\eta} \;=\; \hbar^2 \sum_{pp'} p_z p'_z \,(\beta E^{c}_{p})^{l}\,(\beta E^{c}_{p})^{m} \lim_{k\to 0} \langle v^{c}_{p,k}; v^{c'}_{p',k} \rangle^{(2)}_{\omega+i\eta}\,, \tag{286}$$

see also Eq. (209). The correlation functions of higher moments can be calculated similar to the force-force correlation function, Eq. (208), with different prefactors in p_z and p'_z. We introduce a renormalization factor $r^{(n)}$

$$\sigma_{\rm dc} \;=\; \frac{\epsilon_0\,\omega^2_{\rm pl}}{r^{(n)}\,\nu^{(P_0)}(0)}\,, \tag{287}$$

which relates the n-moment approach of the inverse response function to the one-moment approach according to the static limits of the correlation functions in the determinants in Eq. (125)

$$r^{(n-1)} \;=\; \frac{M^{(n)}}{M^{(1)}} \;=\; \frac{|r_{lm}|}{\begin{vmatrix} 0 & s_m \\ s_l & r_{lm} \end{vmatrix}}\,, \qquad\qquad l,m \;=\; 0,1,2,\ldots n-1 \tag{288}$$

with

$$s_m \;=\; \frac{(\vec{P}^{e}_{0,0}; \vec{P}^{e}_{0,m})}{(\vec{P}^{e}_{0,0}; \vec{P}^{e}_{0,0})}\,, \qquad r_{lm} \;=\; \frac{\langle \dot{\vec{P}}^{e}_{0,l}; \dot{\vec{P}}^{e}_{0,m} \rangle_{i\eta}}{\langle \dot{\vec{P}}^{e}_{0,0}; \dot{\vec{P}}^{e}_{0,0} \rangle_{i\eta}}\,. \tag{289}$$

In the non-degenerate limit is

$$s_m \;=\; \frac{\Gamma\,(m+5/2)}{\Gamma\,(5/2)} \tag{290}$$

and the ratios for r_{nm} have been well investigated, see e.g. [98, 112]. The following ratios are obtained, if we consider the moments $P^{e}_{0,0}, P^{e}_{0,1}$, and $P^{e}_{0,2}$ in the low-density limit

$$\begin{aligned} r_{00} \;&=\; 1\,; \qquad & r_{11} &= 2+\sqrt{2}\,; \\ r_{10} \;&=\; 1\,; \qquad & r_{21} &= 6+11/\sqrt{2}\,; \\ r_{20} \;&=\; 2\,; \qquad & r_{22} &= 24+157/\sqrt{8}\,, \end{aligned}$$

where terms in $\sqrt{2}$ arise from electron-electron collisions. We obtain the renormalization factors, Eq. (288),

$$r^{(0)} = 1 \tag{291}$$
$$r^{(1)} = 0.5176 \tag{292}$$
$$r^{(2)} = 0.5123\,. \tag{293}$$

The behavior of this series, if further moments in the zero-frequency limit are taken into account, was investigated in [49, 98] and found to converge against the Spitzer value $r_{\mathrm{Sp}} = 0.2992/0.591 = 0.506$. In the case of a Lorentz plasma, where only interaction between electrons and ions is considered, the renormalization factor is $r_{\mathrm{L}} = 0.2992/1.0159 = 0.2945$. In that case, the moment expansion converges more quickly with $r^{(1)} = 0.3077$, $r^{(2)} = 0.2949$. Subsequently, different prefactors are obtained for the dc-conductivity, Eq. (282), or the Brooks-Herring result (276). This approach is in analogy to the kinetic theory (Chapman-Enskog approach) where the expansions of the distribution function with respect to Sonine polynomials lead to similar expressions and prefactors [60].

4.4.2 Gould–DeWitt approximation

Following the discussion of the different approximations for the static collision frequency, it becomes apparent that in order to give a consistent description of the effect of collisions in a Coulomb system, we have to combine dynamical screening and strong collisions. Up to now there is no solution available for a dynamically screened ladder approximation. An approximation which interpolates between weak collisions (small q), which have to be screened dynamically, and strong collisions (large q), where a ladder summation has to be performed, has been given by Gould and DeWitt [120, 121]. In this case, a statically screened potential is taken for the ladder summation, Eq. (273), which coincides with a Boltzmann collision integral in kinetic equations. The contribution from the lowest order (Born) collision integral, Eq. (276), is calculated for the same statically screened potential separately. It is subtracted and replaced by the dynamically screened second order (Lenard-Balescu) collision integral, Eq. (246). In an one-moment approximation, the static collision frequency is determined as

$$\nu^{(P_0)}(0) \approx \nu^{\mathrm{GD}} = \nu^{\mathrm{ladder}}(0) - \nu^{\mathrm{Born}}(0) + \nu^{\mathrm{LB}}(0)\,, \tag{294}$$

This approach was also applied to the dc-conductivity of a fully ionized, nondegenerate hydrogen plasma [108]. Instead of Eq. (246), Gould and DeWitt [120, 121] took into account ion dynamics using a dynamic ion structure factor. The electrons were screened statically, according to the static limit of Eq. (247). In [108], an effective screening parameter was used in the ladder approximation in order to take into account the ion dynamics.

4.4.3 Debye–Onsager effect

A further extension of the set of relevant observables is the inclusion of two–particle correlations [51] of the type [122]

$$\delta n^{c,c'}_{l,l'}(k) = \sum_{p,p'} (\hbar\vec{p})^l \, (\hbar\vec{p}')^{l'} \, n^c_{p,k} \, n^{c'}_{p',-k} \tag{295}$$

which leads to a correction of the Coulomb logarithm. The dependence of the leading terms of a virial expansion on density and temperature which goes beyond the Spitzer Coulomb logarithm is given in the low–density, non–degenerate limit as [51]

$$\begin{aligned} L &= \ln\Gamma^{-3/2} + b + c\,\Gamma^{3/2}\ln\Gamma^{-3/2} \\ &= A(T)\ln n + B(T) + C(T)\, n^{1/2}\ln n \ldots . \end{aligned} \tag{296}$$

The factors c and C in Eq. (296) are related to the Debye-Onsager relaxation effect, which is known from the theory of electrolytes [123, 124] as

$$L_{\rm DO} = L_{\rm BH}\left[1 - \frac{\Gamma^{3/2}}{\sqrt{3}(2+\sqrt{2})}\right]^{-1} . \tag{297}$$

It describes the partial compensation of the electric field acting on a charged particle by the formation of an asymmetric screening cloud. Klimontovich and Ebeling [125] found the original Onsager result for the relaxation effect in weakly ionized plasma, where the assumption of a local Maxwellian distribution is well founded. In order to include the Debye-Onsager effect within our approach, the set of relevant observables[42] has to be extended. For the reproduction of the original Onsager result, $\delta n^{e,i}_{0,0}$ has to be taken into account. Furthermore, $C(T)$ in Eq. (296) is modified in comparison to the Onsager result if the assumption of a local Maxwellian distribution is dropped and a further moment $\delta n^{e,i}_{2,0}$ is included, see Ref. [122].

4.4.4 Interpolation Formula

The limiting cases presented above have been used to derive a fit formula for the dc–conductivity of a fully ionized plasma. The quasiclassical limit has been determined [122] as

$$\sigma^{\rm quasiclassic}_{\rm dc}(\Gamma) = 0.591\frac{(4\pi\epsilon_0)^2(k_BT)^{3/2}}{e^2m^{1/2}}\left[\ln\Gamma^{-3/2} + 1.124 + \frac{1.078}{\sqrt{6}+\sqrt{3}}\Gamma^{3/2}\ln\Gamma^{-3/2}\right]^{-1} \tag{298}$$

taking the correct prefactor from the Spitzer result, applying a two–moment approximation, and including two-particle correlations for the Debye-Onsager effect for the determination of the factors in the expansion (296). Following previous attempts for the derivation of an

[42] see discussion in section 2.3

interpolation formula [49, 98, 126, 127] the following expression has been constructed [114] taking into account the limiting cases elaborated above as well as numerical calculations in intermediate parameter ranges,

$$\sigma_{\rm dc}^{\rm ERR}(\Gamma,\Theta) \;=\; a_0 T^{3/2}\left(1+\frac{b_1}{\Theta^{3/2}}\right)\left[D\ln(1+A+B)-C-\frac{b_2}{b_2+\Gamma\Theta}\right]^{-1} \qquad (299)$$

where T in K, σ in $(\Omega{\rm m})^{-1}$, and with the functions

$$\begin{aligned}
A &= \Gamma^{-3}\frac{1+a_4/\Gamma^2\Theta}{1+a_2/\Gamma^2\Theta+a_3/\Gamma^4\Theta^2}\;\left[a_1+c_1\ln(c_2\Gamma^{3/2}+1)\right]^2\,,\\
B &= \frac{b_3(1+c_3\Theta)}{\Gamma\Theta(1+c_3\Theta^{4/5})}\,,\\
C &= \frac{c_4}{\ln(1+\Gamma^{-1})+c_5\Gamma^2\Theta}\,,\\
D &= \frac{\Gamma^3+a_5(1+a_6\Gamma^{3/2})}{\Gamma^3+a_5}\,.
\end{aligned}$$

The set of parameters is persented in TAB. 1. They are fixed by the low-density expansions

a_0	a_1	a_2	a_3	a_4	a_5	a_6
0.03064	1.1590	0.698	0.4876	0.1748	0.1	0.258
b_1	b_2	b_3	c_1	c_2	c_3	c_4	c_5
1.95	2.88	3.6	1.5	6.2	0.3	0.35	0.1

Table 1: Parameters for the interpolation formula (299) for the static conductivity $\sigma_{\rm dc}^{\rm ERR}$

of the dc conductivity (Spitzer), the strong degenerate limit (Ziman) [128] and numerical results by Ichimaru and Tanaka [129, 130] for the dc–conductivity in the degenerate strongly coupled region. In comparison to an earlier version [127], the validity region was improved as well as the accuracy in particular due to the inclusion of the Debye-Onsager effect and the extension into a region where the ion-ion structure factor is relevant.

A comparison of this interpolation formula with experimental results was given in [114]. For the region of plasma parameters of interest, $1 < \Gamma < 2$ and $\Theta > 1$, conductivities obtained from experiments have an accuracy of about 30 % and can be reproduced by the interpolation formula. Another check of accuracy of the interpolation formula for the conductiviy is given by MD simulations to be described below.

4.5 Generalized Drude Formula

As a result of the evaluation of the correlation functions (231) in different approximations and the analysis of the behavior of the collision frequency in the static limit (dc–conductivity),

the frequency-dependent conductivity $\sigma(\omega)$ in the long-wavelength limit, Eq. (227), will be parametrized as follows

$$\sigma(\omega) \;=\; \frac{\epsilon_0\,\omega_{\rm pl}^2}{-i\,\omega \;+\; r(\omega)\,\nu^{(P_0)}(\omega)} \;, \tag{300}$$

where $\nu^{(P_0)}(\omega)$ is the collision frequency calculated in the single moment approach for the distribution function (force-force correlation function), within the dynamically screened binary collision approximation as will be described below. The renormalization factor takes into account corrections due to higher moments in the set of relevant observables, Eq. (122). In the zero-frequency limit (dc-conductivity), results for the static collision frequency $\nu^{(P_0)}(0)$ as well as for the renormalization factor $r(0)$ are known and have been reported in section 4.4. The approach given here allows the extension to finite frequencies.

4.5.1 Dynamically Screened Binary Collision Approximation

In order to give a consistent description of the effect of collisions in a Coulomb system, we have to combine dynamical screening and strong collisions. Up to now, there is no solution available for a dynamically screened ladder approximation which leads to a collision frequency $\nu^{(P_0)}(\omega)$ in a one-moment approach. However, a similar description as it was suggested in the static case by Gould and DeWitt, see section 4.4 and [87], will be used to construct a dynamical collision frequency which interpolates between the Lenard-Balescu expression valid for distant collisions, i.e. small transfer momenta q, where the Born approximation with respect to the dynamically screened interaction can be considered, and the Boltzmann expression valid for close collisions, i.e. large transfer momenta q, where a static potential such as the Debye potential can be taken. To avoid double counting, the collision frequency in Born approximation with respect to the static potential has to be subtracted. As in the static case (294), we use the following ansatz

$$\nu^{(P_0)}(\omega) \approx \nu^{\rm GD}(\omega) \;=\; \nu^{\rm ladder}(\omega) \;-\; \nu^{\rm Born}(\omega) \;+\; \nu^{\rm LB}(\omega) \;, \tag{301}$$

where the Born approximation, Eq. (233), is calculated for the statically screened potential and the adiabatic expression (248) is used for the Lenard-Balescu collision term. The differences between the various approximations discussed are most pronounced in the static limit. Above the plasma frequency, the correction to the convergent collision term, Eq. (301), decreases with increasing frequency due to screening. The high-frequency behavior is the same in all three approximations. This will be shown below.

The differences between the Born and the ladder approximations are most pronounced in the vicinity of the plasma frequency. The effective potential can be introduced in the low-density limit in such a way that in the zero-frequency limit the collision frequency in dynamically screened Born approximation coincides with the collision frequency in Born approximation for the effective interaction, see the introduction of $\kappa_{\rm eff}$ in section 4.4. Considering the static low-density limit, the different terms coincide to give identical results for $\nu(0)$ in the order $n \ln n$. The differences occur with respect to a factor within the argument

of the logarithm, which can be rewritten as a constant (with respect to n) term in addition to $\ln n$. The determination of this constant demands an accurate treatment of dynamically screened binary collisions. As long as we are interested only in the term $\propto n \ln n$, it is sufficient to use the statically screened potential with the effective Debye screening parameter (280) or (247). Then we have $\nu^{(P_0)}(\omega) \approx \nu_{\rm D}^{\rm Born}(\omega)$,

$$\begin{aligned} \nu_{\rm D}^{\rm Born}(\omega) &= -i\frac{(2\pi\beta)^{3/2}\hbar^4 n_i e^4}{3m_e^{3/2}\epsilon_0^2}\int\frac{d^3p}{(2\pi)^3}\int\frac{d^3q}{(2\pi)^3}\,\frac{q^2}{(\kappa_{\rm eff}^2+q^2)^2}\,\frac{{\rm e}^{\beta E^e_{p+q/2}}-e^{\beta E^e_{p-q/2}}}{\Delta E^e_{p,q}-\hbar(\omega+i\eta)}\,\frac{1}{\Delta E^e_{p,q}} \\ &= -ig\,n_i\int_0^\infty\frac{y^4dy}{(\bar n+y^2)^2}\int_{-\infty}^\infty dx\;{\rm e}^{-(x-y)^2}\,\frac{1-{\rm e}^{-4xy}}{xy(xy-w-i\eta)} \end{aligned} \tag{302}$$

with

$$g=\frac{1}{24\sqrt{2}\pi^{5/2}}\,\frac{e^4\beta^{3/2}}{m_e^{1/2}\epsilon_0^2}\,,\qquad w=\frac{\hbar\omega}{4k_{\rm B}T}\,,\quad \bar n=\frac{\hbar^2\kappa_{\rm eff}^2}{8m_e k_{\rm B}T}\,. \tag{303}$$

4.5.2 High frequency behaviour of dynamical conductivity

In this subsection we give details of the determination of the high frequency behavior of the dynamical collision frequency in dynamically screened approximation and in ladder approximation. In the limit $\omega\to\infty$ the real part of the RPA dielectric function fulfills the asymptotic form (60)

$$\lim_{\omega\to\infty}{\rm Re}\,\epsilon(k,\omega) \;=\; 1-\frac{\omega_{\rm pl}^2}{\omega^2}+O(\omega^{-4})\,. \tag{304}$$

and is therefore almost unity, thus ${\rm Im}\,\epsilon^{-1}(k,\omega)\;\approx\;{\rm Im}\,\epsilon(k,\omega)$. Therefore, the limiting behavior of the Born approximation, Eq. (235), as well as the dynamically screened Born approximation, equation (248), is given by

$${\rm Re}\,\nu(\omega)\;\propto\;\frac{1}{\omega}\int_0^\infty{\rm d}k\,k^2\,{\rm Im}\,\epsilon(k,\omega) \tag{305}$$

if the k-dependence of the Coulomb potential is inserted and the static structure factor is assumed to be 1.

In the degenerate limit ($\theta=1/(\beta E_F)\ll 1$), the imaginary part of the dielectric function is [70]

$$\lim_{\theta\to 0}{\rm Im}\,\epsilon_{\rm RPA}(k,\omega) \;=\; \begin{cases} \frac{\pi\chi_0^2}{8z^3}\,\frac{\hbar\omega}{E_F} & : \quad (u\pm z)^2<1 \\ \frac{\pi\chi_0^2}{8z^3}\,(1-(u-z)^2) & : \quad (u-z)^2<1<(u+z)^2 \\ 0 & : \quad 1<(u-z)^2 \end{cases}\quad, \tag{306}$$

using the reduced variables $u=m\omega/(\hbar k_F k)$, $z=k/(2k_F)$, $\chi_0^2=(3/16)(\hbar\omega_{\rm pl}/E_F)^2$. For sufficiently large values of ω, $(u+z)^2$ is always larger than unity. Finite values for the

imaginary part of the dielectric functions are only obtained if the condition $(u-z)^2 < 1$ is obeyed. Applying the transformation $q = k/k_F$, this translates to

$$\left| \frac{m\omega}{\hbar k_F^2 q} - \frac{q}{2} \right| < 1 \tag{307}$$

and leads to an upper and lower bound for the k-integration in equation (305) which can then be performed,

$$\begin{aligned} \int_0^\infty \mathrm{d}k\, k^2\, \mathrm{Im}\, \epsilon_{\mathrm{RPA}}(k,\omega) &\propto \int_{a-1}^{a+1} \frac{\mathrm{d}q}{q} \left[1 - \left(\frac{m\omega}{\hbar k_F^2 q} - \frac{q}{2} \right)^2 \right] \\ &= \left(1 + \frac{m\omega}{\hbar k_F^2} \right) \left[\ln(a+1) - \ln(a-1) \right] - a\,, \quad a = \sqrt{1 + \frac{2m\omega}{\hbar k_F^2}}\,. \end{aligned} \tag{308}$$

The asymptotic form of this expression in the high-frequency limit is proportional to $\omega^{-1/2}$, corresponding to a power law $\omega^{-3/2}$ for $\mathrm{Re}\,\nu(\omega)$.

In the non-degenerate limit ($1/\theta \ll 1$), the imaginary part of the dielectric function is [70]

$$\lim_{1/\theta \to 0} \mathrm{Im}\, \epsilon_{\mathrm{RPA}}(q,\omega) = \frac{\pi \chi_0^2}{8 z^3}\, \theta\, \mathrm{e}^{\beta\mu} \left[\mathrm{e}^{-(u-z)^2/\theta} - \mathrm{e}^{-(u+z)^2/\theta} \right] \tag{309}$$

with defintions of u, z, χ_0 as in Eq. (306).

The integration with respect to q, carried out analytically, results in a collision frequency (305) proportional to a modified Bessel function [131]

$$\mathrm{Re}\,\nu(\omega) \propto \frac{1}{\omega} \sinh\left(\frac{\beta\hbar\,\omega}{2} \right) K_0\left(\frac{\beta\hbar\omega}{2} \right) \quad . \tag{310}$$

The high frequency limit [131] $K_0(z) \sim \sqrt{\pi/(2\,z)}\, e^{-z}\, (1 - 1/(8z) + \dots)$ gives a dependence of $\omega^{-3/2}$ again.

The absorption coefficient $\alpha(\omega)$ for radiation and the imaginary part of the dielectric function are connected via, see Eq. (74)

$$\alpha(\omega) = \frac{\omega}{c\, n(\omega)} \lim_{k \to 0} \mathrm{Im}\, \epsilon(k,\omega) \quad , \tag{311}$$

where c is the speed of light and $n(\omega)$ the index of refraction. Using this relation, the asymptotic scaling of the imaginary part of the dielectric function compares to known results for the frequency dependence of the absorption coefficient of thermal bremsstrahlung at high temperatures [132], see also section 6.2.

The frequency dependence of the dynamical collision frequency in ladder approximation can be determined by exploiting the known off-shell behavior of the Coulomb T–matrix [133].

Inserting the analytic expression of the half-off-shell T–matrix into Eq. (266) results again in a frequency dependence according to $\omega^{-3/2}$, see [87], however with a prefactor depending on density and temperature. Considering the real part of the 2nd Born approximation (270) due to the singularity from the first denominator, the integrals are performed and give in the high-frequency limit $\omega \to \infty$ the same behavior $\propto \omega^{-3/2}$, multiplied with a prefactor $\propto 1/\kappa_D$.

Thus, the asymptotic form of the real part of the collision frequency is given by $\mathrm{Re}\,\nu(\omega) \propto \omega^{-3/2}$ in the degenerate as well as the non-degenerate limit. The latter has been shown for the dynamically screened and the ladder approximation. As a consequence, having in mind that the asymptotic expansion of the dielectric function reads

$$\lim_{\omega\to\infty} \epsilon(\omega) \;=\; 1 - \frac{\omega_{\mathrm{pl}}^2}{\omega^2} \;+\; i\frac{\omega_{\mathrm{pl}}^2 \nu(\omega)}{\omega^3} \;+\; 0(\omega^{-4})\,, \tag{312}$$

we get $\mathrm{Im}\,\epsilon(\omega) \propto \omega^{-9/2}$.

4.5.3 Renormalization Factor $r(\omega)$

So far, only the one-moment approach has been considered within a perturbative treatment, given by the dynamically screened ladder approximation. This is a good approximation in the degenerate case where the Ziman formula follows for the static limit. Electron-electron interactions don't contribute significantly to the scattering processes. However, the inclusion of local-field corrections in the dielectric function could be considered but is an effect in higher order perturbation theory.

A two-moment approach for a non-degenerate hydrogen plasma treating the ions and electrons on the same level was investigated in [62]. Contributions from the ion dynamics are relevant for small frequencies only and lead to a different screening parameter in the static limit, Eq. (183). It is expected that this approach is more relevant in semiconductors where electrons and holes have an effective mass of same order.

Whereas the limiting case of the dc-conductivity is well investigated, see section 205, the method presented here gives results for the optical conductivity at finite frequencies. We are concerned with the evaluation of the prefactor $r(\omega)$ in Eq. (300) as a function of frequency and follow the approach taken in the static limit (288). The renormalization factor within an n-moment approximation is defined as

$$r^{(n-1)}(\omega) \;=\; \frac{M^{(n)}}{M^{(1)}} \;=\; \frac{|r_{lm}(\omega)|}{\begin{vmatrix} 0 & s_m \\ s_l & r_{lm}(\omega) \end{vmatrix}}\,, \qquad\qquad l,m \;=\; 0,1,2,\ldots n-1, \tag{313}$$

where the frequency dependence of $r_{lm}(\omega)$ follows from frequency dependent correlation functions

$$r_{lm} \;=\; \frac{\langle \dot{\vec{P}}^e_{0,l}; \dot{\vec{P}}^e_{0,m} \rangle_{\omega+i\eta}}{\langle \dot{\vec{P}}^e_{0,0}; \dot{\vec{P}}^e_{0,0} \rangle_{\omega+i\eta}} \tag{314}$$

and s_l is given in (289).

The frequency dependent correlation functions of higher moments can be calculated similar to the force-force correlation function, Eq. (208), with different prefactors in p_z and p'_z. We obtain contributions from electron-ion as well as from electron-electron scattering,

$$\langle \dot{\vec{P}}^e_{0,l}; \dot{\vec{P}}^e_{0,m} \rangle_{\omega+i\eta} \;=\; \langle \dot{\vec{P}}^{ei}_{0,l}; \dot{\vec{P}}^{ei}_{0,m} \rangle_{\omega+i\eta} \,+\, \langle \dot{\vec{P}}^{ee}_{0,l}; \dot{\vec{P}}^{ee}_{0,m} \rangle_{\omega+i\eta} \,. \tag{315}$$

In the Debye approximation, Eq. (302), we find

$$\begin{aligned}
&\langle \dot{\vec{P}}^{ei}_{0,l}; \dot{\vec{P}}^{ei}_{0,m} \rangle_{\omega+i\eta} \\
&= -\frac{i\hbar}{\beta}\, n_i \Omega_0\, \frac{n_e \Lambda_e^3}{(2\pi)^6}\, \frac{e^4}{\epsilon_0^2} \int d^3\vec{p} \int d^3\vec{q}\, \frac{1}{(\kappa_{\rm D}^2+q^2)^2}\, \frac{{\rm e}^{\beta E^e_{p+q/2}} - e^{\beta E^e_{p-q/2}}}{\Delta E^e_{p,q} - \hbar(\omega+i\eta)}\, \frac{1}{\Delta E^e_{p,q}} \\
&\qquad \times \Big[(p_z + \frac{q_z}{2})(\beta E^e_{p+\frac{q}{2}})^l \,-\, (p_z - \frac{q_z}{2})(\beta E^e_{p-\frac{q}{2}})^l \Big] \\
&\qquad \times \Big[(p_z + \frac{q_z}{2})(\beta E^e_{p+\frac{q}{2}})^m \,-\, (p_z - \frac{q_z}{2})(\beta E^e_{p-\frac{q}{2}})^m \Big] \\
&= -ig\, \frac{\Omega_0 m_e n_e n_i}{\beta} \int_{-\infty}^{\infty} dx \int_0^{\infty} \frac{y^4\, dy}{(\bar{n}+y^2)^2}\, {\rm e}^{-(x-y)^2}\, \frac{1-{\rm e}^{-4xy}}{xy(xy-w-i\eta)} \Big\{ x; y \Big\}_{lm} .
\end{aligned} \tag{316}$$

The curly brackets stand for polynomials of x and y. After performing angular integrations, for $l = 0, 1$ we find

$$\begin{aligned}
\Big\{ x; y \Big\}_{00} &= 1 \\
\Big\{ x; y \Big\}_{01} &= \Big\{ x; y \Big\}_{10} = 1 + 3x^2 + y^2 \\
\Big\{ x; y \Big\}_{11} &= 2 + 10x^2 + 9x^4 + 2y^2 + 6x^2y^2 + y^4 \,.
\end{aligned} \tag{317}$$

The contributions due to electron-electron collisions follow as

$$\begin{aligned}
\langle \dot{\vec{P}}^{ee}_{0,l}; \dot{\vec{P}}^{ee}_{0,m} \rangle_{\omega+i\eta} \;&=\; -\frac{i\hbar}{\beta}\, \frac{4\Omega_0}{(2\pi)^9}\, \frac{e^4}{\epsilon_0^2} \int d^3\vec{p} \int d^3\vec{p}\,' \int d^3\vec{q}\, \frac{1}{(\kappa_{\rm D}^2+q^2)^2}\, \frac{f^e_{p'+\frac{q}{2}}\, f^e_{p-\frac{q}{2}}}{\Delta E^e_{p',q} - \Delta E^e_{p,q}} \\
&\times \frac{{\rm e}^{\beta(\Delta E^e_{p',q} - \Delta E^e_{p,q})} - 1}{\hbar z + \Delta E^e_{p',q} - \Delta E^e_{p,q}}\, \Big[(p_z + \frac{q_z}{2})(\beta E^e_{p+\frac{q}{2}})^l \,-\, (p_z - \frac{q_z}{2})(\beta E^e_{p-\frac{q}{2}})^l \Big] \\
&\qquad \times \Big[(p_z + \frac{q_z}{2})(\beta E^e_{p+\frac{q}{2}})^m - (p_z - \frac{q_z}{2})(\beta E^e_{p-\frac{q}{2}})^m \\
&\qquad\quad + (p'_z - \frac{q_z}{2})(\beta E^e_{p'-\frac{q}{2}})^m - (p'_z + \frac{q_z}{2})(\beta E^e_{p'+\frac{q}{2}})^m \Big] .
\end{aligned} \tag{318}$$

The first non-vanishing contribution arises for $l = m = 1$,

$$\begin{aligned}
&\langle \dot{\vec{P}}^{ee}_{0,1}; \dot{\vec{P}}^{ee}_{0,1} \rangle_{\omega+i\eta} \\
&= -ig\sqrt{2}\, \frac{\Omega_0 m_e n_e^2}{\beta} \int_{-\infty}^{\infty} dx \int_0^{\infty} \frac{y^4\, dy}{(2\bar{n}+y^2)^2}\, {\rm e}^{-(x-y)^2}\, \frac{1-{\rm e}^{-4xy}}{xy(xy-w-i\eta)} \Big\{ 1 \,+\, \frac{19}{4} x^2 \Big\} .
\end{aligned} \tag{319}$$

The real and imaginary part of expressions (316) and (319) have to be considered for an investigation of the frequency-dependent renormalization factor. One integration in the imaginary part can be obtained using the δ-function. For the real part a partial fraction decomposition has to be performed,

$$
\begin{aligned}
\mathrm{Re}\,\langle \dot{\vec{P}}^{ei}_{0,l}; \dot{\vec{P}}^{ei}_{0,m}\rangle_{\omega+i\eta} &= -g\,\frac{\pi\Omega_0 m_e n_e n_i}{\beta}\,\frac{1-\mathrm{e}^{-4w}}{w}\int_0^\infty \frac{2y^3\,dy}{(\bar{n}+y^2)^2}\,\mathrm{e}^{-(\frac{w}{y}-y)^2}\left\{\frac{w}{y}; y\right\}_{lm}, \\
\mathrm{Re}\,\langle \dot{\vec{P}}^{ee}_{0,1}; \dot{\vec{P}}^{ee}_{0,1}\rangle_{\omega+i\eta} &= -g\,\sqrt{2}\,\frac{\pi\Omega_0 m_e n_e^2}{\beta}\,\frac{1-\mathrm{e}^{-4w}}{w}\int_0^\infty \frac{2y^3\,dy}{(2\bar{n}+y^2)^2}\,\mathrm{e}^{-(\frac{w}{y}-y)^2}\left\{1+\frac{19}{4}\frac{w}{y}^2\right\}, \\
\mathrm{Im}\,\langle \dot{\vec{P}}^{ei}_{0,l}; \dot{\vec{P}}^{ei}_{0,m}\rangle_{\omega+i\eta} &= -g\,\frac{\pi\Omega_0 m_e n_e n_i}{\beta}\int_{-\infty}^\infty dx\,\mathrm{e}^{-x^2} \\
&\times\mathcal{P}\int_0^\infty dy \quad \frac{y}{(\bar{n}+y^2)^2}\left[\frac{\{x+y;y\}_{lm}}{xy+y^2-w}\frac{1}{x+y}-\frac{\{x-y;y\}_{lm}}{xy-y^2-w}\frac{1}{x-y}\right], \\
\mathrm{Im}\,\langle \dot{\vec{P}}^{ee}_{0,1}; \dot{\vec{P}}^{ee}_{0,1}\rangle_{\omega+i\eta} &= -g\,\sqrt{2}\,\frac{\pi\Omega_0 m_e n_e^2}{\beta}\int_{-\infty}^\infty dx\,\mathrm{e}^{-x^2} \\
&\times\mathcal{P}\int_0^\infty dy \quad \frac{y}{(2\bar{n}+y^2)^2}\left[\frac{1+\frac{19}{4}(x+y)^2}{xy+y^2-w}\frac{1}{x+y}-\frac{1+\frac{19}{4}(x-y)^2}{xy-y^2-w}\frac{1}{x-y}\right]. \qquad (320)
\end{aligned}
$$

Numerical results will be given in the next section.

4.6 Numerical Results

The evaluation of the complex collision frequency for a two component Coulomb plasma has been performed for a hydrogen plasma at the conditions of the solar core, i.e. $T = 96.15$ Ryd$=1.52\cdot 10^7$ K, $n_e = n_i = n = 8.9\,a_{\mathrm{B}}^{-3} = 6.0\cdot 10^{25}$ cm^{-3}. These parameters are also relevant for laser-induced plasmas [134]. This is a weakly coupled plasma, $\Gamma = 0.069$, which is not strongly degenerate, $\Theta = 2.34$. The screening parameter is $\kappa_{\mathrm{D}} = (\beta\sum_c e_c^2 n_c/\epsilon_0)^{1/2} = 2.15 a_{\mathrm{B}}^{-1}$ and the plasma frequency $\hbar\omega_{\mathrm{pl}} = 21.15$ Ryd. In FIG. 6, the real part of the collision frequency, Eq. (245), is compared with the collision frequency of the statically screened Born approximation using $\epsilon(q,0) = 1+\kappa_{\mathrm{D}}^2/q^2$ in Eq. (245) or the statically screened potential in (233). The dynamically screened collision frequency coincides with a static description at small as well as high frequencies. Taking into account screening due to ions is crucial in order to reproduce the correct static limit, as was discussed in section 4.4. For the case of static screening, the effective screening parameter κ_{eff}, Eq. (280) as introduced from the comparison of the Brooks-Herring Coulomb logarithm (278) and the static limit of the Lenard-Balescu collision term (279), was applied. It is found that for frequencies larger than the proton plasma frequency only the electrons contribute to the collision frequency. At intermediate frequencies, a pronounced effect due to the inclusion of dynamical screening can be seen. In particular, a peak appears due to the excitation of plasmons, cf. Refs. [111, 135].

The evaluation of the complex collision frequency, Eq. (248), for a classical electron plasma, with $S_i(q) = 1$ and $n_e = n_i$ and an effective Debye screening parameter is shown

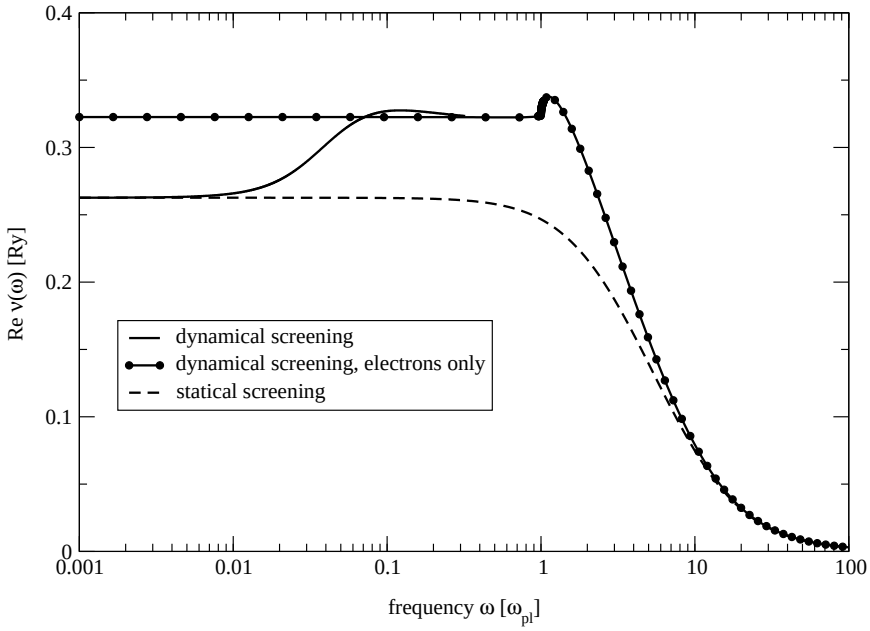

Figure 6: Real part of the dynamical collision frequency $\nu_{LB}(\omega)$ as a function of frequency ω for classical electron and two-component plasma at solar core conditions in comparison to the statically screened Born approximation [87].

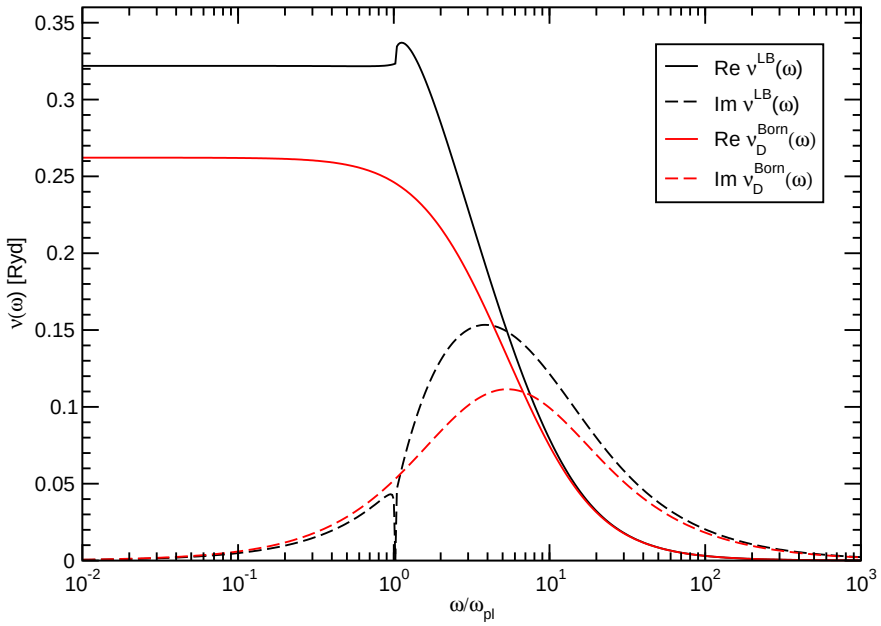

Figure 7: Real and imaginary part of the dynamical collision frequency $\nu_{LB}(\omega)$ for classical electron plasma as a function of frequency ω at solar core conditions in comparison to the statically screened Born approximation $\nu_{\mathrm{D}}^{\mathrm{Born}}(\omega)$.

in FIG. 7. The real and imaginary part of the collision frequency is compared with the statically screened Born approximation, Eq. (302), where the inverse Debye radius $r_{\rm D}$ was used instead of the effective screening parameter $\kappa_{\rm eff}$. As for the real part, the imaginary part shows differences due to dynamical screening in the vicinity of the plasma frequency.

In order to show the consistency of our approximations made for the dielectric function, the Kramers-Kronig relation (56) and the sum rules, Eq. (57), were considered. It was found that the collision frequency and subsequently the dielectric function considered here obey the Kramers-Kronig relation (56). Since the asymptotic form of the real part of the dielectric function is given by $\lim_{\omega\to\infty}\epsilon(0,\omega) = 1-\omega_{\rm pl}^2/\omega^2+...$, see Eq. (60), the first-moment sum rules (57) are fulfilled following the argument in Ref. [30]. This has also been checked numerically. Both of the first-moment sum rules (conductivity and f-sum rule), are fulfilled within a numerical accuracy of better than 0.2 % and 0.5 % for the parameters considered here. To fulfill the first-moment sum rules, the account of the imaginary part of the collision frequency appears to be crucial. It emphasizes that an empirical improvement of the Drude formula introducing solely a frequency dependent relaxation time does not obey sum rules and thus, it is not a consistent approximation.

The high-frequency behavior of the collision frequency is determined by the Born approximation only, Eq. (233), as derived in section 4.5. The real part of the collision frequency is found to be proportional to $\omega^{-3/2}$. It ensures the existence of the third moment of the imaginary part of the dielectric function as required by the corresponding sum rule, Eq. (57). A comparison between the Born approximation calculated for a bare Coulomb potential, a statically screened potential and the dynamical screening result with the high frequency asymptote is shown in FIG. 8. The Born approximation coincides with the asymptote, Eq. (310), for frequencies down to about $4\,\omega_{\rm pl}$.

Of particular interest is the plasmon peak occurring in the response function $\mathrm{Im}\,\epsilon^{-1}(\vec{k},\omega)$ and its dispersion as shown in FIG. 9, see also [86, 136]. While the Drude model shows the plasmon peak at the plasma frequency the more consistent treatment of the dielectric function leads to a shift of the peak in comparison to the plasma frequency due to the imaginary part of the collision frequency. This has also been interpreted as a shift of the plasma frequency, see [90]. The dynamical screening broadens the plasmon peak and reduces the depth of the peak compared with the Drude model.

Following are the results from the evaluation of the ladder approximation (266) for the statically screened Coulomb interaction, replacing the Coulomb potential by the effective Debye potential $V_{ei}^{\rm D}(q) = e_e e_i/[\epsilon_0\Omega(q^2+\kappa_{\rm eff}^2)]$. In this way, the divergences for small q are avoided, anticipating also the dynamical screening. For the exploratory evaluation given here, the higher order products of the T-matrices occurring in Eq. (266) have been neglected. The dynamical collision frequency $\nu^{\rm ladder}(\omega) = \nu^T(\omega)$ in the approximation Eq. (268) is shown in FIG. 10. It is compared with the treatment in dynamically screened Born approximation. The qualitative overall dependence on the frequency is similar to the statically screened Born approximation. Taking into account strong collisions can lead to collision frequencies up to 15 % higher than the Born approximation for frequencies in the vicinity of the plasma frequency, but does not show the peaks at the plasma frequencies as seen in the Lenard-

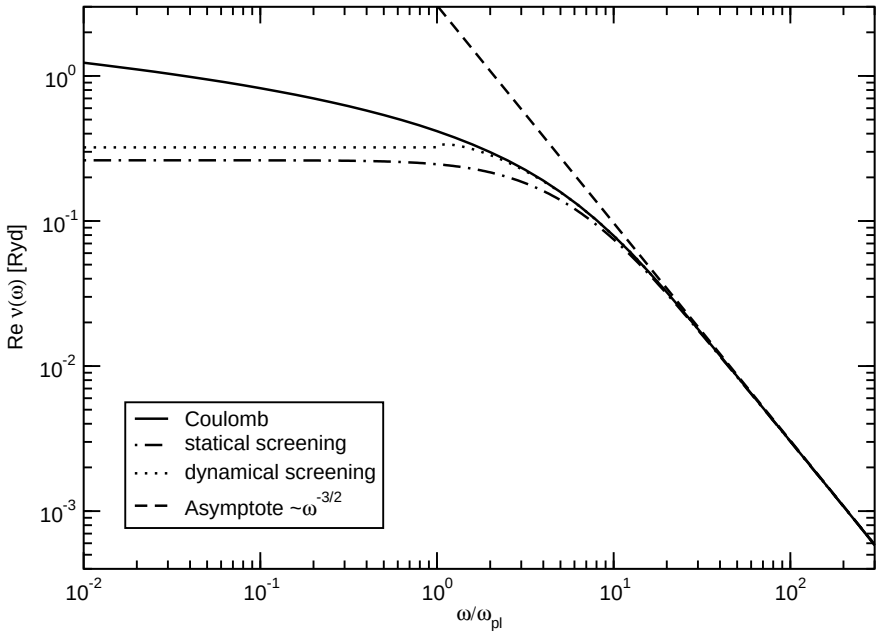

Figure 8: High frequency behaviour of the real part of the dynamical collision frequency in Born approximation calculated for a bare Coulomb potential, a statically and a dynamically screened Coulomb potential as a function of frequency ω for a classical electron plasma at solar core conditions. The asymptote for large frequencies is given.

Balescu approximation.

In order to find a complete and consistent as possible description for the collision frequency including strong collisions and dynamical screening, the Gould-DeWitt (301) scheme is applied for the calculation of the collision frequency in the one-moment approximation. FIGS. 11 and 12 show the real and imaginary part, respectively, of the collision frequency in the dynamically screened binary collision approximation in comparison to the individual approximation discussed above. For the real part, the peak close to the plasma frequency which is due to plasmon excitations in the dynamically screened approximation is preserved in the overall result but shifted to higher collision frequencies due to the additional influence of strong collisions. Static and dynamic screening almost coincide in the high frequency region where the behaviour is determined by strong collisions. In the low frequency regime the collision frequency is dominated by the dynamically screened approximation since the ladder and statically screened Born approximation do have the same low density limit due to the construction of the effective screening parameter used.

In contrast to the Lorentz model [137], the influence of electron-electron interactions can be investigated via the inclusion of higher moments. For this, a renormalization factor was derived in section 4.5. Calculations of the renormalization function $r(\omega)$ as a function of frequency have been performed, again for a hydrogen plasma at solar core conditions. The real and imaginary part of the renormalization factor $r^{(1)}(\omega)$ for a two-moment approach

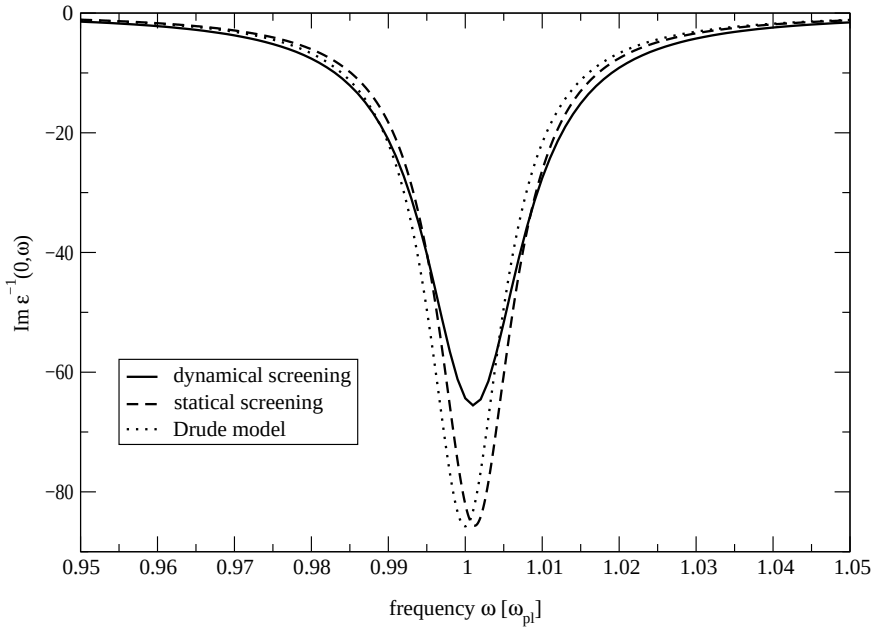

Figure 9: Imaginary part of the inverse dielectric function as a function of frequency ω for a classical two-component plasma at solar core conditions in comparison to the statically screened Born approximation and the Drude model.

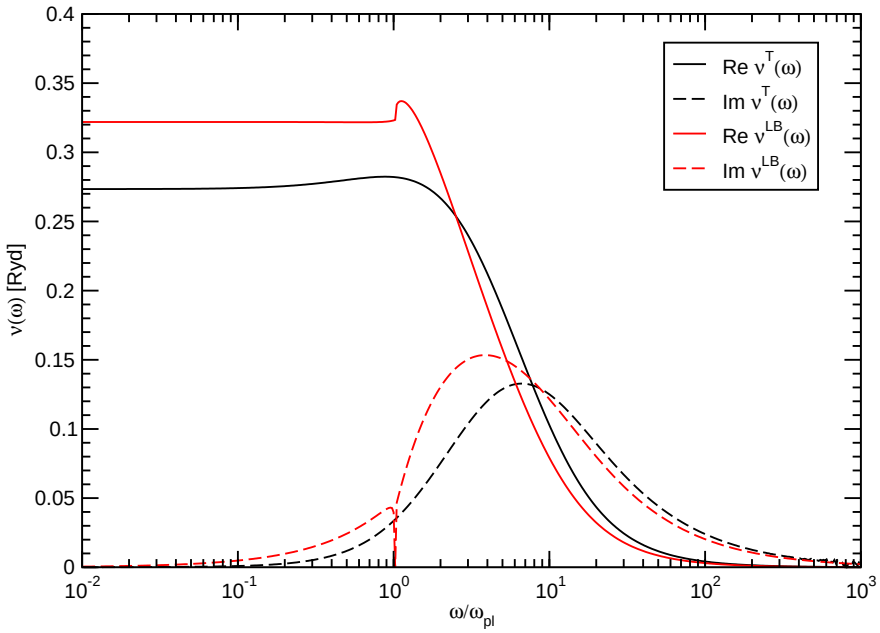

Figure 10: Real and imaginary part of the collision frequency ν^{T} as a function of frequency ω for a classical two-component plasma at solar core conditions.

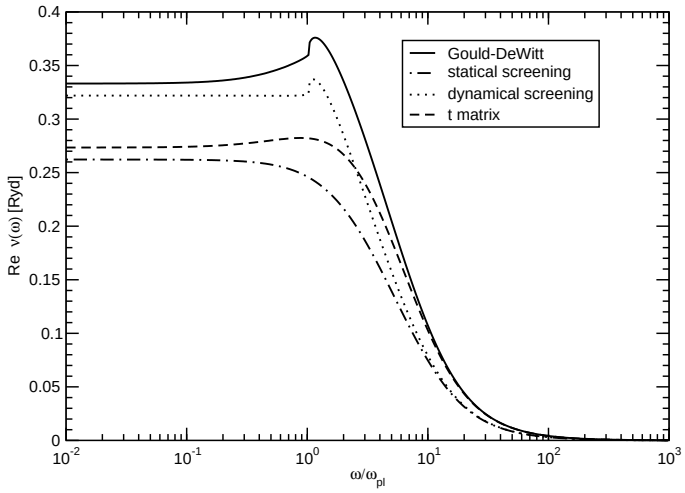

Figure 11: Real part of the dynamical collision frequency in the Gould–DeWitt approximation as a function of frequency ω for classical electron plasma at solar core conditions , seperate contributions are also given: statically screened Born approximation, dynamically screened Born approximation and ladder approximation.

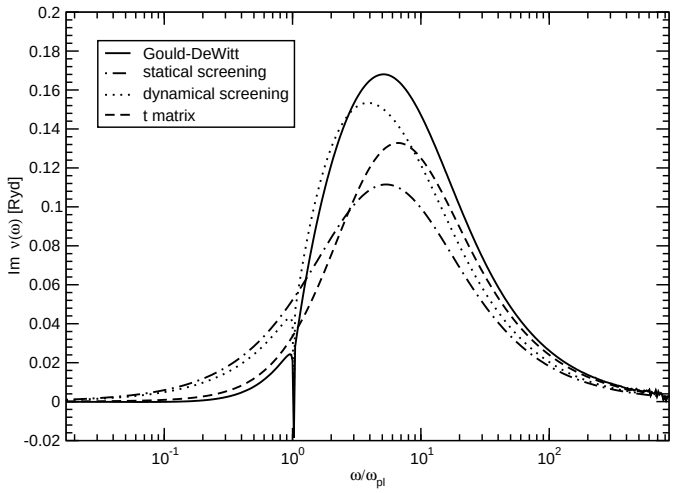

Figure 12: Imaginary part of the dynamical collision frequency in the Gould–DeWitt approximation as a function of frequency ω for classical electron plasma at solar core conditions, separate contributions are also given: statically screened Born approximation, dynamically screened Born approximation and ladder approximation.

where in addition to $\vec{P}^e_{0,0}$ also $\vec{P}^e_{0,1}$ was included are shown in FIG. 13. The static limit of the real part $r^{(1)}(0) = 0.6166$ depends on the density and converges slowly to the zero-density limit $r^{(1)}_{\rm Sp}(0) = 0.5176$ when the density is decreased. In the high-frequency limit, higher moments in the generalized linear response approach can be neglected, and $r(\omega)$ converges to 1. The imaginary part is zero in the static as well as the high-frequency limit. In the intermediate region, the renormalization factor is a complex quantity. As a final result, the real and imaginary part of the collision frequency $\nu(\omega) = r(\omega)\nu^{(P_0)}(\omega)$ as used in the generalized Drude formula (300) has been calculated and presented in FIG. 14 in comparison to the dynamically screened binary collision approximation $\nu^{(P_0)}(\omega)$.

4.7 Conclusions

It was possible to work out a microscopic theory of the dielectric function which is on the same level as the dc-conductivity. By including collisions in a systematic manner, a Drude type relation for the dielectric function was derived. The investigation of a frequency dependent and complex collision term leads to improvements in the description of transport and optical properties. Deviations from the ordinary Drude behaviour were obtained for frequencies in the vicinity and higher than the plasma frequency.

To formulate a quantum statistical approach, special attention has been given to a systematic perturbation expansion. Whereas the perturbation expansion of the response function is divergent near the dc-limit ($\lim_{\omega\to 0}\lim_{k\to 0}$), the perturbation expansion of the dynamical local-field factor or the dynamical collision frequency is convergent near $\omega = 0$ in the long-wavelength limit.

Our main result is the derivation of an expression for the frequency dependent conductivity at arbitrary degeneracy which contains screening and strong collisions. In this way, the static limit reproduces the well known results for the dc-conductivity. An interesting point is that the first-moment sum rules are fulfilled only if the complex character of the dynamical collision frequency is taken into account. This has been shown numerically. The convergence of the third-moment sum rule has been shown analytically and numerically. It is crucial to use a frequency-dependent relaxation time in order to get a convergent third-moment sum rule.

Furthermore, a frequency-dependent renormalization factor was introduced which describes the influence of higher moments of the single-particle distribution function, compared with the one-moment approach, within a given perturbation approximation. This way, the discrepancy between ordinary linear response theory leading, e.g., to the Ziman formula for the dc-conductivity, and kinetic theory, leading to the Spitzer result, is removed.

We restricted ourselves mainly to the long-wavelength limit. The extension for arbitrary wavevectors would be desirable. Then, also in the one-moment approach the collision terms, e.g. in Born approximation and screened Born approximation, are expected to lead to electron-electron contributions.

Another aspect is to treat the local-field corrections in the static limit at finite wavelengths including two-particle correlations in order to bridge with standard approaches like STLS

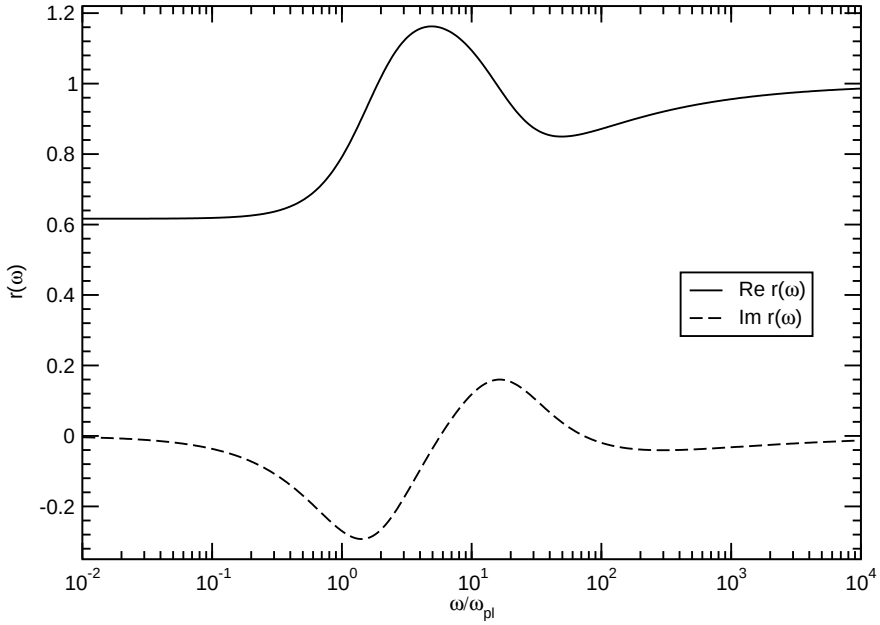

Figure 13: Renormalization factor $r(\omega)$ as a function of frequency ω for a classical two-component plasma at solar core conditions.

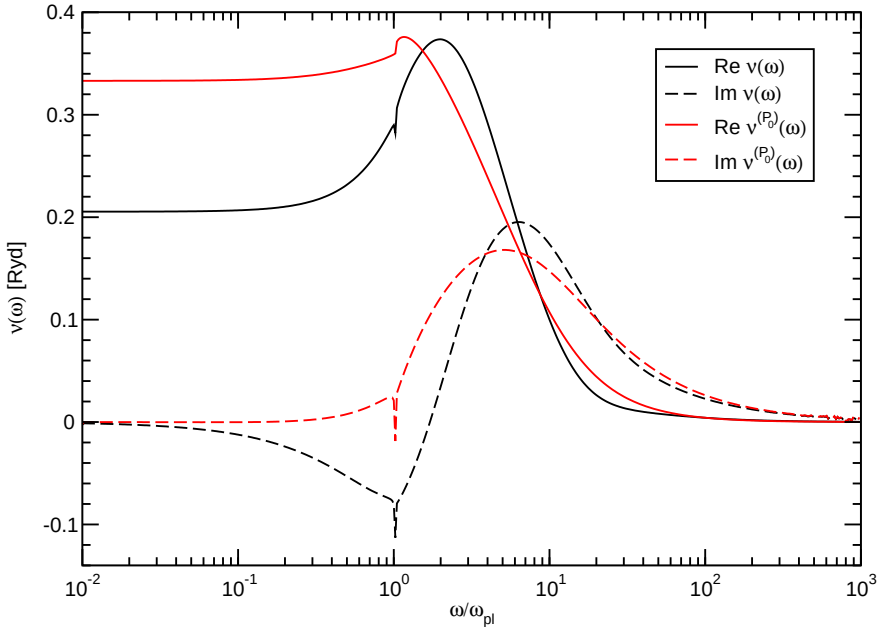

Figure 14: Real and imaginary part of the dynamical collision frequency taking into account the renormalization factor in comparison to the Gould–DeWitt approximation for the one-moment approximation as a function of frequency ω for classical electron plasma at solar core conditions.

[77, 78, 120, 138, 139]. In this context, considering the complex dynamical collision frequency $\nu(\omega;T,n)$ as a function of the plasma density n and performing a virial expansion with respect to n, the approximations given in the present paper allow to determine the correct low-density behaviour of $\nu(\omega;T,n)$, which is obtained taking the single-particle distribution as a set of quantum operators $\{B_n\}$. The inclusion of two-particle correlations into the theory of dc-conductivity is also of interest, see [51, 122], which leads to a virial expansion for the inverse transport properties as the dynamical local-field factors $G(\vec{k},\omega)$ or the dynamical collision frequency $\nu(\omega)$ if considered as function of the plasma density.

4.8 Appendix - Summation of ladder diagrams

The two-particle propagator in ladder approximation is given by the Bethe-Salpeter equation

$$\mathcal{G}_2^L(1,2;\omega_\lambda) \;=\; \mathcal{G}_2^0(1;\omega_\lambda)\delta(1,2) + \sum_3 \mathcal{G}_2^0(1;\omega_\lambda)V(1,3)\mathcal{G}_2^L(3,2;\omega_\lambda) \tag{321}$$

with the free two-particle propagator

$$\mathcal{G}_2^0(1;\omega_\lambda) = \sum_{z_\nu} \frac{1}{z_\nu - E_{p_1}^{c_1}} \; \frac{1}{\omega_\lambda - z_\nu - E_{p_1'}^{c_1'}} = \frac{1-f_1}{\omega_\lambda - E_1} \; . \tag{322}$$

Here and in the following of this Appendix, we use the shorthand notations $E_1 = E_{p_1}^{c_1} + E_{p_1'}^{c_1'}$ and $f_1 = f_{p_1}^{c_1} + f_{p_1'}^{c_1'}$, $\delta(1,2) = \delta_{p_1,p_2}\delta_{p_1',p_2'}\delta_{c_1,c_2}\delta_{c_1',c_2'}$. Also, the ω_λ and z_ν in the denominators have to be seen as energies, the factor $\hbar$ is set to unity but will be reintroduced at the end of this Appendix when making the analytical continuation into the complex frequency plane. Now we have for Eq. (251)

$$\begin{aligned}
\mathcal{G}_{vv}(z_\mu) = \sum_{1234,\omega_\lambda} V(1,2)[K_p(2)-K_p(1)] \frac{1-f_2}{\omega_\lambda + z_\mu - E_2} \Bigg\{ \delta(2,3) + \Bigg[V(2,3) \\
+ \sum_5 V(2,5)\frac{1-f_5}{\omega_\lambda + z_\mu - E_5} V(5,3) + \cdots + \sum_j V(2\ldots j)\frac{1-f_j}{\omega_\lambda + z_\mu - E_j} V(j\ldots 3) \Bigg] \\
\times \frac{1-f_3}{\omega_\lambda + z_\mu - E_3} \Bigg\} \; V(3,4)[K_{p'}(4) - K_{p'}(3)] \\
\times \frac{1-f_4}{\omega_\lambda - E_4} \Bigg\{ \delta(4,1) + \Bigg[V(4,1) + \sum_6 V(4,6)\frac{1-f_6}{\omega_\lambda - E_6} V(6,1) + \ldots \\
+ \sum_i V(4\ldots i)\frac{1-f_i}{\omega_\lambda - E_i} V(i\ldots 1) \Bigg] \frac{1-f_1}{\omega_\lambda - E_1} \Bigg\}.
\end{aligned} \tag{323}$$

The dots in $V(i\ldots j)$ indicate contributions to the series expansion which are not given explicitly. In order to perform the summation over ω_λ we decompose the products of ratios

containing ω_λ into partial fractions so that only one denominator containing ω_λ occurs. We find

$$\begin{aligned}
\mathcal{G}_{vv}(z_\mu) \quad = \quad & \sum_{1234,\omega_\lambda} V(1,2)[K_p(2)-K_p(1)]\Bigg\{\frac{1-f_2}{\omega_\lambda+z_\mu-E_2}\Bigg[\delta(2,3)+V(2,3)\frac{1-f_3}{E_2-E_3}+\dots \\
& +\sum_j V(2\dots j)\frac{1-f_j}{E_2-E_j}V(j\dots 3)\frac{1-f_3}{E_2-E_3}\Bigg] \\
& +\frac{1-f_2}{E_3-E_2}\Bigg[V(2,3)+\dots+\sum_j V(2\dots j)\frac{1-f_j}{E_3-E_j}V(j\dots 3)\Bigg]\frac{1-f_3}{\omega_\lambda+z_\mu-E_3} \\
& +\dots+\sum_j \frac{1-f_2}{E_j-E_2}V(2\dots j)\frac{1-f_j}{\omega_\lambda+z_\mu-E_j}V(j\dots 3)\frac{1-f_3}{E_j-E_3}\Bigg\} \\
& \times V(3,4)[K_{p'}(4)-K_{p'}(3)]\Bigg\{\frac{1-f_4}{\omega_\lambda-E_4}\Bigg[\delta(4,1)+V(4,1)\frac{1-f_1}{E_4-E_1}+\dots \\
& +\sum_i V(4\dots i)\frac{1-f_i}{E_4-E_i}V(i\dots 1)\frac{1-f_1}{E_4-E_1}\Bigg] \\
& +\frac{1-f_4}{E_1-E_4}\Bigg[V(4,1)+\dots+\sum_i V(4\dots i)\frac{1-f_i}{E_1-E_i}V(i\dots 1)\Bigg]\frac{1-f_1}{\omega_\lambda-E_1} \\
& +\dots+\sum_i \frac{1-f_4}{E_i-E_4}V(4\dots i)\frac{1-f_i}{\omega_\lambda-E_i}V(i\dots 1)\frac{1-f_1}{E_i-E_1}\Bigg\}. \qquad (324)
\end{aligned}$$

This expression can be simplified introducing ladder-T matrices according to (258)

$$T(1,2;z)=V(1,2)+\sum_3 V(1,3)\frac{1-f_3}{z-E_3}T(3,2;z) \qquad (325)$$

so that

$$\begin{aligned}
\mathcal{G}_{vv}(z_\mu) = \sum_{1234,\omega_\lambda} V(1,2)[K_p(2)-K_p(1)] \Bigg\{ & \frac{1-f_2}{\omega_\lambda + z_\mu - E_2}\left[\delta(2,3) + T(2,3;E_2)\frac{1-f_3}{E_2-E_3}\right] \\
& + \frac{1-f_2}{E_3-E_2}T(2,3;E_3)\frac{1-f_3}{\omega_\lambda + z_\mu - E_3} \\
& + \sum_j \frac{1-f_2}{E_j-E_2}T(2,j;E_j)\frac{1-f_j}{\omega_\lambda + z_\mu - E_j}T(j,3;E_j)\frac{1-f_3}{E_j-E_3}\Bigg\} \\
& \times V(3,4)[K_{p'}(4)-K_{p'}(3)] \Bigg\{ \frac{1-f_4}{\omega_\lambda - E_4}\left[\delta(4,1) + T(4,1;E_4)\frac{1-f_1}{E_4-E_1}\right] \\
& + \frac{1-f_4}{E_1-E_4}T(4,1;E_1)\frac{1-f_1}{\omega_\lambda - E_1} \\
& + \sum_i \frac{1-f_4}{E_i-E_4}T(4,i;E_i)\frac{1-f_i}{\omega_\lambda - E_i}T(i,1;E_i)\frac{1-f_1}{E_i-E_1}\Bigg\}. \qquad (326)
\end{aligned}$$

After performing the multiplication of these terms and incorporating the remaining $V(1,2)$ and $V(3,4)$ into the T-matrices, one can exchange the indices over which a summation has to be performed in order to get the common factor $\frac{1-f_3}{\omega_\lambda+z_\mu-E_3}\frac{1-f_1}{\omega_\lambda-E_1}$ in all additive terms. The result is

$$\begin{aligned}
\mathcal{G}_{vv}(z_\mu) = \sum_{1234,\omega_\lambda} & \frac{1-f_3}{\omega_\lambda + z_\mu - E_3}\frac{1-f_1}{\omega_\lambda - E_1} \qquad (327) \\
\Bigg\{ & T(1,3;E_3)T(3,1;E_1)K_p(1)K_{p'}(3) - T(3,1;E_1)T(1,3;E_1)K_p(3)K_{p'}(3) \\
& - T(1,3;E_3)T(3,1;E_3)K_p(1)K_{p'}(1) + T(3,1;E_3)T(1,3;E_1)K_p(3)K_{p'}(1) \\
& + T(2,3;E_3)T(3,1;E_1)T(1,2;E_1)\frac{1-f_2}{E_1-E_2}K_p(2)K_{p'}(3) \\
& - T(2,3;E_3)T(3,1;E_3)T(1,2;E_1)\frac{1-f_2}{E_1-E_2}K_p(2)K_{p'}(1) \\
& - \frac{1-f_2}{E_3-E_2}T(2,3;E_3)T(3,1;E_3)T(1,2;E_1)K_p(2)K_{p'}(1)
\end{aligned}$$

$$
\begin{aligned}
&+\frac{1-f_2}{E_3-E_2}T(2,3;E_3)T(3,1;E_1)T(1,2;E_1)K_p(2)K_{p'}(3)\\
&+T(3,2;E_3)\frac{1-f_2}{E_3-E_2}T(2,1;E_1)T(1,3;E_3)K_p(1)K_{p'}(2)\\
&-T(3,2;E_3)\frac{1-f_2}{E_3-E_2}T(2,1;E_1)T(1,3;E_1)K_p(3)K_{p'}(2)\\
&-T(3,2;E_3)\frac{1-f_2}{E_1-E_2}T(2,1;E_1)T(1,3;E_3)K_p(1)K_{p'}(2)\\
&+T(3,2;E_3)\frac{1-f_2}{E_1-E_2}T(2,1;E_1)T(1,3;E_1)K_p(3)K_{p'}(2)\\
&+T(2,3;E_3)T(3,4;E_3)\frac{1-f_4}{E_3-E_4}T(4,1;E_1)T(1,2;E_1)\frac{1-f_2}{E_1-E_2}K_p(2)K_{p'}(4)\\
&-T(2,3;E_3)T(3,4;E_3)\frac{1-f_4}{E_3-E_4}T(4,1;E_1)T(1,2;E_1)\frac{1-f_2}{E_3-E_2}K_p(2)K_{p'}(4)\\
&-T(2,3;E_3)T(3,4;E_3)\frac{1-f_4}{E_1-E_4}T(4,1;E_1)T(1,2;E_1)\frac{1-f_2}{E_1-E_2}K_p(2)K_{p'}(4)\\
&+T(2,3;E_3)T(3,4;E_3)\frac{1-f_4}{E_1-E_4}T(4,1;E_1)T(1,2;E_1)\frac{1-f_2}{E_3-E_2}K_p(2)K_{p'}(4)\Bigg\}.
\end{aligned}
$$

Substituting index 2 by 4 in the fifth and sixth line allows a more compact structure

$$
\begin{aligned}
\mathcal{G}_{vv}(z_\mu) = \sum_{1234,\omega_\lambda} &\frac{1-f_3}{\omega_\lambda+z_\mu-E_3}\frac{1-f_1}{\omega_\lambda-E_1}\Bigg[T(1,3;E_3)K_p(1)-T(1,3;E_1)K_p(3)\\
&+T(1,2;E_1)\left\{\frac{1-f_2}{E_1-E_2}-\frac{1-f_2}{E_3-E_2}\right\}T(2,3;E_3)K_p(2)\Bigg]\Bigg[T(3,1;E_1)K_{p'}(3)\\
&-T(3,1;E_3)K_{p'}(1)+T(3,4;E_3)\left\{\frac{1-f_4}{E_3-E_4}-\frac{1-f_4}{E_1-E_4}\right\}T(4,1;E_1)K_{p'}(4)\Bigg].
\end{aligned}
\tag{328}
$$

Performing the summation over ω_λ,

$$
\begin{aligned}
\sum_{\omega_\lambda}\frac{1-f_3}{\omega_\lambda+z_\mu-E_3}\frac{1-f_1}{\omega_\lambda-E_1} &= \frac{(1-f_1)(1-f_3)(g(1)-g(3))}{E_3-z_\mu-E_1}\\
&= \frac{\mathrm{e}^{\beta\left(E_{p_1}-E_{p_3}+E_{p_1'}-E_{p_3'}\right)}-1}{z_\mu+\left(E_{p_1}-E_{p_3}+E_{p_1'}-E_{p_3'}\right)}\,f_{p_1}[1-f_{p_3}]\,f_{p_1'}[1-f_{p_3'}]
\end{aligned}
\tag{329}
$$

the correlation function, Eq. (213), for the long-wavelength limit in T–matrix approximation is obtained after reintroducing $\hbar$ and is given in Eq. (263).

5 Molecular Dynamics (MD) Simulations

Within linear response theory, transport coefficients, in particular the dielectric function, the dynamical conductivity, and further related quantities such as the dynamical collision frequency, are expressed in terms of equilibrium correlation functions. Analytical expressions have been derived in earlier papers [45, 50, 51, 65, 87] and presented in previous chapters. As pointed out, these quantum statistical approaches are limited to small coupling parameters, e.g. $\Gamma \ll 1$. Simulations are necessary to check the range of validity of these approximations and to extend the range of parameter values. Since we are interested in dynamical properties on the atomic/microscopic scale, MD simulations are a suitable technique which was developed in different directions. Fortunately, the capabilities of computer calculations have increased considerably in recent years and simulations have made an important contribution in many-particle physics.

Classical MD simulations calculate the trajectories of a finite number of particles on the basis of classical equations of motion. In the context of our considerations, the following groups are relevant. Applications to Coulomb systems have been presented by Hansen *et al.* in Refs. [41, 92, 140]. Norman and Valuev [141, 142, 143] developed this approach in order to apply it also to non-equilibrium properties. Zwicknagel *et al.* [144] did extended calculations to determine structure factors and stopping powers of various materials. During the last decades, MD simulations have been successfully applied to various strongly coupled plasma-like systems as the classical one component plasma (OCP), see e.g. [145, 146], or (binary) ionic mixtures [147]. A problem in classical MD simulations of Coulomb systems is the occurrence of singularities in the interaction at zero distance. A consistent quantum treatment eliminates this problem automatically. The quantum character of the dynamical evolution of the many-particle system is considered using wave packet molecular dynamics [148, 149, 150]. In this case, the electrons are treated as wave packets instead of classical particles which propagate through the plasma. Degeneracy effects can be included via the anti-symmetrisation of the fermion wave functions. Another approach was developed by Car and Parrinello [151] where the density functional theory (DFT) [152, 153] is used to determine the electronic states within the MD simulations, see also [154]. Within path integral Monte Carlo (PIMC) techniques, an inclusion of quantum properties is possible as well [155, 156]. Gibbon and Pfalzner [157] used heating rates from which static and dynamic properties were deducted. Filinov *et al.* [158] did MC simulations for plasma systems under consideration of bound states.

We will focus on aspects of classical MD simulations for a two-component plasma (TCP) on the basis of pseudopotentials which mimic quantum effects (CTCMP - classical two-component model plasma). Comparisons with results of analytical approximations as derived in the previous chapters which are restricted to small values of the plasma parameter will be presented. The relevance with respect to a quantum Coulomb plasma is discussed. Results are showing a consistent description of these model plasmas in comparison to quantum statistical approaches and to experimental results, see also section 6.1.

No.	Potential	$T, 10^3 K$	$n_e, 10^{21} cm^{-3}$	Θ	r_D/a_B	$V_{ei}(0)/kT$	$V_{ee}(0)/kT$
1	Kelbg	8	0.0262	21.43	16.11	-10.19	9.88
2	Kelbg	16	0.2096	10.71	8.06	-8.52	7.49
3	Kelbg	33	1.839	5.20	3.91	-6.83	5.61
4	Kelbg	79	25	2.17	1.64	-5.01	3.54
5	Kelbg	350	2194.	0.368	0.49	-2.49	2.31
6	Deutsch	100	51.17	1.71	1.29	-4.49	3.64
7	Deutsch	316	1611	0.54	0.408	-2.51	1.77

Table 2: Parameters of MD simulations for pseudopotentials at $\Gamma = 1$. The corresponding values for the temperature T, the electron density n_e and the degeneracy parameter Θ are given. The interaction potentials at zero distance $V_{ei}(0)/k_{\rm B}T$ and $V_{ee}(0)/k_{\rm B}T$ are shown, see also FIG. 15.

5.1 Model Potentials

Starting from the microscopic description, we will consider as before a two-component fully ionized neutral plasma (TCP), such as a H plasma consisting of electrons and protons, at temperature T and density $n = n_e = n_i$ of each component. Within the Coulomb system, the coupling to a transverse vector potential is neglected, thus not accounting for radiative corrections. This is possible for temperatures not too high as considered here. The interactions are described by the longitudinal part, the Coulomb potential. In this case, the hamiltonian (82) is obtained,

$$H = \sum_{c,\alpha} \frac{p_{c,\alpha}^2}{2m_c} + \frac{1}{2} \sum_{\{c,\alpha\}\neq\{d,\beta\}} \frac{e_c e_d}{4\pi\epsilon_0 |\vec{r}_{c,\alpha} - \vec{r}_{d,\beta}|} \tag{330}$$

with α, β denoting the index of the particle of components c, d (including spin quantum number), respectively. Thus, only longitudinal excitations (plasmons), but no transverse (photons) are described by the Coulomb hamiltonian. In thermal equilibrium, the plasma is characterized by the coupling parameter $\Gamma = e^2(4\pi n/3)^{1/3}(4\pi\epsilon_0 k_{\rm B}T)^{-1}$, and the degeneracy parameter $\Theta = 2m_e k_{\rm B}T\hbar^{-2}(3\pi^2 n)^{-2/3}$, see also Eqs. (1) and (2) in section 1.1. Exemplarily, details on some plasma properties (density, temperature and degeneracy) at $\Gamma = 1$ are given in TAB. 2. Besides those values , we consider densities in the order of 10^{21} cm^{-3} and temperature of $T = 33\,000$ K which is motivated by recent experiments in dense xenon plasmas [159]. TAB. 2 also shows the Debye screening length $r_{\rm D} = (\sum_c n_c e_c^2/\epsilon_0 k_{\rm B}T)^{-1/2}$, see Eq. (183). As a rough estimate, for conditions $r_{\rm D} \leq 1\, a_B$, pressure ionization takes place and the plasma is fully ionized. Otherwise, the plasma has to be considered as partially ionized. While we consider only free charge carriers in the context of a partially ionized plasma, the effects of bound electrons (atoms) are neglected. A comprehensive treatment of these systems should account for bound states as well, see Ref. [160] and section 7.

MD simulations as presented here, are based on classical equations of motion. But in

general, *quantum* effects have to be taken into account which arise (i) due to the symmetry properties for states of identical particles, and (ii) due to the uncertainty principle. As long as the density is lower than the degeneration density, effects of the symmetry (such as Pauli blocking) can be neglected, and in equilibrium, the Fermi distribution function can be replaced by the Maxwell distribution. The uncertainty principle is of relevance in particular for interacting particles at short distances.

For static equilibrium properties such as the equation of state, it can be shown that a quantum treatment can be achieved by a classical approach. For this, the original Coulomb interaction is replaced by a pseudopotential, where the short-range part of the interaction is modified reflecting the quantum character of the interaction [11]. As a first approximation, the Deutsch interaction potential [161, 162] was used for MD simulations of nonideal plasma in the pioneering works [92, 93] and later simulations [163, 164]. It has the form

$$V_{cd}^{D}(r) = \frac{e_c e_d}{4\pi\epsilon_0 r}\left[1 - \exp\left(-\frac{r}{\lambda_{cd}^{D}}\right)\right], \tag{331}$$

where the parameter

$$\lambda_{cd}^{D} = \frac{1}{\sqrt{\pi}}\lambda_{cd} = \frac{\hbar}{\sqrt{2\pi m_{cd} k_{\mathrm{B}} T}}, \quad \frac{1}{m_{cd}} = \frac{1}{m_c} + \frac{1}{m_d}, \tag{332}$$

is related to the thermal wavelength $\Lambda_{cd}^{D} = \sqrt{2\pi\hbar^2/(m_c + m_d)k_{\mathrm{B}}T}$. The Coulomb interaction within a TCP is included as special case when $\lambda_{cd} = 0$.

Introducing the scaling $\tilde{\mathcal{H}} = \mathcal{H}/k_{\mathrm{B}}T$, $\tilde{p} = p/(m_e k_{\mathrm{B}}T)^{1/2}$, $\tilde{r} = r/a$ with $a = (4\pi n/3)^{-1/3}$, and the dimensionless parameters

$$\tilde{\lambda}_{cd}^{D} = \frac{\lambda_{cd}^{D}}{a}, \tag{333}$$

the Hamilton function (330) with the Deutsch interaction (331) reads

$$\tilde{\mathcal{H}} \;=\; \sum_{c,\alpha} \frac{m_e}{m_c}\,\frac{\tilde{p}_{c,\alpha}^{2}}{2} \;+\; \frac{\Gamma}{2} \sum_{\{c,\alpha\}\neq\{d,\beta\}} \frac{e_c e_d}{e^2|\tilde{\vec{r}}_{c,\alpha} - \tilde{\vec{r}}_{d,\beta}|}\left[1 - \exp\left(-\frac{|\tilde{\vec{r}}_{c,\alpha} - \tilde{\vec{r}}_{d,\beta}|}{\tilde{\lambda}_{cd}^{D}}\right)\right]. \tag{334}$$

The system depends on the parameters $\tilde{\lambda}_{cd}^{D}$, and on density n and temperature T through the single classical plasma parameter Γ. For $\tilde{\lambda}_{cd}^{D} \lesssim 1$, weakly coupled systems are characterized by $\Gamma \ll 1$ and nonideal ones by $\Gamma \gtrsim 1$.

A more systematic derivation of a pseudopotential which reproduces the equilibrium properties of the quantum Coulomb system via classical statistics has been given by Kelbg, see [11, 165, 166] on the basis of Slater sums. In particular, we use the so-called "corrected Kelbg" potential [167]

$$V_{cd}^{K}(r) = \frac{e_c e_d}{4\pi\epsilon_0 r}\left[F\left(\frac{r}{\lambda_{cd}}\right) - r\frac{k_{\mathrm{B}}T}{e_c e_d}\tilde{A}_{cd}(\xi_{cd})\,\exp\left(-\frac{r^2}{\lambda_{cd}^{2}}\right)\right], \tag{335}$$

with

$$\xi_{cd} = -\frac{e_c e_d}{k_{\rm B} T \lambda_{cd}}, \quad F(x) = 1 - \exp(-x^2) + \sqrt{\pi} x (1 - \mathrm{erf}(x)),$$

$$\tilde{A}_{ee}(\xi_{ee}) = \sqrt{\pi}|\xi_{ee}| + \ln\left[2\sqrt{\pi}|\xi_{ee}| \int_0^\infty \frac{y \exp(-y^2)\, dy}{\exp(\pi|\xi_{ee}|/y) - 1}\right],$$

$$\tilde{A}_{ei}(\xi_{ei}) = -\sqrt{\pi}\xi_{ei} + \ln\left[\sqrt{\pi}\xi_{ei}^3 \left(\zeta(3) + \frac{1}{4}\zeta(5)\xi_{ei}^2\right) + 4\sqrt{\pi}\xi_{ei} \int_0^\infty \frac{y \exp(-y^2)\, dy}{1 - \exp(-\pi\xi_{ei}/y)}\right],$$

where $\zeta(n)$ is the Riemann-Zeta function. Note, that the definition of the parameter λ_{cd}, Eq. (332), differs by a factor of $\sqrt{\pi}$ from λ_{cd}^D for the Deutsch potential. The interaction potential (335) corresponds to the Coulomb potential at large distances and provides the exact value of the Slater sum and its first derivative at $r = 0$. FIG. 15 shows the pseudopotential for some of the parameters given in TAB. 2 which will be used in the calculations and simulations later on. The temperature determines the depth of the short range part in the corrected Kelbg potential.

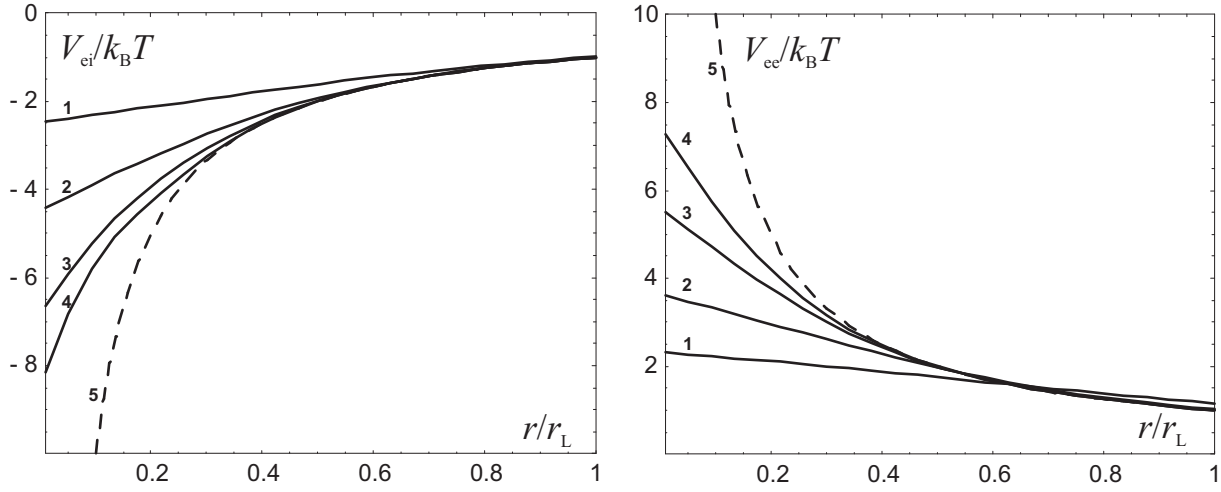

Figure 15: The form of the interaction potentials: (left) ion-electron, (right) electron-electron, for Kelbg potential (335): **1** — $T = 350000$K, **2** — $T = 100000$K, **3** — $T = 33000$K, **4** — $T = 16000$K and Coulomb potential: **5**; $r_L = e^2/(4\pi\epsilon_0 k_B T)$.

The pseudopotentials presented above avoid the Coulomb collapse in a classical treatment of the system. But it is still an unsolved problem whether and under which conditions a quasi-classical MD simulation based on interaction (331) or (335) can reproduce the equilibrium or transport properties of a TCP which has to be treated by quantum statistics.

5.2 MD simulations of equilibrium correlation functions

As shown in the previous chapters, within linear response theory the response of the system to external perturbations is expressed in terms of equilibrium correlation functions such as density, current, force, etc. In general, we have

$$\langle A; B\rangle_{\omega+i\eta} = \int_0^\infty \mathrm{d}t e^{i(\omega+i\eta)t} K_{AB}(t) \tag{336}$$

with

$$K_{AB}(t) = \frac{1}{\beta}\int_0^\beta \mathrm{d}\tau \left\langle A(t-i\hbar\tau)B^\dagger\right\rangle . \tag{337}$$

The average $\langle \dots \rangle = \mathrm{Tr}\{\rho_0 \dots\}$ refers to the equilibrium distribution and the time dependence is due to the Heisenberg picture (24).

For classical systems, the dynamical observables A, B such as charge or current density are commuting variables, and we have simply to evaluate

$$K_{AB}(t) = \langle A(t)B\rangle \tag{338}$$

where the average is taken as the phase space integral over the classical distribution function.

MD simulations calculate the time evolution of the system, solving numerically the equations of motion for the constituting particles. The trajectory in the phase space (Γ space) for a sufficient long time interval can be used to calculate the equilibrium correlation functions. Corresponding to the principle of ergodicity, it is assumed that the long time behavior of a trajectory gives the ensemble average with respect to equilibrium,

$$K_{AB}(t) = \langle A(t)B\rangle = \lim_{t_s\to\infty}\frac{1}{t_s}\int_{t_0}^{t_0+t_s} \mathrm{d}t' A(t+t')B(t') . \tag{339}$$

After some initial time to establish the equilibrium distribution within the system, including the correlations, different pieces of length t_s of a trajectory starting at some time t_0 can be taken to mimic the average over the thermal equilibrium. As shown in [142], these pieces are statistically independent if the starting times t_0 are separated by the dynamical memory time. Alternatively or additionally, the statistical average can be taken by averaging over a large number of independent runs.

The procedure to calculate the trajectories of the CTCMP is conceptually very simple. The $N_{i,\alpha}$ ions (protons) and $N_{e,\alpha}$ electrons $\{\vec{r}_{c,\alpha}, \vec{p}_{c,\alpha}, \alpha = 1\dots N, N = N_i = N_e\}$ follow the classical equations of motion with mutual interactions which determine the forces,

$$\frac{d\tilde{\vec{r}}_{c,\alpha}}{d\tilde{t}} = \frac{m_e}{m_c}\tilde{\vec{p}}_{c,\alpha} , \quad \frac{d\tilde{\vec{p}}_{c,\alpha}}{d\tilde{t}} = -\frac{\partial}{\partial\tilde{\vec{r}}_{c,\alpha}}\left\{\Gamma\sum_{\{d,\beta\}\neq\{c,\alpha\}}\frac{e_c e_d}{e^2|\tilde{\vec{r}}_{c,\alpha}-\tilde{\vec{r}}_{d,\beta}|}\left[1-\exp\left(-\frac{|\tilde{\vec{r}}_{c,\alpha}-\tilde{\vec{r}}_{d,\beta}|}{\tilde{\Lambda}^{\mathrm{D}}_{cd}}\right)\right]\right\} . \tag{340}$$

Here, the Deutsch potential (331) and the scaled variables as introduced in Eq. (334) and $\tilde{t} = t(k_{\mathrm{B}}T/m_e a^2)^{1/2}$ are used. Eqs. (340) are integrated numerically. Thus, the dynamics of the CTCMP depends only on the parameters Γ and $\tilde{\Lambda}^{\mathrm{D}}_{\alpha\beta}$.

MD simulations can be performed only for a finite number $N = N_e = N_i$ of particles. The expense grows quadratically with the particle number N because the long ranged Coulomb part of the force has to be evaluated separately for each pair of particles. The available computing power thus limits the computation to at most a few thousand particles. The actual simulations considered below run with $N = 250$ particles of each species, as well as with $N = 100$.

In order to approximate an infinite system by a finite particle number, the particles are packed into an elementary cubic simulation box of length L and this box is continued periodically in all three spatial directions. The trajectories $\vec{r}_{c,\alpha}(t)$ are simulated in the following way. Initially, all the particles are placed randomly in a cubic box with the edge size $L = (N/n)^{1/3}$ which is determined by the number of particles N in the base cell at a given mean plasma density n. To simulate an infinite homogeneous plasma, images of this charge-neutral basic cell are considered shifting the basic cell by integer multiples of L in different directions. This extended system has a constant mean plasma density n. Artefacts may occur due to the periodicity of the particle positions, but they are suppressed if the basic cell size is increased.

Because particles are leaving the original base cell, the minimum image convention is applied. For this, original particle's images are obtained by periodically shifting their coordinates into the base cell centered around the particle $\{i, c\}$. Thus, the position of each original particle $\vec{r}_{c,\alpha}$ is replaced by the position of an image $\vec{r}^{\,\prime}_{c,\alpha}$

$$r_{c,\alpha}^{\mathrm{n.n.,j}} = r_{c,\alpha}^{j} - mL, \quad \left| r_{c,\alpha}^{\mathrm{n.n.,j}} - r_{d,\beta}^{j} \right| \leq \frac{L}{2}, \tag{341}$$

where $j = x, y, z$ and m is an integer. This method implies that each particle is always surrounded by $2N - 1$ other particles with a constant mean density and the plasma is homogeneous in scales larger than the simulation box.

In general, the dynamics of both electrons and ions are due to forces calculated according to

$$\vec{F}_{c,\alpha} = -\sum_{d,\beta} \frac{\vec{r}_{d,\beta} - \vec{r}_{c,\alpha}}{|\vec{r}_{d,\beta} - \vec{r}_{c,\alpha}|} \frac{\mathrm{d}V_{cd}(\vec{r}_{d,\beta} - \vec{r}_{c,\alpha})}{\mathrm{d}(\vec{r}_{d,\beta} - \vec{r}_{c,\alpha})} \tag{342}$$

at any time step considered. The forces on a particle $\{c, \alpha\}$ are considered to consist of two contributions $\vec{F}_{c,\alpha} = \vec{F}_{c,\alpha}^{\,\mathrm{short}} + \vec{F}_{c,\alpha}^{\,\mathrm{long}}$. The short range contribution $\vec{F}_{c,\alpha}^{\mathrm{short}} = \sum_{\{d,\beta\}\neq\{c,\alpha\}}^{N} \vec{F}_{c,\alpha}(\vec{r}_{d,\beta}^{\,\mathrm{n.n.}} - \vec{r}_{c,\alpha})$ is due to the nearest neighbours which are all original particles or images of original particles found in the base cell centered around the position $\vec{r}_{c,\alpha}$ of the considered particle $\{c, \alpha\}$.

The contribution $\vec{F}_{c,\alpha}^{\mathrm{long}}$ originates from the interaction with particles and images outside the base cell centered around the position $\vec{r}_{c,\alpha}$ of the considered particle. They can be taken

into account considering Ewald sums [92, 168, 169]. If the dimension L of the base cell is large in comparison to the screening length, the contributions of all images except the nearest one can be neglected. In particular, this is justified in the case of a nonideal plasma where the effective interaction potential decreases exponentially with distance due to screening. Therefore, and as will be shown below, the contribution of Ewald sums is not relevant with respect to our simulations for the CTCMP considerd here since the base cell is large in comparison to the Debye sphere.

Equations (340) can be solved using a standard Velocity-Verlet algorithm [170]. But for particles which come very close to each other, in particular for the attractive ion–electron interaction, the arising large forces require a strong reduction of the time step which slows down the numerical propagation. This is avoided by introducing a separate treatment of close collisions, which takes advantage of the fact that the time scales in the close collision region are much shorter than those for the system as a whole. The close colliding particles are thus propagated as subsystems with a much reduced time step [171, 40]. The accuracy and stability of the simulation runs are monitored using the total energy $\mathcal{E}$. The outlined scheme ensures the conservation of $\mathcal{E}$ with an accuracy typically better than 10^{-5} at a global time step $\triangle t = 0.0086\ \omega_{\rm pl}^{-1}$, where $\omega_{\rm pl}$ is the plasma frequency.

The limited simulation box introduces a largest length scale on which collective phenomena can be explored and a discrete set of allowed wave vectors $\vec{k} = 2\pi\vec{n}/L$ with the smallest possible wave number $k_{\rm min} = 2\pi/L$. The unit of the Debye length $r_{\rm D}$ or inverse screening length $\kappa = 1/r_{\rm D}$, see Eq. (183), scales like $k_{\rm min}/\kappa \propto N^{-1/3}\Gamma^{-1/2}$. Thus, small $k_{\rm min}/\kappa$ are only accessible for large Γ (and N). In particular, the long-wavelength limit $k_{\rm min} \to 0$ demands a special consideration. In this case, the collective excitations such as charge density waves are no longer implemented when calculating all positions $\vec{r}_{c,\alpha}(t)$ within the basic cell, but should be treated separately considering a mean field. Obviously, the minimum image method cannot produce such long-wavelength collective excitations because of the periodicity of the particle locations. We will come back to this point in section 5.4 below.

In MD simlations done by Morozov [65, 142, 143, 172], the total number of particles $N = 250$ was found to be enough for $\Gamma \approx 1$. Further increase of the number of particles ($N = 400$) does not affect any simulation results including the mean interaction energy, equilibrium correlation functions and others. The system is brought to equilibrium state of a given temperature using additional Langevin forces in the equations of motions [141]. After equilibrium is reached, these forces are dropped and a long equilibrium MD trajectory is computed. The typical length of the trajectory is $(0.4-4)\cdot 10^7$ time steps which corresponds to the total time $t_{\rm tot} = (0.2-2)\cdot 10^5 \tau_e$, where $\tau_e = 2\pi/\omega_{\rm pl}$ is the period of Langmuir plasma oscillations.

The MD simulations contain, without restrictions on the strength of the interaction, all correlation effects, dynamic screening, close collisions, and multi-particle correlations. They do not rely on a spatial grid and there is no restriction in the spatial resolution. However, the introduction of a basic cell and its periodic images to mimic an infinite system leads to other limitations of this method. If the screening is strong, i.e. for large values of Γ, all relevant interactions are confined within the basic cell, and the treatment of the images

becomes of lower relevance. For a fixed value N this restricts MD simulations to not too small values of Γ. Also, as discussed above in the context with long-wavelength excitations, the limitation $k \gg 1/L$ becomes a serious problem with decreasing Γ. But then one leaves the nonideal regime anyway and can continue with simpler methods, in particular analytical perturbative expansions. It is a general feature, that MD simulations are particularly suited for the case of strong coupling and become inefficient, if not impossible, just where weak coupling approaches are valid.

5.3 Dynamic Structure Factor at finite wavenumber

As a first application for MD simulations, we consider the dynamic structure factor (76) which can be obtained from density-density correlation functions. According to [30, 41] and following Ref. [144], we have

$$\begin{aligned} S(\vec{k},\omega) &= \frac{1}{2\pi N}\int \mathrm{d}t \int \mathrm{d}^3r \int \mathrm{d}^3r' \frac{1}{N^2} \left\langle \sum_{c\alpha,d\beta} e_c \delta(\vec{r}-\vec{r}_{c\alpha}(t)) e_d \delta(\vec{r}'-\vec{r}_{d\beta}) \right\rangle \mathrm{e}^{i\vec{k}\cdot(\vec{r}-\vec{r}')-i\omega t} \\ &= \frac{1}{2\pi N}\int \mathrm{d}t \int \mathrm{d}^3r \int \mathrm{d}^3r' \left\langle \rho(\vec{r},t)\rho(\vec{r}',0)\right\rangle \mathrm{e}^{i\vec{k}\cdot(\vec{r}-\vec{r}')-i\omega t} \\ &= \frac{1}{2\pi N}\int \mathrm{d}t \left\langle \rho_k(t)\rho_k^*(0)\right\rangle \mathrm{e}^{-i\omega t}, \end{aligned} \tag{343}$$

where $\rho_k(t) = \sum_{c,\alpha} e_c \exp[-i\vec{k}\cdot\vec{r}_{c,\alpha}(t)]$ is the Fourier transform of the charge density $\rho(\vec{r},t) = \sum_{c,\alpha} e_c \delta(\vec{r}-\vec{r}_{c,\alpha}(t))$. The angular brackets denote an average over the thermodynamic equilibrium distribution and define the classical correlation function (338) $K_{\rho\rho}(\vec{k},t) = \langle \rho_k(t)\rho_k^*(0)\rangle$.

In MD simulations, observables are calculated as time averages over a certain time interval and/or as ensemble averages over different initial configurations. In order to determine the dynamic structure factor from the classical trajectories $\{\vec{r}_{c,\alpha}(t)\}$, we determine the Fourier transform $\rho_{\vec{k}}(t)$ of the charge density $\rho(\vec{r},t)$ as a function of time for a fixed vector $\vec{k}$. The density-density autocorrelation-function $K_{\rho\rho}(\vec{k},t)$ is calculated from an average over a trajectory during the simulation time t_s, see Eq. (339), as

$$K_{\rho\rho}(\vec{k},t) = \left\langle \frac{1}{t_s}\int_{t_0}^{t_0+t_s} \mathrm{d}t' \rho_{\vec{k}}(t'+t)\,\rho_{-\vec{k}}(t') \right\rangle \ . \tag{344}$$

Additionally, an average denoted by $\langle \ldots \rangle$ over different runs with varying initial microscopic configurations is taken. Transforming the correlation function (344) into the frequency domain, we finally obtain the dynamic structure factor according to (343). Of course, this Fourier transform has to be performed numerically, which restricts the time integral in Eq. (343) to the simulation time t_s and introduces the usual artifacts and problems related to numerical integral transformations [173]. We will resume this when comparing the MD results with the analytical treatment.

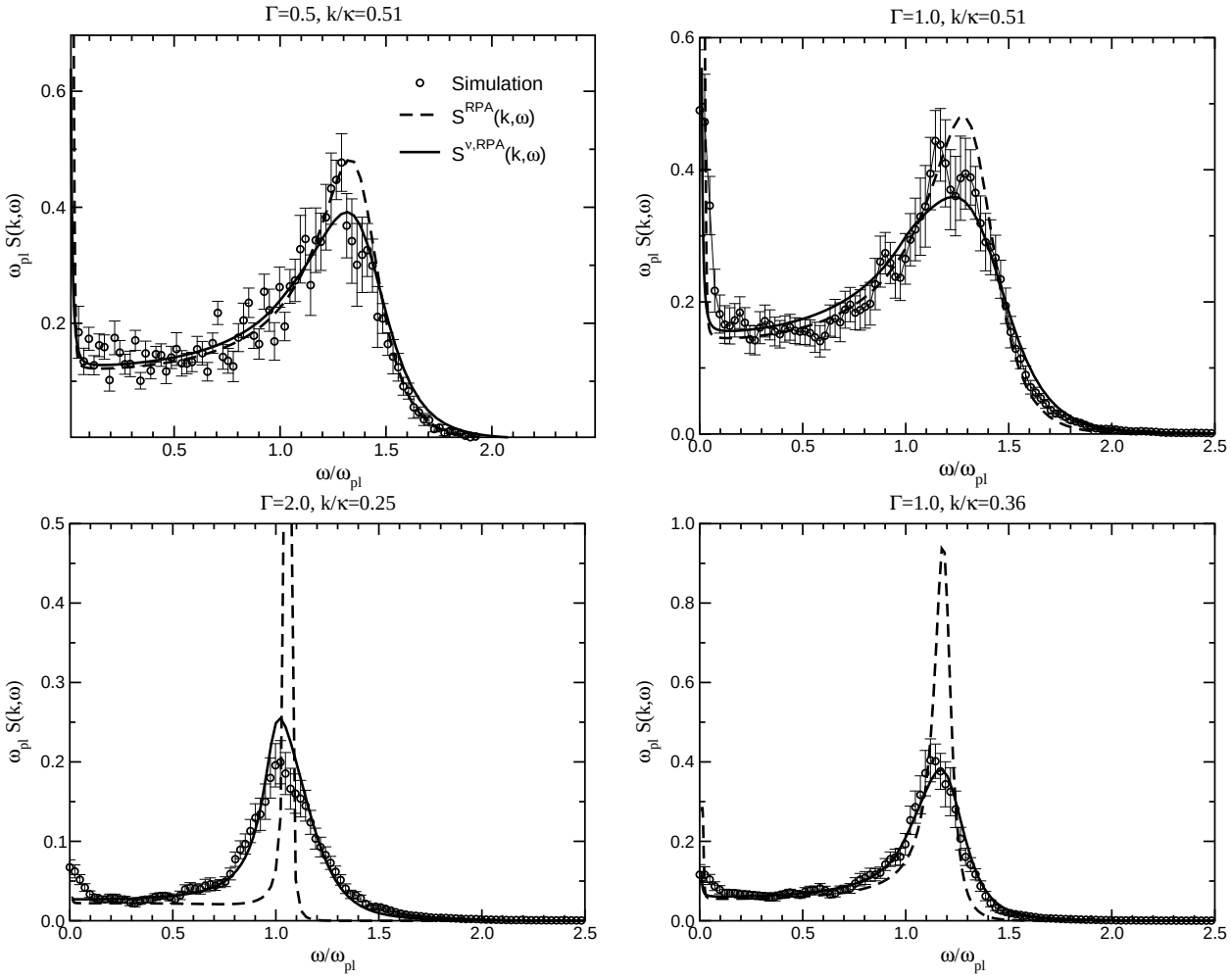

Figure 16: Dynamic structure factor $S(k,\omega)$ for an electron-proton model plasma for different parameter values of $\Gamma, k/\kappa$ as function of frequency ω in units of plasma frequency $\omega_{\rm pl}$: open circle with error bars— MD simulations Eqs. (343), (344), dotted line – evaluation via response function (346) in RPA (355), solid line – evaluation in Mermin-like approximation (357) with dynamically screened dynamic collision frequency $\nu^{\Lambda,\rm RPA}(\omega)$, Eq. (358).

In FIG. 16, results of MD simulations for the structure factor of a CTCMP are shown for different values of the wave vector k [144] (open circles with error bars). Sample times of $t_s = 360\ \omega_{\rm pl}^{-1}$ have been used. The results typically represent an ensemble average over $10 \ldots 20$ individual simulations. The error is deduced from the fluctuations in the ensemble of events. The dynamic structure factor is evaluated at constant total energy in an equilibrium state of the system, which is prepared by a preceding sufficiently long simulation at constant temperature. The same scaled parameters $\tilde{\Lambda}_{cd}^{\rm D}$, see Eq. (333), have been used in all presented simulations. Guided by the quantum statistical derivation [161, 166] of the effective potential (331) where $\tilde{\Lambda}_{cd}^{\rm D} \propto (m_{\alpha\beta})^{-1/2}$ with m_{cd} the reduced masses, we define the scaled parameters via $\tilde{\Lambda}_{cd}^{\rm D} = (m_{ie}/m_{cd})^{1/2}\tilde{\Lambda}_{ie}$. With a fixed $\tilde{\Lambda}_{ie} = 0.4$ we obtain for hydrogen $\tilde{\Lambda}_{ii} = 0.013$ and $\tilde{\Lambda}_{ee} = 0.57$. The simulations show a peak near the plasma frequency $\omega_{\rm pl}$ as well as an enhancement at small ω which represents the ion contribution. The electronic peak is broadened. Further discussions will be given in the following section where comparisons with results of perturbation theory are done.

5.4 Dynamic structure factor: MD simulations versus analytical results

In order to make comparisons between the MD simulations and our quantum statistical approach, we remind the reader of the relationship (77) between the structure factor and the dielectric function,

$$S(\vec{k},\omega) \;=\; \frac{\hbar}{n}\,\frac{\epsilon_0 k^2}{e^2}\,\frac{1}{{\rm e}^{-\beta\hbar\omega}-1}\,{\rm Im}\,\epsilon_{\rm long}^{-1}(\vec{k},\omega)\,. \tag{345}$$

In the classical limit and using the second relation between the longitudinal response function and the longitudinal dielectric function in (73), the dynamic structure factor modifies to

$$S(k,\omega) = -\frac{k_{\rm B}T}{e^2 n\omega}\,{\rm Im}\,\chi_{\rm long}(k,\omega)\;. \tag{346}$$

Using the defintion of the current densities (38), see also (87), the charge-charge density response function (129)

$$\chi_{\rm long}(\vec{k},\omega) = \sum_{cd} e_c e_d \chi_{cd}(\vec{k},\omega) \tag{347}$$

can be expressed in terms of partial response functions

$$\chi_{cd}(\vec{k},\omega) = -\,i\beta\Omega\,\frac{k^2}{\omega}\sum_{pp'}\frac{\hbar^2 p_z p_z'}{m_c m_d}\langle n_{p,k}^c n_{p',k}^d\rangle_{\omega+i\eta}\;. \tag{348}$$

A related quantity is the density-density response function $\chi_{nn}(\vec{k},\omega) = \sum_{cd}\chi_{cd}(\vec{k},\omega)$[43] .

[43]The partial response functions can also be expressed in terms of the Fourier transform of local density fluctuations $\delta n_k^c = \Omega^{-1}\sum_p \delta n_{p,k}^c$ with the fluctuations of occupation numbers $\delta n_{p,k}^c = a_{p-k/2,c}^\dagger a_{p+k/2,c} -$

In the lowest orders of perturbation theory, the partial response functions are derived [144] and can be expressed in terms of the well-known result for the polarization function in RPA (179) [68],

$$\chi^0_{cd}(\vec{k},\omega) = \delta_{cd}\chi^0_c(\vec{k},\omega) = \delta_{cd}\frac{1}{\Omega}\sum_p \frac{f^c_{p+\frac{k}{2}} - f^c_{p-\frac{k}{2}}}{\Delta E^c_{p,k} - \hbar(\omega + i\eta)} = \frac{\delta_{cd}}{e_c^2}\Pi^{c,\mathrm{RPA}}(\vec{k},\omega) \tag{350}$$

with $\Delta E^c_{p,k} = E^c_{p+\frac{k}{2}} - E^c_{p-\frac{k}{2}} = \hbar^2\vec{k}\cdot\vec{p}/m_c$, $f^c_p = [\exp(\beta E^c_p - \beta\mu_c) + 1]^{-1}$ denotes the Fermi distribution function. Taking the response functions (350) in the classical limit, see chapter 3.2, they are given by the expression

$$\chi^0_c(k,z) \;=\; -n_c\beta\Big[1 + i\sqrt{\pi}\, x_c\, \mathrm{w}(x_c)\Big]\,, \tag{351}$$

with $x_c \;=\; \sqrt{m_c\beta/2}\; z/k$ and the Dawson integral (188)

$$\mathrm{w}(x) \;=\; \mathrm{e}^{-x^2}\left[1 + \frac{2i}{\sqrt{\pi}}\int_0^x dt\, \mathrm{e}^{t^2}\right]. \tag{352}$$

The standard random phase approximation (RPA) for the partial response functions of two-component systems is found from summation over ring diagrams [30], equivalent to the introduction of a screened interaction $V^{\mathrm{sc}}_{cd}(\vec{k},\omega) = V_{cd}(\vec{k}) + \sum_{c'} V_{cc'}(\vec{k})\chi^0_{c'}(\vec{k},\omega)\Omega_0 V^{\mathrm{sc}}_{c'd}(\vec{k},\omega)$. Solving

$$\chi^{\mathrm{RPA}}_{cd}(\vec{k},\omega) = \chi^0_c(\vec{k},\omega)\delta_{cd} + \chi^0_c(\vec{k},\omega)\Omega_0 V^{\mathrm{sc}}_{cd}(\vec{k},\omega)\chi^0_d(\vec{k},\omega) \tag{353}$$

we find the RPA expression, c.f. [174]

$$\begin{aligned}
\chi^{\mathrm{RPA}}_{ee}(\vec{k},\omega) &= \frac{\chi^0_e - \chi^0_e\Omega V_{ii}(k)\chi^0_i}{1 - \chi^0_e\Omega V_{ee} - \chi^0_i\Omega V_{ii} + \chi^0_e\chi^0_i\Omega^2(V_{ee}V_{ii} - V^2_{ei})}\,, \\
\chi^{\mathrm{RPA}}_{ei}(\vec{k},\omega) &= \frac{\chi^0_e(\vec{k},\omega)\Omega V_{ei}(k)\chi^0_i(\vec{k},\omega)}{1 - \chi^0_e\Omega V_{ee} - \chi^0_i\Omega V_{ii} + \chi^0_e\chi^0_i\Omega^2(V_{ee}V_{ii} - V^2_{ei})}\,,
\end{aligned} \tag{354}$$

and the corresponding expressions interchanging e and i. The dependence on $\vec{k},\omega$ has been dropped. The complete RPA expression for the TCMP with model interaction V_{cd} follows as

$$\chi^{\mathrm{RPA}}_{\mathrm{long}}(\vec{k},\omega) \;=\; \frac{\chi^0_e + \chi^0_i - \chi^0_e\chi^0_i\Omega(V_{ii} + V_{ee} + 2V_{ei})}{1 - \chi^0_e\Omega V_{ee} - \chi^0_i\Omega V_{ii} + \chi^0_e\chi^0_i\Omega^2(V_{ee}V_{ii} - V^2_{ei})}\,, \tag{355}$$

$\langle a^\dagger_{p-k/2,c}a_{p+k/2,c}\rangle_{\mathrm{eq}}$,

$$\chi_{cd}(\vec{k},\omega) = \Omega\frac{i}{\hbar}\int_0^\infty dt\, e^{i(\omega+i\eta)t}\left\langle\left[\delta n^c_k(t), \delta n^d_k\right]\right\rangle_{\mathrm{eq}}\,. \tag{349}$$

where the partial response functions are taken according to (351) with $z = \omega$. In the special case of vanishing model parameter $\lambda_{cd}^{\mathrm{D}}$ (332) (i.e. the case of the TCP with Coulomb interaction), the expressions simplify considerably since the interactions between the different species have the same q behavior, depending on the species via the charges e_c only.

In order to include collisions, the RPA-Mermin susceptibility is obtained using the partial response functions according to (224) in the form

$$\begin{aligned} \chi_c^{\mathrm{M},0}(k,\omega) &= \left(1-\frac{i\omega}{\nu(\omega)}\right)\left(\frac{\chi_c^0(k,z)\chi_c^0(k,0)}{\chi_c^0(k,z)-\frac{i\omega}{\nu(\omega)}\chi_c^0(k,0)}\right), \qquad (356)\\ z &= \omega + i\nu(\omega) = \omega - \mathrm{Im}\,\nu(\omega) + i\mathrm{Re}\,\nu(\omega), \end{aligned}$$

and replacing the response function $\chi_c^0(k,\omega)$ in Eq. (355) by Eq. (356),

$$\chi_{\mathrm{long}}^{\nu,\ RPA}(\vec{k},\omega) = \frac{\chi_e^{\mathrm{M},0}+\chi_i^{\mathrm{M},0}-\chi_e^{\mathrm{M},0}\chi_i^{\mathrm{M},0}\Omega(V_{ii}+V_{ee}+2V_{ei})}{1-\chi_e^{\mathrm{M},0}\Omega V_{ee}-\chi_i^{\mathrm{M},0}\Omega V_{ii}+\chi_e^{\mathrm{M},0}\chi_i^{\mathrm{M},0}\Omega^2(V_{ee}V_{ii}-V_{ei}^2)}. \qquad (357)$$

The calculation of the dynamic collision frequency can be done in different approximations, as outlined in detail in chapter 4. The Born approximation with respect to the Deutsch potential (331) can be given in analogy to the Born approximation for a screened Coulomb potential (302) replacing the potential accordingly. In the zero-frequency limit $\omega = 0$ a Ziman-Faber like expression (275) is obtained. A more involved description follows the inclusion of dynamic screening according to chapter 4.2 which is used for the comparison with MD simulations. According to Ref. [144], we find ($n_{\mathrm{B}}(\omega) = [\exp(\beta\hbar\omega)-1]^{-1}$)

$$\begin{aligned} \nu^{\mathrm{dyn}}(\omega) = {} & i\frac{\hbar}{\Omega_0 n m_{ei}}\sum_q \frac{q^2}{3}V_{ei}(q)V_{ei}(q)\int\frac{d\omega'}{\pi}\int\frac{d\omega''}{\pi}\frac{n_{\mathrm{B}}(\omega')-n_{\mathrm{B}}(-\omega'')}{(\omega+i\eta+\omega'+\omega'')(-\omega'-\omega'')} \\ & [\mathrm{Im}\chi_{ee}(q,\omega'+i\eta)\mathrm{Im}\chi_{ii}(-q,\omega''+i\eta)-\mathrm{Im}\chi_{ei}(q,\omega'+i\eta)\mathrm{Im}\chi_{ie}(-q,\omega''+i\eta)], \qquad (358) \end{aligned}$$

where the RPA expression (354) and corresponding expressions interchanging e and i are inserted for the partial response functions.

In FIG. 16, the dynamic RPA-Mermin structure factor $S^{\nu,\ RPA}(k,\omega)$ (346), (357) with the dynamically screened collision frequency $\nu^{\mathrm{dyn}}(\omega)$ (358) is compared with the common RPA-structure factor (346), (355) and the results of the MD-simulations (343), (344) at different Γ and k/κ values. With increasing Γ and decreasing k significant differences between the MD-results and the collisionless RPA structure factor develop, indicating a much stronger damping of the plasmon mode at increasing nonideality of the TCMP. In contrast to the collisionless RPA, the values for the dynamic RPA-Mermin structure factor follow this trend very well and are in very good agreement with the simulation data concerning position and width of the peak. Differences between the simulation data and $S^{\nu,\ RPA}(k,\omega)$ appear on the high frequency side for $k/\kappa = 0.51$, where it seems that at higher frequencies the influence of collisions is slightly overestimated. In the case of smaller k-values no such differences arise.

The influence of different approaches for the dynamic collision frequency on the dynamic structure factor $S(k,\omega)$ has been discussed in Ref. [144]. The shift and broadening of the

peak in the structure factor depends on the chosen approximation. In the case of dynamic contributions, as presented in FIG. 16, the peak becomes the broadest and slightly asymmetric. It is desirable, to treat the dynamic collision frequency on the level of a dynamically screened binary collision approximation including a renormalization factor, see chapter 4.5. This is work in progress. As will also be shown in the context of Thomson scattering, see chapter 6.1, qualitativ changes are expected in some parameter regions.

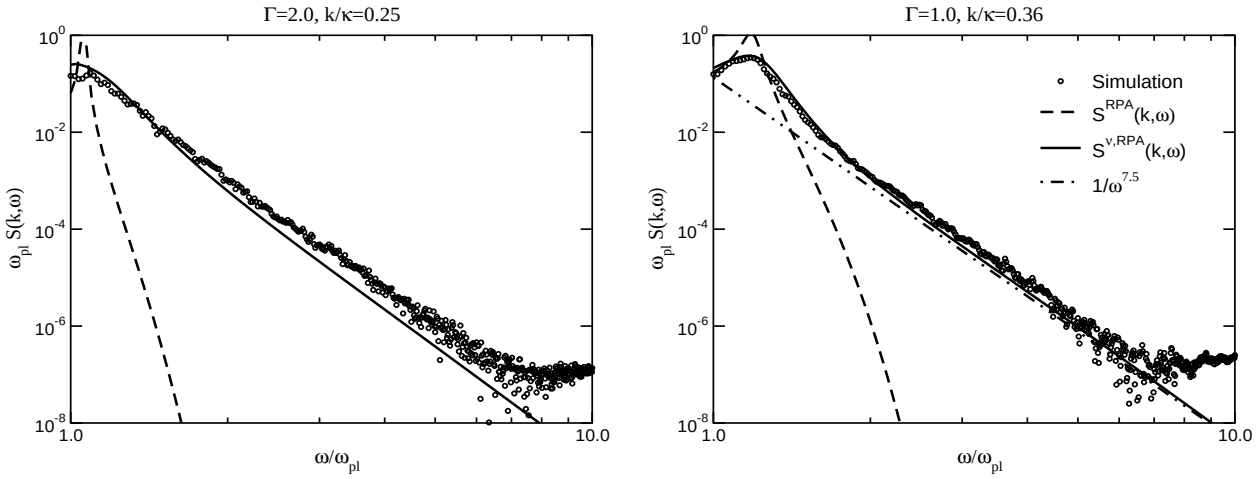

Figure 17: Log-log plot of the dynamic structure factor $S(k,\omega)$ and comparison with an asymptote $\sim 1/\omega^{7.5}$ for different parameter values, compare FIG. 16.

In FIG. 17, the asymptotic behavior of $S(k,\omega)$ is investigated. Due to the unavoidable fluctuations of the MD-simulation data and the usual restrictions of numerical Fourier transformations, the accessible frequency domain for the dynamic structure factor as obtained from the simulations is, however, restricted to frequencies below $\sim 5 \ldots 10\,\omega_{\rm pl}$. While the RPA approximation $S^{\rm RPA}(k,\omega)$ vanishes exponentially the dynamic RPA-Mermin structure factor $S^{\nu,{\rm RPA}}(k,\omega)$ drops down with the asymptote $1/\omega^{7.5}$ [144]. This is in excellent agreement with the simulation data. Note, this is not achieved for the static Born approximation. It also differs from the TCP case with Coulomb interaction where the behaviour is $\propto 1/\omega^{3/2}$ [87], which is related to the difference of the interaction potentials at large values of q.

At stronger coupling, the present pertubative approach becomes questionable. For $\Gamma > 2$, it starts to underestimate the influence of collisions as a damping mechanism, probably because only electron-ion collisions are included and pair correlation effects are neglected. Thus, for higher Γ-values, the theory predicts a more pronounced peak compared to the simulation, as shown for instance in FIG. 18 for $\Gamma > 4$.

As an important test for the consistency of approximations, sum rules and the Krames-Kronig relation should be checked, see chapter 1.5. From the f-sum rule, Eq. (57) with C_1^-,

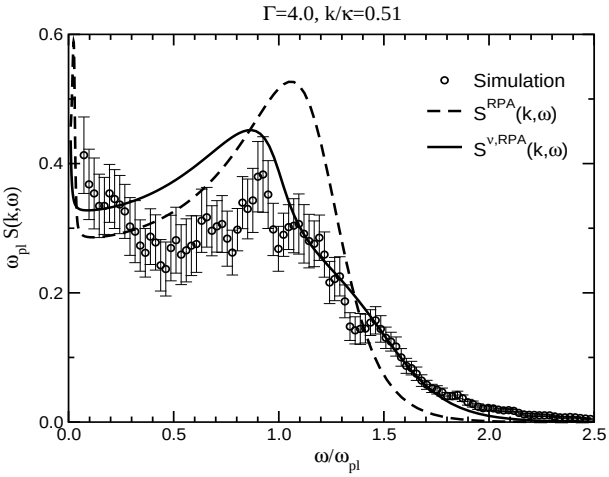

Figure 18: Plot of the dynamic structure factor $S(k,\omega)$ at strong coupling ($\Gamma = 4$). The Mermin-like approximation (357) overestimates the plasmon peak but is able to reproduce the high frequency tail of the simulation.

follows for the structure factor (346) in the classical limit

$$\frac{e^2}{\epsilon_0}\int_0^\infty d\omega\ \omega^2\, S(k,\omega) \quad = \quad -\frac{\pi}{2}\,\frac{k^2}{\kappa^2}\,\omega_{\rm pl}^2\,. \tag{359}$$

This sum rule has been checked for the dynamic RPA-Mermin structure factor (357) and found to be valid within a numerical accuracy of less than 0.5% [144]. In conclusion, we found good agreement of MD simulations and analytical expressions for weakly coupled plasmas, $\Gamma \leq 2$.

5.5 MD simulations in the long-wavelength limit

Calculations of the dynamical structure factor at $k > 1/L$ have been performed for the system considered here, see previous section and, e.g. Ref. [144]. However, for the response to an homogeneous external field, which should lead to the evaluation of the longitudinal dynamical conductivity (202), a separate mean field, see [65, 172], has to be incorporated. This is related to the description of plasma oscillations and will be discussed now.

Plasmon excitations at finite k are described in a mean-field picture in the following way. Considering macroscopic charge density waves $\langle\rho_k\rangle^t = \int d^3r \langle\rho(\vec{r},t)\rangle \exp(i\vec{k}\cdot\vec{r})$, see Eqs. (85) or (44), propagating in z direction with wave vector $\vec{k} = k\vec{e}_z$, we obtain a long-range mean-field $\widetilde{E}_k^z(t) = \int \mathrm{d}^3r\, E^z(\vec{r},t)\exp(i\vec{k}\cdot\vec{r})$ according to the Gauss law (8) as

$$ik\widetilde{E}_k^z(t) = \frac{1}{\epsilon_0}\langle\rho_k\rangle^t. \tag{360}$$

This mean field produces a force on the charges so that they are accelerated. This results in a change of the average macroscopic current (86)

$$\langle J_k^z \rangle^t = \langle j_k^z \rangle^t = \int d^3r \, \langle j^z(\vec{r},t) \rangle \exp(i\vec{k} \cdot \vec{r}) \tag{361}$$

with the longitudinal component of the current density

$$\vec{j}(\vec{r},t) = \sum_{c,\alpha} e_c \vec{v}_{c,\alpha}(t) \delta(\vec{r} - \vec{r}_{c,\alpha}(t)). \tag{362}$$

The current density is related to the time variation of the charge density according to the balance equation (38) $d\langle \rho_k \rangle^t / dt = -ik \langle J_k^z \rangle^t$, and plasma oscillations are obtained.

Since the mean electric field in (360) is long-ranged and not restricted to the screening length, it has to be taken into account adequately and should not be influenced by the size L of the periodic boxes. The MD simulations for the dynamical structure factor presented in the previous section do not treat the mean field explicitly. Therefore, they can only be applied for $k \geq 2\pi/L$. Only in this case, the density fluctuations which lead to plasmon oscillations are included via the particles within the basic MD box. Plasma waves with wavelengths exceeding the length L of the basic box are not correctly implemented by using periodic boundary conditions, so that it is impossible to carry out the long-wavelength limit $k \to 0$ in calculating the dynamical structure factor from the charge ACF, because of the finite extension of the MD basic simulation box. However, it is possible to consider this limit for the current ACF.

For this, we follow the procedure to construct an infinite system by periodic images of a basic cell. We consider this as a limiting case of a finite number of images. Denoting the images in z-direction by N_{images}, then a surface of our system is obtained at $z_- = -(2N_{\text{images}} + 1) \cdot L/2$ and $z_+ = (2N_{\text{images}} + 1) \cdot L/2$. If positive and negative charges are moving at different rates across the surface of the basic cell, the accumulation of surface charge in z direction occurs. The introduction of a finite number of images compensates this effect at the interfaces, but not at the surface of the whole system including all the images. Therfore, charge separation produces a surface charge density. In the limit when the number of images goes to infinity, the surface is far away and produces a homogeneous mean electrical field $\vec{E}(t) = E^z(t)\vec{e}_z$ within the simulation box. Following this reasoning, it is necessary to include a mean field in the long-wavelength limit as shown below. As a consequence, plasma oscillations are obtained.

On the macroscopic level, the Maxwell equations relate this mean field to the z-component of the average current density. Following Eq. (360) and the discussion above, we find in the Fourier space

$$\frac{d}{dt} \widetilde{E}_{k=0}^z(t) = -\frac{1}{\epsilon_0} J^z(t) \,, \tag{363}$$

with the macroscopic current

$$\vec{J}(t) = \langle \vec{J}_{k=0} \rangle^t = \langle \vec{j}(t) \rangle = \langle \sum_{c,\alpha} e_c \vec{v}_{c,\alpha}(t) \rangle \tag{364}$$

as an average over the basic simulation cell. Taking the initial condition $\vec{E}(0) = 0$, the integration of Eq. (363) leads to

$$E^z(t) = \frac{1}{\Omega}\,\widetilde{E}^z_{k=0}(t) = \frac{1}{\epsilon_0 L^3}\left\langle \sum_{c,\alpha} e_c r^z_{c,\alpha}(t) \right\rangle \ . \tag{365}$$

where the normalization volume $\Omega = L^3$ is given by the length of the simulation box. Neglecting the contribution from the Ewald sums, the long-range interaction forces are given by the mean field according to $\vec{F}^{\,\mathrm{long}}_{c,\alpha}(t) = e_c E^z(t)\vec{e}_z$ which contribute to the longitudinal component only. In particular, the equation of motion for an electron reads

$$m_e \frac{d\vec{v}_{e,\alpha}}{dt} = \vec{F}^{\,\mathrm{short}}_{e,\alpha} - eE^z(t)\vec{e}_z. \tag{366}$$

The short-range forces $\vec{F}^{\,\mathrm{short}}_{e,\alpha}$ are fluctuating around a zero mean value. But, the amplitude of these fluctuations is much larger than the fluctuations of the mean field force $-eE^z(t)\vec{e}_z$.

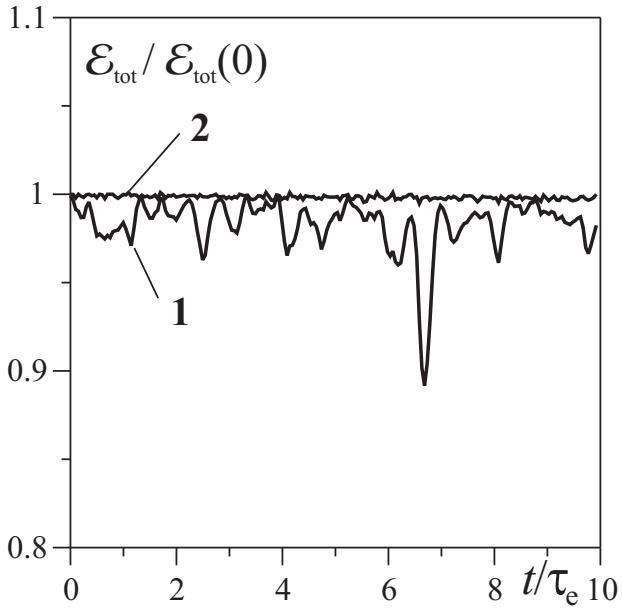

Figure 19: Conservation of the total energy in MD simulations; curve **1** – energy of the particles $\mathcal{E}_{\mathrm{pot}} + \mathcal{E}_{\mathrm{kin}}$ according to Eq. (367), curve **2** – total energy $\mathcal{E}_{\mathrm{tot}}$ including the mean field energy $\mathcal{E}_{\mathrm{field}}$.

An additional indication for the necessity to include the mean field is the investigation of the system energy [65]. In the MD method, if no mean field term is taken into account, the total energy

$$\mathcal{E}_{\mathrm{tot}} = \mathcal{E}_{\mathrm{pot}} + \mathcal{E}_{\mathrm{kin}} = \frac{1}{2}\sum_{\{c,\alpha\}\neq\{d,\beta\}}^{N} V_{cd}(\vec{r}_{d,\beta} - \vec{r}_{c,\alpha}) + \frac{m_e}{2}\sum_{\alpha=1}^{N} v^2_{e,\alpha} + \frac{m_i}{2}\sum_{\alpha=1}^{N} v^2_{i,\alpha} \tag{367}$$

is conserved. If the particle trajectories are calculated including the mean field force, the energy $\mathcal{E}_{\rm pot} + \mathcal{E}_{\rm kin}$ is not conserved. Nevertheless, the conservation law can be fulfilled by including the mean field energy $\mathcal{E}_{\rm field} = L^3\epsilon_0 E^2/2$ so that the total energy $\mathcal{E}_{\rm tot} = \mathcal{E}_{\rm pot} + \mathcal{E}_{\rm kin} + \mathcal{E}_{\rm field}$ is conserved. This is illustrated by simulations' results in FIG. 19.

The occurrence of plasma oscillations can be demonstrated analytically in the following way. If the mass ratio between electrons and ions m_e/m_i is small, the ion current can be neglected. The derivative of the averaged total current density is obtained as

$$\frac{d}{dt}\vec{J}(t) = -e\left\langle \sum_{\alpha=1}^{N} \frac{d}{dt}\vec{v}_{e,\alpha} \right\rangle = \frac{eN}{m_e}(eE^z(t)\vec{e}_z - \langle\vec{\xi}\rangle), \tag{368}$$

$$\vec{\xi} = \frac{1}{N}\sum_{\alpha=1}^{N} \vec{F}_{e,\alpha}^{\ \rm short} = \frac{1}{N}\sum_{\alpha=1}^{N}{\sum_{i,\beta}}' \vec{F}_{ei}(\vec{r}_{i,\beta}^{\ \rm n.n.} - \vec{r}_{e,\alpha})\,. \tag{369}$$

The force $\vec{\xi}$ includes only electron-ion interaction forces. All electron-electron interaction forces are compensated since they do not change the total momentum of the electrons' subsystem. Although the force $\vec{F}_{e,\alpha}^{\ \rm short}$ on each electron is typically much greater than the force $eE^z(t)\vec{e}_z$ from the polarization field, the average over all electrons is of the same order of magnitude as $eE^z(t)$. If we now differentiate Eq. (363) and substitute the derivative of the current using (368), we obtain the equation for the mean field

$$\frac{d^2}{dt^2}E^z(t) + \omega_{\rm pl}^2 E^z(t) = \frac{\omega_{\rm pl}^2}{e}\langle\xi^z\rangle. \tag{370}$$

In the average, $\langle\vec{\xi}\rangle$ vanishes, so that plasma oscillations are described. The corresponding oscillations in the current ACF as obtained from MD simulations are shown below.

Due to the mean field, MD simulations for the z-direction (longitudinal component $j^{\rm long}(t)$) and the x, y directions (transverse components $j^{\rm transv}(t)$) behave in different ways. In particular, two different current ACF can be derived, the longitudinal one $K_{jj}^{\rm long}$ and the transverse one $K_{jj}^{\rm transv}$. In principle, both can be calculated from the same MD simulation if different components are taken. Within MD simulations [41, 140], the normalized current ACF

$$K_{jj}^{\rm long/transv}(t) = \frac{\left\langle j^{\rm long/transv}(t) j^{\rm long/transv}(0)\right\rangle}{\langle j^2\rangle} = \frac{\beta}{\epsilon_0\omega_{\rm pl}^2 L^3}\left\langle j^{z/x}(t) j^{z/x}(0)\right\rangle \tag{371}$$

is calculated. Here, the long-wavelength limit ($k \to 0$) of the Fourier transform (364) of the current density, Eq. (362), is considered, and the normalizing factor is equal to $\langle j^2\rangle = e^2 N\langle v^2\rangle/3 = \epsilon_0\omega_{\rm pl}^2 L^3/\beta$.

For explicit MD simulations, we consider a model plasma consisting of singly charged ions and electrons with density $n = 3.8\times10^{21}$ cm^{-3} at a temperature of $T = 33\,000$ K. This corresponds to recent experiments in dense xenon plasmas [159]. The plasma parameters introduced in section 1.1 take the value $\Gamma = 1.3$, $\Theta = 3.2$. It is a nondegenerate, strongly

coupled plasma. With a Debye radius of $r_D = 2.7\ a_{\mathrm{B}}$, partial ionization is expected. In fact, it is taken into account when the free electron density n is deducted from the experiment. The computations of the current ACF for the ion-electron mass ratios $m_i/m_e = 1836$ and $m_i/m_e = 100$ show no considerable difference. Thus the ratio $m_i/m_e = 100$ is selected for better convergence since the dynamical memory time for ions increases with the ion mass [142]. The current ACF is calculated directly from the velocities of the particles in subsequent moments of time according to Eq. (371). The averaging of the ACF is performed over $(1-5)\cdot 10^5$ initial configurations. These configurations are obtained from a long MD trajectory at different time moments. As shown in [142], two configurations are statistically independent if they are taken at times separated by the dynamical memory time. In our case about $5\cdot 10^3$ initial configurations are already fully statistically independent for electrons.

The results of the MD simulations for the longitudinal and transverse current ACF are shown in FIG. 20, see also [65]. It can be seen that after inclusion of a mean field acting on the z component, the plasma oscillations in $K_{JJ}^{\mathrm{long}}(t)$ become well pronounced in contrast to a monotonously decreasing behavior for the correlation function K_{JJ}^{transv} of the transverse current as it was also obtained in previous MD simulations [92, 93, 140, 142]. It should be stressed that the amplitude of the oscillations in the longitudinal case does not depend on the number of particles N in the simulation. The oscillation frequency tends to ω_{pl} for an ideal plasma (collision frequency $\nu(\omega) = 0$).

As pointed out in section 5.2, the contribution from the Ewald sums can be neglected for the parameter values considered here since the box length is large compared with the screening length. We illustrate this fact by comparing MD simulations with and without Ewald summations. The current ACF for a plasma at $\Gamma = 1$ and temperature of 316 000 K using the Deutsch potential (331) is shown in FIG. 21. As can be seen, the neglect of Ewald sums is of no significance. This is also found for the dynamical collision frequency, which is shown for these particular MD simulations without and including Ewald sums in FIG. 22.

5.6 Dynamical Collision Frequency and Dynamical Conductivity

We will now discuss the results of the current ACF in the context of the dynamical conductivity and the dynamical collision frequency. Within linear response theory, the current ACF can be related to the longitudinal and transverse conductivity, respectively. The dynamical conductivity is related to the dielectric function according to (64)

$$\sigma(\omega) = i\epsilon_0\omega \lim_{k\to 0}[1-\epsilon(\vec{k},\omega)]. \tag{372}$$

From our quantum statistical approach, we find for the longitudinal case from expression (172)

$$\sigma^{\mathrm{long}}(k,\omega) = \frac{(\beta/L^3)\left\langle j_k^{\mathrm{long}}; j_k^{\mathrm{long}}\right\rangle_{\omega+i\eta}}{1-(i\beta/\epsilon_0\omega L^3)\left\langle j_k^{\mathrm{long}}; j_k^{\mathrm{long}}\right\rangle_{\omega+i\eta}}, \tag{373}$$

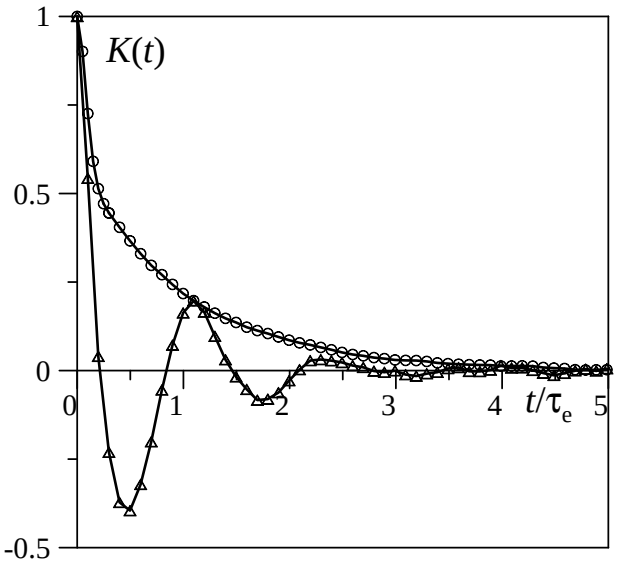

Figure 20: Current auto-correlation function for $\Gamma = 1.28$, $m_i/m_e = 100$; total number of averages 5×10^5; MD trajectory length of $2.5 \times 10^4 \tau_e$, $\tau_e = 2\pi/\omega_{\rm pl}$ – period of electron plasma oscillations; circles – MD simulations $K^{\rm trans}(t)$ of components not influenced by the mean field, triangles – MD simulations $K^{\rm long}(t)$ including the mean-field term in the equations of motion.

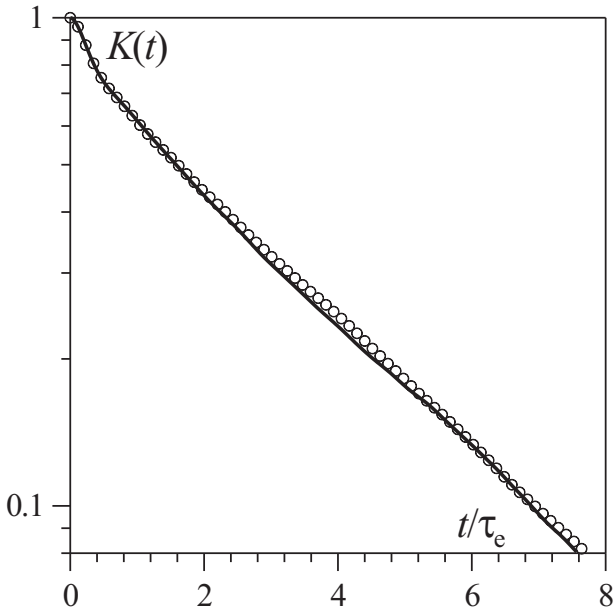

Figure 21: Results of MD simulations with the Deutsch potential (331) for the transverse current ACF using nearest image method without Ewald sums (circles) and simulations including Ewald sums (solid line) for $\Gamma = 1$, $T = 316\,000$ K.

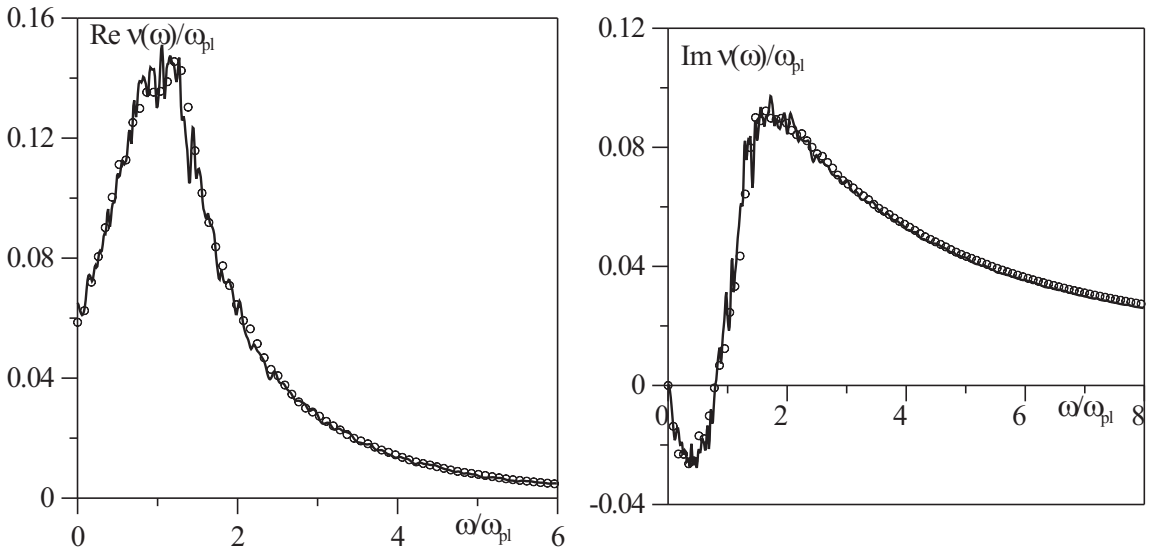

Figure 22: Comparison of dynamical collision frequency, determined from MD simulations via minimum image method without Ewald sums (∘) and simulations including Ewald sums (solid line) for $\Gamma = 1$, $T = 316\,000$ K using the Deutsch potential (331).

and the transverse case from (171)

$$\sigma^{\text{transv}}(k,\omega) = \frac{\beta}{L^3} \left\langle j_k^{\text{transv}}; j_k^{\text{transv}} \right\rangle_{\omega+i\eta} \ . \tag{374}$$

The longitudinal and transverse currents $j_k^{\text{long/transv}}(t)$ and their long-wavelength limit are given by the z-component and x, y-component, respectively, of the Fourier transform of the current density (362), (364). The current correlation functions in the long-wavelength limit (371) are calculated from the current ACF according to

$$\langle j; j \rangle_{\omega+i\eta} = \left\langle j^2 \right\rangle \int_0^\infty \mathrm{e}^{i(\omega+i\eta)t} K_{jj}(t)\, \mathrm{d}t \, . \tag{375}$$

FIG. 23 shows the longitudinal and transverse dynamical conductivity, Eq. 373) and Eq. (374) respectively.

In the long-wavelength limit, the structure of the generalized Drude formula (228) is obtained for the dynamical conductivity. From this, the dynamical collision frequencies $\nu^{\text{long/transv}}(\omega)$ could be deduced, either from the longitudinal case or the transverse case, respectively,

$$\lim_{k\to 0} \sigma^{\text{long/transv}}(\vec{k},\omega) = \frac{\epsilon_0\, \omega_{\text{pl}}^2}{-i\omega + \nu^{\text{long/transv}}(\omega)} \, . \tag{376}$$

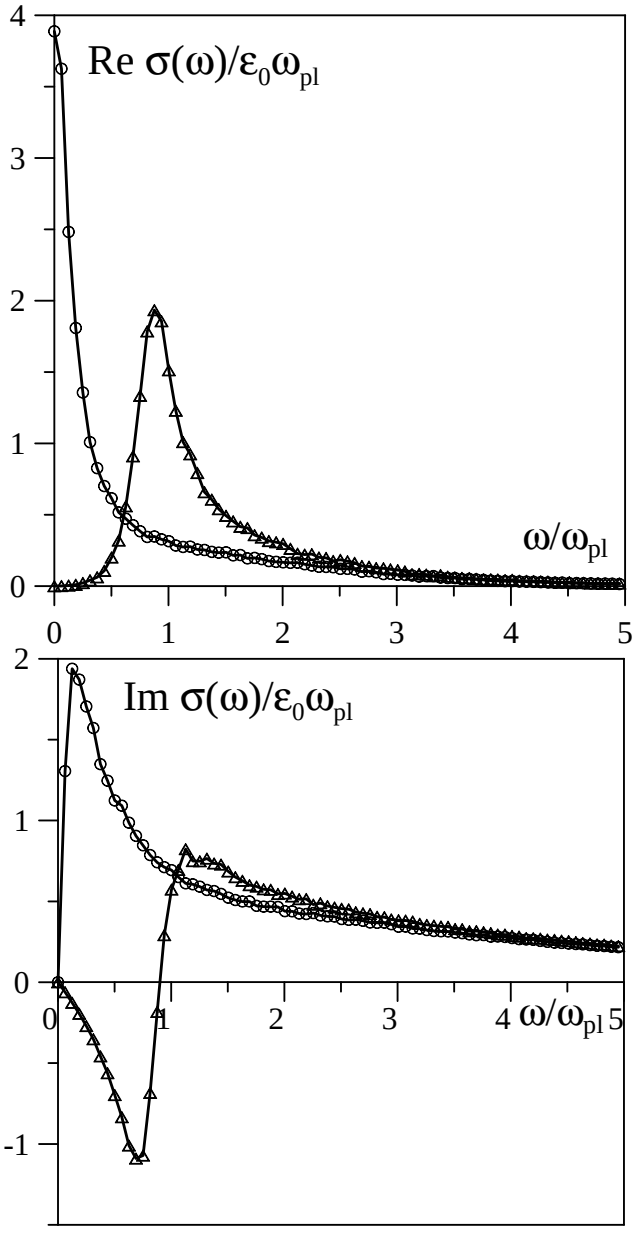

Figure 23: Real and imaginary parts of the Laplace transformation of the current ACF in the transverse case (∘) and the longitudinal case (△), paramters as in FIG. 20.

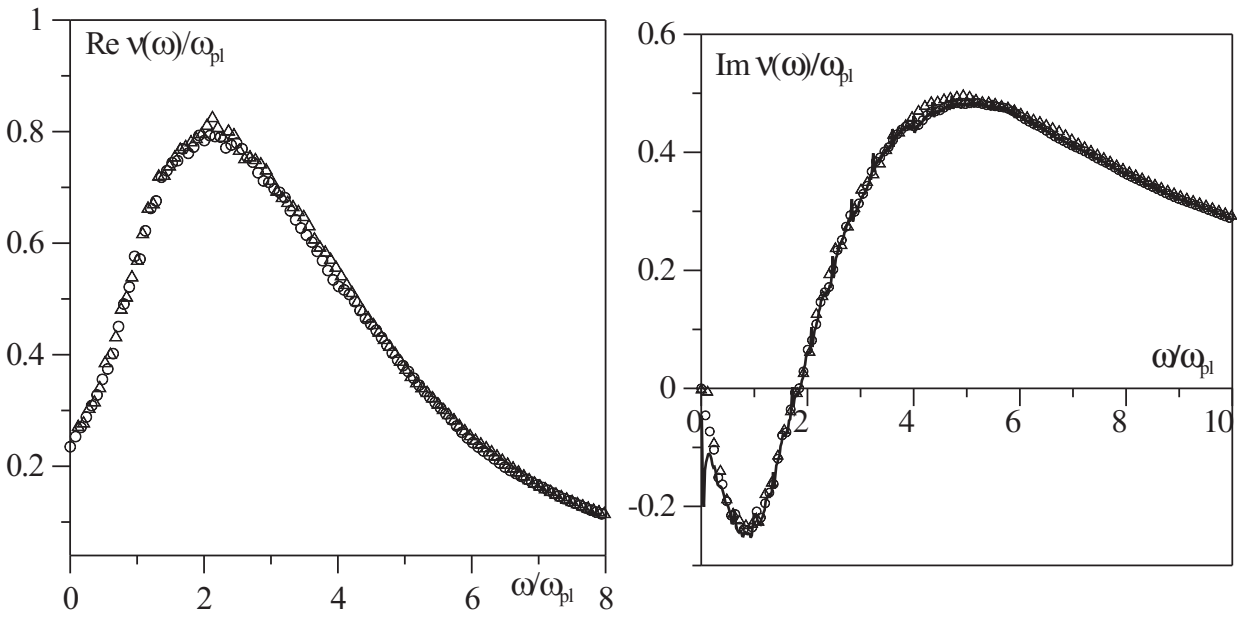

Figure 24: Real and imaginary parts of the dynamic collision frequency from MD simulations for the Kelbg potential (335) in the long-wavelength limit of the transverse case (*circ*) and in the longitudinal case ($\triangle$). Solid line — imaginary part obtained from the real part (transverse case) according to the Kramers-Kronig rule. $T = 33000$K, $\Gamma = 1.28$.

Since the expressions between the conductivities and the current-current correlation functions are different for the longitudinal and the transverse case, the deduced collision frequencies $\nu^{\rm long}(\omega)$ and $\nu^{\rm transv}(\omega)$ are with (373) and (374), respectively,

$$\frac{\nu^{\rm long}(\omega)}{\omega_{\rm pl}} = \frac{\epsilon_0\,\omega_{\rm pl} L^3}{\beta\,\langle j^{\rm long};j^{\rm long}\rangle_{\omega+i\eta}} + i\left(\frac{\omega}{\omega_{\rm pl}} - \frac{\omega_{\rm pl}}{\omega}\right)\,, \tag{377}$$

$$\frac{\nu^{\rm transv}(\omega)}{\omega_{\rm pl}} = \frac{\epsilon_0\,\omega_{\rm pl} L^3}{\beta\,\langle j^{\rm transv};j^{\rm transv}\rangle_{\omega+i\eta}} + i\frac{\omega}{\omega_{\rm pl}}\,. \tag{378}$$

The collision frequencies should be identical for $k \to 0$ since the dynamical conductivities are identical. However, the correlation functions are calculated with different schemes as explained before. The dynamical collision frequencies $\nu^{\rm long/transv}(\omega)$ have been calculated from the simulation data for the current ACFs at zero wavenumber, see FIG. 20, and are shown in FIG. 24. Both coincide quite clearly as expected. Additional verification of self-consistency is performed by calculating $\mathrm{Im}\,\nu(\omega)$ from $\mathrm{Re}\,\nu(\omega)$ in accordance with the Kramers-Kronig rule. Therefore, our analysis showed that the transverse conductivity is identical with the longitudinal conductivity in the long-wavelength limit if the mean field is taken into account in the longitudinal case. This agreement and the validity of the Kramers-Kronig rule prove the high accurracy of our present MD simulations.

Instead of the current ACF, other correlation functions can be considered as well, in particular the force ACF or the current-force correlation function. The following relations

No.	$\nu(0)/\omega_{\rm pl}$	α_r	α_i
1	0.278	—	1.04 ± 0.06
2	0.224	3.4±0.3	1.05
3	0.221	3.8±0.2	1.05±0.02
4	0.142	3.5±4	1.04 ± o.o2
5	0.032	3.4±0.7	1.02± 0.04
6	0.150	3.5±0.4	1.04
7	0.059	3.85	1.02

Table 3: Results of MD simulations. The index number refers to different thermodynamic parameters for $\Gamma = 1$, see TAB. 2 for the corresponding values. The collision frequency at zero frequency $\nu(0)$ and the $\alpha_{r/i}$ characterizing the high-frequency behavior of its real and imaginary part are given.

could be used for this purpose

$$\left\langle \vec{j};\vec{j}\right\rangle_\omega = \frac{i}{\omega}\left(\left\langle \vec{j}^{\,2}\right\rangle - \langle \vec{j};\frac{d}{dt}\vec{j}\,\rangle_\omega\right) = \frac{i}{\omega}\left(\left\langle \vec{j}^{\,2}\right\rangle - \frac{i}{\omega}\langle \frac{d}{dt}\vec{j};\frac{d}{dt}\vec{j}\,\rangle_\omega\right), \tag{379}$$

$$\frac{d}{dt}\vec{j}(t) = \sum_{c,\alpha} e_c \frac{d}{dt}\vec{v}_{c,\alpha}(t) = -e\left(\frac{1}{m_e} + \frac{1}{m_i}\right)\vec{F}_e, \tag{380}$$

where $\vec{F}_e = \sum_\alpha^N \vec{F}_{e,\alpha}$ stands for the resultant force of all ions on electrons as all internal forces between electrons as well as between ions cancel after summation.

Practically, the current ACF provides more accurate results for the low frequencies $\omega < \omega_{\rm pl}$ while the force ACF works better for high frequencies. Due to the finite numerical accuracy of the current ACF obtained from MD simulations, the linear term proportional to $i\omega$ in Eq. (377) and Eq. (378) may lead to a divergent behaviour of $\mathrm{Im}\,\nu(\omega) \sim \omega$ at high frequencies. On the other hand the corresponding relation for the force ACF has no such defect

$$\nu^{\rm long}(\omega) = \frac{i\omega\left\langle \frac{d}{dt}j^{\rm long};\frac{d}{dt}j^{\rm long}\right\rangle_\omega}{i\epsilon_0\omega\,\omega_{\rm pl}^2 L^3/\beta + \left\langle \frac{d}{dt}j^{\rm long};\frac{d}{dt}j^{\rm long}\right\rangle_\omega}. \tag{381}$$

The real and imaginary parts of the dynamic collision frequency are presented in FIG. 25 for different temperatures at a coupling strength of $\Gamma = 1$. TAB. 3 shows details for the simulations where the same parameters as in TAB. 2, section 5.1 are considered. It is seen that with decreasing temperature, absolute values of the real and the imaginary part of the collision frequency increase over the whole frequency range. This is expected from FIG. 15, where the strength of the attractive potential, i.e. βV_{ei}, increases also with decreasing temperature. Note, that the peak in the real part is more pronounced and shifted to higher frequencies with decreasing temperature. Since the collision frequency is shown as a ratio

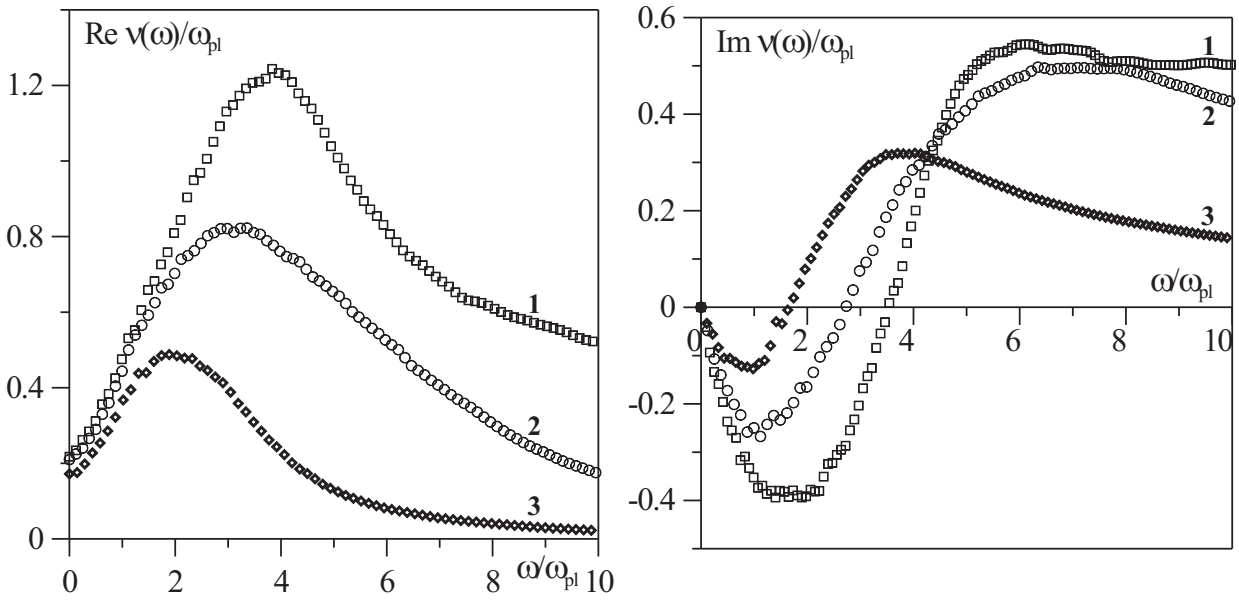

Figure 25: Real and imaginary parts of the effective collision frequency for a Kelbg potential in dependence on temperature. Parameters corresponding to the index numbers 1-2 are given in TAB. 2, curve 3 corresponds to $\Gamma = 1$, $T = 80000$ K.

with respect to the plasma frequency which decreases with decreasing temperature for a fixed Γ, this tendency is slightly suppressed in the presentation.

An important question is to which extent the MD simulations shown here are relevant for real Coulomb systems. The Kelbg potential was constructed to reproduce static equilibrium properties of dense plasmas, and we expect that it should be appropriate at least to describe low-frequency, quasi-static properties. This assumption whether classical simulations based on a pseudopotential can be used to mimic time-dependent properties of dense plasmas can be checked by comparison with quantum statistical calculations

We now compare with the quantum statistical treatment of Coulomb systems using the approximations described in section 4.5 where the collision frequency was defined via the generalized Drude formula (300) as

$$\nu(\omega) = r(\omega)\ \nu^{(P_0)}(\omega). \tag{382}$$

In particular, we consider the Gould–DeWitt scheme (301) for $\nu^{(P_0)}(\omega)$. Furthermore, two moments are taken into account by the frequency-dependent renormalization factor $r^{(1)}(\omega)$, see Eq. (313), which are evaluated in statically screened Born approximation. The results are shown in FIG. 26. Good agreement for both the real and imaginary part is observed for $\omega < \omega_{\rm pl}$, see also [65]. In this region, the quantum mechanical treatment of the Coulomb potential and the classical simulations based on the corrected Kelbg potential are consistent. Note, that an evaluation of the force-force correlation function alone is not sufficient, and the renormalization factor has to be taken into account to obtain correct results, in particular

in the low-density, low-frequency limit.

In the high frequency limit, the asymptotic behaviour of the collision frequency for a Coulomb potential and a Kelbg potential differ. As a consequence, the agreement is poor for $\omega \geq \omega_{\rm pl}$. In order to investigate the high frequency behaviour of the simulation data in more detail, a logarithmic scaling is used in FIG. 27. The real part can be fitted by a power law $\mathrm{Re}\,\nu(\omega) \sim \omega^{-\alpha_r}$. The corresponding values of α_r deduced from the simulation data are shown in TAB. 3. The result is in good agreement with the analytical behavior of $\sim \omega^{-3.5}$ [175] for the Kelbg potential. At frequencies $\omega \gg \omega_{\rm pl}$ the asymptotic expansion of the analytical expression for the collision frequency is possible using the Fourier transform of the corrected Kelbg potential (335)

$$V_{cd}(q) = \frac{e_c e_d \lambda_{cd}}{\epsilon_0 \Omega q} \left[\frac{\sqrt{\pi}}{\lambda_{cd}^2 q^2} \mathrm{Erfi}(\frac{\lambda_{cd}}{2} q) e^{-\frac{\lambda_{cd}^2}{4} q^2} - \frac{\lambda_{cd}^2 k_B T \pi^{3/2} \epsilon_0}{e_c e_d} \tilde{A}_{cd}(\xi_{cd})\, q\, e^{-\frac{\lambda_{cd}^2}{4} q^2} \right]. \qquad (383)$$

However, it is in disagreement with the results for a Coulomb potential which gives $\sim \omega^{-1.5}$ in the high-frequency limit. Therefore, we conclude that the Kelbg pseudopotential is not able to correctly describe the high-frequency behavior of a Coulomb system. Note that the same statement holds for the Deutsch potential (331) for which the collision frequency goes with $1/(\lambda_{cd}\omega^{3.5})$ for high frequencies [176]. However, the imaginary part of the collision frequency follows the power law $\mathrm{Im}\,\nu(\omega) \sim \omega^{-\alpha_i}$ with the exponent α_i deduced from the simulation data close to unity (see TAB. 3), which is in agreement with the analytical result $\sim \omega^{-1}$, valid for all, Coulomb, Kelbg as well as Deutsch potential.

In an earlier paper [176], a comparison of our perturbative approach to results obtained from a MD code by Pfalzner/Gibbon [157] have been reported for $\Gamma = 0.1$. The collision frequency is derived from a heating rate using the high-frequency asymptote of the Drude formula. In this case, good agreement between MD simulations and analytical calculations for a classical model plasma is found for higher frequencies.

FIG. 28 shows the comparison of MD simulations and perturbative results with Schlanges et al. [177] for a fixed density of $n = 10^{22}$ cm^{-3} and frequency of $\omega = 3\omega_{\rm pl}$ as a function of the coupling parameter Γ. Schlanges et al. considered strong fields, which are parameterized via a finite quiver velocity. With decreasing quiver velocity, the limit of linear response is approached [178, 179]. Here, we consider the quiver velocity of $v = 0.2 v_{\rm th}$ which is given in terms of the thermal velocity $v_{\rm th}$ and is low enough to be already in the linear response regime. We find identical results if we evaluate the collision frequency in dynamically screened Born approximation (248), see paragraph 4.2 and Refs. [63, 87]. Dynamical screening within Born approximation was also taken into account in Ref. [177]. On the other hand, MD simulations give results which are significantly higher than the results shown in Ref. [177]. The MD results for the dynamical collision frequency are, however, in qualitative agreement with the Gould – DeWitt result. Strong collisions are of relevance in this region. To support this, we show the result for the collision frequency calculated with the T–matrix collision term. We find significant differences between results for the collision frequency when taking into account beyond static Born approximation either the effects of strong collision or dynamical screening. In agreement with the treatment of the dynamical structure factor [144], see

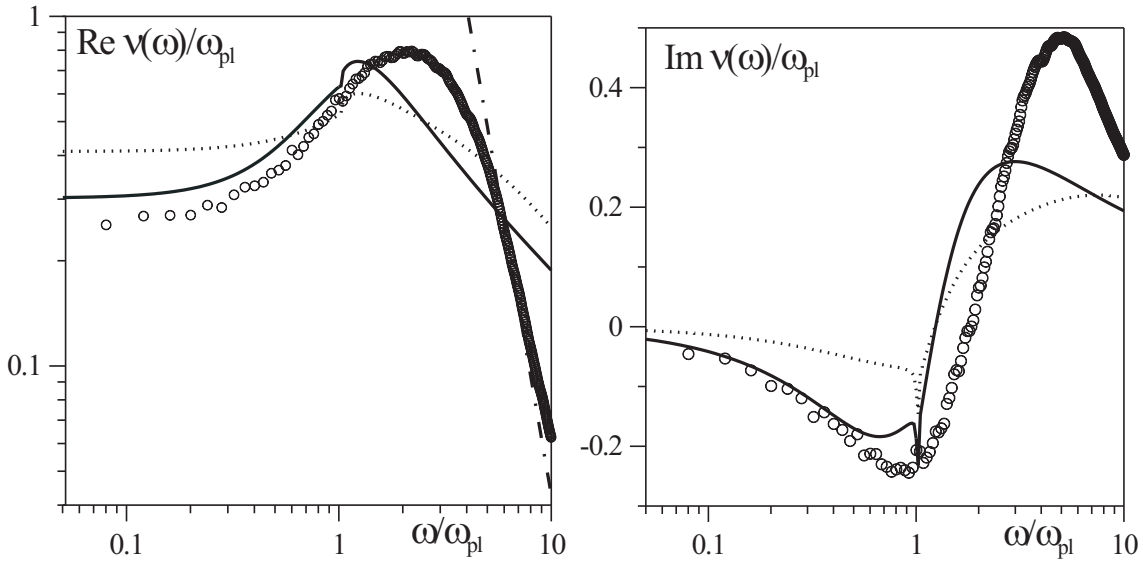

Figure 26: Comparison between MD data for the Kelbg potential (335) (open circles) and the quantum statistical treatment for the Coulomb potential. The Gould–DeWitt scheme is used, accounting for dynamical screening and strong binary collisions. Full line – including renormalization factor $r(\omega)$ in Eq. (382), dotted line – without renormalization factor. The dot-dashed line gives the analytical result for the high-frequency behavior of Re $\nu(\omega)$ for the Born approximation Eq. (302) with Kelbg potential (335). $\Gamma = 1.28$, $T = 33\,000$K.

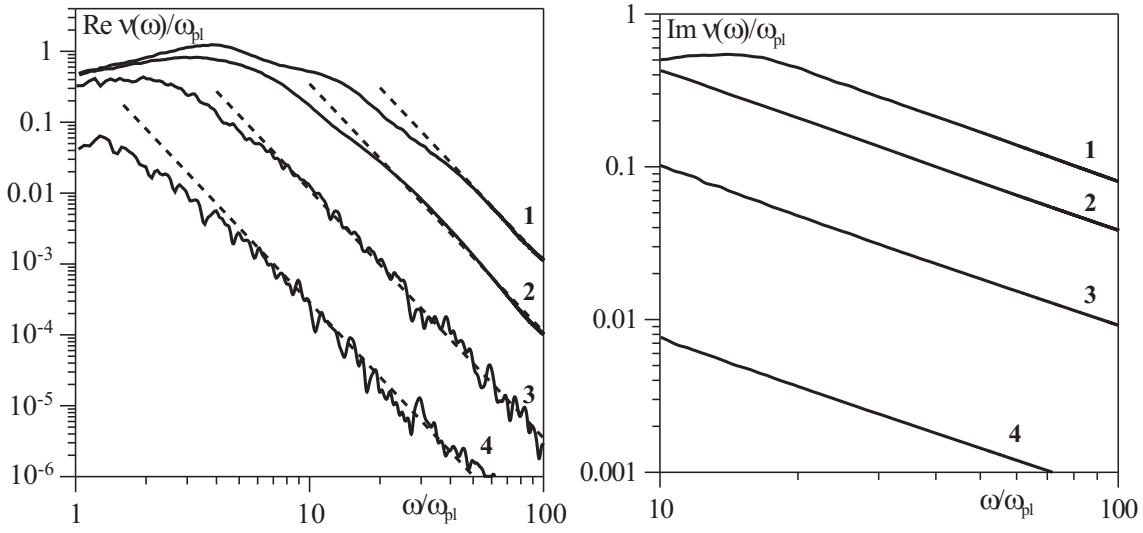

Figure 27: Real and imaginary parts of the effective collision frequency for the Kelbg potential at high frequencies with power fits: **1** — $T = 16000K$, **2** — $T = 33000K$, **3** — $T = 100000K$, **4** — $T = 350000K$. Dashed lines are the power fits $\mathrm{Re}\,\nu \sim \omega^{-3.5}$; $\Gamma = 1$.

paragraph 5.3, the perturbative approach becomes invalid if Γ exceeds the value of about 2. As already seen from FIG. 26, an exact coincidence between MD simulations for the collision frequency based on the Kelbg pseudopotential (or other forms of the pseudopotential) with quantum calculations for the Coulomb system is not expected for frequencies above the plasma frequency. In particular, the high-frequency asymptote is not correctly reproduced.

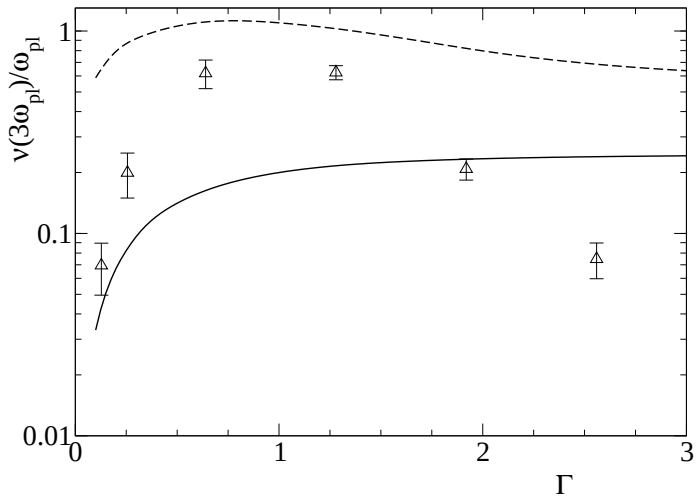

Figure 28: Real part of the collision frequency for charge density $n_e = 10^{22}$ cm^{-3} at frequency $\omega = 3\omega_{\rm pl}$: $\triangle$ - MD results for the Kelbg potential (335); solid curve — Ref. [177] for quiver velocity $v_0 = 0.2 v_{\rm th}$ as well as linear response on the level of dynamically screened Born approximation (Lenard-Balescu collision term), dashed curve — linear response including strong collisions (T–matrix)

5.7 DC-Conductivity of fully ionized plasmas

Another important aspect is the validity range of perturbative results obtained by the quantum statistical approach. As discussed above, see also [65, 144, 172], perturbative analytical results are applicable in the region $\Gamma \leq 2$. For strongly coupled plasmas, interpolation formulas can be constructed based on correct analytical behavior in limiting cases and simulation data for intermediate regions, see section 4.4. In the following, we will discuss the results from MD simulations, analytical approaches, and experimental data for the electrical conductivity in the static limit.

From MD simulations for the current ACF, we have calculated the collision frequency $\nu(\omega)$. According to relation (210), we obtain the dc conductivity $\sigma_{\rm dc} = \epsilon_0 \, \omega_{\rm pl}^2 / \nu(0)$. Results for $\nu(0)$ as function of temperature at fixed nonideality parameter $\Gamma = 1$ are shown in FIG. 29. Apart from the parameter sets given in TAB. 2 for which values for $\nu(0)$ are given in TAB. 3, further simulations have been done. Simulations have also been performed for a fixed temperature of $T = 33\,000$ K and varying coupling parameter Γ. Results for the collision frequency and the static conductivity including error bars are shown in FIGS. 30

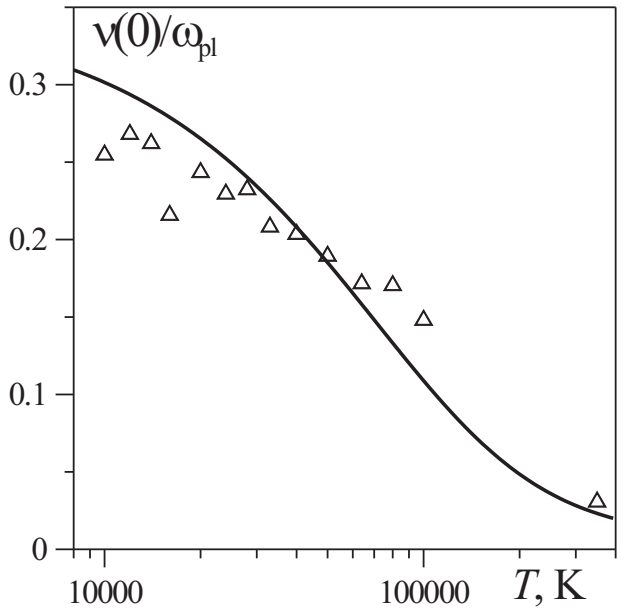

Figure 29: Dependence of the static collision frequency on temperature: △ — MD results for the Kelbg potential, solid line — interpolation formula [114]. $\Gamma = 1$.

and 31. For comparison, collision frequency and dc conductivity are shown which have been calculated using the interpolation formula (299) for the dc conductivity, see section 4.4. Considering the MD simulations for $\Gamma = 1$, FIG. 29, the systematic behaviour agrees very well with the analytical results obtained from the interpolation formula. With respect to the simulations of the dc conductivity for a fixed temperature $T = 33\,000$ K and varying coupling parameter Γ shown in FIG. 30, comparison with the interpolation formula (299) and with experimental data is made. While the agreement between the simulation results and the interpolation formula is excellent for values up to $\Gamma = 1$, discrepancies arise for higher values of Γ. However, the principal behavior of the MD simulations can be reproduced with the interpolation formula. The theoretical description, based on analytical expressions and MD simulations, leads to a good understanding of experimental results which are shown in the figure as well. Note, that the experimental determination of the dc conductivity of a fully ionized plasma is not directly possible, because in general we have a partially ionized plasma where we have to separate the contribution of free charge carriers, and the plasma parameters like temperature and density are not easy to determine.

In contrast, larger discrepancies are found when comparing results for finite frequencies, see FIG. 28. A compilation of various results for the static and the dynamic collision frequencies is shown in FIG. 31. Besides the values for the real part of the collision frequency at $\omega = \omega_{\rm pl}$ as obtained from the current ACF, data for the collisional damping δ_c of the Langmuir waves at $k = 0$ are shown. These were obtained by Morozov *et al.* [143] through extrapolation of MD data for the total damping $\delta(k)$ to the limiting value at $k \to 0$. The data for $\delta(k)$ was found measuring the width of the peak of $S(k, \omega)$ which corresponds to

the Langmuir waves. The interpolation procedure was based on the supposition that the Landau damping in a nonideal plasma does not differ significantly from that in the ideal plasma. This assumption was supported by MD results in [143]. Comments on the static results were already made in the context of FIG. 30 above. Regarding the dynamic results, a reasonable agreement is obtained between the different approaches. The larger value for the collision frequency at $\omega = \omega_{\rm pl}$ compared with the static values $\nu(0)$ has also been shown in FIG. 25 above.

5.8 Concluding remarks on MD simulations

We discussed MD simulations as an alternative tool to evaluate equilibrium correlation functions arising in linear response theory. In particular, we were concerned with the dynamic structure factor related to density-density correlation functions as well as the optical conductivity, which is expressed via current-current autocorrelation functions.

In contrast to analytical expressions from perturbative expansions which are confined to small coupling parameters, MD simulations are appropriate to treat Coulomb systems of any coupling strength. To some extent they are complementary since MD simulations need an increasing numerical effort for small values of the coupling parameter, because the long-range Coulomb interaction is less screened and the number of interacting particles which have to be taken into account is increasing. On the other hand, we found that the perturbative aproaches within the quantum statistical treatment become incorrect if the plasma parameter Γ exceeds the value of about 2. Below this value, reasonable agreement with MD simulations are shown for the dynamical structure factor as well as for the dc conductivity.

Since MD simulations are restricted to finite numbers of particles, we used periodic boundary conditions to get results for infinite systems. If the Debye length is small compared with the simulation box length, the forces acting on a charged particle are mainly caused by the short range contribution, the interactions with all the other particles within the basic box, whereas the contribution of the particles from the images is small and can be expressed by Ewald sums. Special consideration was given to the mean field due to charge separation within the simulation box which leads to collective excitations. They are correctly included in the short-range part of the interaction forces as long as the wave vector k is large compared to the inverse box length $1/L$. We were also able to treat the mean field in the case $k \to 0$ where the different behavior of longitudinal and transverse response of the Coulomb system was analyzed. As a result, we were able to show the plasma oscillations also in long-wavelength limit $k \to 0$.

The classical MD simulations are based on a pseudopotential instead of the original Coulomb interaction. As an appropriate potential to mimic quantum effects, the Kelbg potential is taken which is obtained from a systematic treatment of quantum effects so that static equilibrium properties are correctly reproduced. It is an open question to which extent this potential is able to reproduce dynamic properties of a quantum Coulomb system. From our calculations of the optical conductivity we expect that below the plasma frequency the quantum Coulomb system is fairly well described by a classical pseudopotential of the

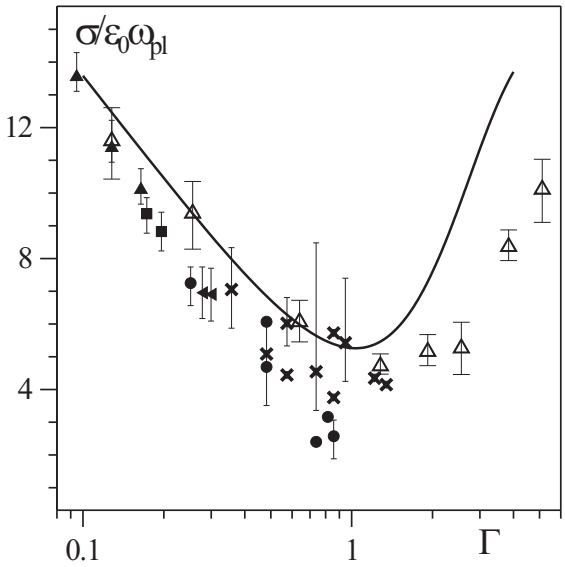

Figure 30: Static conductivity depending on the nonideality parameter Γ. $\triangle$ — MD results for the Kelbg potential (335) for $T = 33\,000$ K, full line — interpolation formula (299) for $T = 33\,000$ K, experimental data: ● – [180], × – [181], ■ – [182], ▲ – [183], ◄ – [184].

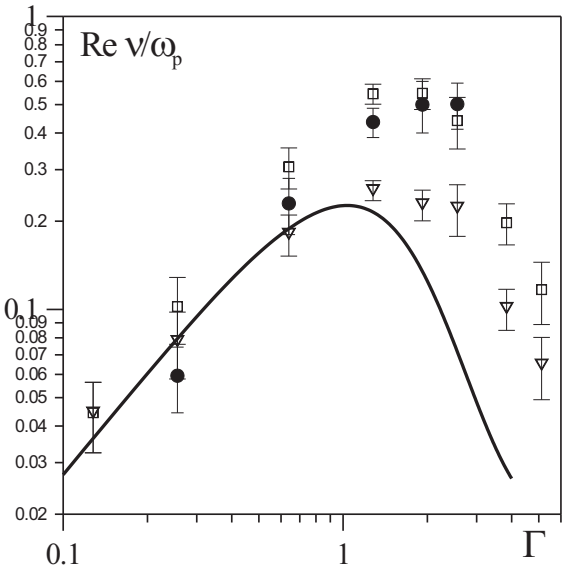

Figure 31: Dynamical conductivity obtained from MD simulations: ∇ — $\omega = 0$, $\square$ — $\omega = \omega_p$ (plasma frequency), • — collisional damping of the Langmuir waves $\nu = 2\delta_c$, solid line — interpolation formula [114], $T = 33000$K.

Kelbg type, whereas above the plasma frequency this pseudopotential does not reproduce the properties of a quantum Coulomb system. This is reflected via the discrepancies in the high-frequency behavior. Further investigations will compare MD simulations with wave packet or path integral simulations which allow for a more consistent treatment of quantum effects.

As shown in chapter 4, investigations based on quantum statistics take adequately into account the Coulomb interaction and quantum effects. In this approach, the formation of bound states can also correctly be included. Present perturbative treatments lead to analytical results. However, they are restricted to small nonideality parameter values $\Gamma \leq 1$ and small plasma densities n. In our approach, the weak-coupling limit has been improved taking into account dynamical screening and strong binary collisions. Considering also the renormalization factor $r(\omega)$, the correct low-density limit of transport coefficients is achieved. The comparison with MD simulations shows that the low-frequency behavior of the optical conductivity is given in good approximation as long as $\Gamma \leq 1$. For higher values of Γ, the quantum statistical approach has to be evaluated using methods beyond perturbation theory or by deriving interpolation formulas. On the other hand, MD simulations based on the Kelbg pseudopotential cannot reproduce the correct high-frequency ($\omega > \omega_{\rm pl}$) behavior of the optical conductivity for quantum Coulomb systems. Various known properties such as the high frequency behaviour and analytic constraints like the Kramers-Kronig relations were used to assess the MD results and to show the consistency of our approach. For all conditions considered here, these restrictions were fulfilled within the numerical precision.

Within the quantum statistical treatment, the formation of bound states is described in the low-density limit applying the model of a partially ionized plasma. At high densities, this model breaks down, and one has to apply adequate concepts such as the spectral function in order to describe the density modification due to medium effects, in particular the dissolution of bound states. This problem becomes more involved when, instead of a simple hydrogen plasma, ions with higher charges are considered allowing for different stages of ionization. The formation of bound states will be an essential aspect in the future development of numerical simulations.

MD simulations as well as quantum statistical calculations of dynamical conductivity have to be confronted with experimental data. In this paper we focused on the dc conductivity. For small nonideality up to $\Gamma \approx 1$, we found satisfactory coincidence between theory, MD simulations and experiments. In the next chapter we will address applications to bremsstrahlung [144] as well as Thomson scattering [185, 186] which should be analysed in order to investigate the dynamical collision frequency at higher frequencies. As already discussed above, classical MD simulations based on pseudopotentials such as the Kelbg one fail to reproduce the correct high-frequency asymptote for the collision frequency so that larger discrepancies compared with experiments are expected. Instead of classcal MD simulations, consistent quantum simulations such as wave-packet molecular dynamics or path integral techniques have to be used to compare with experimental data for high frequencies.

For the dc conductivity, a satisfactory agreement between analytical results, MD simulations and measured values has been found. Other experimental results suffer e.g. from

the transient nature of the produced plasma. Ionization, density, and temperature profiles have to be considered to infer local plasma conditions in order to compare with simulations or calculations. Experiments are performed not only with hydrogen plasmas, but also with other materials in which case the electron interactions are not pure Coulombic any more. The formation of bound states is an important feature in present experiments, since the contribution of the ionized component is extracted by applying the model of the partially ionized plasma. Nevertheless, for the plasma conditions considered here, the consistency between MD simulations, perturbative calculations, and experimental results is inferred.

6 Further Applications

As already discussed in the Introduction and shown in section 1.5, the dielectric function is a physical property which is of relevance in various situations where the coupling of a charged particle system with the radiation field is considered. In a first approximation, often the RPA, see section 3.2., is applied to describe the dielectric response of the Coulomb system. The RPA provides closed analytical expressions and can be implemented in an easy way. However, it describes no correlations in the charged particle system. Based on a mean-field approximation, collective excitations such as plasmons are described, but no collisions are considered in the Coulomb system. Despite this, the RPA has been proven to be a successfull description of plasma response in many applications, the relevance of collisions has to be investigated in concrete applications in order to achieve a description of desired accuracy.

A systematic microscopic approach to the treatment of collisions in a charged particle system should be given within a quantum statistical treatment as presented in the previous chapters. As a consequence, a generalized Drude formula (203) was derived containing a collision frequency $\nu((\vec{k},\omega))$ depending on frequency and wavenumber. We claim that we are able to give a consistent description of the response of a Coulomb system interacting with radiation, and we are able to evaluate the respective expressions using different many-particle methods. Exemplarily, we give some applications here, in particular to Thomson scattering, bremsstrahlung and reflectivity. In each case, there is a very close link to experiments which have been either done or are intended. This chapter is by no means exhaustive. We hope to inspire the reader, to consider further applications to physical situations where the interaction of charged particle systems with radiation is relevant.

6.1 Thomson Scattering

Thomson scattering in plasmas has been studied for a long time [187, 188, 189, 190, 191]. Dense plasmas are not transparent in the optical region when the frequency of the light $\omega_0 = 2\pi c/\lambda_0$ becomes less than the plasma frequency $\omega_{\rm pl}^2 = ne^2/(\epsilon_0 m_{\rm e})$. However, the method of X-ray Thomson scattering can be used which has been developed and applied for the diagnostic of dense plasmas recently [6]. This method requires intense X-ray sources as obtained e.g. from high–power optical laser in order to pump and probe samples of solid densities [192, 193, 194]. Alternatively, a free electron laser (FEL) test facility at DESY, Hamburg, has already demonstrated its capabilities for high–flux and time–resolved experiments at about 100 nm wavelength [195]. An X-ray FEL operating in the VUV range from 60-5 nm has started operation at the beginning of 2005 [196] at a wavelength of 35 nm. A similar facility is under construction at Stanford Linear Acceleration Center (SLAC) in Stanford [197].

First experiments to measure the averaged ionization state $\bar{Z}$, the electron density, and the electron temperature by using incoherent Thomson scattering at a probe wavelength of $\lambda_0 = 263\,\text{nm}$ were performed for high-Z (gold) plasmas [198, 199] with uncertainties of $< 20\%$. Spectrally resolved X-ray Thomson scattering at $\lambda = 0.24$ nm was applied to

determine plasma parameters for dense Be plasma [193]. Results for Be and C at solid state-like densities were given recently [7, 200, 201]. Comparison of the experimentally determined ionization state with the ACTEX model [202, 203] and calculations within the chemical picture [204] shows good agreement. In the latter approach, the various ionization stages up to Be^{4+} or C^{6+} are coupled via mass action laws. These are evaluated by considering nonideality corrections to the equation of state, see [205] for details.

Within this paragraph, we follow the terminology as found in [188, 200, 191]. The differential scattering cross section of Thomson scattering is related to the total dynamic structure factor $S_{\rm ee}(k,\omega)$ of all electrons in the plasma according to

$$\frac{d^2\sigma}{d\Omega\, d\omega} = \left(\frac{\mathrm{d}\sigma}{\mathrm{d}\Omega}\right)_{\rm T} \frac{k_1}{k_0} S_{\rm ee}(k,\omega) \tag{384}$$

where $(\mathrm{d}\sigma/\mathrm{d}\Omega)_{\rm T}$ is the Thomson cross section [191]; k_0 and k_1 are the wavenumbers of the incident and the scattered light, respectively. The energy and momentum transfer are characterized by $\hbar\omega = \hbar\omega_0 - \hbar\omega_1$ and $\hbar\mathbf{k} = \hbar\mathbf{k_0} - \hbar\mathbf{k_1}$, respectively. In the limit $\hbar\omega \ll \hbar\omega_0$ the transfer momentum is related to the scattering angle θ according to $k = 4\pi\sin(\theta/2)/\lambda_0$. A scattering parameter

$$\alpha = \frac{1}{k\lambda_{\rm D}}\ , \tag{385}$$

is introduced, where the screening length in the plasma $\lambda_{\rm D} = 1/\kappa = \sqrt{\epsilon_0 k_{\rm B} T_{\rm e}/(n_{\rm e} e^2)}$ is the inverse of the screening parameter κ, Eq. (183). Short-range correlations (within the Debye sphere) are relevant for $\alpha \leq 1$ and long-range, collective scattering is dominant for $\alpha \geq 1$. Furthermore, the plasma will be characterized by dimensionless parameters Γ and Θ which reflect the nonideality and degeneracy, respectively, of the plasma. The dynamic structure factor is defined in Eq. (76). According to Chihara [191] it can be decomposed into

$$S_{\rm ee}(k,\omega) = |f_{\rm I}(k) + q(k)|^2\, S_{\rm ii}(k,\omega) + Z_{\rm f} S^0_{\rm ee}(k,\omega) + Z_c \int d\omega'\, \widetilde{S}(k,\omega-\omega') S_{\rm s}(k,\omega'). \tag{386}$$

Eq. (386) contains contributions from electrons tight to the ion motion including screening (first term), from free electrons (second term) and from inelastic scattering due to excitations of core electrons (third term). Z_f is the average number of free electrons and Z_c the average number of core electrons per atom. As outlined by Chihara *et al.* [188, 191, 200], f_I denotes the ionic form factor, $q(k)$ the free electron cloud arround the ions, $S_{\rm ii}$ the ion-ion structure factor, $S^0_{\rm ee}$ the electron-electron structure factor of the free electrons, $\widetilde{S}$ the structure factor of core electrons in the ions and $S_{\rm s}$ the self-motion part of the ions described by the ion-ion density correlation function $S_{\rm ii}$. In the limit of fully ionized hydrogen, expression (386) reduces to

$$S_{\rm ee}(k,\omega) = |q(k)|^2\, S_{\rm ii}(k,\omega) + S^0_{\rm ee}(k,\omega). \tag{387}$$

It can be shown that this leads to identical expressions as if calculated from the electronic part of the RPA density-density response function (354) via the relation (346)

$$S_{\rm ee}(k,\omega) = -\frac{k_{\rm B}T}{e^2 n\omega}\,{\rm Im}\,\chi_{\rm ee}^{\rm RPA}(k,\omega)\,. \tag{388}$$

Within this paragraph, we focus on the free electron part of the structure factor

$$S_{\rm ee}^{0}(k,\omega) = -\frac{k_{\rm B}T}{e^2 n\omega}\,{\rm Im}\,\chi_{\rm e}^{0}(k,\omega)\,. \tag{389}$$

Analytical results on this level of the RPA are given in Eq. (350) and Section 3.2, and have been applied, see Gregori *et al.* Gregori03. We are interested in special conditions where RPA is not sufficient to describe X-ray Thomson scattering and collisions have to be taken into account. The adequate treatment of the dynamical structure factor including collisions is expected to improve plasma diagnostics using Thomson scattering. In this case the response function $\chi_{\rm e}^{0}(k,\omega)$ in Eq. (389) is replaced by the Mermin expression (356),

$$S_{\rm ee}^{0}(k,\omega) = -\frac{k_{\rm B}T}{e^2 n\omega}\,{\rm Im}\,\chi_{\rm e}^{\rm M.0}(k,\omega)\,. \tag{390}$$

We will now apply this formalism in order to calculate the structure factor $S_{\rm ee}^{0}(k,\omega)$ for parameters relevant for Thomson scattering, which are shown in TAB. 4 denoted as sets **a1**,. . ., **e3** [186]. The densities of sets **a**, **c** and **e** had been considered in a previous paper [185] since they are relevant for experimental situations given in Ref. [200]. Additionally, intermediate parameter sets **b** and **d** have been chosen in Ref. [186].

The parameter sets **a1**...**a3** are accessible with optical lasers, the sets **c1**...**c3** are in the extreme ultraviolet (EUV), and the parameter sets **e1**...**e3** are in the X-ray regime. In the last column of TAB. 4, we give also the results for the static collision frequency ${\rm Re}\,\nu_{\rm D}^{\rm Born}(\omega=0)$, Eq. (302), for all parameter sets. These values provide a rough estimate for typical collision frequencies, but neglect the dynamics and strong collisions. One clearly sees that for the cases **a** and **b** collisions are less important than for higher densities, i.e. cases **c**–**e**. For the parameter sets **c**, the collision frequencies are largest. Pauli blocking prevents the collisions to have a major influence in the case of highest densities, i.e. sets **d** and **e**.

The results for the electron dynamic structure factor Eq. (389) obtained from the RPA dielectric function, Eq. (350), and for the Mermin approximation (390) taking the frequency dependent collision frequency in the dynamical Born approximation, Eq. (235), are shown for the corresponding parameters of TAB. 4 in FIG. 32. For these calculations, the Kramers–Kronig relation (56) as well as sum rules (57) for the Mermin dielectric function are fulfilled within a numerical accuracy of better than 0.1%.

The well-known form for the structure factor in RPA is recovered. For small recoil energy (compared to the thermal energy) two symmetric peaks are found, see sets **a** and **b**. With increasing recoil energy these peaks become asymmetric and the red-shifted peak is more pronounced. The influence of collisions is most effective in the EUV domain at densities

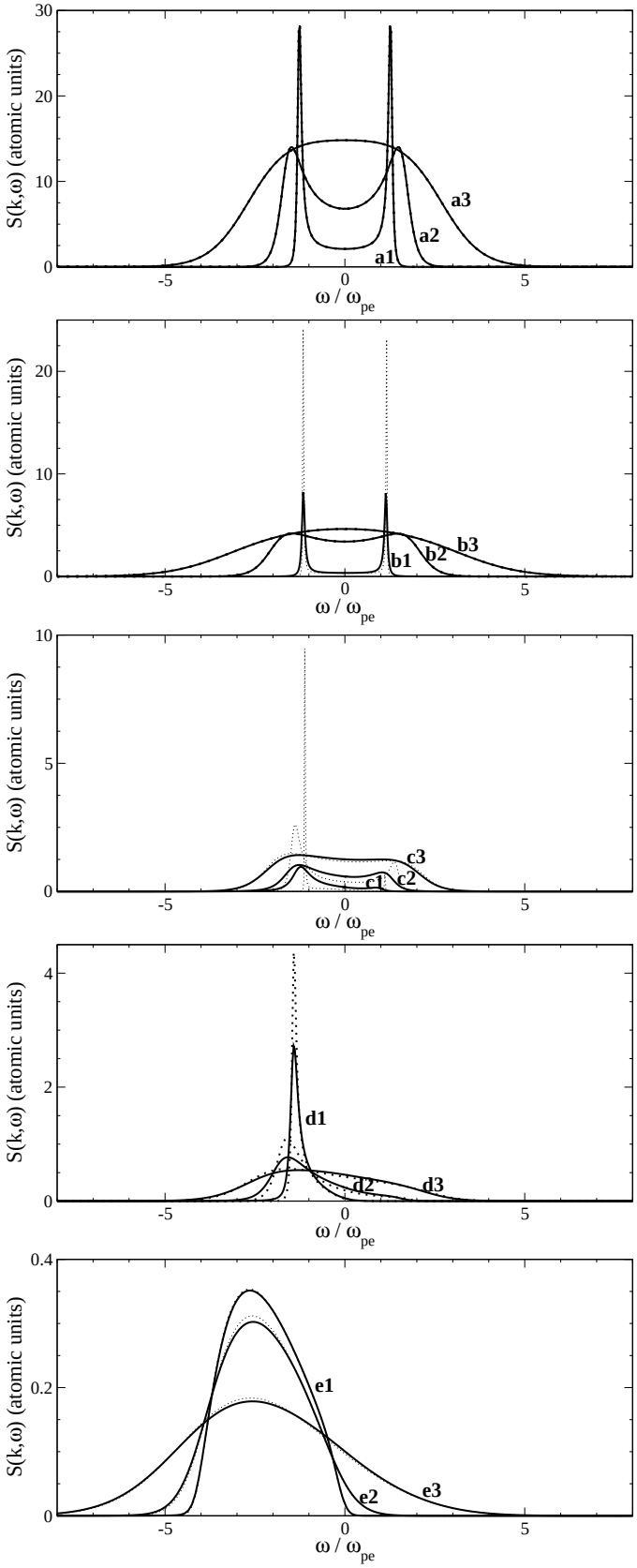

Figure 32: Dynamic structure factor $S^0_{\rm ee}(k,\omega)$ for an electron plasma at parameter values according to TAB. 4. Dotted lines: in RPA; full lines: from Mermin approach (390) with dynamical collision frequency in Born approximation, Eq. (235). Taken from [186].

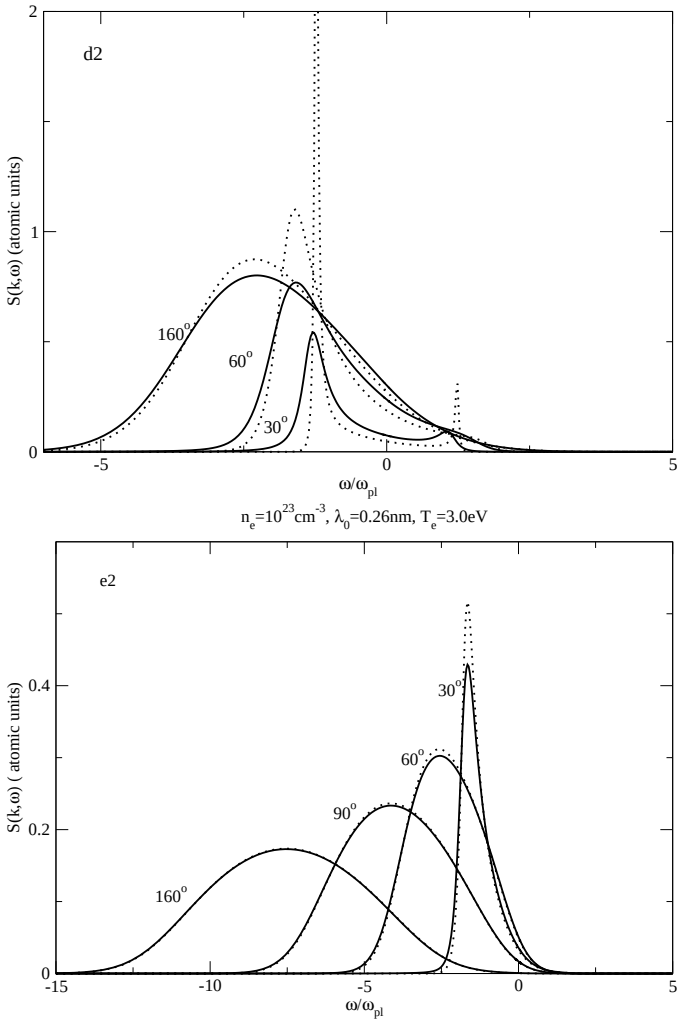

Figure 33: Angular dependence of the dynamic structure factor for sets **d2** (upper figure) and **e2** (lower figure). Dotted lines: RPA; solid lines: Mermin approach (390) with dynamic collision frequency in Born approximation, Eqs. (235).

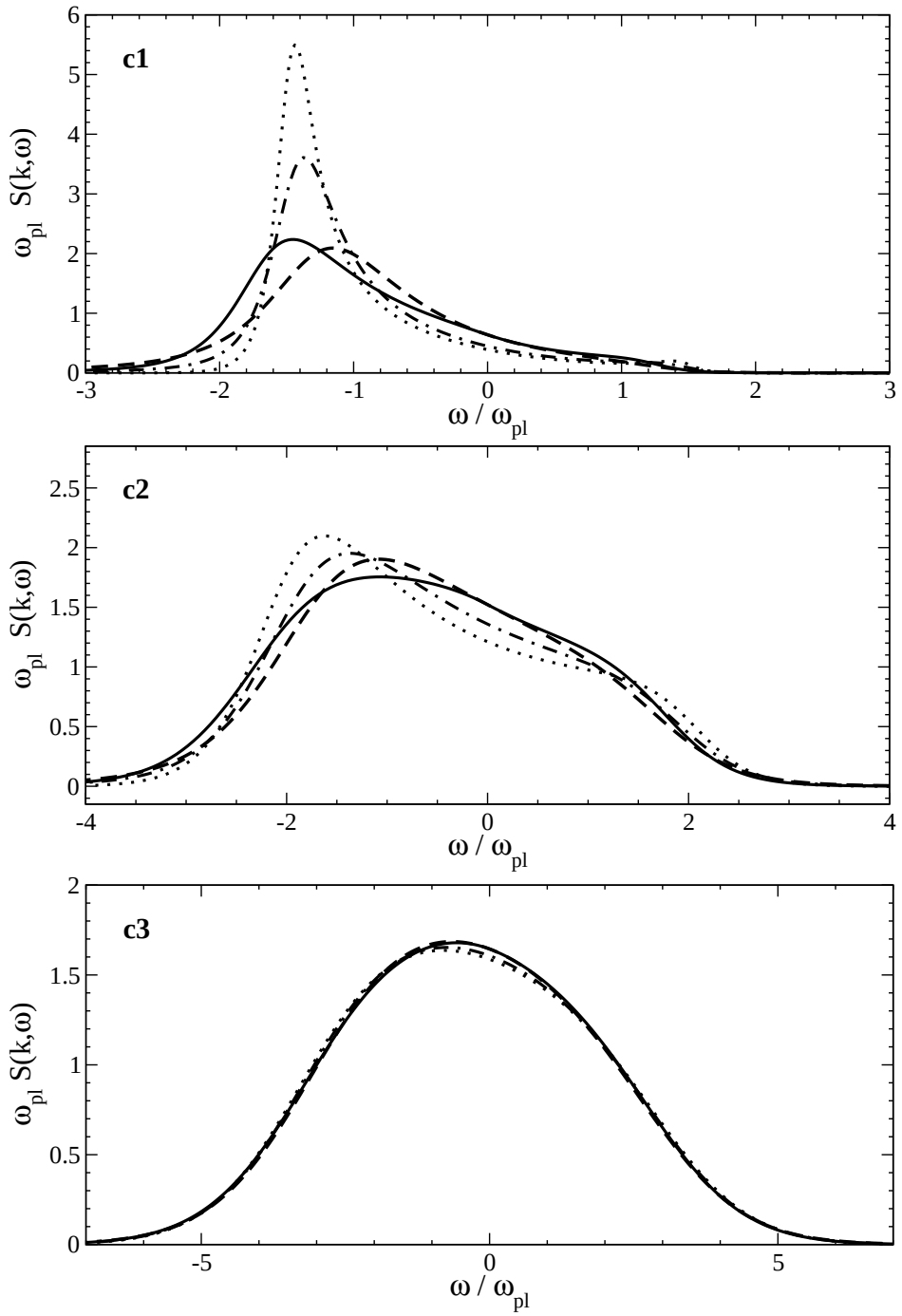

Figure 34: Dynamic structure factor for the conditions **c1**, **c2**, and **c3**. Dotted lines: in RPA; Mermin approach (390) taking collision frequency in different approximations. Full line: dynamical collision frequency in Born approximation (235); dashed line: static collision frequency in Born approximation (274); dot-dashed lines: interpolation formula (299). Taken from [186].

Table 4: Plasma parameters as used for the calculation of the dynamic structure factor: electron density n_e and the corresponding electron plasma frequency ω_{pl}, initial laser wavelength λ_0, electron temperature T_e, degeneracy parameter Θ, coupling parameter Γ, and static collision frequency in Born approximation $\mathrm{Re}\,\nu_D^{\mathrm{Born}}(\omega = 0)/\omega_{pl}$.

	n [cm^{-3}]	ω_{pl} [eV]	λ_0 [nm]	T_e [eV]	Θ	Γ	$\mathrm{Re}\,\nu_{\mathrm{stat}}^{\mathrm{Born}}$ [ω_{pe}]
a1				200	12000	0.0025	0.00044
a2	10^{19}	0.117	532	600	36000	0.0008	0.00010
a3				3000	180000	0.0002	0.00001
b1				10	130	0.12	0.0578
b2	10^{20}	0.371	50	100	1300	0.012	0.0030
b3				500	6400	0.0022	0.0003
c1				0.5	1.4	4.6	0.6538
c2	10^{21}	1.174	4.13	2.0	5.5	1.2	0.5305
c3				8.0	22	0.29	0.1574
d1				0.5	0.30	10	0.098
d2	10^{22}	3.713	1.0	2.0	1.2	2.5	0.399
d3				8.0	4.7	0.62	0.254
e1				0.8	0.10	13	0.0137
e2	10^{23}	11.742	0.26	3.0	0.38	3.6	0.1393
e3				13.0	1.7	0.83	0.2090

around $n_e = 10^{21}$ cm^{-3}, i.e. for sets **c**. For these parameters it is seen that collisions broaden the structure factor and the position of the peak is red-shifted.

The dependence of the dynamic struture factor on the scattering angle θ_{sc} can also be studied. In this way, the scattering parameter α, Eq. (385), is changed and we probe short-range correlations (small angle scattering) up to collective modes (back scattering). The angular dependence is shown for set **e2** in FIG. 33. As typical for the RPA, the dynamic structure factor is red-shifted and broadened with increasing scattering angle. Collisions are more important for smaller angles and yield modifications of the RPA results.

In FIG. 34 we give a more detailed comparison of the dynamic structure factor for parameter set **c**. We compare the RPA result with the Mermin result taking the static and dynamic collision frequency in Born approximation, Eqs. (274) and (235), respectively. In addition, also the Mermin result taking the static collision frequency derived from the interpolation formula, Eq. (299), is shown. The differences are most pronounced for the parameter set **c1**, i.e. for a degeneracy parameter $\Theta \approx 1$ and a large coupling parameter $\Gamma \gg 1$. As a general feature, the inclusion of the collisions leads to a broadening of the structure factor. Comparing the static and dynamic Born result for the case **c1** it is seen that the frequency dependence of the collision frequency leads to a red-shift of the maximum position in the structure factor. In particular, the high frequency tail of the curve is modified if the frequency dependence of the collision frequency is taken into account.

The peaks are located at values $|\omega|$ slightly above the plasma frequency, which can be understood from the plasmon dispersion relation. In the high-frequency case ($\omega^2 \gg k^2 v_{\mathrm{Te}}^2$) one has [206, 207]

$$\omega_{\mathrm{max}}^2 \approx \omega_{\mathrm{pl}}^2 + 3k^2 v_{\mathrm{Te}}^2 + \left(\frac{\hbar k^2}{2m_e}\right)^2 \ , \tag{391}$$

with the electron thermal velocity v_{Te}. In TAB. 5 we have summarized the information on the position of the red-shifted maximum of the structure factor and the width (FWHM) for the parameter set **c1** in the different approximations shown in FIG. 34. The position of the red-shifted peak in the RPA can be compared with the plasmon dispersion relation, Eq. (391), $\omega_{\mathrm{max}}/\omega_{\mathrm{pl}} = -1.321$. However, this dispersion relation is a classical result and gives a better agreement if compared with the RPA in the classical limit, $\omega_{\mathrm{max}}/\omega_{\mathrm{pl}} = -1.380$.

Table 5: Position of the infrared peak $\omega_{\mathrm{max}}/\omega_{\mathrm{pl}}$ and its FWHM for the dynamic structure factor shown in FIG. 34 for the case **c1**.

	FWHM	$\omega_{\mathrm{max}}/\omega_{\mathrm{pl}}$
$\bar{\nu} = 0$ (RPA)	0.494	-1.437
Mermin, $\bar{\nu}_{\mathrm{dyn}}^{\mathrm{Born}}$	1.244	-1.456
Mermin, $\bar{\nu}_{\mathrm{stat}}^{\mathrm{Born}}$	1.285	-1.155
Mermin, $\bar{\nu}_{\mathrm{stat}}^{\mathrm{ERR}}$	0.674	-1.373

It is the intention to extract plasma temperatures from the high-frequency part of the structure factor. The sensitivity of such a temperature adjustement via the dynamic structure factor with respect to the inclusion or the neglect of collisions was demonstrated in Ref. [185] for case **c1**. In analogy to [6], the temperature is determined by adjusting the electron temperature in the calculations with the dynamical Born approximation in order to obtain a satisfactory coincidence in the high-frequency crest of the structure factor. For the case **c1** the result is shown in FIG. 35 at a fixed density. It can be seen that the electron temperature inferred from the RPA structure factor overestimates the electron temperature derived from the dynamic Born result by a factor of about 2 which is important for plasma diagnostics.

Another approach to determine plasma parameters is the fact that the double peak structure in the regime $\alpha > 1$ where collective scattering is dominant shows an asymmetry according to (76),

$$S(k, -\omega) = \mathrm{e}^{-\frac{\hbar\omega}{k_{\mathrm{B}}T}} S(k, \omega) \tag{392}$$

If it were possible to spectrally resolve these side-peaks from the ion acoustic and the Rayleigh peak at the probe frequency and measure their intensities, one can directly determine the plasma temperature. Since the position of the plasmon resonance in a solid density plasma is given by the dispersion relation (391), the plasma frequency and subsequently the free

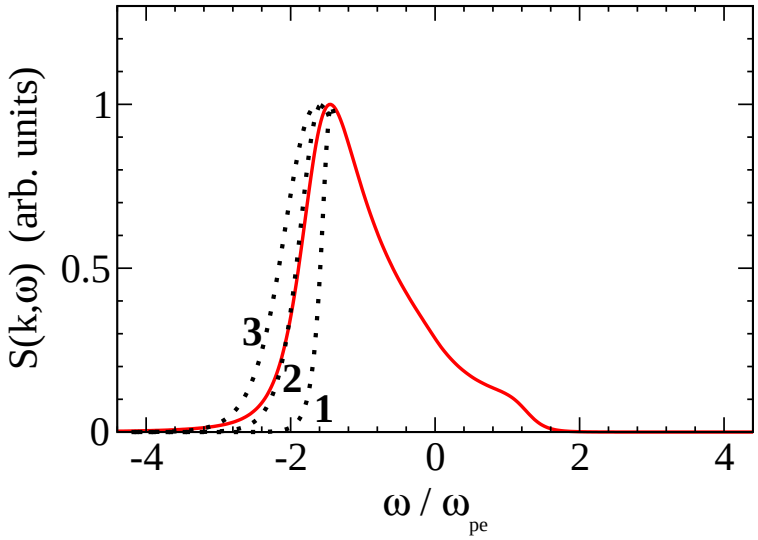

Figure 35: Dynamic structure factor $S(k,\omega)$ for parameter set **c1** ($T = 0.5$ eV) using Mermin approach with a dynamical collision frequency in Born approximation (235) (full line) in comparison to RPA results (dotted lines) for the same density and different electron temperatures, **1**: 0.5 eV, **2**: 1.0 eV, and **3**: 1.5 eV.

electron density can be determined with the temperature and therefore the thermal velocity known.

We have also performed calculations of the dynamic structure factor using the concept of the local-field factor, see Eq. (191). Taking the static local-field factor according to Hubbard [76] we observed only marginal deviations from the RPA result, see FIG. 36.

A more pronounced modification of the structure factor is obtained if dynamic local-field corrections are taken into account. Ichimaru *et al.* [208] suggested a fit formula for the dynamic local-field factor which interpolates between the low- and high-frequency limits. Gregori *et al.* [209] have used this expression, Eq. (214) and obtained strong deviations from the RPA result. In particular, a peak structure (entropy fluctuations) arises at zero frequency, which possibly reflects elastic contributions due to scattering on ions.

A peak structure of the dynamic structure factor near the plasma frequency has been obtained within the dynamic collision frequency approach, see FIG. 36. Evaluating the dynamic collision frequency within Born approximation with respect to a dynamically screened interaction $\nu_{\rm LB}$, an enhancement of the dynamic collision frequency is obtained near the plasma frequency, see also [62, 87]. Results for the dynamic structure factor show a structure which, however, is not so pronounced as the result given in [209].

Because of the good agreement with molecular dynamics simulations [144] we assume that our approach based on the dynamic collision frequency is more appropriate than the result obtained by using the fit [208] of the dynamic local-field corrections. However, possibly structures due to dynamic effects in collisions may lead to visible profiles in the Thomson scattering cross sections. A more detailed discussion should be done within the context of

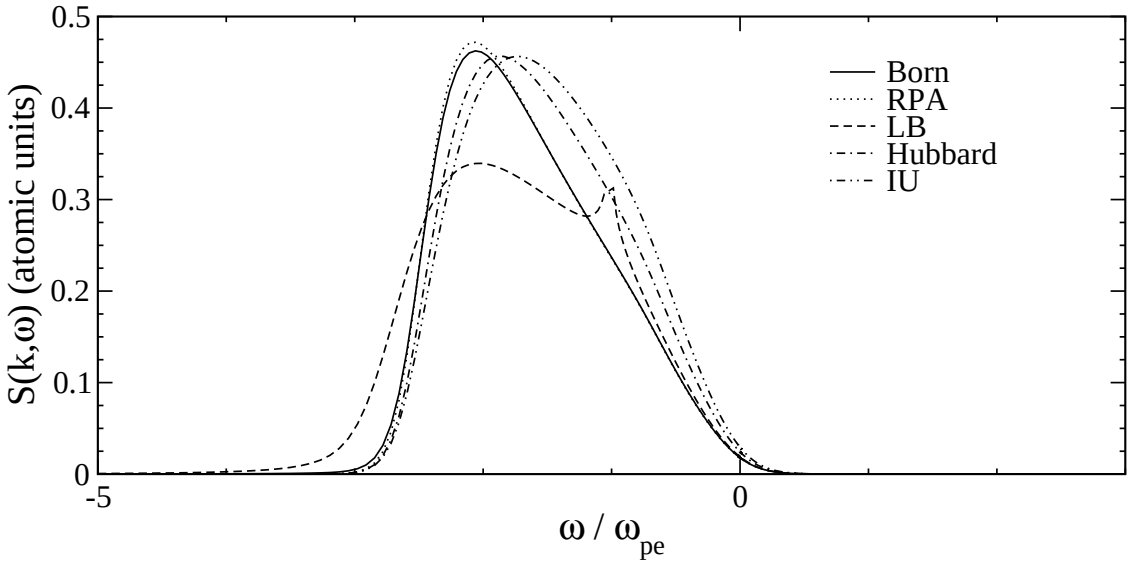

Figure 36: Structure factor $S(k,\omega)$ utilizing a dynamic collision frequency in Born approximation with respect to a statically screened potential (Born) and a dynamically screened potential (LB), RPA results and local-field corrections (Hubbard [76], Ichimaru and Utsumi (IU) [208]) for parameters as given in Ref. [209]: $n_e = 10^{23}$ cm^{-3}, $\lambda_0 = 0.66$ nm, $\theta_{\rm sc} = 135°$, and $T = 1$ eV.

the Gould-DeWitt approximation for the dynamic collision frequency, see section 4.5.

We have treated X-ray Thomson scattering in a wide range of temperatures and densities. Those scattering experiments are an important diagnostic tool to infer plasma temperatures and densities if reliable results for the dynamic structure factor $S(\mathbf{k},\omega)$ are known. The contribution of free electrons to the structure factor is usually studied on the level of the RPA. We have extended this approach by considering collisions in the free electron part of the structure factor, see also Ref. [185]. These results indicate that collisions have only a minor influence on the dynamic structure factor in a wide parameter range so that RPA can be applied there. However, we also identified a parameter region (degeneracy parameter $\Theta \approx 1$ and coupling parameter $\Gamma \gg 1$) where major deviations from the RPA results are found and collisions are important to get reliable results for the plasma parameters, see also Refs. [186, 200, 209]. More refined calculations are necessary and are in progress. Besides the contribution of free electrons, also those of bound states and of inelastic collisions with weakly bound electrons have to be included in the evaluations when comparing with experimental scattering spectra, see Ref. [200].

6.2 Bremsstrahlung

In fully ionized isotropic plasmas, bremsstrahlung emitted in collisions between charged particles is the dominant emission process. Even in partially ionized plasmas, bremsstrahlung

is an important contribution to the continuum background spectrum. As pointed out, e.g. in Refs. [210, 211], this continuum spectrum can be used to infer density and temperature conditions in plasmas.

The emission of radiation by a plasma is characterized by the emission coefficient $j(\omega)$, which gives the rate of radiation energy per unit volume, frequency and solid angle. For a system in thermal equilibrium the emission coefficient is related to the absorption coefficient $\alpha(\omega)$ by Kirchhoff's law

$$j(\omega) \;=\; L_\omega^H(\omega)\,\alpha(\omega) \quad , \tag{393}$$

where $L_\omega^H(\omega) = \hbar\omega^3/(4\pi^3c^2)\,[\exp(\hbar\omega/k_BT)-1]^{-1}$ is the spectral power density of blackbody radiation, and c is the speed of light. The absorption coefficient describes the inverse process to bremsstrahlung, namely the absorption of a photon upon collision leading to the attenuation of electromagnetic waves in a plasma. Since it is a main contribution to radiation loss in plasmas its understanding is crucial for modeling radiation transport.

Continuum emission of hot and dense plasmas was measured in a number of experiments, see, e.g. Ref. [212, 213]. However, the bremsstrahlung spectrum has contributions from free-free as well as bound-free transitions. Hence, a description of the bremsstrahlung spectrum requires also an appropriate treatment of bound states in a hot and dense plasma. In addition, the transient nature of the expanding laser-induced plasma requires the knowledge of density and temperature profiles as well as ionization degrees, which can be taken e.g. from a hydrodynamical code. Here, we will focus on the free–free transitions. The presentation follows mainly Ref. [214].

The thermally averaged emission coefficient for a non-relativistic plasma considering free-free transitions without particle correlations reads according to Kramers [215]

$$j_{\rm ff}(\omega) \;=\; A^{-1}\,Z^2\,n_e\,n_i\,g(\omega)\,\frac{\exp\left(-\frac{\hbar\omega}{k_BT}\right)}{\sqrt{k_BT}} \quad , \tag{394}$$

with a constant A given by $A = 12\pi^2\sqrt{6\pi}\epsilon_0^3c^3m_e^{3/2}/e^6$. The Gaunt factor $g(\omega)$ was introduced later by Gaunt [216] in order to account for quantum-mechanical modifications. Considering particle correlations leads to further changes of Kramer's expression.

Modifications due to particle correlations have been discussed in the literature to some extent. Dawson and Oberman [135, 217] derived the Gaunt factor from an approximation for the dynamical collision frequency based on kinetic theory accounting for screening. Their expression is widely used to describe the collisional absorption of intense laser radiation by plasmas [218]. The expression of Dawson and Oberman was improved by Bekefi [110] replacing the necessary cut-off parameters by a quantum mechanical analysis. Further improvements to treat correlations in the electron gas have been performed by Berkovsky et al. [90] considering local-field corrections. Effects due to the degeneracy of the electron gas are included by Kawakami et al. [219]. Effects due to strong correlations of the ions represented by an ion structure factor were treated in Refs. [220, 221]. Strong collisions

were considered by Berkovsky *et al.* [90] using thermodynamic Green's function techniques, similar to the approach presented in chapter 4. Nonlinear inverse bremsstrahlung in high-frequency fields was calculated by Silin [222], see also Ref. [223, 224]. A somewhat similar approach is presented in Ref. [225]. A refined quantum-statistical treatment starting from the Kadanoff-Baym equations is given by Kremp *et al.* [226, 227].

In what follows, we apply the approach to the dielectric function as obtained in the previous chapters. We again restrict ourselves to fully ionized classical Maxwellian plasmas at moderate values of the nonideality parameter and to weak perturbing fields. Different expressions for the Gaunt factor including already known expressions are given. Numerical results for the bremsstrahlung spectrum of the solar core plasma and a comparison with computer simulations for a plasma at moderate values of the nonideality parameter are given.

Medium modifications of the propagation of electromagnetic waves in an isotropic, unmagnetized plasma are described by the transversal dielectric permittivity $\epsilon_t(k,\omega)$. In the long-wavelength limit $k \to 0$, relevant for the emission and absorption of visible light, the transverse and longitudinal dielectric function are identical $\epsilon(\omega) = \lim_{k\to 0} \epsilon_{\rm transv}(k,\omega) = \lim_{k\to 0} \epsilon_{\rm long}(k,\omega)$. The dielectric function $\epsilon(\omega)$ is connected to the index of refraction $n(\omega)$ and the absorption coefficient $\alpha(\omega)$ by, see e.g. [228],

$$n(\omega) + \frac{ic}{2\omega}\,\alpha(\omega) \;=\; \sqrt{\epsilon(\omega)}, \tag{395}$$

and we obtain

$$n(\omega) = \frac{1}{\sqrt{2}}\,\left[\mathrm{Re}\,\epsilon(\omega) \,+\, \sqrt{\left(\mathrm{Re}\,\epsilon(\omega)\right)^2 + \left(\mathrm{Im}\,\epsilon(\omega)\right)^2}\right]^{1/2}, \qquad \alpha(\omega) \;=\; \frac{\omega}{c\,n(\omega)}\,\mathrm{Im}\,\epsilon(\omega). \tag{396}$$

The dielectric function is taken in the generalized Drude-like form (228),

$$\epsilon(\omega) \;=\; 1 - \frac{\omega_{\rm pl}^2}{\omega\,\left[\omega + i\nu(\omega)\right]}, \tag{397}$$

with a dynamical and complex collision frequency $\nu(\omega)$. Using Eq. (396), we obtain the absorption coefficient as a function of the real part of the dynamical collision frequency

$$\alpha(\omega) \;=\; \frac{\omega_{\rm pl}^2}{c}\,\frac{\mathrm{Re}\,\nu(\omega)}{\left(\omega^2 + |\nu(\omega)|^2\right)\,n(\omega)}. \tag{398}$$

Usually, a high-frequency expansion of this expression is considered, taking the imaginary part of the dielectric function as proportional to the real part of the dynamical collision frequency, $\mathrm{Im}\,\epsilon(\omega) \;\approx\; \omega_{\rm pl}^2\,\mathrm{Re}\,\nu(\omega)/\omega^3$ and $\mathrm{Re}\,\epsilon(0,\omega) \;\approx\; 1$. With this approximation one can introduce the high-frequency limit $\bar{\alpha}(\omega) = \omega_{\rm pl}^2\,\mathrm{Re}\nu(\omega)/c\omega^2$. However, being interested in frequencies comparable or smaller than the plasma frequency, the absorption coefficient $\bar{\alpha}(\omega)$ derived in the high-frequency limit should be corrected as $\alpha(\omega) = \bar{\alpha}(\omega)/\left[(1 + |\nu(\omega)|^2/\omega^2)n(\omega)\right]$.

6.2.1 Evaluation of the Gaunt factor

First of all, we consider corrections due to the dynamically screened Born approximation, which was derived in section 4.2. The collision frequency was given in Eq. (248).

$$\nu^{\mathrm{LB}}(\omega) \;=\; i\,\frac{\epsilon_0 n_i\,\Omega_0^2}{6\pi^2 e^2\,n_e m_e}\int_0^\infty dq\,q^6\,V_{ei}^2(q)\,S_i(q)\,\frac{1}{\omega}\left[\epsilon_{\mathrm{RPA},e}^{-1}(q,\omega)\;-\;\epsilon_{\mathrm{RPA},e}^{-1}(q,0)\right]. \quad (399)$$

The dielectric function $\epsilon_{\mathrm{RPA},e}(q,\omega)$ is taken in the Random Phase Approximation (RPA). For a Maxwellian plasma, we give the imaginary part of the dielectric function, see e.g. [70],

$$\mathrm{Im}\,\epsilon_{\mathrm{RPA},e}(q,\omega) = \frac{m_e\omega_{\mathrm{pl},e}^2}{\hbar q^3}\left(\frac{2\pi m_e}{k_B T}\right)^{1/2}\sinh\left(\frac{\hbar\omega}{2k_B T}\right)\exp\left(-\frac{m_e}{2k_B T}\,\frac{\omega^2}{q^2}-\frac{1}{8k_B T}\,\frac{\hbar^2 q^2}{m_e}\right) \quad (400)$$

This result was first derived by Bekefi [110] using kinetic theory and was also obtained by Bobrov and Trigger [99] analyzing the force-force correlation function. To account for a finite ion mass, the collision frequency for a two-component plasma has to be determined including dynamical screening effects [87]. Substantial deviations between the two-component calculation and the adiabatic model have been found for frequencies small compared to the ion plasma frequency. Going beyond the RPA approximation (400) for the inverse dielectric function, further correlation effects can be incorporated. We report some of the extensions without being exhaustive. Kawakami [219] included degeneracy effects by considering the general expression for the RPA at arbitrary degeneracy. Berkovsky and Kurilenkov considered local field corrections using a method suggested by Ichimaru et al. [130]. Tkachenkov and Fernández de Córdoba [229] employed the method of moments to include correlations. An extension of the Lenard-Balescu collision term, Eq. (399), for a two-temperature plasma is presented by Dharma-Wardana [102]. Effects due to the quiver motion have recently been studied by Mulser et al. [224] and Kremp et al. [226, 227]. Within our approach, an iterative treatment can be carried out inserting the improved dielectric function into Eq. (399). However, since we are only interested in weakly coupled plasmas so far, we keep the level of the RPA.

From the general expression (399), we derive further approximations, see also Ref. [230]. A statically screened dynamical collision frequency is obtained by $\epsilon_{\mathrm{RPA},e}^{-1}(q,\omega)\approx[\mathrm{Re}\,\epsilon_{\mathrm{RPA},e}(q,\omega)-i\mathrm{Im}\,\epsilon_{\mathrm{R}}$ The corresponding real part of the collision frequency reads

$$\mathrm{Re}\,\nu^{\mathrm{D}}(\omega) \;=\; \frac{\epsilon_0 n_i\,\Omega_0^2}{6\pi^2 e^2\,n_e m_e}\int_0^\infty dq\,q^6\,V_D^2(q)\,S_i(q)\,\frac{1}{\omega}\,\mathrm{Im}\,\epsilon_{\mathrm{RPA},e}(q,\omega), \quad (401)$$

where $V_D(q)=V_{ei}(q)/\left[\mathrm{Re}\,\epsilon_{\mathrm{RPA},e}(q,0)\right]$ is the Debye potential. The collision frequency $\nu^{\mathrm{B}}(\omega)$ in Born approximation with respect to the Coulomb potential is obtained by the approximation $\mathrm{Im}\,\epsilon^{-1}(k,\omega)\;\approx\;-\mathrm{Im}\,\epsilon(k,\omega)$. In this approximation, the integration in Eq. (399) can be carried out analytically, resulting in

$$\mathrm{Re}\,\nu^{\mathrm{B}}(\omega) = \frac{e^4 n_i}{12\pi^2\epsilon_0^2 m_e}\left(\frac{2\pi m_e}{k_B T}\right)^{1/2}\frac{1}{\hbar\omega}\left[\exp\left(\frac{\beta\hbar\omega}{2}\right)-\exp\left(-\frac{\beta\hbar\omega}{2}\right)\right]K_0\left(\frac{\hbar\omega}{2k_B T}\right), \quad (402)$$

where $K_0(z)$ is a modified Bessel function[44]. The static ion structure factor is approximated as $S_i(q) \approx 1$. Since $\mathrm{Im}\,\epsilon^{-1}(k,\omega) \approx -\mathrm{Im}\,\epsilon(k,\omega)$ for $\omega \gg \omega_{\mathrm{pl}}$, the Born approximation coincides with the high frequency limit of the dynamically screened collision frequency. Using Kirchhoff's law, Eq. (393), and comparing with Kramers result, the well known Gaunt factor in Born appoximation [211] is obtained, $g^{\mathrm{B}}(\omega) = \exp(\hbar\omega/[2k_BT])\,\sqrt{3}\,K_0(\hbar\omega/[2k_BT])/\pi$.

There are several points of criticism connected with the result of Bekefi, Eq. (399). First, the formula of Bekefi does not yield the correct static value for the conductivity. For a classical fully ionized plasma in the low density limit, the conductivity is given by the Spitzer formula, see section 4.4. The Spitzer result can be attributed to strong collisions not accounted for in the Eq. (399). Secondly, the high-frequency asymptote for a dilute plasma should be given by the Sommerfeld result []. Although, Sommerfeld's formula coincides with the result by Bekefi in first Born approximation, they disagree in higher orders of perturbation theory. We will show below how to remove these deficiencies by taking into account strong collisions in a T–matrix approximation of the dynamical collision frequency.

The first calculation of inverse bremsstrahlung in a plasma accounting for screening effects was performed by Dawson and Oberman [135, 217] starting from the Vlasov equation. Their result is similar to the one obtained by Bekefi. However, they used the classical Maxwellian dielectric function (189) to describe the dynamical screening of the potential. As a consequence they had to introduce a wave-vector cut-off at $q_{\max}$ to regularize the integration over q. The need of a cut-off parameter is avoided in Eq. (399) by using the quantum mechanical RPA expression for the dielectric function which implies an effective cut-off with the thermal de Broglie wavelength. Dawson and Oberman obtained the following absorption coefficient

$$\alpha^{\mathrm{DO}}(\omega) = \frac{e^6}{12 m_e \hbar c \epsilon_0^3} \left(\frac{2\pi\beta}{3m_e}\right)^{1/2} n_e\, n_i\, \frac{1}{\omega^3} \left(1 - \mathrm{e}^{-\beta\hbar\omega}\right) \frac{\ln\Lambda}{\left(1 - \omega_{\mathrm{pl}}^2/\omega^2\right)^{1/2}}, \qquad (403)$$

where $\ln\Lambda$ is a Coulomb logarithm. Λ is given by the minimum of $q_{\max} v_T/\omega_{\mathrm{pl}}$ and $q_{\max} v_T/\omega$. The quantity $q_{\max}$ in turn is given by the minimum of $k_BT/(Ze^2)$ and $(m_e k_B T)^{1/2}/\hbar$. Here, $v_T = (k_BT/m)^{1/2}$ is the thermal velocity, m_e the electron mass. Note, that the dc conductivity derived from the Dawson-Oberman expression $\sigma_{\mathrm{dc}} = \sigma(0) = \lim_{\omega\to 0} \epsilon_0\omega\,(\epsilon(0,\omega) - 1)$ coincides in the Coulomb logarithm with the Spitzer formula, see [59], alas the prefactors differ. A discussion on improvements of the Coulomb logarithm introduced here can be found in Ref. [232]. Some work on dynamical effects within a classical straight-line trajectory was recently published by Jung [233]. Furthermore, the index of refraction, Eq. (403), is derived from the approximation $\mathrm{Re}\,\epsilon(0,\omega) = 1 - \omega_{\mathrm{pl}}^2/\omega^2$ assuming $\mathrm{Im}\,\epsilon(0,\omega) \ll \mathrm{Re}\,\epsilon(0,\omega)$.

A systematic treatment of strong collisions can be obtained by performing a ladder approximation with respect to a static screened potential $V^{\mathrm{D}}(q) = e^2/[\epsilon_0\Omega_0(q^2 + \kappa_{\mathrm{eff}}^2)]$ with an effective inverse screening length κ_{eff}, see section 4.3. The corresponding collision frequency ν^{T}, Eq. (253), can be rewritten as an integration over the dipole matrix element, as was

[44] Using the identity $\int_0^\infty dx\, x^{\alpha-1}\,\mathrm{e}^{-px}\,\mathrm{e}^{-q/x} = 2(q/p)^{\alpha/2}\,K_\alpha\left(2\sqrt{pq}\right)$.

shown by Wierling *et al.* in the appendix of Ref. [214]. Assuming a classical Maxwellian plasma and taking into account scattering states only, the real part is given by [214]

$$\begin{aligned}\mathrm{Re}\,\nu^{\mathrm{T}}(\omega) &= \frac{\pi n_e\sqrt{\mu}}{(2\pi)^{9/2}\,m_e}\left(1-\mathrm{e}^{-\beta\hbar\omega}\right)(\hbar\omega)^3\int_0^\infty dk_1\,k_1^2\int_0^\infty dk_2\,k_2^2\,\delta(\hbar\omega+\frac{\hbar^2k_1^2}{2\mu}-\frac{\hbar^2k_2^2}{2\mu}) \\ &\quad\times\exp\left(-\beta\hbar^2k_1^2/2\mu\right)\int d\Omega_1\int d\Omega_2\left|\int d^3r\Psi^*_{\vec{k}_2}(\vec{r})\,z\,\Psi_{\vec{k}_1}(\vec{r})\right|^2 \quad , \end{aligned} \tag{404}$$

where μ is the reduced mass, Ω_1, Ω_2 are the solid angles of the momenta $\vec{k}_1, \vec{k}_2$, respectively. This expression shows the proportionality of the dynamical collision frequency to the dipole matrix element. In the high-frequency limit, our treatment corresponds to the approach of Lamoureux et al. [234]. The free-free dipole matrix element for a Debye potential can be determined from the numerical solution of the Schrödinger equation, see, e.g., Ref. [235]. Taking the limit $\kappa_{\mathrm{eff}} \to 0$, we obtain Sommerfeld's result [231] for the free-free Gaunt factor of an uncorrelated Maxwellian plasma.

6.2.2 Numerical results for a hydrogen plasma

As given by Eq. (398), the absorption coefficient reads in terms of the collision frequency and the renormalization factor, see Eq. (300),

$$\alpha(\omega) = \frac{\omega_{\mathrm{pl}}^2}{c\,n(\omega)}\,\mathrm{Im}\,\frac{1}{\omega + i\,r(\omega)\,\nu^{(P_0)}(\omega)} \quad . \tag{405}$$

The collision frequency $\nu^{(P_0)}(\omega)$ is the one-moment approximation in dynamically screened T–matrix approach which is approximated via the Gould-deWitt scheme, see section 4.5, in particular Eq. (301). We apply our improved expression of the absorption coefficient to a hydrogen plasma at two different physical situations. In a first step, we compare our results with computer simulations by Pfalzner and Gibbon [157]. As was done in the simulation, we choose a nonideality parameter $\Gamma = 0.1$. In order to avoid contributions from bound states, we fix the effective inverse screening length to be $\kappa_{\mathrm{eff}} = 1.4\,a_B^{-1}$. This leads to a density of $n = 1.51 \times 10^{25}$ cm^{-3} and a temperature of $T = 573$ eV. Although the degeneracy parameter amounts to $\theta = 2.58$, degeneracy effects are neglected to be on the same level with the simulation.

The real part of the dynamical collision frequency $\nu^{(P_0)}(\omega)$, Eq. (301), is shown in FIG. 37. Besides the Gould-DeWitt result, the contributions from dynamical screening, Eq. (399), and strong collisions, Eq. (266), as well as the static screening result, Eq. (401), are shown. In the high-frequency limit, the dynamical screening and static screening almost coincide, since $\mathrm{Re}\,\epsilon(q,\omega) \approx 1$. In consequence, the Gould-DeWitt result is dominated by the contribution from strong collisions. In the static limit, the dc conductivity with a Spitzer-like Coulomb logarithm is found. The peak in the contribution from dynamical screening close to the plasma frequency is due to plasmon excitation and was found earlier by Dawson and Oberman, see FIG. 1 in Ref. [135, 217] and also Ref. [236]. It is smoothed out by improving

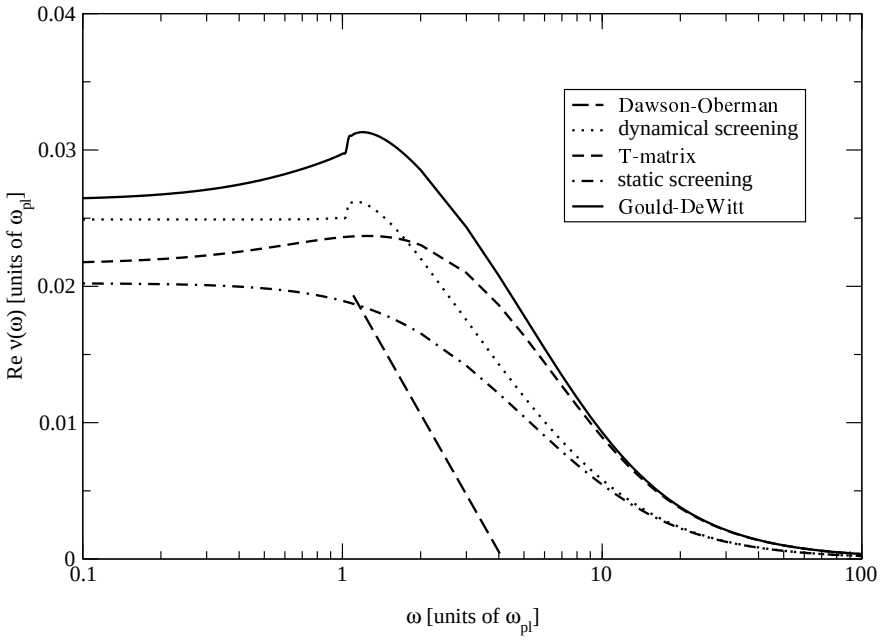

Figure 37: Frequency dependence of the real part of the collision frequency $\nu(\omega)$. A hydrogen plasma with $n = 1.51 \times 10^{25}$ cm^{-3}, $T = 573$ eV corresponding to $\Gamma = 0.1$ is considered. Different approximations are compared.

the inverse dielectric function beyond RPA taking into account collisions. The Dawson-Oberman result significantly underestimates the collision frequency. As discussed above, it is adjusted to coincide with the low-frequency ($\hbar\omega \ll k_B T$) asymptote of the Born approximation. Since the plasma frequency is comparable with the thermal energy ($\hbar\omega_{\rm pl} \approx k_B T/4$), the Dawson-Oberman result is not an appropriate approximation. Besides the sum rules for the dielectric function and its inverse (57), we have also tested the following sum rules for the index of refraction $n(\omega)$ and the extinction coefficient $\mathrm{Im}\,\epsilon(\omega)/(2\,n(\omega))$, see Ref. [237],

$$\int_0^\infty d\omega \, \frac{\omega \, \mathrm{Im}\, \epsilon(\omega)}{2\, n(\omega)} \;=\; \frac{\pi\, \omega_{\rm pl}^2}{4} \;, \tag{406}$$

$$\int_0^\infty d\omega \; (n(\omega) - 1) \;=\; 0 \;. \tag{407}$$

The agreement is in the order of the numerical accuracy of 0.1%.

The renormalization factor $r(\omega)$, Eq. (313) was calculated within a 2–moment-approximation, for the plasma conditions under consideration it is displayed in FIG. 38. The real part is substantially smaller than unity at low frequencies, being 0.62 in the static limit. This corresponds to a higher conductivity as compared with the one obtained from the Gould-DeWitt approach, see section 4.5. For high frequencies the real part converges to unity, implying that higher order moments do not contribute in the high-frequency limit. In between, for frequencies above the plasma frequency, the real part shows an increase to

about 1.2. The imaginary part is connected to the real part by a Kramers-Kronig relation. Thus, it is zero in the static as well as high-frequency limit and exposes a maximum and a minimum in between corresponding to the structure of the real part. Detailed numerical studies show, that the maximum of the real part is located close to $k_B T$. This can also be estimated using a high frequency expansion of Eq. (402) leading to expressions in terms of Bessel functions, which have $\hbar\omega/(2k_B T)$ as an argument.

The real part of the modified collision frequency $\nu(\omega) = r(\omega)\,\nu^{(P_0)}(\omega)$ is shown in FIG. 39. It is compared to the unmodified collision frequency and to data points obtained via computer simulation by Pfalzner and Gibbon [157]. For low frequencies the collision frequency is decreased compared to the unmodified one while for frequencies higher than about $2\,\omega_{\rm pl}$, the collision frequency is increased. For these frequencies, the calculated collision frequencies agree with the one obtained by computer simulation within the errors. For frequencies around $\omega_{\rm pl}$ there is disagreement of a factor of 2 to 3. Note, that the comparison with the results of Pfalzner and Gibbon is delicate. Within the simulation approach the degeneracy parameter θ is infinite, while our approach starts from fixed density and temperature conditions, thus having a finite θ. Furthermore, Pfalzner and Gibbon derived the collision frequency from a simulation of the heating rate of the plasma. Converting the heating rate to a collision frequency, they have used the high-frequency asymptote of the Drude formula. Thus, to compare with their results a refined analysis of the observables should be carried out.

In a second step, we study a hydrogen plasma with density $n = 6.0 \times 10^{25}\,\mathrm{cm}^{-3}$ and temperature $T = 1.3$ keV corresponding to the conditions at the solar center. Since the energy transport in the inner region of the sun is due to radiation, the absorption coefficient is crucial for standard solar models where it enters via the opacities. The Gaunt factor for the solar core center was calculated by Iglesias and Rose [239, 240] using the Lenard-Balescu formula Eq. (401) for the dynamical collision frequency. The overall frequency dependence as well as the differences of the various approximations for solar core conditions are similar to the ones discussed above. We only show the resulting Gaunt factor in FIG. 40. The range of frequencies is chosen as in Ref. [239]. Note that higher frequencies are already in the x-ray range where a treatment of the dielectric function in the long-wavelength limit is no longer sufficient to describe the propagation of the photon. The Gaunt factor is given in units of the Gaunt factor $g_D(\omega)$ which is obtained when comparing the absorption coefficient Eq. (398) using a dynamical collision frequency with a statically screened approximation, see Eq. (401).

In FIG. 40, various approximations are shown. The dynamically screened approximation corresponds to the result of Iglesias. Our final result is given by the solid line. For low frequencies $\omega < \omega_{\rm pl}$ the deviations from unity are small implying that the Gaunt factor is well approximated by a statically screened treatment. However, for frequencies above the plasma frequency $\omega_{\rm pl} \approx 0.2 k_B T$ considerable deviations appear. These are due to changes in the index of refraction as well as the real part of the collision frequency, cf. Eq. (398). The onset at the plasma frequency is connected to the minimum of the index of refraction. While dynamical screening corrections are small for high frequencies, the account of strong collisions (T–matrix) not included in the Born-like Gaunt factor $g_D(\omega)$ leads to an increase

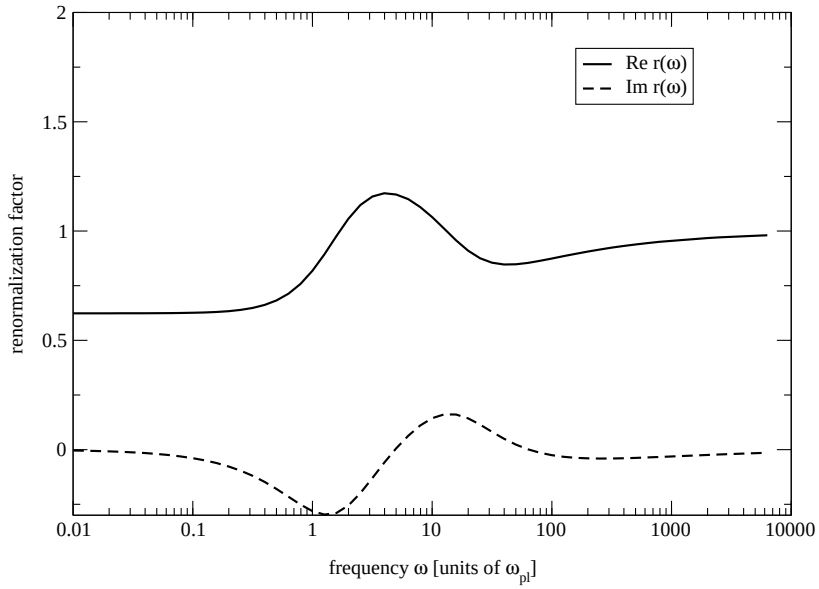

Figure 38: Frequency dependence of the renormalization factor $r(\omega)$. A hydrogen plasma with $n = 1.51 \times 10^{25}$ cm^{-3}, $T = 573$ eV, corresponding to $\Gamma = 0.1$ is considered.

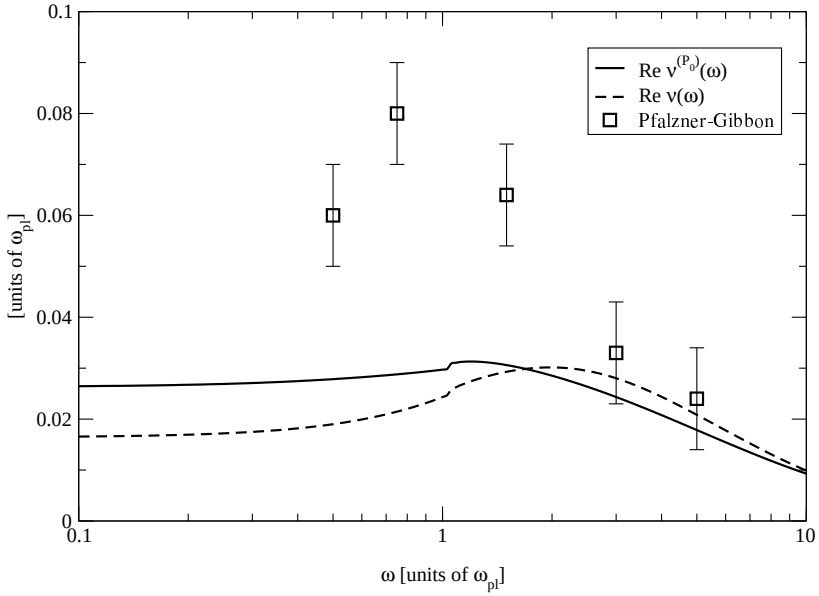

Figure 39: Dynamical collision frequency $\nu(\omega)$ modified by the renormalization factor $r(\omega)$ compared to the unrenormalized collision frequency $\nu^{(P_0)}(\omega)$ and the numerical simulation of Pfalzner and Gibbon [157]. The indicated error bars are from [238]. P. Gibbon, private communication, (2000) A hydrogen plasma with $n = 1.51 \times 10^{25}$ cm^{-3}, $T = 573$ eV, corresponding to a nonideality parameter $\Gamma = 0.1$ is considered.

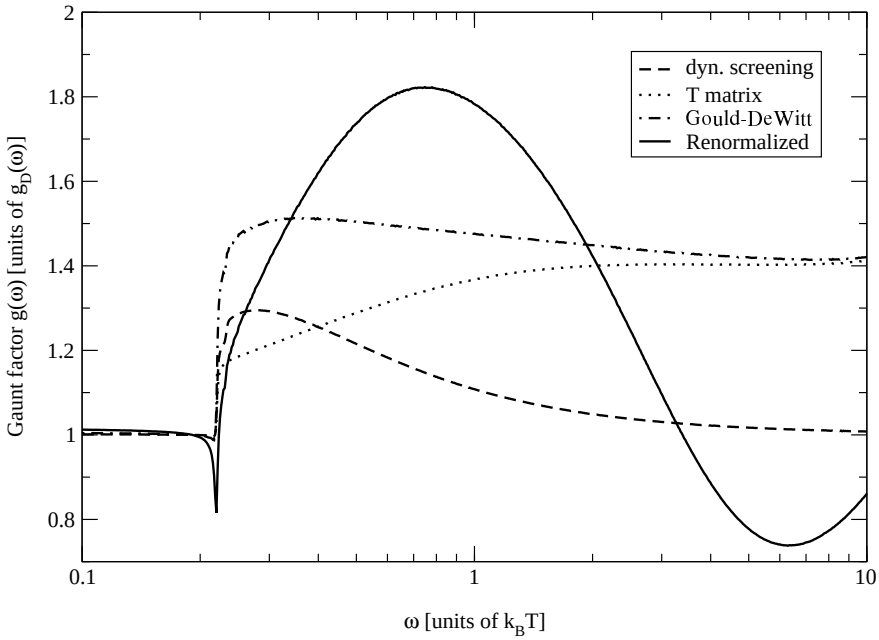

Figure 40: Frequency dependence of the Gaunt factor. The correction to the Gaunt factor in the statically screened approximation is shown. The solid curve is our final result and is compared with other approximations. Solar core conditions with $n = 6.0 \times 10^{25}$ cm^{-3}, $T = 1.3$ keV are considered.

of the real part of the collision frequency. A further increase is due to the renormalization factor. As was already noted by Iglesias and Rose, the account of dynamical screening is not important for the calculation of Rosseland mean opacities. The differences are small in the important region around $\hbar\omega/(k_B T) = 4$. However, including strong collisions and the renormalization due to higher moments lead to pronounced deviations. Since the maximum of the real part of the renormalization factor is located at $k_B T$, the Gaunt factor is affected even at large frequencies compared to the plasma frequency $\omega_{\rm pl}$. Thus, a recalculation of the Rosseland mean opacities [240] would be interesting. However, the effect has to be confirmed by augmenting the number of moments in Eq. (313).

6.3 Reflectivity

Recently, dense plasmas showing the transition from dielectric to metallic behavior were investigated extensively [241, 242, 243, 244, 245, 246, 247]. Highly compressed matter can be produced by shock waves from explosions or high intense laser pulses. Heavy ion beams or z-pinch discharges are also used to create dense plasmas. For the diagnostics of properties in such highly compressed plasmas, optical measurements are most favorable. E.g. the reflectivity is expected to give information on the free charge carrier density.

Reflectivity measurements under shock wave compression have been performed for dif-

ferent materials. For instance, Basko et al. [244, 245] discussed experiments in Al and Si. Whereas the electron density is estimated to change at the shock wave front within a small intervall of several nanometers, the change in temperature occurs within a layer of about 0.3 μm. Of high interest are recent experiments in liquid deuterium and water [246, 247] which show a saturation of the reflectivity at values above 50% indicating that a conducting state was attained. We will consider experiments on xenon plasmas.

To generate dense xenon plasma we used explosively driven shock waves which lead to compression and irreversible heating of the investigated gas. The detailed discussion of the reflectivity experiments can be found in [159]. Three series of experiments to measure the reflectivity have been performed. In the earlier one [241], a laser beam with wavelength $\lambda = 1.064$ μm was used. In recent experiments, laser beam wavelengths of $\lambda = 0.694$ μm [242, 159, 160] and $\lambda = 0.532$ μm [243, 248] were chosen. A strong increase of the reflectivity has been observed indicating metallization.

In papers by Kurilenkov *et al.* [100, 249], the first series of experiments by Mintsev *et al.* [241] was analyzed. The dielectric function was calculated via a dynamical collision frequency. The Born approximation was improved by including structure factor and local field corrections, but no consistent description of the measured reflectivities has been achieved. A different approach to the reflectivity was taken by Norman *et al.* [250, 251], who proposed that the assumption of non-equilibrium excitations of plasma waves might provide a reasonable agreement with the experimental results. However, the structure of possible excitations of plasma waves in the shock wave front is an open question.

The thermodynamic parameters of the plasma were determined from the measured shock wave velocity. The plasma composition was calculated within a chemical picture [13, 252]. Working with a grand canonical ensemble [253] virial corrections have been taken into account due to charge-charge interactions (Debye approximation). Short range repulsion of heavy particles was considered within the framework of a soft sphere model.

In the parameter range of the shock wave experiments, derivations of up to 20 % for the composition have been obtained depending on the approximations for the equation of state. This is within the accuracy of the experimental values of the reflectivity.

In accordance with these calculations, plasma densities of $\rho \approx$ 0.3-4 g cm^{-3}, pressures of $P \approx 1.6 - 20$ GPa and temperatures about $T \approx 3 \cdot 10^4$ K were realised during the experiments. Under these conditions the Coulomb interaction is characterised by the nonideality parameter $\Gamma = e^2(4\pi n_e/3)^{1/3}(4\pi\epsilon_0 k_B T)^{-1} = 1.1$ - 1.9. For the different wavelengths, results of the reflectivity measurements on dense xenon plasma and the respective thermodynamic parameters are presented in TABS. 6 to 8. The parameter $\Theta = 2m_e k_B T(3\pi^2\hbar^3 n_e)^{-2/3}$ with m_e the electron mass, is the ratio of temperature and Fermi energy. The relative importance of quantum effects increases with Θ^{-1}.

6.3.1 Reflectivity on step-like profile

Assuming a step-like profile of the shock wave front, the laser beam reflection is determined by the electronic properties of the plasma behind the shock wave front. The reflection

P/ GPa	R^{exp}	T/ K	ρ/ g cm^{-3}	n_e/ cm^{-3}	n_a/cm^{-3}	α_{ion}	Γ	Θ
1.6	0.096	30 050	0.51	1.8×10^{21}	6.1×10^{20}	0.75	1.1	4.8
3.1	0.12	29 570	0.97	3.2×10^{21}	1.4×10^{21}	0.70	1.3	3.2
5.1	0.18	30 260	1.46	4.5×10^{21}	2.2×10^{21}	0.67	1.5	2.6
7.3	0.26	29 810	1.98	5.7×10^{21}	3.5×10^{21}	0.62	1.6	2.2
10.5	0.36	29250	2.70	7.1×10^{21}	5.4×10^{21}	0.57	1.8	1.9
16.7	0.47	28810	3.84	9.1×10^{21}	8.6×10^{21}	0.51	1.9	1.6

Table 6: Experimental results [241] for the reflectivity R of xenon plasma at wavelength $\lambda = 1.06\ \mu$m and thermodynamic parameter values: pressure P, temperature T, mass density ρ, free electron number, density n_e, density of neutral atoms n_a, ionization degree $\alpha_{\text{ion}} = n_e/n_a$, non-ideality parameter Γ and degeneracy parameter Θ.

P/ GPa	R^{exp}	T/ K	ρ/ g cm^{-3}	n_e/ cm^{-3}	n_a/cm^{-3}	α_{ion}	Γ	Θ
0.93	0.02	32 070	0.27	1.1×10^{21}	2.1×10^{20}	0.78	0.87	7.1
1.9	0.05	32 900	0.53	2.1×10^{21}	4.8×10^{20}	0.72	1.0	4.8
4.1	0.11	33 100	1.1	4.0×10^{21}	1.3×10^{21}	0.69	1.3	3.2
6.1	0.14	33 120	1.6	5.2×10^{21}	2.1×10^{21}	0.64	1.4	2.6
9.1	0.18	32 090	2.2	6.6×10^{21}	3.6×10^{21}	0.60	1.6	2.1
12.0	0.26	32 020	2.8	7.8×10^{21}	5.0×10^{21}	0.56	1.7	1.9
16.0	0.40	31 040	3.4	8.8×10^{21}	7.3×10^{21}	0.54	1.8	1.7

Table 7: Experimental results [242] for the reflectivity R of xenon plasma at wavelength $\lambda = 0.694\,\mu$m. Same notation for thermodynamic parameters as in TAB. 6.

P/ GPa	R^{exp}	T/ K	ρ/ g cm^{-3}	n_e/ cm^{-3}	n_a/cm^{-3}	α_{ion}	Γ	Θ
4.1	0.02	33 100	1.1	4.0×10^{21}	1.3×10^{21}	0.69	1.3	3.2
6.1	0.05	33 120	1.6	5.2×10^{21}	2.1×10^{21}	0.64	1.4	2.6
9.1	0.11	32 090	2.2	6.6×10^{21}	3.6×10^{21}	0.60	1.6	2.1
12.0	0.16	32 020	2.8	7.8×10^{21}	5.0×10^{21}	0.56	1.7	1.9

Table 8: Experimental results [243] for the reflectivity R of xenon plasma at wavelength $\lambda = 0.532\,\mu$m. Same notation for thermodynamic parameters as in TAB. 6.

$\lambda/\ \mu$m	ω/fs^{-1}	$n_e^{\mathrm{cr}}/\mathrm{cm}^{-3}$
1.060	1.78	$1.02\ \times 10^{21}$
0.694	2.72	$2.35\ \times 10^{21}$
0.532	3.52	$4.04\ \times 10^{21}$

Table 9: Laser wavelength λ, frequency ω and critical density n_e^{cr} (for explanation see text).

coefficient is given by [254]

$$R(\omega) \;=\; \left|\frac{1-Z(\omega)}{1+Z(\omega)}\right|^2 \tag{408}$$

with the surface impedance

$$Z(\omega) \;=\; -\frac{i\omega}{\pi c}\int_{-\infty}^{\infty}\mathrm{d}k\,\frac{1}{k^2-\omega^2\epsilon_t(k,\omega)/c^2}\,, \tag{409}$$

where $\epsilon_t(k,\omega)$ is the transverse dielectric function depending on the wavenumber k and the frequency ω. The influence of the dependence on the wavenumber k has been investigated in [255] and found to be of insignificance at the parameter values of the considered experiments. As detailed below, only small values of k are relevant when performing the integration in the surface impedance. A comparison of the mean free path and the much larger skin depth also shows that nonlocal effects are not releveant here. Therefore, we take the long–wavelength limit of the dielectric function $\epsilon_t(0,\omega)=\epsilon(\omega)$ and find the Fresnel formula after performing the k integration,

$$R(\omega) = \left|\frac{\sqrt{\epsilon(\omega)}-1}{\sqrt{\epsilon(\omega)}+1}\right|^2 \;. \tag{410}$$

The frequency ω has to be taken at the laser frequency, see TAB. 9.

If the relationship between the dielectric function and the thermodynamic parameters were known the measurement of the reflectivity would provide information about, e.g., the particle density. Assuming the RPA approximation for the dielectric function in the long–wavelength limit $\epsilon(\omega) = 1-\omega_{\mathrm{pl}}^2/\omega^2$, with the plasma frequency $\omega_{\mathrm{pl}} = \sqrt{n_e e^2/(\epsilon_0 m_e)}$, a critical density n_e^{cr}, see TAB. 9, is obtained, at which the plasma frequency coincides with the frequency ω of the probing laser pulse. Total reflection occurs at densities higher than n_e^{cr} due to a negative dielectric function. However, investigating the experimental data in TABS. 6, 7 and 8, it is not possible to confirm such a direct relationship between the values of free electron density n_e and the reflectivity R. The observed reflection coefficient increases smoothly with the free electron density. It approaches only slowly values characteristic for metals, although the critical density for metallic behaviour is exceeded even at the lowest densities, see TAB. 9. Taking collisions into account a reflectivity smaller than 1 is expected even in a metallic system. Within the present section, we will discuss various improvements

in the approximations for the dielectric function beyond RPA, but preserving the assumption of a step-like shock wave front.

Firstly, we consider the contributions from the free charge carriers to the dielectric function in the form of the generalized Drude formula, see section 3.4, in particular Eqs. (202) and (203),

$$\epsilon(\omega) = 1 + \frac{i}{\epsilon_0 \omega}\sigma(\omega) = 1 - \frac{\omega_{\rm pl}^2}{\omega[\omega + i\nu(\omega)]}. \tag{411}$$

In order to investigate the influence of the frequency dependent collision frequency, we use the leading term which is covered by the first Born approximation for the statically screened potential with an effective Debye screening parameter, see Eq. (302). In the static limit, $\nu(0) = \epsilon_0 \omega_{\rm pl}^2/\sigma_{\rm dc}$ is related to the static (dc) conductivity $\sigma(0) = \sigma_{\rm dc}$ which is the phenomenological Drude formula. Evaluating the collision frequency in the static limit ($\omega = 0$), Eq. (274), the result is the Ziman formula [115]. Applied to a Debye potential in the case of non–degeneracy we obtain

$$\nu_{\rm dc}^{ei,{\rm Born}} = n_e \frac{e^4 \beta^{3/2}}{6\sqrt{2}\pi^{3/2}\epsilon_0^2 m_e^{1/2}} \int_0^\infty dy \frac{y^3}{(\bar{n} + y^2)^2} e^{-y^2} \quad . \tag{412}$$

The resulting values for the reflectivity calculated from the Drude formula (411) with the static collision frequency (412) are shown in TABS. 10 and 11, together with the reflectivities resulting from the dynamical collision frequency in Born approximation (235) taken at the laser frequencies ω. Compared with the observed reflectivities, the results obtained from the static collision frequency in Born approximation do not show the strong increase in the reflectivity as a function of the electron density. The use of the dynamical conductivity in comparison to the static collision frequency increases the reflectivity by about 15 %, but it also fails to produce the steep dependence of the reflectivity on the electron density as observed in the experiment, see TABS. 6 to 8. Similar results were obtained in [100] where a dynamical collision frequency in Born approximation was calculated using a pseudopotential for the electron-ion interaction and taking into account structure factor and local field corrections. However, these improvements do not lead to a qualitatively different behaviour of the reflectivity.

The generalization of the dielectric function (411) to the nonlocal k dependent case is possible and has been considered in [87, 144, 160], using a Mermin ansatz. A comparison of results for the reflectivity (408), (409) using a k dependent Born approximation for the collision frequency $\nu(k, \omega)$ in $\epsilon(k, \omega)$ and the Fresnel formula with the frequency dependent collision frequency in Born approximation (235) has shown deviations less than 5 %. However, in general, the Born approximation is not appropriate in the region of plasma parameters under consideration, as pointed out e.g. in [87, 100]. Further improvements will be discussed in the following.

The Born approximation (Faber-Ziman result) underestimates the value of the dc conductivity. The correct low-density limit of $\sigma_{\rm dc}$ is given by the Spitzer formula and can be obtained considering strong collisions and using a renormalization factor as discussed in sections 4.3. A constant correction factor following from the static limit was used in the case

P/GPa	$R^{\rm exp}$	$R(\nu_{\rm dc}^{ei,{\rm Born}})$	$R(\nu^{ei,{\rm Born}}(\omega))$	$R_{\rm dc}^{\rm ERR}$	$R_{\rm dc}^{{\rm ERR},ea}$	$R^{\rm MD}$
1.6	0.096	0.272	0.304	0.502	0.452	0.27
3.1	0.12	0.342	0.351	0.588	0.531	0.50
5.1	0.18	0.381	0.380	0.630	0.572	0.59
7.3	0.26	0.404	0.399	0.661	0.593	0.60
10.5	0.36	0.429	0.419	0.692	0.616	0.67
16.7	0.47	0.457	0.447	0.729	0.646	0.68

Table 10: Reflectivities from step-like density profiles, calculated at the experimental parameter values for $\lambda = 1.06$ μm. $R(\nu_{\rm dc}^{ei,{\rm Born}})$ – Drude formula (411) with static collision frequency (412), $R(\nu^{ei,{\rm Born}}(\omega))$ – dynamical collision frequency in Born approximation, $R_{\rm dc}^{\rm ERR}$ – Drude formula (411) with static collision frequency (299), $R_{\rm dc}^{{\rm ERR},ea}$ – Drude formula (411) with static collision frequency (299) and contribution of bound states to dielectric function, $R^{\rm MD}$ - dielectric function from Monte Carlo calculations, see section 5.6.

of small frequencies in [100]. On the other hand, screening of the interaction potential plays a role on a dynamical level which leads to the Lennard–Balescu scattering term. Taking these various limiting cases into account, an interpolation formula for the dc conductivity of a fully ionized Coulomb plasma was derived in [114].

Using the Drude formula (411) with the collision frequency $\nu(0)$ from the interpolation formula (299) for the conductivities $\sigma_{\rm dc}^{\rm ERR}$, see section 4.3 and Ref. [114]), we obtain the reflectivities $R_{\rm dc}^{\rm ERR}$. They are shown as $R_{\rm dc}^{\rm ERR}$ and $R_{\rm ERR}$,static in TABS. 10, 11 and FIGS. 41, 42, respectively. $R_{\rm ERR}$,dynamic in the FIGS. denotes a dynamic approximation obtained from scaling the static result according to the Born case. The results for the reflectivities are up to 60 % higher than the Born approximation indicating that in contrast to the use of a dynamical collision frequency, which will change the reflectivity by about 10–15 %, the account of strong collision in the collision frequency is more essential. Compared with the experimental results, the calculated reflectivities are too high, and the strong increase of the measured values with density can not be explained.

The fraction of neutral particles in the plasma gives a contribution to the dielectric function which is not negligible. For high densities, this fraction increases to about 50%, see TABS. 6 and 7. Contributions due to additional scattering mechanisms of the free electrons

P/GPa	$R^{\rm exp}$	$R(\nu_{\rm dc}^{ei,{\rm Born}})$	$R(\nu^{ei,{\rm Born}}(\omega))$	$R_{\rm dc}^{\rm ERR}$	$R_{\rm dc}^{{\rm ERR},ea}$	$R^{\rm MD}$
4.1	0.11	0.264	0.309	0.510	0.439	0.18
9.1	0.18	0.357	0.375	0.635	0.546	0.47
16.0	0.40	0.396	0.405	0.698	0.540	0.52

Table 11: Reflectivities from step-like density profiles, calculated at the experimental parameter values for $\lambda = 0.694$ μm. Same notation as in TAB. 10.

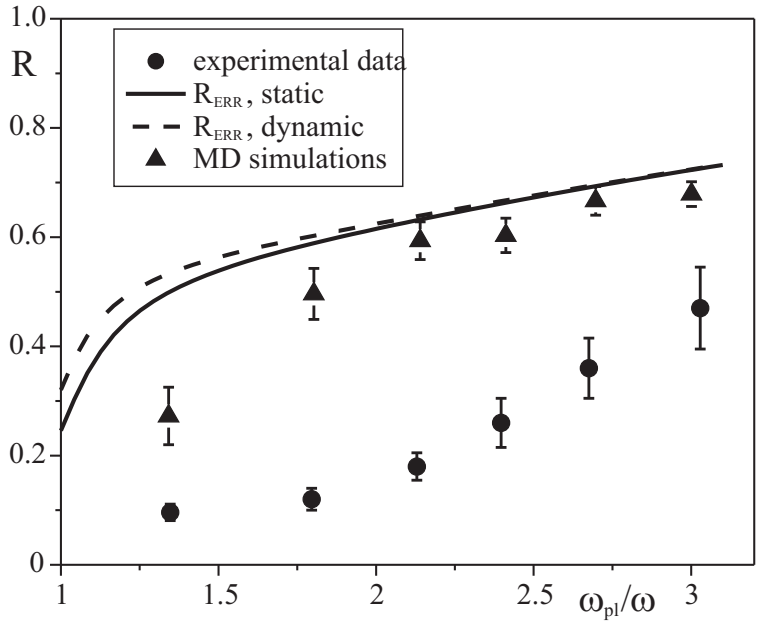

Figure 41: Comparison of expermient and different theoretical approximations for reflectivity coefficient with probe laser of $\lambda_1 = 1.06\,\mu$m, assuming a step–like shock wave front.

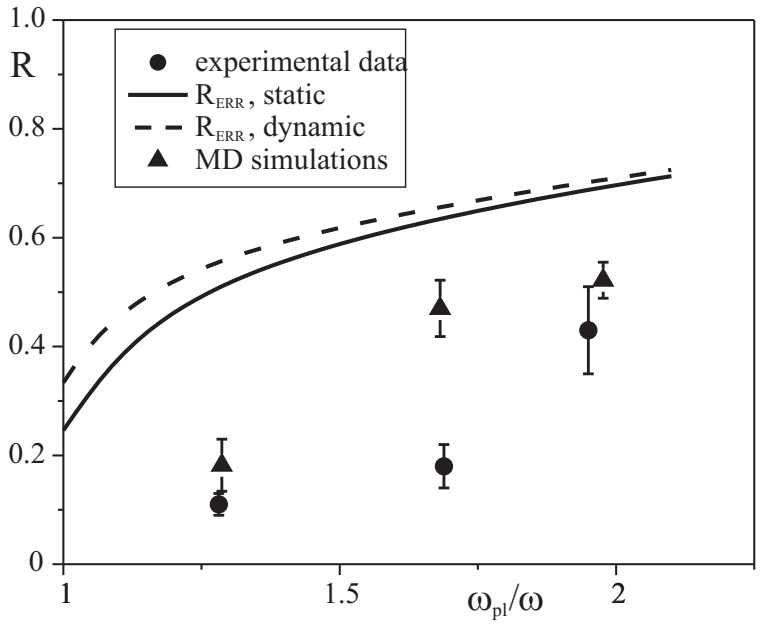

Figure 42: Comparison of expermient and different theoretical approximations for reflectivity coefficient with probe laser of $\lambda_2 = 0.694\,\mu$m, assuming a step–like shock wave front.

with atoms as well as a direct contribution of the neutral component to the dielectric function should be taken into account in such a partially ionized system and will affect the reflectivity.

The scattering of free electrons on the atoms can be described by a screened polarization potential [14]

$$V_{\rm p}(r) \;=\; \frac{e^2}{4\pi\epsilon_0}\,\frac{\alpha_{\rm p}}{2\left(r^2+r_0^2\right)^2}{\rm e}^{-2\kappa r}(1+\kappa r)^2 \tag{413}$$

with the polarizability $\alpha_{\rm p} = 27.3\,a_{\rm B}^3$ [256] for xenon and the screening parameter $\kappa^2 = 2n_e\beta e^2/\epsilon_0$. The cut–off parameter r_0 ensures the finite size of the polarization potential at small distances $r \to 0$ from the atom. It is caused by the finite extension of the atomic charge distribution so that the simple $1/r^4$ dependence is modified at short distances. According to the discussion in [160], the cut–off parameter was chosen to be the atomic radius r_0= 0.1 nm =1.89 $\rm a_B$ [256].

The electron-atom interaction leads to an additional contribution to the collision frequency in the following manner, $\nu = \nu^{ei} + \nu^{ea}$. In static Born approximation, the respective collision frequency is

$$\nu_{\rm dc}^{ea} \;=\; n_a\frac{e^4\beta^{3/2}}{6\sqrt{2}\pi^{3/2}\epsilon_0^2 m_e^{1/2}}\left(\frac{m_e\pi\alpha_{\rm p}}{\beta\hbar^2 r_0}\right)^2\frac{1}{2}\int_0^\infty dy\frac{y^5}{(y+\kappa^2 l^2)^4}{\rm e}^{-y-2r_0\sqrt{y}/l} \tag{414}$$

where $l^2 = \beta\hbar^2/(8m_e)$. The strength of the electron–atom scattering is about one third of that of the electron–ion scattering. Improving the Born approximation, the electron-atom collision frequency should be obtained from a T–matrix calculation as has been done for the transport cross sections for xenon [257]. The inert gases show a typical Ramsauer minimum. However, at energies typical for the temperatures considered here, exploratory T–matrix calculations give larger collision frequencies compared to the Born approximation which will be reduced if screening effects are taken into account.

The neutral component of the partially ionized plasma also gives an additional direct contribution to the dielectric function. According to a cluster expansion of the polarization function [11], several terms can be discussed. The main contribution comes from transitions bound-continuum and can be approximated by

$$\epsilon^{ea}(\omega) = 4\pi\alpha_{\rm p}\,n_a\frac{1}{1-(\hbar\omega/E_0)^2}\;. \tag{415}$$

Both contributions to the dielectric function, (414) in the collision frequency as well as (415) have been taken into account in the calculation of the reflectivity, see row $R_{\rm dc}^{\rm ERR,ea}$ in TABS. 10 and 11. It leads to a reduction of the reflectivity by about 10 % and increases with decreasing ionization degree.

Excited states may also contribute to the dielectric function. The lowest excited state occurs at about 8.3 eV above the ground state of $E_0 = -12.13$ eV. Its population is low at the considered temperatures of about 2.6 eV. Furthermore, considering the high densities which are near to condensed matter densities, the shift of the continuum of scattering states becomes quite large. Neglecting dynamical effects, an estimation is given by the Debye shift

$-\kappa e^2/(4\pi\epsilon_0) = 36.2$ eV$/(\sqrt{\Gamma}\Theta)$. It is reasonable to assume that the excited states have already merged into the continuum and should be included in the continuum contribution (415).

6.3.2 Density profile of shock wave front

The spacial structure of the ionizing shock wave was discussed in [241]. In the region of the shock wave front a steep increase of the free electron density is expected. The width of the wave front is determined by relaxation processes in the plasma. In Ref. [241] it was estimated to be of the order $d \approx 0.1$ μm, which is about one order of magnitude less than the laser wavelength. Preliminary calculations in a recent paper [255], which were based on the assumption that the density profile is linear within the shock wave front, found values for the thickness of the shock wave front in the order of $0.1 - 1$ μm. This is in contrast to other systems like metals [244, 245] where free charge carriers are already present, and not produced by ionization processes. Subsequently, the width of the wave front density profile is small.

If a density profile of the shock wave front is considered where the free electron density smoothly increases from zero to its maximum value, the reflection of electromagnetic radiation occurs already in the outer region where the density is low. To perform an exploratory calculation, different density profiles were assumed where the electron density $n_e(z)$ increases with distance z from zero up to the saturation value n_e. The temperature is taken as a constant throughout the shock wave front. However, in a more refined approach, also a temperature profile $T(z)$ could be considered. It is also expected that the fraction of the neutral component would change within the shock wave front leading to a profile $n_a(z)$ which has been neglected so far.

A rigorous treatment of the propagation of laser radiation through a shock wave front should take into account the dependence of the collision frequency on the local electron density and temperature. A precise result for the reflectivity from an arbitrary plasma front can be obtained from the direct solution of the equation for the electromagnetic field. Let us consider a planar wave propagating along z-axis. Neglecting nonlocal effects for the conductivity we write the following Helmholtz equation for the complex amplitude of the electric field with frequency ω:

$$\frac{d^2E(z)}{dz^2} + 4\pi^2\epsilon(\omega, z)E(z) = 0, \tag{416}$$

where z is the distance in units of the wavelength. The function $\epsilon(\omega, z)$ has to be calculated for given density and temperature profiles $n_e(z)$, $T(z)$. In the local approximation, the dielectric function $\epsilon(\omega, n_e(z))$ is considerd to be dependent only on the local density. This approximation is justified here since the characteristic length of variation of $n_e(z)$ which is of the order of 1 μm is large compared with the microscopic correlation length which is in the order of the Debye radius of about 1 nm .

The appropriate solution of (416) is selected by taking the boundary condition

$$E(z_0) = E_0 \exp\left\{-2\pi i z_0 \sqrt{\epsilon(\omega, z_0)}\right\}, \quad E'(z_0) = -2\pi i \sqrt{\epsilon_0(\omega, z_0)}\, E(z_0).$$

Then the equation (416) is solved numerically starting from the initial point z_0. The reflectivity is given by [258],

$$R = \frac{|E_r(z_1)|^2}{|E_i(z_1)|^2}, \tag{417}$$

where

$$E_i(z) = \frac{1}{2}\left(E(z) - \frac{E'(z)}{2\pi i}\right) \quad \text{and} \quad E_r(z) = \frac{1}{2}\left(E(z) + \frac{E'(z)}{2\pi i}\right) \tag{418}$$

describe incident and reflected waves correspondingly and z_1 is taken at the free space region ($\epsilon(\omega, z_1) = 1$).

We now consider a density profile as a given quantity [248]. The temperature is assumed to be uniform at the plasma temperature throughout the shock wave front. Smooth empirical density profiles for a shock wave front such as a linear decrease or a spatial variation according to a Fermi function have been considered in various combinations [159, 160, 255, 259]. As already mentioned in Ref. [241], the density profile across the shock front is expected to increase at first slowly and to become steeper towards the plasma region. Such a behaviour was already reproduced using a bi-linear profile [160], see Fig. 43. The disadvantage of a previously assumed continuous profile consisting of two Fermi functions [160] was its symmetry with respect to the gradual changes at the boundary of the profile. Therefore, we now propose an asymmetric Fermi profile:

$$\begin{aligned} n_{\mathrm{aF}}(n_{\mathrm{e}}, z) &= \frac{n_{\mathrm{e}}}{e^{Y(z)} + 1}, \\ Y(z) &= -\frac{z}{A} - e^{z/B} + C. \end{aligned} \tag{419}$$

This is shown in comparison to the bi-linear profile for one parameter set. As shown in Fig. 44, the expected general behaviour of the density pofile is reproduced. For the suitably chosen parameters A, B, C see the following section.

In particular, the parameter A affects the width of the ordinary Fermi profile in the low density region for negative z. The second parameter B influences the order of asymmetric compression in the high density region for positive z. With the last parameter C one is able to choose the point, were the ordinary Fermi function starts to be compressed. The details of the density profile can be controled by measuring the reflectivity at different laser frequencies ω_{L}. As will be shown in the next section, we are able to justify the ansatz (419) in an empirical way. In detail, we use two different laser frequencies ω_{L} to dermine the parameters of the density profile (419) and show that the experimental values of the reflectivity R for a third laser frequency are also well reproduced.

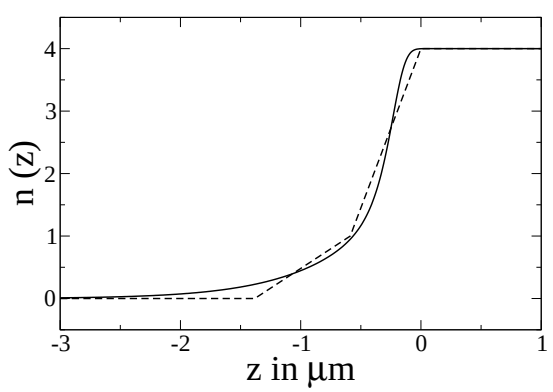

Figure 43: Comparison between the bi-linear profile (dashed line) [160] and asymmetric Fermi profile (419) (solid line) fitted to the reflectivity R at $n_\mathrm{e} = 4 \cdot 10^{21}\mathrm{cm}^{-3}$.

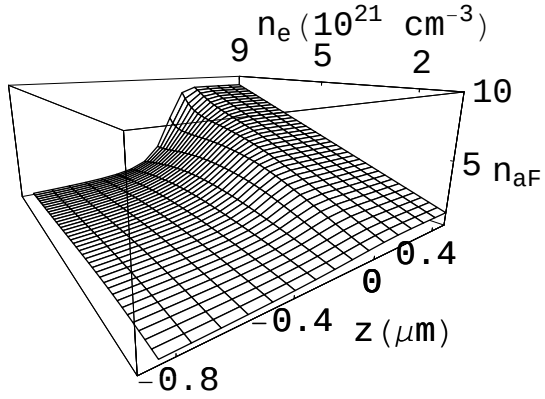

Figure 44: Profile of the shock front density $n_\mathrm{aF}(n_\mathrm{e}, z)$, Eq. (419) for different maximum densities n_e.

6.3.3 Parametrization of the density profile

Using measurements of the reflectivity at different wavelengths, it is possible to determine the details of the density profile. We use the ansatz (419) with open parameters A, B, C. The parameters were fitted to reproduce the experimental values for the wavelengths 1.06 μm and 0.694 μm. Interpolating for the reflectivity between different density values n_e in the plasma according to the experiments [241, 242, 243], we found the following parametrization for the profile,

$$\begin{aligned} A(n_\mathrm{e}) &= a_1 + a_2 \cdot e^{a_3 \cdot n_\mathrm{e}}, \\ B(n_\mathrm{e}) &= b_1 \cdot n_\mathrm{e}^3 + b_2 \cdot n_\mathrm{e}^2 + b_3 \cdot n_\mathrm{e} + b_4, \\ C(n_\mathrm{e}) &= c_1 \cdot n_\mathrm{e}^2 + c_2 \cdot n_\mathrm{e} + c_3 \end{aligned} \tag{420}$$

and $a_1 = 0.03254$ $a_2 = 1.437$, $a_3 = -0.4909$, $b_1 = -0.003687$, $b_2 = 0.05775$, $b_3 = -0.2560$, $b_4 = 0.47905$, $c_1 = 0.03155$, $c_2 = -0.05537, c_3 = 0.4720$. The densities have to be taken in units of 10^{21} cm^{-3} and the position z in μm. A landscape of the density profiles for different values of n_e is shown in Fig. 44. The results for the reflectivity R, calculated for the asymmetric Fermi profile $n_\mathrm{aF}(n_\mathrm{e}, z)$, Eq. (419), and fixed temperature $T = 33000$ K are shown in Fig. 45 for three different laser frequencies ω_L. The critical densities are indicated. Above those, the reflectivity R starts to increase. Also experimental values are shown. As in former works [160, 159, 255, 259], the experimental values at laser wavelengths 1.06 μm and 0.694 μm are well reproduced. Data at the third wavelength of 0.532 μm have then been calculated from the derived shock wave profiles. The experimental data are reproduced within the error bars except in the region of very low densities. The good qualitative agreement shows, that the adjustment of the parameters using two wavelengths is sufficient to describe the behaviour of the reflectivity for the third wavelength and probably other wavelengths as well.

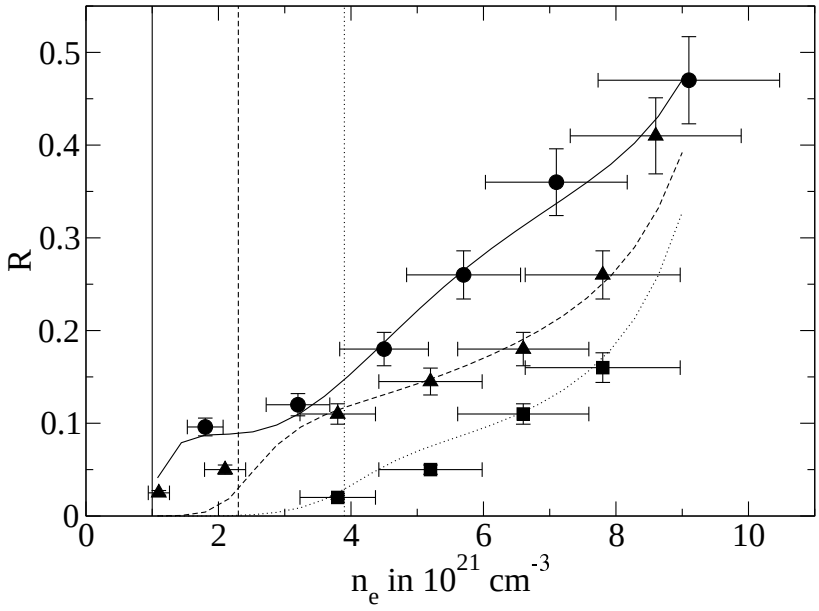

Figure 45: Reflectivity coefficient R for Xenon calculated with asymmetric Fermi profile $n_{\rm aF}$ (lines) in comparison with measurements (symbols with error bars) [241, 242, 243] for laser wavelengths 1.06 μm (solid line, ●), 0.694 μm (dashed line, ▲), and 0.532 μm (dotted line, ■), the corresponding critical densities $n_{\rm e}^{\rm cr}$ are indicted with vertical lines.

We conclude that by choosing appropriate values for the fit parameters the measured reflectivities can be reproduced within the error bars. The aim was to demonstrate that experimental reflectivities at different frequencies can be interpreted assuming a corresponding profile. In particular, we find that the density gradient is higher at higher densities.

It is of interest to show the consequences of the determination of the density profiles $n_{\rm aF}(n_{\rm e}, z)$ which vary with the maximum pressure or maximum density n_e obtained behind the shock wave front, see FIG. 44. The corresponding curves for the reflectivity show a steep increase when $n_{\rm aF}$ approaches the critical density $n_{\rm cr}$ for the respective laser frequencies. Then the reflectivity as function of n_e remains nearly constant, but rises once more at higher values of $n_{\rm e}$. Here, the width of the shock front d_λ as function of $n_{\rm e}$ is decreasing. Possibly, the formation of the precursor ionization sheet is reduced if the velocity of the shock front is high. This should be discussed on the basis of a hydrodynamical code including ionization processes. Nonequilibrium processes may be of importance in order to describe the formation of free carriers.

Measurements at different frequencies show a bending of the density profile, from a sharp decrease near the shock front to a moderate decay at larger distances. Such a structure was also assumed in Ref. [241]. The dependence of the density profile on the maximum pressure or maximum density n_e obtained behind the shock wave front is of interest for further investigations. Note also, that instead of the static conductivity we have to consider a dynamical one. However, as was shown for the step-like shock wave front, it is expected

that the dynamical collision frequency leads to only minor modifications.

Compared with the value given in Ref. [241], our estimation of the width of the shock wave front comes out to be larger. We also observe a structure of the density profile, see FIG. 44. In a more sophisticated description, the temperature variation has to be considerd as well as the variation of density of the neutral component. We can think about ionization processes due to heating in a precursor sheet in front of the shock wave and a steeper increase of the free electron density at the shock wave. We have to include nonequilibrium processes given by the velocity of the wave front. Experiments at different wavelengths of the laser beam are important to get more information about the density profile of the shock front.

6.4 Concluding Remarks

For the diagnostic of dense plasmas photons in the VUV or X-ray regime are required. First experiments have demonstrated the great capacity of X-ray Thomson scattering for the determination of respective plasma parameters such as density, temperature, and ionization state. For a proper interpretation of the experimental data, the interaction of energetic photons with strongly coupled plasmas has been considered beyond the usual random phase approximation (RPA). The cross section for Thomson scattering is related to the dynamical structure factor $S(k, \omega)$. We improved the RPA by including collisions. We studied the effect of dynamical screening and strong collisions. Results for typical plasma situations where collisions are of relevance and which are of experimental interest have been presented.

A systematic approach to inverse bremsstrahlung in hot, weakly coupled plasmas is given employing the relation between the absorption coefficient and the dielectric function. For the first time, dynamical screening and strong collisions were treated on the same footing in Ref. [87], leading to a consistent approximation of the absorption coefficient. Several known expressions for the absorption coefficient are re-derived in simplifying approximations. Compared with the well-known Sommerfeld result, which can be derived as a limiting case, strong collisions are treated by a numerical determination of the T–matrix. Compared with the Dawson-Oberman expression and its generalization, the introduction of the renormalization factor $r(\omega)$ leads to the correct Spitzer dc conductivity.

We carried out numerical calculations for two sets of parameters corresponding to moderate coupling. At high frequencies compared to the plasma frequency corrections due to strong collisions dominate while the account of dynamical screening is of less importance. Furthermore, the renormalization factor leads to an increase of the Gaunt factor at moderate frequencies and a decrease at higher frequencies. These kind of corrections have not be considered so far in the calculation of Rosseland mean opacities for solar core conditions, see Ref. [239].

We confirm the high-frequency behavior of the simulation results by Pfalzner and Gibbon. However, for frequencies around the plasma frequency a careful analysis of the observables to be compared has to be carried out. Furthermore, additional data points from the simulation would be helpful to confirm the trend at high frequencies.

In order to infer plasma parameters from optical reflection coefficient measurements of

dense xenon plasma produced in shock experiments, we have to take into account a finite width of the shock wave front of the order of $1\,\mu$m. Different forms of profiles $n_e(z)$ have been considered, and the reflectivity can be obtained by solving the Helmholtz equation.

Our calculations are based on an interpolation formula for the dc conductivity, obtained from a systematic quantum statistical treatment of different limiting cases. In particular, the account of the renormalization factor and of strong collisions is essential to obtain the correct low-density limit for the dc–conductivity. The uncertainty in using the interpolation formula increases for $\Gamma \geq 1$. The values of the plasma parameter Γ for dense xenon plasmas considered here are in the region $1 < \Gamma < 2$, and $5 > \Theta > 1.5$ for the degeneracy. Improving this approach by taking a dynamical collision frequency or even a non-local instead of the static one, only marginal modifications of the reflectivity are expected. An alternative approach is given by MD simulations, which have been performed for classical model plasmas where the Coulomb interaction is replaced by a pseudopotential.

Xenon under the conditions considered is a partially ionized plasma. The composition is shown in TABS. 6-8. The conductivity as well as the related quantities are influenced by the neutral component, which lead to a modification of the reflection coefficient. However, we find that neither analytical expressions for the collision frequency (static or dynamic, local or nonlocal) nor MD simulations as well as the account of neutral components can explain satisfactorily the behavior of the measured reflectivity as long as a step-like front profile is assumed.

Instead of step-like density profiles which are not able to explain the measured reflectivities, smooth density profiles were considered. We have shown that the experimental values of the reflectivity at different frequencies allow to determine the density profile. For this, the density profile was parameterized by an ansatz using an asymmetric Fermi profile dependence on the position. The parameters were given as smooth functions of the electron density in the shock wave fitting the measured reflectivities in the considered region. It has been found that the gradient of the density profile is higher for higher densities, i.e. closer to the step–like shock wave front. In order to explain the smooth density profiles, the propagation of a shock wave should be considered within a non–equilibrium approach containing ionization and compression processes. The treatment of ionization kinetics and the inclusion of possible further non–equilibrium processes is the subject of future work.

As discussed above, improvements of our exploratory calculations on the finite shock wave front are possible replacing the static collision frequency by a dynamical one and considering non–local effects, which are expected to give only marginal effects. The density profile of the free electrons can be further modified, and we can include different profiles for temperature and the neutral component. Further items which should be addressed are the accuracy in determining the composition, in particular the free electron density, and the relevance of the assumption of local equilibrium.

7 Outlook

We presented a quantum statistical approach to the dielectric function and related quantities, describing the response of a charged particle system to an external perturbation. Analytical expressions were obtained within perturbative expansions after partial summations. The comparison with (classical) MD simulations have been done with a special emphasis on the explanation of experiments. We focussed on weak external fields where linear response is applicable. Furthermore, our evaluations are confined to non-relativistic homogeneous systems.

Within the following sections, we will discuss a few aspects which lead to a generalization and a broader field of possible applications. As one of the main issues, we address the formation of bound states within the treatment of many-particle systems. They cannot be obtained within a classical approach and have to be considered as an intrinsic quantum phenomenon. Starting from the low-density limit, bound states can be treated on the same level as elementary particles (chemical picture). The advantage of the Green's function approach used here is that this concept can be realized in a consistent way, and density corrections can be given systematically. The simplest concept is the model of a partially ionized plasma (PIP) where free and bound states are considered within a chemical picture, and medium modifications are incorporated as shift of the energies of the corresponding quasiparticles. We will present some issues which go beyond the chemical pictures and in particular the connection with condensed matter theories.

7.1 Bound state formation and Mott effect

Assuming non-interacting charged particles, an ideal quantum system is obtained, for which all properties can be evaluated in closed form. However, due to the Coulomb interaction, it is possible that bound states (clusters) of 2,3,4, ... particles can be formed. Their discrete energy levels $E_{\mathrm{n}P} < 0$ follow from the solution of the respective few-body Schrödinger equations. In the case of two particles, in momentum representation, we have

$$[E(1) + E(2)]\psi_{\mathrm{n}P}(12) + \sum_{1'2'} V(1,2;1',2')\psi_{\mathrm{n}P}(1'2') = E_{\mathrm{n}P}\psi_{\mathrm{n}P}(12) \tag{421}$$

with $E(1) = p_1^2/2m_1$ and the total momentum $\vec{P} = \vec{p}_1 + \vec{p}_2$ and internal quantum number n. For the Coulomb interaction between an electron and a proton, $V(12,1'2') = -e^2/(\epsilon_0\Omega|\vec{p}_1 - \vec{p}_1'|^2)$, the well-known solutions for the hydrogen atom wave functions $\psi_{\mathrm{n}P}(12)$ and energy levels $E_{\mathrm{n}P}$ follow. In general, more complex bound states can build up in Coulomb systems. The formation of molecules and higher clusters, neutral as well as ionized, has to be taken into account.

The properties of a charged particle system are modified in an essential way if bound states are formed. E.g., a plasma consisting of free charge carriers will absorb electromagnetic radiation at arbitrary frequencies, whereas a gas of neutral atoms is transparent for different regions in the electromagnetic spectrum. Therefore it is an important question, to which

many-particle system	*elementary particles*	*bound states*	high *density limit*
ionic plasma	electrons, ions	atoms, molecules	liquid metal
semiconductor plasma	electrons, holes	excitons	electron-hole liquid
many-nucleon system	protons, neutrons	nuclei	nuclear matter
many-quark system	quarks	hadron	quark-gluon plasma

Table 12: Bound states and condensed matter phase in QED and QCD systems, taken from [261].

extent free charged particles are present in the plasma, which can be given via e.g. the ionization degree of the plasma. In a simple approximation, the electrical current can be considered to be determined by the free charge carriers only. However, in a more detailed description, the inclusion of additional microscopic processes is necessary. E.g., the collision frequency in a partly ionized plasma can be decomposed into collisions with free carriers and bound states.

A more delicate question is the modification of bound states themselves in a dense medium. Due to the influence of surrounding particles, the binding energies and wave function of the bound states as well as the scattering states are modified. Note, that bound states (correlations) disappear at high densities due to screening of the interaction (Mott effect) and phase space occupation (Pauli blocking), see Kremp *et al.* [11] as well as Schmidt *et al.* [260]. At high densities, the fermion system can be understood as a condensed state in which the bound states are dissolved and the single-particle excitations are described by itinerant quasiparticles. This process can be found in various many-particle systems. Some examples [261] are given in TAB. 12, the first two are based on QED, the latter two on quantum chromodynamics (QCD).

A particularly interesting phenomenon in quantum systems is the formation of quantum condensates, which can be interpreted as the Bose condensation of bound states, e.g., consisting of two fermions. This effect in interacting fermion systems is related to the phase coherence of the wave function and needs more subtle considerations. At low temperatures, quantum condensates may appear. A crossover from Bose-Einstein condensation of bound states to Cooper pairing at increasing densities may occur, in correspondence with the dissolution of bound states, see Schmidt *et al.* [260], and Noziere and Schmitt-Rink [262]. This phenomenon was observed for Coulomb systems in ultracold atomic gases in traps and expected for low dimensional excitonic systems in excited semiconductors at low temperatures. Although it is closely related to the Mott effect in charged particle systems, we will not go into further details here.

A consistent description of medium effects on two-particle states, including bound and scattering states, and larger clusters can be given within a systematic quantum statistical approach such as perturbation expansions, simulation techniques or path integral approaches. Interestingly, the very different physical systems given in TAB. 12 can be described by applying similar mathematical methods. Equilibrium as well as nonequilibrium properties can be obtained. In spite of the fact that there are generally no exact solutions known

for non-ideal quantum systems, many-particle methods have been elaborated to treat such systems. In the following, we will discuss the perturbation expansion in more detail.

The density of states as well as the equation of state $n(\beta, \mu)$ can be deduced from the single particle spectral functions $A(p, \omega)$. On the other hand, $A(p, \omega)$ is determined by the self-energy $\Sigma(p, \omega)$ which has to be evaluated in an appropriate approximation. Within a simple perturbative expansion of the self-energy, no bound states are obtained in any finite order. To take bound states into account we have to perform infinite summations of ladder diagrams. Two-particle bound states are obtained from the two-particle propagator $G_2(12, 1'2', i\omega_\lambda)$ in ladder approximation, which leads to the Bethe-Salpeter equation, see Kremp *et al.* Ref. [11]. In the low-density limit, its solution is equivalent to the solution of the corresponding few-particle Schrödinger equation.

Within this chemical picture or partially ionized plasma model (PIP), bound states are treated in the same way as the elementary particles. They are considered as new species, and the many-particle system behaves like an ideal mixture of elementary particles and bound states. For $\Sigma(p, \omega)$, a cluster decomposition can be given, see Kremp *et al.* [11], and Röpke *et al.* [261, 263]. The expansion of the spectral function with respect to the imaginary part of $\Sigma(p, \omega)$ leads to the Beth-Uhlenbeck formula, which explicitly contains the different contributions of free, bound and scattering states to the density of states. The components are considered to be in chemical equilibrium which leads to a mass action law, see Ebeling *et al.* [10], and Redmer [14] and references therein.

For higher densities, the properties of the elementary particles as well as of the bound states are modified by the dense medium. The generalized Beth-Uhlenbeck formula contains the quasiparticle shifts as well as the medium modification of the two-particle system, see Zimmermann *et al.* [264, 265], Schmidt *et al.* [260] as well as Nozieres and Schmitt-Rink [262]. They are obtained in first Born approximation, from the single-particle self-energy as well as from the Bethe-Salpeter equation for the two-particle propagator. An important issue is that the inclusion of medium effects in the self-energy and in the effective interaction of the Bethe-Salpeter equation has to be performed in a consistent manner. Ward identities relate both quantities and guarantee the validity of sum rules and conservation laws. In this way, also consistent approximations with respect to higher orders of density or interaction are constructed.

For short-range interactions, the lowest order correction for the single-particle state is given by the Hartree-Fock shift, which has to be complemented in a consistent approximation by the Pauli-blocking of the interaction in the two-particle wave equation. For Coulomb systems, the use of a screened interaction in the self-energy (Montroll-Ward approximation, GW approximation) as well as in the two-particle wave equation as a consistent approximation has been investigated by, e.g., Kremp, Zimmermann *et al.* [11, 264, 266, 267]. In particular, the energy shifts of free particles and bound states due to screening effects will lead to the Mott effect where the bound states merge with the continuum of scattering states. As a consequence, the metal-insulator transition (MIT) from a dielectric to a metal-like behavior happens when the lowest bound state disappears. Zimmermann [264] pointed out that one has to take care of compensation effects between weakly bound states and scattering states

so that no artificial discontinuities arise.

However, these mean-field approximations treat the particles as uncorrelated since the screening is described by the dielectric function for a collisionless plasma in RPA. Going beyond but still keeping within the chemical picture, we extend the approximation by taking along additional contributions which can be found when replacing the free particle propagators by the two-particle propagators ect. At the same time, the vertex e which couples the single particles to the interaction is extended by vertex contributions describing the coupling of a few-particle system to the interaction, see Röpke, Der *et al.* [11, 75]. Based on these considerations, a systematic improvement of the Hartree-Fock approximation is given by the cluster-mean field approximation, see Zimmermann, Röpke *et al.* [264, 268, 269, 270]. Clusters are now considered in the mean field of a correlated medium. The influence of the surrounding clusters is included in effective interactions which have to be solved self-consistently within a system of generalized mass action laws. An important issue is the correct antisymmetrization of the wave function of the cluster considered and the surrounding clusters. Thus the mean-field concept becomes invariant with respect to the definition of "elementary" particles.

In next order, the second Born approximation, collisions within the medium are taken into account. Contributions from the interaction of the considered single particle or cluster, respectively, with the elementary particles in the medium as well as bound states and higher clusters are considered. Within Coulomb systems, these are the leading terms contributing to the polarization potential and the van der Waals interaction if free charged particles and neutral atoms, respectively, are considered to interact with bound states, see Refs. [11, 14, 266, 267]. Alternatively, such systematic approximations can also be derived treating the screening of the interaction via the dielectric function considering the first order of the polarization function with respect to interactions. Within the chemical picture, the polarization bubbles of free elementary particles in RPA are extended by bubble diagrams formed by cluster propagators, see Röpke and Der [75]. Shifts of the energies of single particles and bound states are found which are of the order of the density of free or bound states, respectively.

Applying perturbation expansions, we should be able to derive systematic expansions with respect to the interaction or with respect to the density. However, within the considerations so far, important aspects like the broadening of the bound state energy levels cannot be described adequately. Other diagrammatic contributions have to be considered. In particular singular terms may arise, which demand a special treatment to get convergent results. It was shown by Röpke and Reinholz [261] that such contributions to the self-energy do arise. Considering the self-energy, a T–matrix contribution occurs describing an atomic bound state which is interrupted by a T–matrix insertion with another ion, forming also a bound state. It can be interpreted as an electron in a bound state which brakes up to form a bound state with a different ion, the electron is effectively hopping from one ion to another. Such divergent terms can be treated by solving the three-particle problem, see Röpke *et al.* [263, 271, 272]. By including hopping processes in this way, the splitting of bound state energies and the formation of a band structure is obtained.

Whereas splitting of energy levels due to hopping processes is not described within the PIP model, it is a phenomenon familiar to condensed matter physics. In the case of ions forming a periodic lattice the solution of the single-particle mean-field approximation is well known. The energy levels are broadened into bands, and the band width is related to the overlap integral. Since the dependence of this overlap integral on the ion-ion distance (lattice parameter $\propto n^{-1/3}$) is exponential, it is not expected that a simple perturbation expansion can reproduce the broadening of the bound state energy levels.

Further alternative approaches to describe an electron-ion system have been developed starting from an adiabatic approximation, solving the single electron Schrödinger equation in an effective potential at a given ionic configuration. At high densities, models known from liquid metals or disordered solids have been used to describe the electron structure in dense plasmas. The average atom model [273, 274, 275] and the bounded atom model [276, 277] consider the formation of bands from atomic bound states, if the atoms approach each other, as an important feature. However, since each atom is treated in an effective environment as given by boundary conditions, the formation of charged clusters and molecules or Hubbard-like correlation effects are not well reproduced within such models. Aspects of a description of disordered systems are relevant since dense plasmas can be considerd as a system with a liquid like disorder. In particular, the density functional formalism can be used as an appropriate approach describing the electron subsystem at a given ionic configuration.

Another concept to describe bound states and hopping of electrons between them within a tight binding model is the Anderson model. It considers the modification of the band structure due to (diagonal, non-diagonal, or topological) disorder, in particular the filling of band gaps by localized states and the formation of mobility edges. Thus, the role of disorder and the transition from localized to delocalized states relevant for the MIT is elaborated in this model, but other processes such as electron correlations, screening, higher excitations and bands are not consistently covered.

In contrast to the optimal treatment of cluster quasiparticle states due to the disordered ionic potentials, the systematic inclusion of electron-electron correlations remains a problem which can be treated only in certain approximations. One well explored possibility is the Hubbard model which accounts for the on-site electron-electron interaction. It is leading to a correlation gap in the density of states. Winn and Logan [278] were able to show that the Hubbard transition is related to the correlation-gap closure in a half-filled band if the ratio of bandwidth and correlation energy exceeds a critical value. As a consequence, a transition from dielectric to metallic behavior (MIT) occurs. However, important aspects like screening by and of free electrons and the related shifts of the energies of bound and scattering states are not described adequately within this picture.

At high densities, a disordered Anderson-Hubbard model (DAH model) is of interest. The electronic properties are determined by the electrons moving in a potential formed by the disordered system of ions, similar to amorphous solids or liquids, which can be described by a dynamical structure factor, as well as the on-site electron-electron interaction.

Several questions arise when comparing the different approaches and concepts, such as:

i. Are the concepts of free-particle density, bound-state density, ionization degree etc.

well defined in dense plasmas?

ii. How can the formation of bands, of localized and itinerant states be described in a plasma model? What is the role of disorder?

iii. How are correlations to be included, e.g. within the density functional formalism or the Hubbard model? How are excited states and screening by free electrons to be treated?

iv. How is the transition from dielectric behavior to metallic behavior best described? What is the relationship between the Mott effect and the Hubbard transition?

With respect to the last item, different mechanisms have been suggested to explain this metal-insulator transition (MIT) in strongly coupled Coulomb systems at intermediate densities. Coming from low densities where the PIP model is valid, screening and Pauli blocking are considered as the relevant mechanisms for this transition. Starting from high densities, band splitting and cloasure of band gaps, such as described in the averaged atom model, or disorder and localization as described in the Anderson model are the relevant microscopic phenomena for the MIT. Alternatively, electron-electron correlations described, e.g., in the Hubbard model are discussed as the microscopic mechanism for the formation of a correlation gap in the density of states which is closed at the MIT. It is a challenge to future work to give a unified description of dense plasmas including the PIP model as well as the DAH model. In a unified approach which contains both aspects, the chemical picture in the partially ionized plasma model as well as the band-like properties, the spectral function should be the key quantity. A systematic approach to the self-energy should incorporate the mean-field energy shifts, the band formation and electron correlation, see Röpke, Reinholz *et al.* [263, 272].

7.2 Influence of bound states on plasma response properties

The consideration of bound states in the dielectric function within the Green's function approach was discussed by Röpke and Der [75], for further references and applications see Kremp *et al.* [11]. A cluster decomposition of the polarizability according to the chemical picture yields contributions of free carriers and bound states (atoms). This is the PIP model if considered in the limit of low densities. The cluster decomposition also leads to a further improvement of the RPA and the dynamical collision frequency as well as additional contributions to the dielectric function due to bound states. It is an appropriate starting point to describe optical properties in ionic as well as in semiconductor plasmas. We will not give here an exhaustive description of the influence of bound states on plasma response properties, but only briefly report some work relevant for the applications given in chapter 6, in particular absorption and emission spectra, the static transport coefficients and the dynamical structure factor.

Treating the dynamical collision frequency $\nu(\omega)$, we have shown how the Born approximation is improved considering dynamical screening, strong collisions and the renormalization

factor describing the deformation of the distribution function due to electron-electron collisions. E.g., the Kramers result for the bremsstrahlung can be improved considering strong collisions leading to the Sommerfeld formula, see section 6.2 and Wierling *et al.* [214]. However, bound states have not been considered in the T–matrix approach given in section 4.3. Whereas the radiative transitions between (free) scattering states contributes to the continuum in the optical emission or absorption spectra, the transition between bound states gives the line spectrum. Bound–free transitions also will contribute to the continuum of the optical spectrum.

The evaluation of spectral line shapes in dense Coulomb systems within a consistent Green's function approach has been developed by Röpke and Hitzschke [29]. Besides the modification of the bound state due to the medium also vertex corrections (interference terms) have been investigated by Günter *et al.* [279]. Optical line profiles are determined by the natural width, the Doppler broadening, and pressure broadening. The standard description of the electron contribution within the impact approximation was reproduced. It was found that a dynamical microfield for ions is a suitable approximation. Improving semiempirical approaches, see Griem [210], effects in dense plasmas such as dynamical screening and collective excitations (plasmons) have been incorporated in addition to the collisions with free or bound states by Günter *et al.* [280, 281, 282, 283, 284, 285]. Virtual transitions to neighbouring states do not contribute if the energy difference is comparable to the plasma frequency. In particular, the nonlinear behavior of shift and width of spectral lines in high-dense plasmas has been discussed. For hydrogen plasmas, theoretical results by Könies and Günter [281, 282] and experimental results by Böddeker *et al.* [286] are in reasonable agreement. Könies and Günter [287] also investigated further properties caused by the surrounding dense plasma, in particular the asymmetry of the line shape . Spectra of hydrogen-like carbon ions, see Sorge *et al.* [288], and neutral Helium atoms, see Omar *et al.* [289, 290] have also been calculated and are compared with MD simulations of the electrical field and experimental data.

In discussing the Thomson scattering, we again focussed on the contribution of free-free transitions. However, also the bound electrons will contribute to the measured spectrum. In Eq. (386), the different contributions are given including also the bound–bound and bound–free transitions. This relation is based on a simple chemical picture considering the different components of the plasma as well–defined entities. As pointed out before, in addition to the scattering states, also bound states will contribute to the T–matrix. In accordance to the cluster decomposition of the dielectric function by Röpke and Der [75], the structure factor can be decomposed into different contributions describing free–free, free–bound and bound–bound transitions of the electrons. We would like to mention that our systematic quantum statistical approach can be extended also to higher densities, where in the strongly coupled Coulomb system the bound states are modified by the medium and eventually dissolved near the Mott density. The bound electrons which are strongly correlated with ions in a physical picture, should be described by a spectral function as outlined in the previous section.

The role of bound states in calculating the thermoelectric transport coefficients has long been extensively investigated. The partially ionized plasma (PIP) model takes the formation

of bound states into account with respect to different aspects, see Redmer *et al.* [14, 53, 291]. Firstly, the ionization degree determines the part of charge carriers which contributes to the electrical current. Secondly, in addition to free states, also atoms (bound states) will contribute to the collision frequency. From the force autocorrelation approach [53, 291], the scattering cross sections of free and bound electrons contribute additively. However, within a more general approach, also the bound states will contribute to the conductivity due to hopping processes [292]. As an application, the influence of bound states on the reflectivity has already been discussed in section 6.3.2. Calculating the contribution of the scattering with neutral atoms, the collision frequency has been improved.

In conclusion, the formation of bound states can be taken into account within the PIP model. Some references have been given. However, an exhaustive description of the influence of bound states on plasma response properties is beyond the scope of the present work. In particular, a systematic approach to the MIT based on the spectral function, as sketched in section 7.1, has to be elaborated which extends the applicability of the PIP model to higher densities.

7.3 Further developments

A first remark should be made with respect to a relativistic generalization of the dielectric response given here. As already discussed in the beginning, the general treatment of the dense charged particle system should start from a many-particle QED. The manifestation of a covariant formulation of the response to external perturbations as well as a kinetic theory has been attacked in various papers. An exhaustive discussion would exceed the present work, and we refer to only some approaches within a Green's function approach [26, 293, 294]. In particular, a many-particle QED for open systems in non-equilibrium was developed in recent papers by Höll, Morozov and Röpke [23, 24, 25]. The main point was the generalization of the linear response theory, in particular the relation between the collision frequency and the force autocorrelation function, from the nonrelativistic to the relativistic case. As already well-known, it is possible to express the response to external perturbations in terms of the relativistic current density autocorrelation function. Similar approaches have also been formulated in quantum chromodynamics, see [295, 296, 297].

We expect that the use of force correlation functions, i.e. the so-called second fluctuation-dissipation theorem, which holds for the inverse transport coefficients, will also be of use in the relativistic case. In the low-density limit, within Born approximation, the Bethe-Heitler result for the bremsstrahlung has been reproduced by Höll *et al.* [25]. In contrast to the treatment of transition probabilities on the basis of Fermi's Golden rule, this relativistic quantum statistical approach allows to include many-particle effects in dense charged particle systems in a systematic way.

Higher order density effects such as dielectric screening and quasiparticle propagation can be incorporated and will be subject to further considerations, for references see [298, 299, 300, 301]. Also, pair creation is an important relativistic effect, which has been discussed by Blaschke *et al.* [302, 303, 304, 305] and its modification in dense plasmas is of interest in

forthcoming work Thus, nonequilibrium many-particle QED is an interesting broad field for future investigations.

A very different topic is the treatment of inhomogeneous systems, such as surfaces or finite clusters. A local approximation can be given such that the collision frequency is determined according to the actual local values of density and temperature. A more detailed approach will take into account the eigenstates of electrons instead of plane waves, e.g., in clusters [306, 307], and will modify the collision frequency correspondingly. The solution of the Maxwell equations in inhomogeneous media such as a shock wave fronts was considered in section 6.3. Considering states in strong non-equilibrium, the local equilibrium approach might not be justified any more.

In the case of experiments with high intense laser beams, the occurrence of strong fields creates conditions which exceed the applicability of linear response, and concepts such as the dielectric function and transport coefficints have to be extended. A kinetic theory of plasmas in strong electric fields has been elaborated. Some references [178, 179, 222, 223, 224] were already discussed in section 7.3. They have investigated the collision frequency for strong fields. Our approach of linear response is restricted to weak external perturbations. However, the approach of constructing a generalized statistical operator for non-equilibrium situations allows evaluations in nonlinear regimes as well.

A last comment shall be made with respect to exotic plasmas. For dusty plasmas, the classical description is applicable and the dynamical structure factor has been measured. Excitonic energy levels in semiconductor heterostructures of reduced dimensionality are presently of increasing interest, since the manufacturing of such nanostructured materials is experimentally feasible and of technological importance. Many of the results given in the present work can be transferred to such two- or one-dimensional structures, see also Reinholz *et al.* [308, 309].

Acknowledgment

This work is in large parts a review of a collection of publications which were prepared in collaboration with a number of people. These are V. Fortov, V. Gryaznov, F. Höhne, A. Höll, S. Kuhlbrodt, T. Millat, V. Mintsev, I. Morozov, S. Nagel, C. Neißner, T. Pschiwul, R. Redmer, G. Röpke, A. Selchow, R. Thiele, A. Wierling, Yu. Zaporoghets, and G. Zwicknagel. It is my pleasure to thankfully acknowledge their contributions.
I would like to thank D. Blaschke, T. Bornath, W. Ebeling, S. Günter, K. Henneberger, I. McArthur, W.-D. Kraeft, D. Kremp, G. Manzke, V. Morozov, F. Reinholz, M. Schlanges, M. Schmidt, and B. Stamps who provided a continuously challenging background and encouraged with stimulating discussions. I very much enjoy working with J. Adams, C. Fortmann, C. Gocke, B. Holst, M. French, B. Omar, T. Raitza, and V. Schwarz.
Over the years I got to know some great scientist and closer collaboration developed with some of them. I would like to thank in particular J. Clark, M. Das, S. Glenzer, F. Hensel, D. Hoffmann, S. Hernandez, E. Krotschek, D. Logan, D. Nielson, and I. Tkachenko and acknowledge the support of the late E. Bashkin and T. Maslen.

The University of Western Australia provided a fellowship and the German DFG granted a Habilitandenstipendium. Furthermore, I acknowledge the financial support from the DFG-Sonderfoschungsbereich SFB 198 "*Kinetics of partially ionized plasmas*", the Graduiertenkolleg GK 567, the Virtual Institute VH-VI-104 "*Plasma physics research using FEL radiation*" by the Helmholtz Society, and the DFG-Sonderforschungsbereich SFB 652 "*Strong correlations and collective phenomena in radiation fields: Coulomb systems, clusters and particles*".

References

[1] A. Einstein, Ann. Physik (Leipzig) **17**, 132 (1905).

[2] V. Mintsev, V. Gryaznov, M. Kulish, and V. Fortov, Contrib. Plasma Phys. **41**, 119 (2001).

[3] in *Report 2002: High Energy Density Physics with Intense Laser and Ion Beams*, edited by D. Hoffmann (GSI, Darmstadt, 2003).

[4] K. Eidmann, J. Meyer-ter-Vehn, T. Schlegel, and S. Hüller, Phys. Rev. E **62**, 1202 (1999).

[5] C. Gahn, G. Tsakiris, A. Pukhov, J. Mezer-ter-Vehn, G. Pretzler, P. Thirolsf, D. Habs, and K. J. Witte, Phys. Rev. Lett. **83**, 4772 (1999).

[6] S. Glenzer, G. Gregori, R. Lee, F. Rogers, S. W. Pollaine, and O. Landen, Phys. Rev. Lett. **90**, 175002 (2003).

[7] S. Glenzer, G. Gregori, F. Rogers, D. Froula, S. W. Pollaine, R. Wallace, and O. Landen, Phys. Plasmas **10**, 2433 (2003).

[8] R. Kodama, P. A. Norreys, K. Mima, A. E. Dangor, R. G. Evans, H. Fujita, Y. Kitagawa, K. Krushelnick, T. Miyakoshi, N. Miyanaga, T. Norimatsu, S. J. Rose, T. Shozaki, K. Shigemori, A. Sunahara, M. Tampo, K. A. Tanaka, Y. Toyama, T. Yamanaka, and M. Zepf, Nature **412**, 798 (2001).

[9] G. Röpke, Contrib. Plasma Phys. **43**, 350 (2003).

[10] W. Ebeling, W. D. Kraeft, and D. Kremp, *Theory of bound states and ionization equilibrium in plasmas and solids* (Akademie-Verlag, Berlin, 1976).

[11] W.-D. Kraeft, D. Kremp, W. Ebeling, and G. Röpke, *Quantum Statistics of Charged Particle Systems* (Akademie-Verlag, Berlin, 1986).

[12] V. Fortov, and I. Iakubov, *Physics of Nonideal Plasma* (Hemisphere Publ. Corp., New York, 1990).

[13] W. Ebeling, A. Förster, V. Fortov, V. Gryaznov, and A. Polishchuk, *Thermophysical properties of Hot Dense Plasmas* (Teubner-Verlag, Stuttgart-Leipzig, 1991).

[14] R. Redmer, Physics Reports **282**, 35 (1997).

[15] D. Kremp, M. Schlanges, and W.-D. Kraeft, *Quantum Statistics of Nonideal Plasmas* (Springer, Berlin, 2005).

[16] Contr. Plasma Phys. **29** (4/5), 1989 Wustrow; Contr. Plasma Phys. **33** (5-6), 1993 Markgrafenheide; Contr. Plasma Phys. **39** (1-2), 1999 Rostock ; Contr. Plasma Phys. **41** (2-3), 2001 Greifswald; Contr. Plasma Phys. **43** (5-6) 2003 Valencia.

[17] *Physics of Strongly Coupled Plasmas*, eds. W.D. Kraeft and M. Schlanges (World Scientific, Singapore, 1996), Binz 1995; Journ. de Phys. IV **10** (5) 2000, St. Malo 1999; J. Phys. A: Math. Gen. **36** (22), 2003 Santa Fe.

[18] C. Itzykson, and J.-B. Zuber, *Quantum Field Theory* (McGraw-Hill, Singapore, 1980).

[19] M. E. Peshkin, and D. V. Schroeder, *An Introduction to Quantum Field Theory* (Addison-Wesley, New York, 1995).

[20] N. Bogolyubov, and D. Shirkov, *Introduction to the Theory of Quantized Fields* (Interscience, New York, 1959).

[21] S.S. Schweber, *An Introduction to Relativistic Quantum Field Theory* (Harper and Row, New York, 1961).

[22] G. Fleming, J. Math. Phys. **7**, 1959 (1966).

[23] V. Morozov, G. Röpke, and A. Höll, Theor. Math. Phys. **131**, 812 (2002).

[24] V. Morozov, G. Röpke, and A. Höll, Theor. Math. Phys. **132**, 1029 (2002).

[25] A. Höll, G. Röpke, and V. Morozov, Contr. Plasma Physics **319**, 371 (2003).

[26] B. Bezzerides, and D. F. DuBois, Ann. Phys. **70**, 10 (1972).

[27] D. F. DuBois, in *Lectures in Theoretical Physics* (Gordon and Breach, New York, 1967), Chap. Nonequilibrium Quantum Statistical Mechanics of Plasmas and Radiation, pp. 469–619.

[28] A. Bechler, Ann. Phys. **135**, 19 (1981).

[29] G. Röpke, and L. Hitzschke, in *Spectral Line Shapes*, edited by J. Szudy (Ossolineum Publishing House, Wrozław, 1989), pp. 49–72.

[30] G. D. Mahan, *Many-Particle Physics*, 2nd ed. (Plenum Press, New York, 1990).

[31] L. Schiff, *Quantum Mechanics* (McGraw-Hill, Tokyo, 1968).

[32] L. P. Kadanoff, and G. Baym, *Quantum Statistical Mechanics*, *Frontiers in Physics* (Addison-Wesley, New York, 1962).

[33] A. L. Fetter, and J. D. Walecka, *Quantum Theory of Many-Particle systems* (McGraw-Hill, New York, 1971).

[34] D. Zubarev, V. Morozov, and G. Röpke, *Statistical Mechanics of Nonequilibrium Processes* (Akademie-Verlag, Berlin, 1996), Vol. 1.

[35] D. Zubarev, V. Morozov, and G. Röpke, *Statistical Mechanics of Nonequilibrium Processes* (Akademie-Verlag, Berlin, 1997), Vol. 2.

[36] D. Forster, *Hydrodynamic Fluctuations, Broken Symmetry, and Correlation Functions* (W.A. Benjamin, Inc., London, 1975).

[37] A. Gold, Z. Phys. B **103**, 491 (1997).

[38] S. Adamyan, J. Ortner, and I. Tkachenko, Europhys. Lett. **25**, 11 (1994).

[39] J. Hong, and M. Lee, Phys. Rev. Lett. **70**, 1972 (1993).

[40] G. Zwicknagel, C. Toepffer, and P.-G. Reinhard, Phys. Rep. **309**, 117 (1999).

[41] J. P. Hansen, and I. R. McDonald, *Theory of Simple Liquids* (Academic Press, London, 1986).

[42] R. Kubo, J. Phys. Soc. Jpn. **12**, 570 (1957).

[43] H. Mori, Progr. Theor. Phys. **33**, 423 (1965).

[44] D. Zubarev, *Nonequilibrium Statistical Thermodynamics* (Plenum Press, New York, 1974).

[45] G. Röpke, Physica A **121**, 92 (1983).

[46] V. Christoph, and G. Röpke, phys. stat. sol. (b) **131**, 11 (1985).

[47] Y. Tserkovnikov, Theor. Math. Phys. **49**, 993 (1981).

[48] M. Lee, J. Math. Phys. **24**, 2512 (1983).

[49] H. Reinholz, Phd thesis, Institut für Physik, Rostock, 1989.

[50] G. Röpke, Phys. Rev. E **57**, 4673 (1998).

[51] G. Röpke, Phys. Rev. A **38**, 3001 (1988).

[52] F. Höhne, R. Redmer, H. Wegener, and G. Röpke, Physica A **128**, 643 (1984).

[53] H. Reinholz, R. Redmer, and S. Nagel, Phys. Rev. E **52**, 5368 (1995).

[54] G. Röpke, and F. Höhne, phys. stat. sol. (b) **107**, 603 (1984).

[55] F. Goedsche, R. Richter, H. Wegener, and G. Röpke, Physica Status Solidi (B) **120**, 631 (1983).

[56] H. Reinholz, and R. Redmer, J. Non-Cryst. Solids **156-158**, 654 (1993).

[57] H. Reinholz, R. Redmer, and D. Tamme, Contrib. Plasma Phys. **29**, 395 (1989).

[58] J. L. Spitzer, and R. Härm, Phys. Rev **89**, 977 (1953).

[59] J. L. Spitzer, *Physics of Fully Ionized Gases* (Interscience, New York, 1962).

[60] S. Chapman, and T. Cowling, *The Mathematical Theory of Non-Uniform Gases* (University Press, London, 1952).

[61] H. Grad, in *Handbuch der Physik*, edited by S. Flügge (Springer, Berlin, 1958), Vol. XXII, p. 205.

[62] G. Röpke, and A. Wierling, Phys. Rev. E **57**, 7075 (1998).

[63] H. Reinholz, Aust. J. Phys. **53**, 133 (2000).

[64] pp. 68-71 in [35].

[65] H. Reinholz, I. Morozov, G. Röpke, and T. Millat, Phys. Rev. E **69**, 066412 (2004).

[66] Y. L. Klimontovich, *Kinetic Theory of Nonideal Gases and Nonideal Plasmas (in Russian)* (Nauka, Moscow, 1975).

[67] S. Ichimaru, *Statistical Plasma Physics I* (Addison-Wesley, Redwood City, 1992).

[68] J. Lindhard, K. Dan. Vidensk. Selsk. Mat. Fys. Medd. **28**, 8 (1954).

[69] Y. L. Klimontovich, and V. Silin, Zh. Éksp. Teor. Fiz. **23**, 151 (1952).

[70] N. Arista, and W. Brandt, Phys. Rev. A **29**, 1471 (1984).

[71] N. Iwamoto, Phys. Rev. A **30**, 3289 (1984).

[72] K. Kliewer, and R. Fuchs, Phys. Rev. **181**, 552 (1969).

[73] F. Stern, Phys. Rev. Lett. **18**, 546 (1967).

[74] A. Ganguly, and C. Ting, Phys. Rev. B **16**, 3541 (1977).

[75] G. Röpke, and R. Der, phys. stat. sol. (b) **92**, 501 (1979).

[76] J. Hubbard, Proc. R. Soc. London A **243**, 336 (1957).

[77] K. Singwi, M. Tosi, R. Rand, and A. Sjölander, Phys. Rev. **176**, 589 (1968).

[78] S. Tanaka, and S. Ichimaru, Phys. Rev. A **32**, 3756 (1985).

[79] L. Świerkowski, D. Neilson, and J. Szymański, Aust. J. Phys. **46**, 423 (1993).

[80] G. Kalman, and K. Golden, Phys. Rev. B **57**, 8834 (1998).

[81] C. Richardson, and N. Ashcroft, Phys. Rev. B **50**, 8170 (1994).

[82] G. Kalman, and K. Golden, Phys. Rev. A **38**, 5516 (1990).

[83] H. Reinholz, R. Redmer, G. Röpke, and A. Wierling, Contrib. Plasma Phys. **39**, 77 (1999).

[84] E. Engel, and S. Vosko, Phys. Rev. B **42**, 4940 (1990).

[85] S. Hong, and G. Mahan, Phys. Rev. B **50**, 8182 (1994).

[86] G. Röpke, R. Redmer, A. Wierling, and H. Reinholz, Phys. Rev. E **60**, R2484 (1999).

[87] H. Reinholz, R. Redmer, G. Röpke, and A. Wierling, Phys. Rev. E **62**, 5648 (2000).

[88] V. Adamyan, T. Meier, and I. Tkachenko, Fiz. Plasm. (in Russian) **11**, 826 (1985).

[89] V. Rylyik, and I. Tkachenko, Phys. Rev. A **44**, 1287 (1991).

[90] M. Berkovsky, and Y. Kurilenkov, Physica A **197**, 676 (1993).

[91] Y. Kurilenkov, M. Berkovsky, S. Hocini, and M. Skowronek, J. Phys. B: At. Mol. Opt. Phys. **28**, 2021 (1995).

[92] J. P. Hansen, and I. R. McDonald, Phys. Rev. A **23**, 2041 (1981).

[93] L. Sjögren, J. Hansen, and E. Pollock, Phys. Rev. A **24**, 1544 (1981).

[94] N. Mermin, Phys. Rev. B **1**, 2362 (1970).

[95] A. Selchow, G. Röpke, and A. Wierling, Contrib. Plasma Phys. **42**, 43 (2002).

[96] G. Röpke, A. Selchow, A. Wierling, and H. Reinholz, Phys. Lett. A **260**, 365 (1999).

[97] K. Morawetz, and U. Fuhrmann, Phys. Rev. E **61**, 2272 (2000).

[98] H. Reinholz, R. Redmer, and D. Tamme, Contr. Plasma Physics **29**, 395 (1989).

[99] V. Bobrov, and S. Trigger, Solid State Commun. **56**, 210 (1985).

[100] M. Berkovsky, Y. Kurilenkov, and H. Milchberg, Phys. Fluids B **4**, 2423 (1992).

[101] M. Berkovsky, Physica A **214**, 461 (1995).

[102] M. Dharma-wardana, in *Laser Interactions with Atoms, Solids, and Plasmas*, Vol. 327 of *NATO Advances Study Institute Series B: Physics*, edited by R. More (Plenum Press, New York, 1992), p. 311.

[103] M. Dharma-wardana, and F. Perrot, Phys. Lett. A **163**, 223 (1992).

[104] D. Pines, and F. Nozières, *Theory of Quantum Fluids* (Benjamin, New York, 1958).

[105] A. Lenard, Annales of Physics (N.Y.) **10**, 390 (1960).

[106] R. Balescu, Phys. Fluids **3**, 52 (1960).

[107] R. Gurnsey, Phys. Fluids **7**, 1600 (1964).

[108] R. Redmer, G. Röpke, F. Morales, and K. Kilimann, Phys. Fluids B: Plasma Phys. **2**, 390 (1990).

[109] W. Hänsch, and G. Mahan, Phys. Rev. B **28**, 1902 (1983).

[110] G. Bekefi, *Radiation Processes in Plasmas* (Wiley, New York, 1966).

[111] J. Hopfield, Phys. Rev. **139**, A419 (1965).

[112] H. Reinholz, R. Redmer, and S. Nagel, Contributed Papers of the XXII. Int. Conf. on Phenomena in Ionized Gases (ICPIG) in Hoboken **2**, 37 (1995).

[113] G. Röpke, C.-V. Meister, K. Kollmorgen, and W. Kraeft, Ann. Physik (Leipzig) **36**, 377 (1979).

[114] A. Esser, R. Redmer, and G. Röpke, Contrib. Plasma Phys. **43**, 33 (2003).

[115] J. Ziman, Philos. Mag. **6**, 1013 (1961).

[116] T. Faber, *Introduction to the Theory of Liquid Metals* (University Press, Cambridge, 1972).

[117] D. Boercker, F. Rogers, and H. DeWitt, Phys. Rev. A **25**, 1623 (1982).

[118] H. Brooks, Phys. Rev. **83**, 879 (1951).

[119] F. Blatt, Solid State Phys. **4**, 199 (1957).

[120] J. Hubbard, Proc. R. Soc. London A **262**, 371 (1961).

[121] H. Gould, and H. DeWitt, Phys. Rev. **155**, 68 (1967).

[122] A. Esser, and G. Röpke, Phys. Rev. E **58**, 2446 (1998).

[123] L. Onsager, Phys. Z. **28**, 277 (1927).

[124] H. Falkenhagen, *Electrolyte* (Hirzel, Stuttgart, 1953).

[125] Y. L. Klimontovich, and W. Ebeling, Sh. Eksp. Teor. Fiz. **43**, 146 (1962).

[126] G. Röpke, and R. Redmer, Phys. Rev. A **39**, 907 (1989).

[127] H. Reinholz, R. Redmer, and G. Röpke, in *Physics of Nonideal Plasmas - Selected Papers of the Int. Workshop on the Physics of Nonideal Plasmas (PNP) in Gosen 1991*, edited by W. Ebeling, A. Förster, and R. Radtke (Teubner-Verlag, Leipzig, 1992), pp. 190–195.

[128] J. Ziman, *Principles of the Theory of Solids* (University Press, Cambridge, 1972).

[129] S. Ichimaru, and S. Tanaka, Phys. Rev. A **32**, 1790 (1985).

[130] S. Ichimaru, H. Iyetomi, and S. Tanaka, Phys. Rep. **149**, 91 (1987).

[131] *Handbook of Mathematical Functions*, edited by M. Abramowitz, and I. Stegun (Dover, New York, 1972).

[132] W. Karzas, and R. Latter, Astrophys. J. Suppl. **6**, 167 (1961).

[133] H. van Haeringen, L. Kok, and J. de Maag, Phys. Rev. A **32**, 677 (1985).

[134] T. Wilhein, J. Opt. Soc. Am. B **15**, 1235 (1998).

[135] J. Dawson, and C. Oberman, Phys. Fluids **5**, 517 (1962).

[136] G. Röpke, H. Reinholz, R. Redmer, and A. Wierling, J. Phys. IV France **10**, Pr5 (2000).

[137] H. Reinholz, and G. Röpke, in *Condensed Matter Theories*, edited by G. Anagnostatos, R. Bishop, K. Gernoth, J. Ginis, and A. Theophilou (Nova Science Publ., New York, 2000), Vol. 15, pp. 337–356.

[138] R. Dandrea, N. Ashcroft, and A. Carlsson, Phys. Rev. B **34**, 2097 (1986).

[139] H. Schweng, and H. Bohm, Phys. Rev. B **48**, 2037 (1993).

[140] J.-P. Hansen, in *Strongly Coupled Plasma Physics*, edited by F. Rogers, and H. DeWitt (Plenum Press, New York, 1987), p. 111.

[141] I. Morozov, G. Norman, and A. Valuev, Doklady Physics **43**, 608 (1998).

[142] I. Morozov, G. Norman, and A. Valuev, Phys. Rev. E **63**, 036405 (9 pages) (2001).

[143] I. Morozov, and G. Norman, JETP **100**, 370 (2005).

[144] A. Selchow, G. Röpke, A. Wierling, H. Reinholz, T. Pschiwul, and G. Zwicknagel, Phys. Rev. E **64**, 056410 (2001).

[145] J. Hansen, I. R. McDonald, and E. Pollock, Phys. Rev. A **11**, 1025 (1975).

[146] P. Schmidt, G. Zwicknagel, P.-G. Reinhard, and C. Toepffer, Phys. Rev. E **56**, 7310 (1997).

[147] J. Hansen, I. R. McDonald, and P. Vieillefosse, Phys. Rev. A **20**, 2590 (1979).

[148] M. Knaup, Ph.D. thesis, Friedrich-Alexander-Universität Erlangen-Nürnberg, unpublished, 2001.

[149] D. Klakow, C. Toepffer, and P.-G. Reinhard, J. Chem. Phys. **101**, 10 766 (1994).

[150] M. Knaup, P.-G. Reinhard, and C. Toepffer, Contrib. Plasma Phys. **41**, 159 (2001).

[151] R. Car, and M. Parrinello, Phys. Lett. A **60**, 317 (1977).

[152] P. Hohenberg, and W. Kohn, Phys. Rev. Lett. **136**, 864 (1964).

[153] W. Kohn, and L. Sham, Phys. Rev. **140**, 1133 (1965).

[154] G. Kresse, and J. Hafner, Phys. Rev. B **47**, 558 (1993).

[155] D. M. Ceperley, Rev. Mod. Phys. **67**, 279 (1995).

[156] B. Militzer, and D. M. Ceperley, Phys. Rev. Lett. **85**, 1890 (2000).

[157] S. Pfalzner, and P. Gibbon, Phys. Rev. E **57**, 4698 (1998).

[158] V. S. Filinov, M. Bonitz, P. Levashov, V. E. Fortov, W. Ebeling, M. Schlanges, and S. W. Koch, J. Phys. A **36**, 6069 (2003).

[159] H. Reinholz, Y. Zaporoghets, V. Mintsev, V. Fortov, I. Morozov, and G. Röpke, Phys. Rev. E **68**, 036403 (2003).

[160] H. Reinholz, G. Röpke, I. Morozov, V. Mintsev, Y. Zaporoghets, V. Fortov, and A. Wierling, J. Phys. A: Math. Gen. **36**, 5991 (2003).

[161] C. Deutsch, Phys. Lett. A **60**, 317 (1977).

[162] C. Deutsch, M. Combert, and H. Minoo, Phys. Lett. A **66**, 3810 (1978).

[163] T. Pschiwul, and G. Zwicknagel, J. Phys. A **36**, 6251 (2003).

[164] T. Pschiwul, and G. Zwicknagel, Contrib. Plasma Phys. **43**, 393 (2003).

[165] W. Ebeling, G. Norman, A. Valuev, and I. Valuev, Contrib. Plasma Phys. **39**, 61 (1999).

[166] G. Kelbg, Ann. Physik (Leipzig) **129**, 2193 (1963).

[167] A. Filinov, M. Bonitz, and W. Ebeling, J. Phys. A **36**, 5957 (2003).

[168] B. Nijboer, and F. D. Wette, Physica (Utrecht) **23**, 309 (1957).

[169] J. Hansen, Phys. Rev. A **8**, 3096 (1973).

[170] M. Allen, and D. Tildesley, *Computer Simulation of Liquids* (Clarendon Press, Oxford, 1975).

[171] G. Zwicknagel, Ph.D. thesis, Friedrich-Alexander-Universität Erlangen-Nürnberg, unpublished, 1994.

[172] I. Morozov, H. Reinholz, G. Röpke, A. Wierling, and G. Zwicknagel, Phys. Rev. E **71**, 066408 (2005).

[173] W. Press, B. Flannery, S. Teukolsky, and W. Vetterling, *Numerical Recipes* (Cambridge University Press, Cambridge, 1989).

[174] T. Pschiwul, Master's thesis, Friedrich-Alexander-Universität Erlangen-Nürnberg, unpublished, 2001.

[175] T. Millat, Ph.D. thesis, Universität Rostock, 2003.

[176] T. Millat, A. Selchow, A. Wierling, H. Reinholz, R. Redmer, and G. Röpke, J. Phys. A: Math. Gen. **36**, 6259 (2003).

[177] M. Schlanges, T. Bornath, P. Hilse, and D. Kremp, Contrib. Plasma Phys. **43**, 360 (2003).

[178] T. Bornath, M. Schlanges, P. Hilse, and D. Kremp, Phys. Rev. E **64**, 026414 (2001).

[179] T. Bornath, M. Schlanges, P. Hilse, and D. Kremp, J. Phys. A: Math. Gen. **36**, 5941 (2003).

[180] V. Sechenov, E. Son, and O. Shchekotov, Sov. Phys.-TVT **15**, 415 (1977).

[181] Y. Ivanov, V. Mintsev, V. Fortov, and A. Dremin, Sov. Phys.-TVT **71**, 216 (1976).

[182] A. Bakeev, and R. Rovinskii, Sov. Phys.-TVT **8**, 1121 (1970).

[183] V. Batenin, and P. Minaev, Sov. Phys.-TVT **92**, 676 (1971).

[184] S. Andreev, and T. Gavrilova, Sov. Phys.-TVT **13**, 176 (1975).

[185] A. Höll, R. Redmer, G. Röpke, and H. Reinholz, Eur. J. Phys. D **29**, 159 (2004).

[186] R. Redmer, H. Reinholz, G. Röpke, R. Thiele, and A. Höll, IEEE Transactions on Plasma Science **33**, 77 (2005).

[187] D. Evans, and J. Katzenstein, Rep. Prog. Phys. **327**, 207 (1969).

[188] J. Chihara, J. Phys. F: Met. Phys. **172**, 295 (1987).

[189] V. Tsytovich, Astropart. Phys. **5**, 285 (1996).

[190] E. Nardi, Z. Zinamon, D. Riley, and N. Woolsey, Phys. Rev. E **57**, 4693 (2000).

[191] J. Chihara, J. Phys. Condens. Matter **129**, 231 (2000).

[192] D. Riley, N. Woolsey, D. McSherry, I. Weaver, A. Djaoui, and E. Nardi, Phys. Rev. Lett. **84**, 1704 (2000).

[193] O. Landen, S. Glenzer, M. Edwards, R. Lee, G. Collins, R. Cauble, W. Hsing, and B. Hammel, J. Quant. Spectrosc. Radiat. Transf. **71**, 465 (2001).

[194] H. Baldis, J. Dunn, M. Foord, and W. Rozmus, Rev. Sci. Instr. **73**, 4223 (2002).

[195] H. Wabnitz, L. Bittner, A. R. B. de Castro, R. Dührmann, P. Gürtler, T. Laarmann, W. Laasch, J. Schulz, A. Swiderski, K. von Haeften, T. Müller, B. Faatz, A. Fateev, J. Feldhaus, C. Gerth, U. Hahn, E. Saldin, E. Schneidmiller, K. Sytchev, K. Tiedtke, R. Treusch, and M. Yurkov, Nature **420**, 482 (2002).

[196] R. Brinkmann, B. Faatz, K. Flöttmann, J. Rossbach, J. Schneider, H. Schulte-Schrepping, D. Trines, T. Tschentscher, and H. Weise, DESY Rep. 2002-167, DESY, Hamburg (unpublished).

[197] T. L. D. S. Group, Technical Report No. SLAC-R-0521, SLAC, Stanford 1998, CA (unpublished).

[198] S. Glenzer, W. Rozmus, B. MacGowan, L. Estabrook, J. D. Groot, G. Zimmermann, H. Baldis, J. Harte, R. Lee, E. Williams, and B. Wilson, Phys. Rev. Lett. **82**, 97 (1999).

[199] M. Foord, S. Glenzer, R. Thoe, K. Kwong, K. Fournier, B. Wilson, and P. Springer, Phys. Rev. Lett. **85**, 992 (2000).

[200] G. Gregori, S. Glenzer, W. Rozmus, R. Lee, and O. Landen, Phys. Rev. E **67**, 026412 (2003).

[201] G. Gregori, S. Glenzer, F. Rogers, S. Pollaine, O. Landen, S. Blancard, G. Faussurier, P. Renaudin, S. Kuhlbrodt, and R. Redmer, Phys. Plasmas **11**, 2754 (2004).

[202] F. J. Rogers, Physics of Plasmas **7**, 51 (2000).

[203] F. Rogers, and D. Young, Phys. Rev. E **56**, 5876 (1997).

[204] S. Kuhlbrodt, H. Juranek, V. Schwarz, and R. Redmer, Contrib. Plasma Phys. **43**, 342 (2003).

[205] S. Kuhlbrodt, and R. Redmer, Phys. Rev. E **62**, 7191 (2000).

[206] A. Sitenko, and V. Malnev, *Plasma Physics Theory* (Chapman and Hall, London, 1995).

[207] S. Ichimaru, Rev. Mod. Phys. **54**, 1017 (1982).

[208] S. Ichimaru, and K. Utsumi, Phys. Rev. B **24**, 7385 (1981).

[209] G. Gregori, S. Glenzer, and O. Landen, J. Phys. A: Math. Gen. **36**, 5971 (2003).

[210] H. Griem, *Principles of Plasma Spectroscopy* (Cambridge University Press, Cambridge, 1997).

[211] I. Hutchinson, *Principles of Plasma Spectroscopy* (Cambridge University Press, Cambridge, 1987).

[212] A. Mostovych, K. Kearney, J. Stamper, and A. Schmitt, Phys. Rev. Lett. **66**, 612 (1990).

[213] M. Lamoureux, P. Waller, P. Charles, and N. Avdonina, Phys. Rev. E **62**, 4091 (2000).

[214] A. Wierling, T. Millat, G. Röpke, R. Redmer, and H. Reinholz, Physics of Plasmas **8**, 3810 (2001).

[215] H. Kramers, Philos. Mag. **46**, 836 (1923).

[216] J. Gaunt, Proc. R. Soc. London A **126**, 654 (1930).

[217] T. Johnston, and J. Dawson, Phys. Fluids **16**, 722 (1973).

[218] W. Kruer, *The Physics of Laser Plasma Interaction* (Addison-Wesley, Redwood City, 1988).

[219] R. Kawakami, K. Mima, H. Totsuji, and Y. Yokoyama, Phys. Rev. A **38**, 3618 (1988).

[220] R. Cauble, and W. Rozmus, Phys. Fluids **28**, 3387 (1985).

[221] N. Dagdeviren, and S. Koonin, Astrophys. J. **319**, 192 (1995).

[222] V. Silin, Zh. Éksp. Teor. Fiz. **47**, 2254 (1964).

[223] C. Decker, W. Mori, J. Dawson, and T. Katsouleas, Phys. Plasmas **1**, 4043 (1994).

[224] P. Mulser, F. Cornolti, E. Bèsuelle, and R. Schneider, Phys. Rev. E **63**, 016406 (2001).

[225] S. Rae, and K. Burnett, Phys. Fluids B **2**, 1015 (1990).

[226] D. Kremp, T. Bornath, M. Bonitz, and M. Schlanges, Phys. Rev. E **60**, 4725 (1999).

[227] M. Bonitz, T. Bornath, D. Kremp, M. Schlanges, and W.-D. Kraeft, Contrib. Plasma Phys. **39**, 329 (1999).

[228] J. Jackson, *Classical Electrodynamics* (Wiley, New York, 1975).

[229] I. Tkachenkov, and P. F. de Córdoba, Phys. Rev. E **57**, 2222 (1998).

[230] M. Murillo, and J. Weisheit, Phys. Rep. **302**, 1 (1998).

[231] A. Sommerfeld, *Atombau und Spektrallinien* (Vieweg-Verlag, Braunschweig, 1949), Vol. 1-2.

[232] S. Skupsky, Phys. Rev. A **36**, 5701 (1987).

[233] Y.-D. Jung, Phys. Rev. E **55**, 3369 (1997).

[234] M. Lamoureux, I. Feng, R. Pratt, and H. Tseng, J. Quant. Spectrosc. Radiat. Transf. **27**, 227 (1982).

[235] B. Gao, and A. Starace, Comp. Phys. **1**, 70 (1987).

[236] A. Salat, and P. Kaw, Phys. Fluids **12**, 342 (1969).

[237] M. Altarelli, D. Dexter, H. Nussenzveig, and D. Smith, Phys. Rev. B **6**, 4502 (1972).

[238] P. Gibbon, private communication (2000).

[239] C. Iglesias, and S. Rose, Astrophys. J. Lett. **466**, L115 (1996).

[240] C. Iglesias, Phys. Lett. A **213**, 313 (1996).

[241] V. B. Mintsev, and Y. B. Zaporoghets, Contrib. Plasma Phys. **29**, 493 (1989).

[242] Y. B. Zaporoghets, V. B. Mintsev, V. Gryaznov, and V. Fortov, in *Physics of Extreme Matter*, edited by V. F. *et al.* (Inst. Probl. Chem. Phys. RAN, Chernogolovka, 2002), p. 188.

[243] Y. Zaporoghets, V. Mintsev, V. Gryaznov, V. Fortov, H. Reinholz, T. Raitza, and G. Röpke, J. Phys. A: Math. Gen. **39**, 4329 (2006).

[244] M. Basko, T. Löwer, V. Kondrashov, A. Kendl, R. Sigel, and J. M. ter Vehn, Phys. Rev. E **56**, 1019 (1997).

[245] T. Löwer, V. Kondrashov, M. Basko, A. Kendl, J. M. ter Vehn, R. Sigel, and A. Ng, Phys. Rev. Lett. **80**, 4000 (1998).

[246] P. Celliers, G. Collins, D. Silva, L.B., D. Gold, R. Cauble, R. Wallace, M. Foord, and B. Hammel, Phys. Rev. Lett. **84**, 5564 (2000).

[247] R. Cauble, D. Bradley, P. Celliers, G. Collins, L. D. Silva, and S. Moon, Contr. Plasma Physics **41**, 239 (2001).

[248] T. Raitza, H. Reinholz, G. Röpke, V. Mintsev, and A. Wierling, J. Phys. A: Math. Gen. **39**, 4393 (2006).

[249] Y. Kurilenkov, M. Berkovsy, S. Hocini, and M. Skowronek, in *Transport and Optical Properties of Nonideal Plasma*, edited by G. Kobzov, I. Iakubov, and M. Popovich (Plenum Press, New York, 1995), pp. 270–274.

[250] A. Kaklyugin, G. Norman, and A. Valuev, in *Physics of Strongly Coupled Plasmas*, edited by W. Kraeft, and M. Schlanges (World Scientific, Singapore, 1996), pp. 435–440.

[251] G. Norman, and A. Valuev, in *Strongly Coupled Coulomb Systems*, edited by G. Kalman, M. Rommel, and K. Blagoev (Plenum Press, New York, 1998), pp. 103–116.

[252] W. Ebeling, Physica A **43**, 293 (1969).

[253] A. Likalter, Zh. Eksp. Teor. Fiz. **56**, 340 (1969).

[254] W. Rozmus, V. Tikhonchuk, and R. Cauble, Phys. Plasmas **327**, 360 (1996).

[255] H. Reinholz, G. Röpke, A.Wierling, V. Mintsev, and V. Gryaznov, Contrib. Plasma Phys. **43**, 3 (2003), arXiv:physics/0207040.

[256] S. Fraga, J. Karwowski, and K. Saxena, *Handbook of Atomic Data* (Elesevier, Amsterdam, 1976).

[257] V. Atrazhev, I. Chernysheva, and T. Doke, Jpn. J. Appl. Phys. Part 1 **41**, 1572 (2002).

[258] J. Lekner, *Theory of Reflection* (Martinus Nijhoff Publ, Dordrecht, 1987).

[259] T. Raitza, Master's thesis, Institut für Physik, Univeristät Rostock, Rostock, 2005.

[260] M. Schmidt, G. Röpke, and H. Schulz, Ann. Physik (Leipzig) **202**, 57 (1990).

[261] G. Röpke, and H. Reinholz, phys. stat. sol (b) **234**, 254 (2002).

[262] P. Nozières, and S. Schmitt-Rink, J. Low Temp. Phys. **59**, 159 (1985).

[263] G. Röpke, H. Reinholz, and C. Neißner, J. Phys. A **36**, 5931 (2003).

[264] R. Zimmermann, *Many-Particle Theory of Highly Excited Semiconductors*, Vol. 18 of *Teubner–Texte zur Physik* (Teubner, Leipzig, 1987).

[265] R. Zimmermann, and H. Stolz, phys. stat. sol. (b) **131**, 151 (1985).

[266] G. Röpke, K. Kilimann, W. D. Kraeft, D. Kremp, and R. Zimmermann, phys. stat. sol. (b) **88**, K59 (1978).

[267] R. Zimmermann, K. Kilimann, W.-D. Kraeft, D. Kremp, and G. Röpke, phys. stat. sol. (b) **90**, 175 (1978).

[268] G. Röpke, Ann. Physik (Leipzig) **3**, 145 (1994).

[269] G. Röpke, A. Schnell, and P. Schuck, in *Condensed Matter Theories*, edited by J. Clark, and P. V. Panat (Nova Science Publ., New York, 1994), Vol. 12, p. 237.

[270] H. Stolz, R. Zimmermann, and G. Röpke, phys. stat. sol. (b) **105**, 585 (1981).

[271] C. Neißner, Ph.D. thesis, Universität Rostock, 2004.

[272] H. Reinholz, G. Röpke, and C. Neißner, in *Condensed Matter Theories*, edited by M. Belkacem, and M. Dinh (Nova Science Publ., New York, 2005), Vol. 19, p. 33. .

[273] B. Rozsnyai, Phys. Rev. A **5**, 1137 (1972).

[274] J. Yuan, Y. Sun, and S. Zheng, Phys. Rev E **53**, 1059 (1996).

[275] F. Perrot, and M. Dharma-wardana, Int. J. Thermophys. **20**, 1299 (1999).

[276] V. Gryaznov, M. Zhernokletov, and V. Zubarev, Sov. Phys.-JETP **51**, 288 (1980).

[277] V. E. Fortov, V. Y. Ternovoi, M. V. Zhernokletov, M. A. Mochalov, A. L. Mikhailov, A. S. Filimonov, A. A. Pyalling, V. B. Mintsev, V. K. Gryaznov, and I. L. Iosilevski, JETP **97**, 259 (2003).

[278] M. Winn, and D. Logan, J. Phys.: Condensed Matter **1**, 1753 (1989).

[279] S. Günter, L. Hitzschke, and G. Röpke, Phys. Rev. A **44**, 6834 (1991).

[280] S. Sorge, Ph.D. thesis, Universität Rostock, 2000.

[281] A. Könies, Ph.D. thesis, Universität Rostock, 1995.

[282] S. Günter, Habilitation thesis, Universität Rostock, 1995.

[283] S. Günter, and A. Könies, Phys. Rev. E **49**, 4732 (1994).

[284] A. Könies, S. Günter, and G. Röpke, J. Phys. B: At. Mol. Opt. Phys. **29**, 6091 (1996).

[285] S. Sorge, S. Günter, and G. Röpke, J. Phys. B: At. Mol. Opt. Phys. **32**, 675 (1999).

[286] S. Böddeker, S. Günter, A. Könies, L. Hitzschke, and H.-J. Kunze, Phys. Rev. E **47**, 2785 (1993).

[287] A. Könies, and S. Günter, J. Quant. Spectrosc. Radiat. Transf. **52**, 825 (1994).

[288] S. Sorge, A. Wierling, G. Röpke, W. Theobald, R. Sauerbrey, and T. Wilhein, J. Phys. B: At. Mol. Opt. Phys. **33**, 2983 (2000).

[289] B. Omar, A. Wierling, S. Günter, and G. Röpke, in *Spectral Line Shapes*, edited by E. Dalimier (Frontier Group, Paris, 2004), pp. 150–152.

[290] B. Omar, A. Wierling, S. Günter, and G. Röpke, J. Phys.: Conf. Series **11**, 147 (2005).

[291] R. Redmer, G. Röpke, S. Kuhlbrodt, and H. Reinholz, Contrib. Plasma Phys. **41**, 163 (2001).

[292] R. Redmer, G. Röpke, S. Kuhlbrodt, and H. Reinholz, Phys. Rev. B **63**, 233104 (2001).

[293] W. Botermans, and R. Malfliet, Phhys. Rep. **198**, 115 (1990).

[294] J. Knoll, and D. Voskresensky, Ann. Phys. **249**, 532 (1996).

[295] A. Das, *Finite Temperature Field Theory* (World Scientific, Singapore, 1997).

[296] J. Kapusta, *Finite Temperature Field Theory* (University Press, Cambridge, 1993).

[297] M. LeBellac, *Thermal field theory* (University Press, Cambridge, 1996).

[298] L. Landau, and I. Pomeranchuk, Dokl. Akad. Nauk SSSR **92**, 535 (1953).

[299] A. Migdal, Phys. Rev. **103**, 1811 (1956).

[300] S. Klein, Rev. Mod. Phys. **71**, 1501 (1999).

[301] H. Hansen, U. Uggerhøj, C. Biino, S. Ballestrero, A. Mangiarotti, P. Sona, T. Ketel, and Z. Vilakazi, Phys. Rev. Lett. **91**, 014801 (2003).

[302] A. Ringwald, Phys. Lett. B **510**, 107 (2001).

[303] C. Roberts, and S. Schmidt, Prog. Part. Nucl. Phys. **45**, 1 (2000).

[304] D. Blaschke, Y. Kalinovsky, S. Schmidt, and H. Schulze, Phys. Rev. C **57**, 438 (1998).

[305] D. Blaschke, M. Volkov, and V. Yudichev, Eur. Phys. J. A **17**, 103 (2002).

[306] T. Fennel, G. Bertsch, and K.-H. Meiwes-Broer, Eur. Phys. J. D **29**, 367 (2004).

[307] V. Krainov, and M. Smirnov, Phys. Rep. **370**, 237 (2002).

[308] H. Reinholz, Solid State Comm. **123**, 489 (2002).

[309] H. Reinholz, and G. Röpke, Contrib. Plasma Phys. **43**, 346 (2003).